Numerical Homogenization: Multi-resolution and Super-localization Approaches

Dissertation

zur Erlangung des akademischen Grades

Dr. rer. nat.

eingereicht an der

Mathematisch-Naturwissenschaftlich-Technischen Fakultät

der Universität Augsburg

von

Moritz Hauck

Augsburg, April 2023

Erstgutachter: Prof. Dr. Daniel Peterseim
Zweitgutachter: Prof. Dr. Martin Kronbichler
Drittgutachter: Prof. Dr. Patrick Henning

Tag der mündlichen Prüfung: 16. Juni 2023

Abstract

Multi-scale problems arise in many scientific and engineering applications, where the effective behavior of a system is determined by the interaction of effects at multiple scales. To accurately simulate such problems without globally resolving all microscopic features, numerical homogenization techniques have been developed. One such technique is the Localized Orthogonal Decomposition (LOD). It provides reliable approximations at coarse discretization levels using problem-adapted basis functions obtained by solving local sub-scale correction problems. This allows the treatment of problems with heterogeneous coefficients without structural assumptions such as periodicity or scale separation.

This thesis presents recent achievements in the field of LOD-based numerical homogenization. As a starting point, we introduce a variant of the LOD and provide a rigorous error analysis. This LOD variant is then extended to the multi-resolution setting using the Helmholtz problem as a model problem. The multi-resolution approach allows to improve the accuracy of an existing LOD approximation by adding more discretization levels. All discretization levels are decoupled, resulting in a block-diagonal coarse system matrix. We provide a wavenumber-explicit error analysis that shows convergence under mild assumptions. The fast numerical solution of the block-diagonal coarse system matrix with a standard iterative solver is demonstrated.

We further present a novel LOD-based numerical homogenization method named Super-Localized Orthogonal Decomposition (SLOD). The method identifies basis functions that are significantly more local than those of the LOD, resulting in reduced computational cost for the basis computation and improved sparsity of the coarse system matrix. We provide a rigorous error analysis in which the stability of the basis is quantified a posteriori. However, for challenging problems, basis stability issues may arise degrading the approximation quality of the SLOD. To overcome these issues, we combine the SLOD with a partition of unity approach. The resulting method is conceptually simple and easy to implement. Higher order versions of this method, which achieve higher order convergence rates using only the regularity of the source term, are derived.

Finally, a local reduced basis (RB) technique is introduced to address the challenges of parameter-dependent multi-scale problems. This method integrates a RB approach into the SLOD framework, enabling an efficient generation of reliable coarse-scale models of the problem. Due to the unique localization properties of the SLOD, the RB snapshot computation can be performed on particularly small patches, reducing the offline and online complexity of the method. All theoretical results of this thesis are supported by numerical experiments.

Acknowledgments

First and foremost, I would like to express my gratitude to my advisor, Daniel Peterseim, for giving me the opportunity to work in his research group and for his guidance, encouragement, and mentorship throughout my Ph.D. studies. I am also very grateful to Martin Kronbichler and Patrick Henning for agreeing to serve as co-examiners of my dissertation. Furthermore, I would like to thank my co-authors Francesca Bonizzoni, Zhaonan Dong, Philip Freese, Tim Keil, Roland Maier, and Axel Målqvist for the successful collaboration over the past three years, which has directly or indirectly contributed to the content of this dissertation. I would also like to thank Philip Freese, Fabian Kröpfl, Roland Maier, Hannah Mohr, and Christoph Zimmer for their meticulous proofreading and insightful suggestions, which significantly improved my dissertation. Moreover, I would like to thank all my current and former colleagues at the Chair for Computational Mathematics, the Research Unit for Applied Analysis, the Research Unit for High-Performance Scientific Computing, and the Chair for Inverse Problems at the University of Augsburg for the welcoming working environment, the stimulating discussions, and their support. I would like to acknowledge the financial support from the European Research Council (ERC) through the Horizon 2020 Research and Innovation Program of the European Union (Grant agreement No. 865751 – RandomMultiScales). Last but not least, I would like to thank my family and friends for their constant presence and support. I am especially grateful to my parents, my brother and sister, and my girlfriend Veronika for their endless encouragement, affection, and unwavering belief in me.

Augsburg, April 2023 *Moritz Hauck*

Contents

List of Figures

List of Algorithms

1 Introduction

1.1 Motivation

The interplay of effects at different scales plays an important role in many scientific and engineering applications. One example is the fluid flow in porous media, such as groundwater flow through heterogeneous geological subsurface formations composed of sediment and rock. Here, a reliable model must account for effects on multiple length scales, ranging from the micrometer scale to the meter scale [Hel97]. Another prominent example is the use of short fibers to reinforce materials such as concrete or polymers. In this application, the fiber microstructure increases the tensile strength of the resulting composite material, see for example [FL96; BS07; Lau+21]. A particularly surprising example comes from optics. As shown in [PE03; EP04], materials with certain microstructures can cause interactions of effects on different length scales, resulting for example in negative effective refractive indices. Such materials, known as metamaterials, have extraordinary properties that do not exist in nature. They can be used to construct perfectly flat lenses [Pen00] and invisibility cloaks [PSS06].

In the above mentioned applications, a complex interplay of effects on multiple scales determines the effective flow or material properties. Mathematically, one describes the underlying physical processes as solutions to partial differential equations (PDEs) with coefficients varying on multiple scales. Because of the nature of the coefficients, such PDEs are typically referred to as multi-scale PDEs or multi-scale problems. The direct numerical solution of such problems by means of classical finite element methods (FEMs) is very challenging due to the presence of microstructures that need to be resolved, resulting in a very large, possibly intractable number of degrees of freedom. In addition, the coefficients often have a high contrast, which makes the numerical solution even more difficult. Since in practice, one is mainly interested in the effective behavior of the PDE solution, one may try to average the coefficients at a macroscopic scale. However, the naive averaging of the coefficients generally produces a macroscopic problem with significantly different effective properties than the original problem, see, e.g., [MP20, Ch. 2]. Under strong assumptions on the coefficients (i.e., periodicity and scale separation), sophisticated analytical averaging techniques, known under the term homogenization, can be used to construct macroscopic coefficients, see, e.g., [Tar09]. However, such approaches fail whenever one leaves the idealized periodic regime. We note that the groundwater flow example has non-periodic coefficients due to the heterogeneous subsurface geology, while the

coefficients for a reinforced material and a metamaterial may be non-periodic due to material imperfections.

In the general setting with minimal structural assumptions on the coefficients, so-called numerical homogenization methods provide an alternative to analytical homogenization. Given a coarse mesh, the idea is to construct problem-adapted coarse approximation spaces whose basis functions are obtained by solving local PDEs. Because of the microscopic information encoded in the approximation space, numerical homogenization methods are able to provide reliable approximations even on coarse meshes that do not resolve the coefficients. Note that for numerical homogenization methods, the coarse scale is not predetermined by the problem. Instead, it is a design choice made by the user, depending on the available computational resources and the desired accuracy. Numerical homogenization methods typically have a moderate computational overhead compared to classical FEMs, e.g., a slightly larger support of the basis functions or a moderately increased number of basis functions per mesh entity.

Surprisingly, numerical homogenization methods also prove to be effective beyond homogenization problems. An inconspicuous application is the stabilization of numerical schemes for time-harmonic wave propagation problems, such as the Helmholtz problem. To obtain a reliable approximation, classical FEMs require the mesh size to be much smaller than the minimal requirement needed to resolve the oscillatory nature of the solution. This is known as the pollution effect [BS97]. Numerical homogenization methods, however, are able to suppress the pollution effect at a moderate wavenumber-dependent computational overhead, see for example [Pet17]. An overview of the origin and development of numerical homogenization methods is given in the next section.

1.2 Literature review

Analytical techniques such as G- and H-convergence [Spa68; MT78] provide a fairly general framework for the homogenization of elliptic operators. Given a sequence of elliptic differential operators indexed by a fine-scale parameter ε tending to zero, they establish the existence of an elliptic limit problem along with weak and strong convergence results. This limit problem, called homogenized PDE, describes the effective behavior of the solution. Furthermore, the concept of Γ-convergence [DG75] can be used for the homogenization of ε-dependent energy functionals, e.g., in nonlinear elasticity, see [BD98]. Note that the above analytical homogenization techniques are generally non-constructive unless the coefficient of the elliptic problem allows a separation of scales into a slow variable and a fast ε-periodic variable. Under this assumption, popular analytical tools, such as the energy method [MT78], two-scale convergence [Ngu89; All92], and periodic unfolding [CDG02] can be used to derive implicit characterizations of the homogenized coefficient. Note that such a clear separation of scales is not satisfied in many applications, such as groundwater flow. Furthermore, one

may not be interested in the limit problem a priori, but rather in the problem for a fixed value of ε.

Besides these analytical techniques, there are various numerical approaches to homogenization. In the following, we give an overview of these numerical homogenization approaches using a classification inspired by [AHP21].

Homogenization-based approaches

Popular numerical homogenization approaches based on the above-mentioned analytical homogenization results include the Multiscale Finite Element Method (MsFEM) [HW97], the Two-Scale Finite Element Method [MS02], and the Heterogeneous Multiscale Method (HMM) [EE03]. The idea of the MsFEM is to solve local versions of the considered PDEs on all elements of a given coarse mesh. The solutions of these local PDEs are then used as basis functions of the method. Choosing the boundary conditions of the local PDEs is delicate, since a mismatch between the coarse mesh and the periodic microstructure can lead to large errors, so-called resonance errors. An oversampling approach, where the local PDEs are solved on domains that are a few ε-layers larger than the original elements, can be used to reduce these resonance errors. For advances in the homogenization-based error analysis of the MsFEM and further developments, see for example [HWC99; HWZ04; Glo12] and [LBLL13; LBLL14; HOS14; CL18; Leg+22].

The Two-Scale Finite Element Method is inspired by the concept of two-scale convergence. More specifically, for the construction of its coarse basis functions, the method mimics the choice of test functions in the theory of two-scale convergence. Note that, by definition, the method is limited to periodic microstructures. Later, in [HS05; Hoa08; HS11], the method was extended to the concept of multi-scale convergence [AB96].

The idea of the HMM is to compute a macroscopic FEM approximation of the homogenized PDE. This requires approximations of the homogenized coefficients at the quadrature points, which are computed by solving local PDEs on small cells around the quadrature points. This method is particularly efficient since these cells are typically much smaller than the coarse elements. Similar to the MsFEM, resonance errors can be reduced by oversampling. For results on the error analysis of the HMM, see for example [Abd05; Ohl05]. A review of the HMM can be found in [Abd+12]. We emphasize that the analysis of the above methods is based on (constructive) homogenization techniques and therefore strong structural assumptions on the coefficients of the considered problem are necessary.

Variational approaches

These strong structural assumptions are overcome by another class of numerical homogenization methods that can be derived from the Variational Multiscale

Method (VMM) [Hug+98]. This class includes methods such as the popular Localized Orthogonal Decomposition (LOD) [MP14; HP13]. The construction of the VMM is based on a decomposition of the solution space into a coarse finite element (FE) space and a fine-scale space. In order to obtain an accurate approximation in the underresolved regime, it incorporates the fine-scale Green's function of the residual into the discrete bilinear form. Note that the VMM can be viewed as a generalization of the local Green's function approach [Hug95], which avoids the original limitation that microscopic features must be strongly localized to coarse elements. In [HS07], it was discovered that projection operators from FE theory are particularly useful for constructing decompositions of the solution space. More specifically, it was suggested to choose the coarse space and the fine-scale space as the image and kernel of a projection operator. The empirical observation that the fine-scale Green's operator applied to FE shape functions decays exponentially fast justifies its localized computation on patches of the coarse mesh. This results in a practical variant of the VMM that requires only local fine-scale computations. A posteriori error control strategies for this method were developed in [Mål05; LM05; Mål11]. The first rigorous proof of the exponential decay properties of the fine-scale Greens operator was presented in [MP14], which led to the introduction of the LOD. Note that in the context of the LOD, the fine-scale Green's operator is usually referred to as corrector, since it is used to correct coarse FE shape functions. The LOD uses a problem-adapted approximation space defined as the span of corrected coarse FE shape functions. Under minimal structural assumptions on the coefficients, the LOD achieves optimal orders of convergence, provided that the support of the basis functions (the patch size) is increased logarithmically with the desired accuracy. More precisely, given a coarse mesh of mesh size H, an accuracy of $\mathcal{O}(H)$ is achieved when using basis functions with supports of diameter $\mathcal{O}(H \log(\frac{1}{H}))$. This results in a moderate (logarithmic) computational overhead compared to the coarse-scale FEM. The original construction of the LOD was later refined in [HP13; HM14]. The LOD can be interpreted as an additive Schwarz method, allowing an alternative proof of its exponential localization properties, see [KY16; KPY18]. Higher order variants of the LOD were first introduced in [Mai21] and later refined in [DHM22]. For a complete overview of LOD-based numerical homogenization, see [MP20; AHP21].

Although the LOD provided the first constructive exponential localization result, the general question of localization was already theoretically studied in [GGS12], where so-called Adaptive Local Bases (ALB) were introduced. Under minimal structural assumptions, the ALB achieve an accuracy of $\mathcal{O}(H)$ using $\mathcal{O}((\log \frac{1}{H})^{d+1})$ local basis functions per mesh entity. Note that this is only a theoretical result, since the computation of the local basis functions requires the solution to global problems. This problem is later addressed in [Wey17], where a practical variant of the ALB is introduced.

Another related approach with many conceptual similarities to the LOD are the so-called Rough Polyharmonic Splines (RPS) introduced in [OZB14]. The

basis functions of this method, which are determined by constrained energy minimization problems, can be viewed as generalized problem-adapted splines. Note that the decay properties of the basis functions and the resulting computational overhead are similar to the LOD. The extension of the game-theoretic interpretation of the RPS in [Owh15] to hierarchical information games led to the multi-resolution numerical homogenization approaches [Owh17; OS19], also known as gamblets. This also gave rise to the multi-resolution method [FP20] in the context of the LOD.

Spectral approaches

Another class of methods are spectral numerical homogenization methods, known as Multiscale Spectral Generalized Finite Element Methods (MS-GFEMs). This class of methods goes back to [BL11] and has been further developed in [BHL14; Bab+20; MSD22; MS22; SS22; MAS23]. In the spirit of generalized finite element methods [MB96; BM97], the domain is divided into a collection of overlapping subdomains using a partition of unity (PU). The idea of the MS-GFEM is then to decompose the solution to be approximated locally (on each subdomain) into a local particular function solving a local version of the considered PDE and an operator-harmonic part. Optimal approximation spaces for the approximation of the operator-harmonic part can be constructed by solving local spectral problems. This is done using the concept of Kolmogorov n-widths [Pin85] for a compact restriction operator defined on an oversampling domain. For strategies that allow the efficient practical computation of the optimal approximation spaces, we refer for example to [BS18]. By multiplication with a PU, the local approximation spaces are made conformal. The resulting set of local basis functions can then be used in a standard Galerkin approach. The MS-GFEM achieves a sub-exponential rate of convergence in the number of local basis functions per subdomain. More precisely, to achieve an accuracy of $\mathcal{O}(H)$, one needs $\mathcal{O}((\log \frac{1}{H})^{d+1})$ local basis functions, where d denotes the spatial dimension. Note that for the MS-GFEM, convergence is established in the number of local basis functions and not in the diameter of the subdomains.

We also mention the Generalized Multiscale Finite Element Method (GMsFEM) introduced in [EGH13], which combines features of the MsFEM and the MS-GFEM. The idea of the GMsFEM is to select a few relevant basis functions from a typically large local snapshot space by solving local spectral problems. For further developments related to the GMsFEM, see for example [Cal+16; CEL18; CEL19].

Numerical homogenization for stabilization purposes

The numerical solution of problems such as convection-dominated flow problems or time-harmonic wave propagation problems is particularly challenging since the mesh size must satisfy very restrictive assumptions in order to obtain a re-

liable approximation. For convection-dominated flow problems, classical FEMs exhibit spurious oscillations unless the mesh size resolves the thin boundary layers of the solution, see [Mel02]. For time-harmonic wave propagation problems, accurate approximations with classical FEMs even require a mesh size much smaller than that one needed to resolve the oscillations of the solution. If such strong mesh size requirements are not met, the numerical approximation exhibits accumulating phase errors due to numerical dispersion, see [IB95]. Popular techniques for dealing with the above problems include *hp*-FEMs [Mel02; MS10; MS11; MPS13], the Streamline Upwind Petrov–Galerkin method [BH82; HMA86; Hug87] for convection-dominated flow problems and Trefftz methods [Moi11; HMP14; HMP16] for time-harmonic wave-propagation problems.

The relevance of numerical homogenization in this context was recognized for example in [Bre+97], where the equivalence of the local Green's function approach (the origin of the VMM) to the residual-free bubble stabilization of FEMs introduced in [BR94] was shown. At that time, residual-free bubbles were a popular tool for stabilizing the numerical solution of convection-dominated flow problems, see [FNS98; Bre+99]. A particularly powerful framework in this context is the VMM, which has given rise to a number of LOD-based stabilization approaches for convection-dominated flow problems [LPS18] and time-harmonic wave propagation problems [GP15; Pet16; BG22]. For the latter class of Helmholtz-type problems, the LOD achieves an accuracy of $\mathcal{O}(H)$, provided that a minimum resolution condition is satisfied and that the diameter of the supports of the basis functions is increased like $\mathcal{O}(H \log(\frac{\kappa}{H}))$, where κ denotes the wavenumber. Note that also the MS-GFEM can be used to stabilize the numerical solution of Helmholtz problems, see [MAS23]. For an accuracy of $\mathcal{O}(H)$, it requires that the number of local basis functions per subdomain is increased like $\mathcal{O}((\log \frac{\kappa}{H})^{d+1})$.

Numerical homogenization for parametric problems

Parameter dependence adds another layer of complexity to multi-scale problems. Classical model order reduction techniques such as the reduced basis (RB) method, which typically rely on direct numerical simulations, require the repeated computation of global snapshots. For multi-scale problems where even one global solve is considered challenging, the repeated solution of global problems is intractable. Approaches capable of dealing with parameter-dependent multi-scale problems perform a localization of the snapshot computation to subdomains. Such a localization is typically achieved by either domain decomposition techniques or numerical homogenization methods.

Approaches based on domain decomposition construct local reduced spaces on subdomains and couple these local reduced spaces across interfaces in either a conforming or non-conforming manner. A prominent example is the Reduced Basis Element Method, which was first introduced in [MR02] and further developed in [KOH11; APQ16; HKP12; IQR12]. It uses a non-overlapping domain

decomposition and glues the reduced spaces together using Lagrange multipliers in a Mortar-like fashion, cf. [BMP93]. Further related methods are the Localized Reduced Basis Multiscale method [Alb+12; OS15] and the Arbitrary Local Modifications method [Buh+17].

Approaches that use numerical homogenization to localize the snapshot computation employ RB techniques within a numerical homogenization method to accelerate the typically costly basis computation. For numerical homogenization methods such as the MsFEM, the HMM, and the LOD, this led to the development of the RB-MsFEM [HZZ15], the RB-HMM [AB12; AB13], and the RB-LOD [AH15; KR21], respectively. Clearly, the properties of the above methods depend strongly on the properties of the underlying numerical homogenization method. While the RB-MsFEM and the RB-HMM are restricted to settings with (spatial) periodicity and scale separation, the RB-LOD is able to handle more general settings. For a review of localized model reduction techniques for parameter-dependent PDEs, see [Buh+21].

1.3 Outline and contributions

The goal of this thesis is to present recent achievements in the field of LOD-based numerical homogenization. As a starting point, Chapter 2 introduces prototypical approximation spaces obtained by applying the solution operator of the considered PDE to classical FE spaces such as piecewise constants. We prove that the corresponding Galerkin method provides accurate approximations of optimal order without having to resolve the underlying coefficients. However, since in general global problems must be solved to compute the basis functions of the prototypical method, such approaches are not feasible without modification.

One approach to localize the basis computation and thereby obtain a practical method is the LOD, which is introduced in Chapter 3 in the general setting of inf–sup stable problems. We present a variant of the LOD that uses a novel construction based on a tailor-made quasi-interpolation operator. This allows approximations without numerical pollution, at the cost of slightly increasing the support of the basis functions. We present a rigorous analysis showing the exponential localization properties of the LOD.

The LOD is then extended to the multi-resolution setting in Chapter 4 using the Helmholtz problem as a model problem. Given an LOD approximation on a coarse mesh, the presented Multi-resolution Localized Orthogonal Decomposition (MRLOD) allows to add additional discretization levels to improve the accuracy of the approximation. All discretization levels are decoupled, resulting in a block-diagonal coarse system matrix. We present a rigorous wavenumber-explicit error analysis that shows optimal order convergence of the MRLOD without any pre-asymptotic effects under mild assumptions on the discretization. Special emphasis is placed on the fast solution of the block-diagonal coarse system matrix. We prove that all but the first small block can be solved with a

standard iterative solver within a fixed number of iterations.

A very recent localization approach is the Super-Localized Orthogonal Decomposition (SLOD), which is introduced in Chapter 5 for inf–sup stable problems. The idea of the SLOD is to identify (normalized) local FE source terms that yield responses under the local solution operator of the PDE with minimal conormal derivatives. These responses are then used as the problem-adapted basis functions of the method. The SLOD has significantly improved localization properties compared to the LOD, resulting in smaller patch problems and a sparser coarse system matrix. More precisely, numerical experiments show that the SLOD achieves an accuracy of $\mathcal{O}(H)$ if the diameter of the supports of the basis functions is increased like $\mathcal{O}(H(\log \frac{1}{H})^{(d-1)/d})$. We put special emphasis on the theoretical and practical study of the decay of the localization error. We also provide an error analysis of the SLOD in which the basis stability is quantified a posteriori. For Helmholtz problems, the SLOD improves the oversampling condition of the LOD needed for optimal order convergence to $\mathcal{O}(H(\log \frac{\kappa}{H})^{(d-1)/d})$.

For challenging problems, such as problems with high-contrast channeled coefficients, the SLOD may suffer from basis stability issues, which degrade its approximation quality. Therefore, in Chapter 6, we introduce the Super-Localized Generalized Finite Element Method (SL-GFEM) for an elliptic model problem. The SL-GFEM combines the SLOD with a PU approach to overcome these basis stability issues. The SL-GFEM computes local spectral problems in a space spanned by a few deterministic snapshots. Therefore, random sampling strategies as for the MS-GFEM can be avoided. From an application point of view, the SL-GFEM is conceptually simple and easy to implement. We prove a posteriori and a priori error estimates for the SL-GFEM showing that its approximation quality is at least as good as that of the SLOD and at the same time not worse than that of the LOD. Special emphasis is placed on the study of higher order versions of the SL-GFEM, which achieve higher order convergence rates using only the regularity of the source term.

Finally, Chapter 7 introduces the Reduced Basis Super-Localized Orthogonal Decomposition (RB-SLOD) for reaction–convection–diffusion problems with parameter-dependent multi-scale coefficients. The RB-SLOD is a local RB technique resulting from the integration of a RB approach into the SLOD framework. Given a parameter, the RB-SLOD quickly generates coarse-scale models of the considered problem that accurately capture the effective behavior of the problem. Note that the unique localization properties of the SLOD allow one to perform the RB snapshot computation on particularly small patches, which is crucial to the low offline and online complexity of the RB-SLOD. A major strength of the RB-SLOD is that it is affected only by parameters in the PDE operator and not by parametric, possibly non-affine, source terms. In contrast, classical RB approaches require the use of the empirical interpolation method [Bar+04], which increases the overall computational cost.

Parts of this thesis have already been published in scientific journals. The

work on the MRLOD has been published in *Multiscale Modeling & Simulation* [HP22a] and the original work on the SLOD has been published in *Mathematics of Computation* [HP22b]. Furthermore, an article on the SLOD for Helmholtz problems and the articles introducing the SL-GFEM and the RB-SLOD have been submitted to scientific journals and are available as preprints, see [FHP21; Fre+22a; BHP22]. The presentation of the results in this thesis follows in part the presentation in the respective journal or preprint articles. Note that some parts have been rephrased or expanded, and that the notation may differ for consistency. We emphasize that the research articles [HM22; DHM22], written by the author of this thesis, are not directly included in the thesis. The latter has been accepted for publication in *SIAM Journal on Numerical Analysis*.

The numerical experiments presented in this thesis were performed either in `Matlab`, based on code developed at the Chair for Computational Mathematics at the University of Augsburg, or in `Python`, using an adaptation of the `gridlod` software from [HK17].

Notation. Throughout this work, we denote by $C > 0$ a constant, which is independent of discretization parameters such as the mesh size and the oversampling parameter, but which may depend on the spatial dimension d and the domain D. We emphasize that C may change from estimate to estimate. In order to simplify the notation, we abbreviate $a \leq Cb$ and $a \geq Cb$ by $a \lesssim b$ and $a \gtrsim b$, respectively. Further, provided that $a \lesssim b$ and $a \gtrsim b$, we write $a \approx b$.

2 Problem-adapted approximation

As mentioned in the introduction, classical FEMs based on universal polynomial approximation spaces can perform arbitrarily poorly for multi-scale PDEs. In fact, to obtain a reliable approximation, it is a minimal requirement for FEMs that the underlying mesh resolves the coefficients of the considered PDE. Additionally, the convergence of FEMs can be arbitrarily slow due to the possibly low regularity of the solution. In order to obtain reliable approximations on meshes that do not necessarily resolve the coefficients, problem-specific information can be added to the approximation space. This idea was first proposed for one-dimensional problems in [BO83].

In this chapter, we construct such problem-adapted approximation spaces by applying the solution operator of the PDE to coarse classical FE spaces. This is a common strategy used explicitly or implicitly in many works, see for example [OZ11; GGS12; MP14; OZB14; Owh17]. We further prove that the Galerkin method based on such problem-adapted spaces gives optimal convergence orders on arbitrarily coarse meshes without any pre-asymptotic effects. This is done in the general setting of inf–sup stable problems, which includes all PDEs considered in the remainder of this thesis (e.g., the Helmholtz problem in Chapters 4 and 5 and the reaction–convection–diffusion problem in Chapter 7).

However, this construction cannot be used in practice without modification, since it generally requires the solution to global problems for the computation of the basis functions. To derive a practical numerical homogenization method, one needs to localize the basis computation. Several localization techniques are presented in the following chapters (see Chapters 3 to 6).

2.1 Abstract model problem

We consider a linear second order PDE in weak form with possibly highly heterogeneous coefficients. It is posed on a bounded Lipschitz domain $D \subset \mathbb{R}^d$ ($d = 1, 2, 3$), which is either an interval ($d = 1$), a polygonal domain ($d = 2$), or a polyhedral domain ($d = 3$). Without loss of generality, we assume that D is scaled such that its diameter is of order one. We define the space $L^2(D)$ as the space of possibly complex-valued square integrable functions on D and denote by $(\cdot\,,\cdot)_{L^2}$ and $\|\cdot\|_{L^2}$ the L^2-inner product and the L^2-norm, respectively. Given a subdomain $S \subset D$, we write $\|\cdot\|_{L^2(S)}$ and $(\cdot\,,\cdot)_{L^2(S)}$ for their restriction to S. Furthermore, we denote by $H^k(D)$, $k \in \mathbb{N}_0$, the Sobolev space consisting of functions in $L^2(D)$, which have square integrable weak derivatives of order

up to k. We denote by $\|\cdot\|_{H^k}$ and $|\cdot|_{H^k}$ the H^k-norm and the H^k-seminorm on D, respectively. Note that for $k = 0$, it holds that $H^0(D) = L^2(D)$ and that $\|\cdot\|_{H^0} = |\cdot|_{H^0} = \|\cdot\|_{L^2}$. For a precise introduction to Lebesgue and Sobolev spaces, see for example [Alt16, Ch. 3].

The solution space of the considered second order PDE is a closed subspace $\mathcal{V} \subset H^1(D)$, which takes into account a possible Dirichlet boundary condition on a relatively closed boundary segment of ∂D of positive surface measure. As subspace of $H^1(D)$, one can equip $\mathcal{V}$ with the inner product

$$(\cdot\,,\cdot)_{\mathcal{V}} \coloneqq (\cdot\,,\cdot)_{L^2} + (\nabla\cdot\,,\nabla\cdot)_{L^2}, \tag{2.1}$$

where ∇ is the weak gradient, and denote its induced norm by $\|\cdot\|_{\mathcal{V}}$. The restriction of $\mathcal{V}$ to the subdomain $S \subset D$ is denoted by $\mathcal{V}(S) \coloneqq \mathcal{V}|_S$. This space can be equipped with the inner product $(\cdot\,,\cdot)_{\mathcal{V}(S)}$, which is the restriction of (2.1) to S and its induced norm $\|\cdot\|_{\mathcal{V}(S)}$. Furthermore, we denote by $\mathcal{V}^*$ the anti-dual space of $\mathcal{V}$ consisting of all continuous anti-linear functionals on $\mathcal{V}$ and write $\|\cdot\|_{\mathcal{V}^*}$ for the operator norm on $\mathcal{V}^*$.

The weak formulation of the considered PDE is based on a continuous sesquilinear form $a\colon \mathcal{V}\times\mathcal{V}\to\mathbb{C}$, which is typically a sum of integrals of its arguments, the derivatives of its arguments, and coefficient functions. For such sesquilinear forms, the continuity also holds in a local sense, i.e., there exists $C_a > 0$ such that

$$|a(v,w)| \le C_a \|v\|_{\mathcal{V}(S_1\cap S_2)} \|w\|_{\mathcal{V}(S_1\cap S_2)} \tag{2.2}$$

holds for all $v, w \in \mathcal{V}$ with $\operatorname{supp}(v) \subset S_1$, $\operatorname{supp}(w) \subset S_2$. This is an important ingredient for the localization proof of the LOD in Chapter 3 and will therefore be assumed in the following. Given a source term $F \in \mathcal{V}^*$, the weak formulation seeks a solution $u \in \mathcal{V}$ such that it holds

$$a(u,v) = F(v) \tag{2.3}$$

for all $v \in \mathcal{V}$.

The unique existence of a solution $u \in \mathcal{V}$ can be guaranteed by the Banach–Nečas–Babuška theorem [Bab71]. It requires the inf–sup conditions

$$\inf_{v\in\mathcal{V}} \sup_{w\in\mathcal{V}} \frac{|a(v,w)|}{\|v\|_{\mathcal{V}}\|w\|_{\mathcal{V}}} = \inf_{w\in\mathcal{V}} \sup_{v\in\mathcal{V}} \frac{|a(v,w)|}{\|v\|_{\mathcal{V}}\|w\|_{\mathcal{V}}} \ge \alpha_{\mathrm{c}}, \tag{2.4}$$

where the inf–sup constant $\alpha_{\mathrm{c}} > 0$ typically depends on the type of the problem at hand, the bounds of the coefficients, and the geometry of the domain. Note that the values of the inf–sup constants in (2.4) are the same as long as they do not vanish, cf. [Dem06]. The inf–sup stability (2.4) implies the stability of the problem (2.3), i.e.,

$$\|u\|_{\mathcal{V}} \le \alpha_{\mathrm{c}}^{-1} \|F\|_{\mathcal{V}^*}. \tag{2.5}$$

2.2 Classical finite element method

This section introduces the FEM, which is one of the most common and widely used discretization techniques for PDEs. Furthermore, we demonstrate the failure of the FEM to provide accurate approximations in the context of highly oscillatory coefficients, which motivates numerical homogenization techniques.

The construction of the FEM is based on a sequence of meshes $\{\mathcal{T}_H\}_{H>0}$, where each mesh is a finite subdivision of $\overline{D}$ (the closure of D) into closed convex elements K, and H is a mesh size parameter to be defined subsequently. For simplicity, we restrict ourselves to Cartesian meshes, which implicitly restricts the possible geometries of the considered domain D. We assume that all meshes are geometrically conformal in the sense of [EG04, Def. 1.55], which means that each face of an element is either a subset of the boundary ∂D or it coincides with the face of another element. Let us further assume that all elements are shape regular [EG04, Def. 1.107], i.e., there exists $C_{\mathrm{rg}} > 0$ such that

$$\max_{K\in\mathcal{T}_H} \frac{H_K}{\rho_K} \leq C_{\mathrm{rg}}$$

holds for all meshes in the sequence, where $H_K \coloneqq \operatorname{diam}(K)$ (the diameter of the smallest ball that contains K) and ρ_K denotes the diameter of the largest ball that is contained in K. Moreover, we assume that the sequence of meshes is quasi-uniform [EG04, Def. 1.140], i.e., there exists $C_{\mathrm{qu}} > 0$ such that

$$H \coloneqq \max_{K\in\mathcal{T}_H} H_K \leq C_{\mathrm{qu}} \min_{K\in\mathcal{T}_H} H_K$$

holds for all considered meshes. The set of all (interior and boundary) nodes of the mesh $\mathcal{T}_H$ is denoted by $\mathcal{N}_H$.

In this thesis, we will frequently use the $\mathcal{Q}^1$-FEM, which is a particular FEM based on the following approximation space:

$$V_H^{\mathrm{fem}} \coloneqq \big\{v \in \mathcal{V} : \ v|_K \text{ is a polynomial of coordinate degree } \leq 1, \ K \in \mathcal{T}_H\big\}.$$

It seeks an approximation $u_H^{\mathrm{fem}} \in V_H^{\mathrm{fem}}$ such that it holds

$$a(u_H^{\mathrm{fem}}, v) = F(v) \tag{2.6}$$

for all $v \in V_H^{\mathrm{fem}}$. The unique existence of a solution $u_H \in V_H^{\mathrm{fem}}$ is guaranteed by an inf–sup condition similar to (2.4) with the difference that, in the finite-dimensional setting, it is sufficient to require only one of the two inf–sup conditions in (2.4), cf. [EG04, Prop. 2.21]. More precisely, we assume that there exists $\alpha_{\mathrm{fem}} > 0$ such that

$$\inf_{v\in V_H^{\mathrm{fem}}} \sup_{w\in V_H^{\mathrm{fem}}} \frac{|a(v,w)|}{\|v\|_{\mathcal{V}}\|w\|_{\mathcal{V}}} \geq \alpha_{\mathrm{fem}}. \tag{2.7}$$

Note that in the remainder of this thesis we will just write FEM for the $\mathcal{Q}^1$-FEM.

To derive an error estimate of the FEM, one typically uses Céa's lemma (see, e.g., [EG04, Lem. 2.28]), which states the quasi-optimality of the FE approximation. This means that one can estimate the approximation error of the FEM against the approximation error for any $v_H \in V_H^{\mathrm{fem}}$, i.e.,

$$\|u - u_H^{\mathrm{fem}}\|_{\mathcal{V}} \leq \left(1 + \frac{C_a}{\alpha_{\mathrm{fem}}}\right) \min_{v_H \in V_H^{\mathrm{fem}}} \|u - v_H\|_{\mathcal{V}}. \tag{2.8}$$

The latter term can be estimated by choosing v_H as quasi-interpolation of the solution u, see, e.g., [EG04, Thm. 3.16 & Rem. 3.17]. To quantify the convergence of the FEM with respect to the mesh size H, we need additional regularity of the solution u. For non-negative s, we denote by $H^s(D)$ the Sobolev–Slobodeckij spaces [Rou13, Ch. 1.2.3], which are generalizations of the usual Sobolev spaces to non-integer s. We denote by $|\cdot|_{H^s}$ the Sobolev–Slobodeckij-seminorm on D. Provided that $u \in H^{1+r}(D)$ for some $r \in [0,1]$, the quasi-interpolation operator from [EG17, Thm. 6.4] can be used to show that

$$\|u - u_H^{\mathrm{fem}}\|_{\mathcal{V}} \lesssim \left(1 + \frac{C_a}{\alpha_{\mathrm{fem}}}\right) H^r |u|_{H^{1+r}}. \tag{2.9}$$

In particular, this estimate shows optimal first order convergence provided that $u \in H^2(D)$. However, the estimate also indicates, that the approximation quality of the FEM may be poor for large seminorms or low regularity of u.

To demonstrate the failure of the FEM, we use the example in [MP20, Ch. 2], where for a highly oscillatory coefficient A_ε, the one-dimensional diffusion problem $-(A_\varepsilon u_\varepsilon')' = f$ on the interval $D = (0,1)$ with homogeneous Dirichlet boundary conditions is considered. The coefficient A_ε is smooth but highly oscillatory, where $0 < \varepsilon \ll 1$ denotes the length scale of the oscillations. It is defined by

$$A_\varepsilon(x) = \frac{1}{2 + \cos\left(\frac{2\pi x}{\varepsilon}\right)}. \tag{2.10}$$

The weak formulation of the problem seeks $u_\varepsilon \in \mathcal{V} \coloneqq H_0^1(D)$ such that

$$a_\varepsilon(u_\varepsilon, v) \coloneqq \int_0^1 A_\varepsilon u_\varepsilon' v' \,\mathrm{d}x = \int_0^1 f v \,\mathrm{d}x =: F(v) \tag{2.11}$$

holds for all $v \in \mathcal{V}$. Using that $\frac{1}{3} \leq A_\varepsilon(x) \leq 1$ for all $x \in D$, we obtain that a is continuous and that $a(v,v) \gtrsim \|v\|_{\mathcal{V}}^2$ holds for all $v \in \mathcal{V}$ with constants independent of ε. The latter condition is known as coercivity (see also Section 6.1) and ensures that the inf–sup conditions (2.4) and (2.7) hold independently of ε. For the particular choice of the source term $f \equiv 1$, the solution u_ε can be calculated explicitly, cf. [MP20, Ch. 2]. Using the explicit form of the solution, one easily verifies that $u_\varepsilon \in H^2(D)$ with $|u_\varepsilon|_{H^2} \approx \varepsilon^{-1}$. Inserting this into estimate (2.9), we obtain that the FEM yields reliable and first order convergent approximations

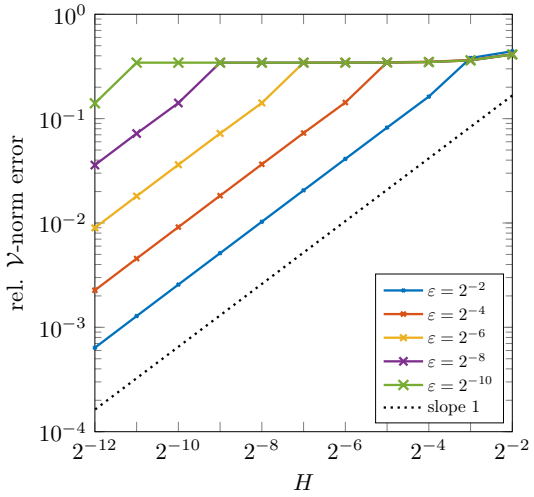

Figure 2.1: Error of the FE approximation of (2.11) with $f \equiv 1$ as a function of H for several values of ε.

provided that the resolution condition $H \lesssim \varepsilon$ is satisfied. In the pre-asymptotic regime, where the oscillations of the coefficient are not resolved by the mesh, i.e., $H \gtrsim \varepsilon$, the error is generally large. This can also be observed in Figure 2.1.

We emphasize that it is a general observation that FEMs based on universal polynomial approximation spaces give unsatisfactory approximations if the coefficients are not resolved by the mesh, cf. [PS12]. In such cases, neither the macroscopic behavior of the solution nor its microscopic features are well approximated. Note that the previous one-dimensional example had a large seminorm of the solution. In practice, also the regularity of the solution is typically low, i.e., r is close to zero. This creates additional difficulties for the FEM as seen in the estimate (2.9). In fact, it is shown in [BO00] that classical FEMs can perform arbitrarily poorly for PDEs with rough coefficients.

2.3 Prototypical problem-adapted approximation

To obtain reliable approximations even when the coefficients are not resolved or the regularity of the solution is low, problem-specific information can be incorporated into the approximation space. In this section, we introduce such problem-adapted approximation spaces and prove that the respective Galerkin method achieves optimal convergence orders under minimal structural assumptions. The construction we use is inspired by that in [OS19; AHP21]. It is based on a set of pairwise linearly independent anti-linear functionals

$$\{q_j : j \in J\} \subset \mathcal{V}^*, \tag{2.12}$$

where J is a suitable index set. These functionals, typically called quantities of interest (QOIs), select the information to be extracted from the solution u. To obtain an accurate approximation of the solution on the mesh $\mathcal{T}_H$, one typically uses QOIs defined with respect to $\mathcal{T}_H$. Note that there is much flexibility in choosing the QOIs, see for example [AHP21, Ex. 3.1]. Throughout this thesis, we will only use the (complex conjugate) element averages with respect to $\mathcal{T}_H$ as QOIs, which are for all $K \in \mathcal{T}_H$ defined as

$$q_K(v) \coloneqq \frac{1}{|K|} \int_K \overline{v} \, \mathrm{d}x \tag{2.13}$$

for all $v \in \mathcal{V}$, where $|K|$ denotes the volume of K and $\overline{\cdot}$ denotes the complex conjugation. Note that the complex conjugation ensures that the q_K are anti-linear, i.e., it holds that $q_K \in \mathcal{V}^*$, cf. (2.12).

For the definition of the problem-adapted approximation spaces, we define the solution operator and its adjoint version by $\mathcal{L}\colon \mathcal{V}^* \to \mathcal{V}$, $F \mapsto u$ and $\mathcal{L}^*\colon \mathcal{V}^* \to \mathcal{V}$, $F \mapsto w$, respectively, where u and w are for all $v \in \mathcal{V}$ defined as

$$a(u, v) = F(v), \qquad \overline{a(v, w)} = F(v). \tag{2.14}$$

The well-posedness of the operators $\mathcal{L}$ and $\mathcal{L}^*$ is an immediate consequence of the inf–sup stability (2.4). The problem-adapted trial and test spaces are then defined as follows:

$$U_H^{\mathrm{a}} \coloneqq \operatorname{span}\{\mathcal{L} q_K : K \in \mathcal{T}_H\}, \qquad V_H^{\mathrm{a}} \coloneqq \operatorname{span}\{\mathcal{L}^* q_K : K \in \mathcal{T}_H\}. \tag{2.15}$$

Note that for hermitian problems the operators $\mathcal{L}$ and $\mathcal{L}^*$ coincide, and therefore also U_H^{a} and V_H^{a} coincide. We emphasize that such problem-adapted spaces are not feasible in practice without modification. This is due to the typically slow (algebraic) decay of the Green's function corresponding to the problem (2.3), which implies that also the canonical basis functions $\{\mathcal{L} q_K : K \in \mathcal{T}_H\}$ and $\{\mathcal{L}^* q_j : K \in \mathcal{T}_H\}$ of U_H^{a} and V_H^{a} decay slowly, cf. [Eva10, Ch. 2]. Therefore, global problems need to be solved to compute the canonical basis functions, which is considered intractable in practice. Figure 2.2 illustrates the canonical basis functions in one dimension.

The prototypical problem-adapted approximation seeks $u_H^{\mathrm{a}} \in U_H^{\mathrm{a}}$ such that

$$a(u_H^{\mathrm{a}}, v) = F(v) \tag{2.16}$$

holds for all $v \in V_H^{\mathrm{a}}$. To ensure the existence of a unique solution $u_H^{\mathrm{a}} \in U_H^{\mathrm{a}}$, we do not require the inf–sup stability of a on $U_H^{\mathrm{a}} \times V_H^{\mathrm{a}}$, since in many applications, such as Helmholtz problems, this condition may be difficult to prove. Instead, we require an inf–sup condition of a on the subspace $\mathcal{W} \subset \mathcal{V}$ defined by

$$\mathcal{W} \coloneqq \bigcap_{K \in \mathcal{T}_H} \ker q_K, \tag{2.17}$$

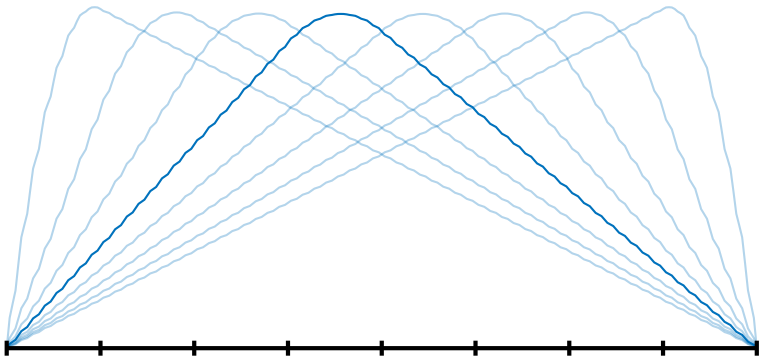

Figure 2.2: Canonical prototypical basis functions for problem (2.11) with $\varepsilon = 2^{-6}$.

where ker denotes the kernel of a linear operator. The space $\mathcal{W}$ is a closed subspace of $\mathcal{V}$, since it is an intersection of kernels of continuous functionals. It can be interpreted as the space of functions that are not resolved by the prototypical method (2.16). Therefore, the space $\mathcal{W}$ is typically referred to as the fine-scale space. Note that the space $\mathcal{W}$ will play an essential role in the construction of the LOD in Chapters 3 and 4. We assume that a is inf–sup stable on $\mathcal{W} \times \mathcal{W}$, i.e., there exists $\alpha_{\mathrm{f}} > 0$ such that

$$\inf_{v \in \mathcal{W}} \sup_{w \in \mathcal{W}} \frac{|a(v,w)|}{\|v\|_{\mathcal{V}} \|w\|_{\mathcal{V}}} = \inf_{w \in \mathcal{W}} \sup_{v \in \mathcal{W}} \frac{|a(v,w)|}{\|v\|_{\mathcal{V}} \|w\|_{\mathcal{V}}} \geq \alpha_{\mathrm{f}}. \tag{2.18}$$

The following lemma shows that this condition ensures the inf–sup stability of a on $U_H^{\mathrm{a}} \times V_H^{\mathrm{a}}$ and hence the well-posedness of (2.16).

Lemma 2.3.1 (Inf–sup stability of the problem-adapted approximation)**.** *If the inf–sup conditions* (2.4) *and* (2.18) *are satisfied, it holds that the sesquilinear form a is inf–sup stable on $U_H^{\mathrm{a}} \times V_H^{\mathrm{a}}$, i.e.,*

$$\inf_{v \in U_H^{\mathrm{a}}} \sup_{w \in V_H^{\mathrm{a}}} \frac{|a(v,w)|}{\|v\|_{\mathcal{V}} \|w\|_{\mathcal{V}}} \geq \alpha_{\mathrm{a}} \tag{2.19}$$

with $\alpha_{\mathrm{a}} \coloneqq C_a^{-1} \alpha_{\mathrm{c}} \alpha_{\mathrm{f}} > 0$.

Proof. The proof of this lemma can be obtained by combining results from [AHP21, Sec. 3.2 & 3.3]. □

The special choice of the problem-adapted approximation spaces ensures that the prototypical approximation exactly satisfies the QOIs. This is shown in the following lemma.

Lemma 2.3.2 (Exactness of QOIs)**.** *The prototypical approximation u_H^{a} defined in* (2.16) *has the same QOIs as the solution u of* (2.3)*, i.e., it holds that*

$$q_K(u) = q_K(u_H^{\mathrm{a}}) \tag{2.20}$$

for all $K \in \mathcal{T}_H$.

Proof. For all $K \in \mathcal{T}_H$, we obtain using the Galerkin orthogonality and the definition of the adjoint solution operator $\mathcal{L}^*$ in (2.14) that

$$0 = \overline{a(u - u_H^{\mathrm{a}}, \mathcal{L}^* q_K)} = q_K(u - u_H^{\mathrm{a}}). \qquad \square$$

Next, we prove the optimal order convergence of the prototypical approximation (2.16) under minimal structural assumptions. For this, we note that the choice of the problem-adapted approximation spaces in (2.15) allows to transform the approximation problem of the solution u in the space $\mathcal{V}$ into an approximation problem of the source term F in the space $\mathcal{V}^*$. In the latter approximation problem, the source F is approximated by a linear combination of the QOIs defined in (2.13). In order to quantify the convergence of the prototypical method, we need to assume additional regularity of the source term, e.g., L^2-regularity, which means that there exists a function $f \in L^2(D)$ such that

$$F = (f\,,\,\cdot)_{L^2}. \tag{2.21}$$

To define an approximation of f, we introduce the space of $\mathcal{T}_H$-piecewise constants as

$$\mathcal{P}^0(\mathcal{T}_H) \coloneqq \operatorname{span}\{\mathbf{1}_K : \; K \in \mathcal{T}_H\} \tag{2.22}$$

with $\mathbf{1}_K$ denoting the characteristic function of the element K. The corresponding L^2-orthogonal projection $\Pi_H^0 \colon L^2(D) \to \mathcal{P}^0(\mathcal{T}_H)$ can then be expressed explicitly in terms of the QOIs as

$$\Pi_H^0 v = \sum_{K \in \mathcal{T}_H} q_K(\overline{v}) \mathbf{1}_K. \tag{2.23}$$

From its definition, it immediately follows that Π_H^0 is locally stable with respect to the L^2-norm, i.e., for all $K \in \mathcal{T}_H$, it holds that

$$\|\Pi_H^0 v\|_{L^2(K)} \leq \|v\|_{L^2(K)} \tag{2.24}$$

for all $v \in L^2(D)$. Furthermore, recalling the assumption that all elements K are convex, we obtain by Poincaré's inequality [PW60; Beb03] that

$$\|v - \Pi_H^0 v\|_{L^2(K)} \leq \pi^{-1} H \|\nabla v\|_{L^2(K)} \tag{2.25}$$

holds for all $K \in \mathcal{T}_H$ and $v \in H^1(T)$.

Using the above results, we are able to prove the desired optimal order convergence result for the prototypical approximation. This result requires only the regularity of the source term and, in contrast to the FEM, no additional regularity assumptions on the solution are necessary.

Lemma 2.3.3 (Convergence of the prototypical approximation)**.** *For any $f \in H^k(D)$, $k \in \{0,1\}$, the prototypical approximation* (2.16) *satisfies that*

$$\|u - u_H^{\mathrm{a}}\|_{\mathcal{V}} \leq \alpha_{\mathrm{f}}^{-1} \pi^{-1-k} H^{1+k} |f|_{H^k}.$$

Proof. By Lemma 2.3.2, we obtain that $u - u_H^{\mathrm{a}} \in \mathcal{W}$. Thus, using the inf–sup stability (2.18), there exists $w \in \mathcal{W}$ with $\|w\|_{\mathcal{V}} = 1$ such that

$$\alpha_{\mathrm{f}} \|u - u_H^{\mathrm{a}}\|_{\mathcal{V}} \leq |a(u - u_H^{\mathrm{a}}, w)| = |(f\,,\, w - \Pi_H^0 w)_{L^2}| \leq \pi^{-1} H \|f\|_{L^2}.$$

Here, we used that $a(u_H^{\mathrm{a}}, w) = 0$, $\Pi_H^0 w = 0$, and (2.25) for w. In the case $k = 1$, we additionally use that

$$(f\,,\, w - \Pi_H^0 w)_{L^2} = (f - \Pi_H^0 f\,,\, w - \Pi_H^0 w)_{L^2},$$

which holds due to the definition of Π_H^0. Applying (2.25) again then gives the result. □

Note that using interpolation techniques, one can extend this result to source terms $f \in H^s(D)$, $s \in [0,1]$, i.e., one can show convergence of order $1+s$ for the prototypical approximation. The corresponding estimate is similar to the one in Lemma 2.3.3, but it includes an additional constant resulting from the interpolation. We emphasize that choosing the QOIs as in [AHP21, Ex. 3.1b] yields prototypical approximations with higher orders of convergence, see [Mai21; DHM22].

2.4 Overview of localization strategies

To obtain a practically feasible numerical method, one needs to localize the computation of the basis functions of the prototypical trial and test spaces U_H^{a} and V_H^{a}. In this section, we introduce the general concept of localization and give an overview of the localization strategies presented in this thesis.

Concept of localization

When performing a localization, one usually first identifies rapidly decaying basis functions of U_H^{a} and V_H^{a}, where we assign each basis function to a mesh entity (elements in our case). Despite their fast decay, these basis functions are usually globally supported. However, the fast decay allows one to construct accurate local approximations of the basis functions by localizing their computation to patches. For this, one typically chooses patches of $m \in \mathbb{N}$ layers of coarse elements around the respective elements. The error resulting from this approximation, the so-called localization error, is determined by the choice of the basis functions of the trial and test spaces and the oversampling parameter m. We define the localized trial and test spaces as the span of the respective localized basis functions. Finally, a practical method can be defined as the Galerkin approximation with respect to these localized trial and test spaces.

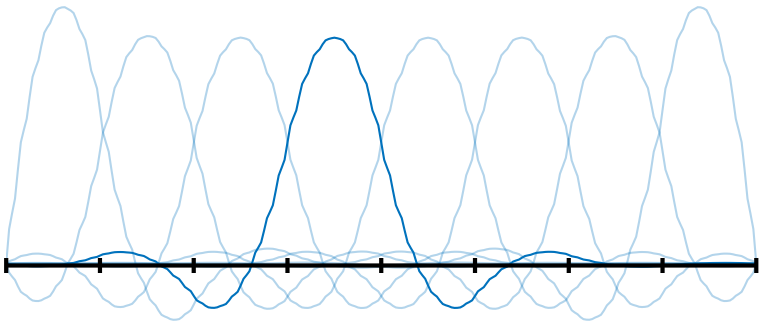

Figure 2.3: Prototypical basis functions of the LOD for problem (2.11) with $\varepsilon = 2^{-6}$.

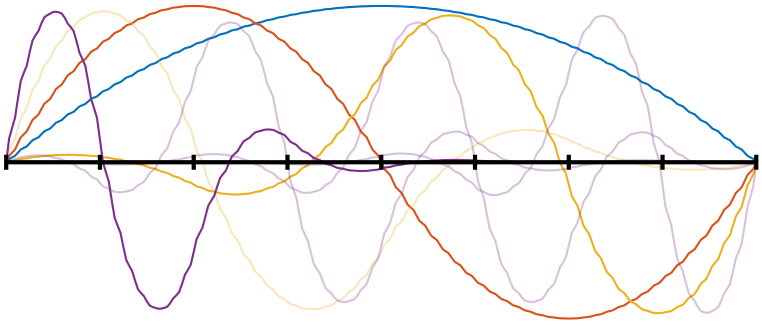

Figure 2.4: Prototypical MRLOD basis functions for problem (2.11) with $\varepsilon = 2^{-6}$. The colors indicate the different discrete scales the basis functions are associated to.

Ideas of the presented localization approaches

Four different localization strategies are considered in this thesis, namely the LOD, the MRLOD, the SLOD, and the SL-GFEM. Their ideas have already been briefly sketched in Chapter 1. In the following, we recall the main ideas and illustrate their choice of basis functions in one dimension.

The LOD is a popular localization technique, which constructs its trial and test spaces based on problem-adapted decompositions of the solution space into a coarse approximation space and an infinite-dimensional remainder space. By adding fine-scale corrections to classical FE shape functions, the LOD constructs exponentially decaying prototypical basis functions of the coarse approximation space. These functions are shown in Figure 2.3 in one dimension. The prototypical basis functions are then localized to patches in order to obtain a practical method. The LOD is discussed in detail in Chapter 3.

In the spirit of gamblets [Owh17], the LOD is extended to the multi-resolution setting in Chapter 4. For this, we employ a discrete hierarchy of scales induced by a Haar basis. The resulting MRLOD has the desirable property that its

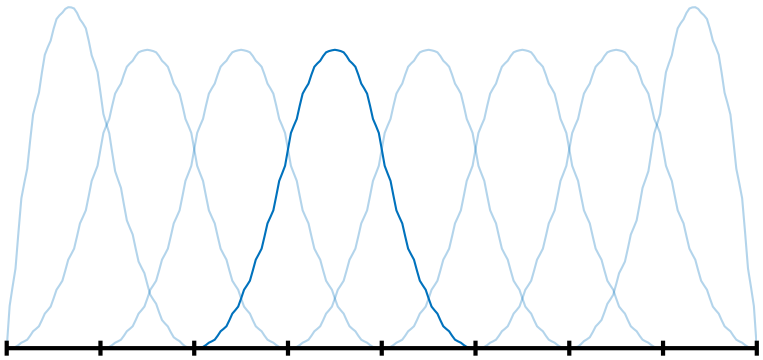

Figure 2.5: SLOD basis functions for problem (2.11) with $\varepsilon = 2^{-6}$.

discrete scales are decoupled. More precisely, the resulting linear system is block-diagonal with blocks that are easily invertible. For an illustration of the prototypical basis functions of the MRLOD, see Figure 2.4. To obtain a practical method, the prototypical basis functions are localized using LOD techniques at each discretization level.

Another localization approach is the SLOD introduced in Chapter 5. For all patches of elements in the coarse mesh, the SLOD solves a local minimization problem. More precisely, it minimizes the conormal derivative among the responses to local piecewise constant functions under the local solution operator. The resulting local responses are then used as the basis function of the SLOD. Compared to the exponential decay of the localization error for the LOD, we observe a super-exponential decay for the SLOD. In one dimension, super-exponential means that the basis is truly local, i.e., the localization error is zero. Figure 2.5 shows the local SLOD basis functions in one dimension. Note that the stability of the basis of the SLOD can only be guaranteed a posteriori. To overcome this, the SLOD is combined with a partition of unity in Chapter 6, resulting in the SL-GFEM.

3 Localized Orthogonal Decomposition

This chapter gives a brief introduction to the Localized Orthogonal Decomposition (LOD), which was originally introduced in [MP14; HP13] for an elliptic model problem. Given a coarse mesh, the idea of the LOD is to decompose the solution space of the considered problem into an infinite-dimensional fine-scale space consisting of functions not resolved by the coarse mesh and a finite-dimensional complement space. If this decomposition is chosen in a problem-adapted way, the finite-dimensional complement space contains fine-scale information of the problem at hand and allows an accurate approximation of the solution to the problem. To obtain a practical method, the LOD approximates the complement space by a localized version, whose basis functions can be computed by solving sub-scale correction problems on patches of the coarse mesh. The LOD approximation is then obtained by performing a Galerkin approach using the localized complement space as approximation space. We note that for non-hermitian problems, the LOD uses two different decompositions of the solution space, resulting in different trial and test spaces. While the classical FEM yields reliable approximations only if the mesh resolves all fine-scale features of the considered problem (see for example Figure 2.1), the LOD yields reliable approximations for arbitrarily coarse meshes. More precisely, provided that the diameter of the patches for the local sub-scale correction problems is increased logarithmically with the desired accuracy, the LOD is able to achieve optimal orders of convergence independent of the smoothness of the coefficients.

In the following, we use the LOD to localize the problem-adapted approximation spaces introduced in Chapter 2 and to obtain a practically feasible variant of the prototypical method defined in (2.16). For this, we again consider the general setting of inf–sup stable problems, which includes all PDEs considered in the remainder of this thesis. We emphasize that the presentation of this chapter is inspired by [Mai20; AHP21]. In contrast to these works, however, we include a tailor-made quasi-interpolation operator in the definition of the method, which cures numerical pollution effects as observed for example in [Mai21]. This approach goes back to [HP22a]. Note that most of the proofs presented are based on rather standard LOD theory and are adaptations of for example those in [MP20; AHP21] to the present setting.

3.1 Correctors

The LOD uses correctors to incorporate fine-scale information of the considered problem into its coarse approximation space. Recalling the definition of the fine-scale space $\mathcal{W}$ in (2.17), we define the correctors $\mathcal{C}, \mathcal{C}^*\colon \mathcal{V} \to \mathcal{W}$ such that

$$a(\mathcal{C}v, w) = a(v, w), \qquad a(w, \mathcal{C}^* v) = a(w, v) \tag{3.1}$$

holds for all $v \in \mathcal{V}$ and $w \in \mathcal{W}$. Due to the inf–sup stability of a on $\mathcal{W} \times \mathcal{W}$, cf. (2.18), the correctors $\mathcal{C}$ and $\mathcal{C}^*$ are well-defined and continuous, i.e., it holds for all $v \in \mathcal{V}$ that

$$\|\mathcal{C}v\|_{\mathcal{V}} \leq \alpha_{\mathrm{f}}^{-1} C_a \|v\|_{\mathcal{V}}, \qquad \|\mathcal{C}^* v\|_{\mathcal{V}} \leq \alpha_{\mathrm{f}}^{-1} C_a \|v\|_{\mathcal{V}}. \tag{3.2}$$

The following lemma characterizes the images and kernels of $\mathcal{C}$ and $\mathcal{C}^*$. We denote by im and ker the image and kernel of a linear operator, respectively.

Lemma 3.1.1 (Properties of $\mathcal{C}$ and $\mathcal{C}^*$)**.** *The operators $\mathcal{C}$ and $\mathcal{C}^*$ are projection operators with*

$$\mathrm{im}(\mathcal{C}) = \mathrm{im}(\mathcal{C}^*) = \mathcal{W}, \qquad \ker(\mathcal{C}) = U_H^{\mathrm{a}}, \qquad \ker(\mathcal{C}^*) = V_H^{\mathrm{a}}.$$

Furthermore, it holds for the complementary projection operators that

$$\mathrm{im}(\mathtt{id} - \mathcal{C}) = U_H^{\mathrm{a}}, \qquad \mathrm{im}(\mathtt{id} - \mathcal{C}^*) = V_H^{\mathrm{a}}, \qquad \ker(\mathtt{id} - \mathcal{C}) = \ker(\mathtt{id} - \mathcal{C}^*) = \mathcal{W},$$

where $\mathtt{id}$ *denotes the identity operator.*

Proof. Note that the codimension of $\mathcal{W} \subset \mathcal{V}$ (the dimension of any complement space of $\mathcal{W}$ in $\mathcal{V}$) is equal to the number of elements in $\mathcal{T}_H$. The proof of this result can be found in [AHP21, Thm. 3.5]. The identity $\mathrm{im}(\mathcal{C}) = \mathcal{W}$ holds by definition since $\mathcal{C}$ is a projection onto $\mathcal{W}$. To prove that $\ker(\mathcal{C}) = U_H^{\mathrm{a}}$, we first show the inclusion "$\supset$". Since any $v \in U_H^{\mathrm{a}}$ can be written as $v = \sum_{K \in \mathcal{T}_H} c_K \mathcal{L} q_K$ for some coefficients $(c_K)_{K \in \mathcal{T}_H}$, we obtain for all $w \in \mathcal{W}$ that

$$a(\mathcal{C}v, w) = a(v, w) = \sum_{K \in \mathcal{T}_H} c_K q_K(w) = 0,$$

where we used definitions (2.17) and (3.1). This directly implies that $v \in \ker(\mathcal{C})$ and thus, since $v \in U_H^{\mathrm{a}}$ was arbitrary, that $\ker(\mathcal{C}) \supset U_H^{\mathrm{a}}$. Since $\mathcal{C}$ is a projection, we have that $\mathcal{V} = \mathrm{im}(\mathcal{C}) \oplus \ker(\mathcal{C})$ (see, e.g., [Alt16, Thm. 9.13]). Using this and the fact that the codimension of $\mathcal{W}$ is equal to the number of elements in $\mathcal{T}_H$, it follows that $\ker(\mathcal{C}) = U_H^{\mathrm{a}}$. The result for the complementary projection $(\mathtt{id} - \mathcal{C})$ follows using standard identities for the kernel and image of projections, cf. [Alt16, Thm. 9.13]. The proof for $\mathcal{C}^*$ is analogous. □

The following corollary states problem-adapted decompositions of $\mathcal{V}$.

Corollary 3.1.2 (Decomposition of $\mathcal{V}$)**.** *The solution space can be decomposed as follows:*

$$\mathcal{V} = U_H^{\mathrm{a}} \oplus \mathcal{W} = V_H^{\mathrm{a}} \oplus \mathcal{W}. \tag{3.3}$$

These decompositions are "a-orthogonal" (recall that a is in general not an inner product) in the sense that

$$a(U_H^{\mathrm{a}}, \mathcal{W}) = 0, \qquad a(\mathcal{W}, V_H^{\mathrm{a}}) = 0. \tag{3.4}$$

Proof. The proof of this corollary uses exactly the same arguments as the proof of Lemma 3.1.1 and is therefore omitted. □

3.2 Coarse-scale bases

In this section, we construct basis functions of the problem-adapted trial and test spaces U_H^{a} and V_H^{a} by applying the operators $(\mathtt{id}-\mathcal{C})$ and $(\mathtt{id}-\mathcal{C}^*)$ to coarse $\mathcal{V}$-conforming functions. In Section 3.3 it is then proved that basis functions constructed in this way decay exponentially fast, which justifies their localization in Section 3.4.

As coarse $\mathcal{V}$-conforming functions we use non-negative bubble functions. The bubble function corresponding to the element $K \in \mathcal{T}_H$ is chosen such that it holds $b_K \in H_0^1(K)$ and $\Pi_H^0 b_K = \mathbf{1}_K$ as well as

$$\|b_K\|_{L^2(K)} \leq \pi^{-1} H \, \|\nabla b_K\|_{L^2(K)} \lesssim \|\mathbf{1}_K\|_{L^2(K)}, \tag{3.5}$$

where the hidden constant depends only on the shape regularity of $\mathcal{T}_H$. There are many reasonable choices of bubble functions. For example one can choose b_K as the appropriately scaled product of the FE hat functions associated with nodes contained in K. We define the operator $\mathcal{B}_H \colon L^2(D) \to \mathcal{V}$, which maps an L^2-function to its $\mathcal{V}$-conforming bubble companion with the same element averages by

$$\mathcal{B}_H(v) \coloneqq \sum_{K \in \mathcal{T}_H} q_K(\overline{v}) b_K, \tag{3.6}$$

where the q_K are the QOIs defined in (2.13). It is a direct consequence that the kernels of $\mathcal{B}_H$ and Π_H^0 coincide, i.e., $\ker \mathcal{B}_H = \ker \Pi_H^0$. Using estimate (3.5), one can prove the local stability of $\mathcal{B}_H$, i.e., there exists $C_{\mathcal{B}_H} > 0$ such that

$$\|\mathcal{B}_H v\|_{L^2(K)} + H \|\mathcal{B}_H v\|_{\mathcal{V}(K)} \leq C_{\mathcal{B}_H} \|v\|_{L^2(K)} \tag{3.7}$$

holds for all $K \in \mathcal{T}_H$ and $v \in L^2(D)$, where the constant $C_{\mathcal{B}_H}$ depends only on the shape regularity of $\mathcal{T}_H$. Note that in (3.7) we give a bound on the local $\mathcal{V}$-norm of $\mathcal{B}_H v$ (instead of the local H^1-seminorm), which will simplify the analysis in the following sections.

We define the space of bubble functions by

$$U_H \coloneqq \operatorname{span}\{b_K : K \in \mathcal{T}_H\}. \tag{3.8}$$

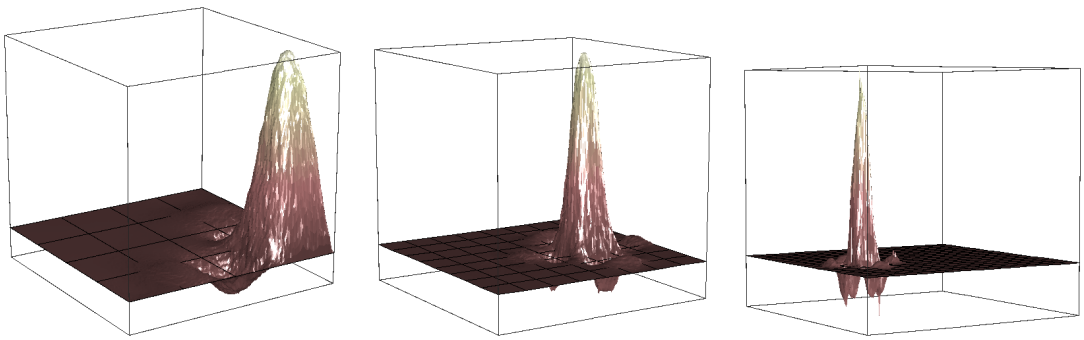

Figure 3.1: Prototypical LOD basis functions for several coarse meshes for the problem considered in Section 3.6.

The following lemma provides alternative characterizations of the problem-adapted trial and test spaces U_H^{a} and V_H^{a}.

Lemma 3.2.1 (Characterizations of U_H^{a} and V_H^{a})**.** *The spaces U_H^{a} and V_H^{a} can alternatively be characterized as*

$$U_H^{\mathrm{a}} = (\mathtt{id} - \mathcal{C})U_H, \qquad V_H^{\mathrm{a}} = (\mathtt{id} - \mathcal{C}^*)U_H. \tag{3.9}$$

In particular, it holds that

$$\big\{(\mathtt{id} - \mathcal{C})b_K : K \in \mathcal{T}_H\big\}, \qquad \big\{(\mathtt{id} - \mathcal{C}^*)b_K : K \in \mathcal{T}_H\big\} \tag{3.10}$$

are bases of the spaces U_H^{a} and V_H^{a}, respectively.

Proof. Using $(\mathtt{id} - \mathcal{B}_H)\mathcal{V} \subset \mathcal{W}$, which implies that $(\mathtt{id} - \mathcal{C})(\mathtt{id} - \mathcal{B}_H)\mathcal{V} = 0$, we obtain the first identity in (3.9) as follows:

$$U_H^{\mathrm{a}} = (\mathtt{id} - \mathcal{C})\mathcal{V} = (\mathtt{id} - \mathcal{C})(\mathtt{id} - \mathcal{B}_H)\mathcal{V} + (\mathtt{id} - \mathcal{C})\mathcal{B}_H\mathcal{V} = (\mathtt{id} - \mathcal{C})U_H.$$

The second identity in (3.9) can be proved analogously and (3.10) is an immediate consequence of (3.9). □

For a depiction of the basis functions (3.10), see Figure 3.1. These basis functions are typically called prototypical LOD basis functions due to their generally global support.

3.3 Decay and localization

In this section, we prove the exponential decay of the prototypical LOD basis functions, which justifies their localization in Section 3.4. To this end, we introduce patches with respect to the coarse mesh $\mathcal{T}_H$. We define the first order element patch $\mathsf{N}(S) = \mathsf{N}_1(S)$ of a union of elements $S \subset \overline{D}$ as follows:

$$\mathsf{N}_1(S) := \bigcup \{K \in \mathcal{T}_H : K \cap S \neq \emptyset\}.$$

For any $m \geq 2$, the m-th order patch $\mathsf{N}_m(S)$ of S is then recursively given as

$$\mathsf{N}_m(S) := \mathsf{N}_1(\mathsf{N}_{m-1}(S)). \tag{3.11}$$

3.3.1 Splitting into element correctors

To construct localized correctors, we use the concept of element correctors, cf. [HP13]. Note that the use of element correctors allows for improved stability properties of the resulting LOD method. To define the element correctors, we decompose the sesquilinear form a into the element sesquilinear forms

$$a_K \colon \mathcal{V} \times \mathcal{V} \to \mathbb{C} \tag{3.12}$$

for any $K \in \mathcal{T}_H$. Recalling that a is typically a sum of integrals of its arguments, the derivatives of its arguments, and coefficient functions, we can define the form a_K by appropriately restricting the integrals to the element K. It then holds that

$$a(v,w) = \sum_{K \in \mathcal{T}_H} a_K(v,w) \tag{3.13}$$

for all $v, w \in \mathcal{V}$. We require that for all $K \in \mathcal{T}_H$ the sesquilinear forms a_K are locally continuous in the sense that

$$|a_K(v,w)| \leq C_a \|v\|_{\mathcal{V}(K)} \|w\|_{\mathcal{V}(K)} \tag{3.14}$$

holds for all $v, w \in \mathcal{V}$. In practice, the constant C_a is usually the same as the constant in (2.2). Therefore, for simplicity, we will not introduce a new constant.

For any $K \in \mathcal{T}_H$, we define the element correctors $\mathcal{C}_K, \mathcal{C}_K^* \colon \mathcal{V} \to \mathcal{W}$ such that

$$a(\mathcal{C}_K v, w) = a_K(v,w), \qquad a(w, \mathcal{C}_K^* v) = a_K(w,v) \tag{3.15}$$

is satisfied for all $v \in \mathcal{V}$ and $w \in \mathcal{W}$. Note that the inf–sup stability of a on $\mathcal{W} \times \mathcal{W}$, cf. (2.18), and the local continuity (3.14) ensure the well-posedness of the operators $\mathcal{C}_K$ and $\mathcal{C}_K^*$. Furthermore, by (3.13) the sum of the element correctors $\mathcal{C}_K$ and $\mathcal{C}_K^*$ is equal to the correctors $\mathcal{C}$ and $\mathcal{C}^*$, respectively, i.e.,

$$\mathcal{C} = \sum_{K \in \mathcal{T}_H} \mathcal{C}_K, \qquad \mathcal{C}^* = \sum_{K \in \mathcal{T}_H} \mathcal{C}_K^*. \tag{3.16}$$

3.3.2 Exponential decay of element corrections

To prove the exponential decay of the element corrections, we require that the sesquilinear form a is inf–sup stable on local subspaces of $\mathcal{W}$, defined for any $K \in \mathcal{T}_H$ and $m \in \mathbb{N}$ as

$$\mathcal{W}_{K,m}^{\mathrm{c}} \coloneqq \{w \in \mathcal{W} : \ \operatorname{supp}(w) \subset \overline{D \backslash \mathsf{N}_m(K)}\}, \tag{3.17}$$

i.e., we assume that there exists $\alpha_{\mathrm{d}} > 0$ such that

$$\inf_{v \in \mathcal{W}_{K,m}^{\mathrm{c}}} \sup_{w \in \mathcal{W}_{K,m}^{\mathrm{c}}} \frac{|a(v,w)|}{\|v\|_{\mathcal{V}} \|w\|_{\mathcal{V}}} = \inf_{w \in \mathcal{W}_{K,m}^{\mathrm{c}}} \sup_{v \in \mathcal{W}_{K,m}^{\mathrm{c}}} \frac{|a(v,w)|}{\|v\|_{\mathcal{V}} \|w\|_{\mathcal{V}}} \geq \alpha_{\mathrm{d}} \tag{3.18}$$

holds for all $K \in \mathcal{T}_H$ and $m \in \mathbb{N}$.

Under this assumption, the following lemma shows that the element corrections decay exponentially fast away from their associated elements.

Lemma 3.3.1 (Exponential decay of element corrections)**.** *There exists $C_{\mathrm{d}} > 0$ depending only on C_a and α_{d} and the shape regularity of $\mathcal{T}_H$, such that*

$$\|\mathcal{C}_K v\|_{\mathcal{V}(D\setminus \mathsf{N}_m(K))} \leq \exp(-C_{\mathrm{d}} m)\|\mathcal{C}_K v\|_{\mathcal{V}}$$

holds for all $K \in \mathcal{T}_H$, $v \in \mathcal{V}$, and $m \in \mathbb{N}$. An analogous result holds for $\mathcal{C}_K^*$.

Proof. To simplify the notation, we abbreviate $\varphi \coloneqq \mathcal{C}_K v$ and denote by $\mathcal{N}_H$ the set of all (interior and boundary) nodes of $\mathcal{T}_H$. We define η as the FE cut-off function with $\eta(z) = 0$ for all $z \in \mathcal{N}_H \cap \mathsf{N}_{m-1}(K)$ and $\eta(z) = 1$ for all other nodes, i.e.,

$$\begin{aligned} \eta &\equiv 0 && \text{in } \mathsf{N}_{m-1}(K),\\ \eta &\equiv 1 && \text{in } D\setminus\mathsf{N}_m(K),\\ 0 \leq \eta &\leq 1 && \text{in } R \coloneqq \mathsf{N}_m(K)\setminus\mathsf{N}_{m-1}(K). \end{aligned}$$

Its gradient satisfies that $\|\nabla\eta\|_{L^\infty(D)} \leq C_\eta H^{-1}$ with $C_\eta > 0$ depending only on the shape regularity of $\mathcal{T}_H$.

By the local inf–sup stability (3.22), there exists $w \in \mathcal{W}^{\mathrm{c}}_{K,m-1}$ with $\|w\|_{\mathcal{V}} = 1$ such that

$$\begin{aligned} \alpha_{\mathrm{d}}\|\varphi\|_{\mathcal{V}(D\setminus \mathsf{N}_m(K))} &= \alpha_{\mathrm{d}}\|(\mathtt{id} - \mathcal{B}_H)\varphi\|_{\mathcal{V}(D\setminus \mathsf{N}_m(K))}\\ &\leq \alpha_{\mathrm{d}}\|(\mathtt{id} - \mathcal{B}_H)\eta\varphi\|_{\mathcal{V}}\\ &\leq |a((\mathtt{id} - \mathcal{B}_H)\eta\varphi, w)|\\ &= |a((\mathtt{id} - \mathcal{B}_H)\varphi, w) - a((\mathtt{id} - \mathcal{B}_H)(1-\eta)\varphi, w)|, \end{aligned} \tag{3.19}$$

where we used that $\mathcal{B}_H\varphi = 0$ and $(\mathtt{id} - \mathcal{B}_H)\eta\varphi \in \mathcal{W}^{\mathrm{c}}_{K,m-1}$. For the first term on the right-hand side of (3.19), we use that $\mathcal{B}_H\varphi = 0$ and $\operatorname{supp}(w) \subset \overline{D\setminus\mathsf{N}_{m-1}(K)}$, as well as (3.14) and (3.15), to obtain that

$$a((\mathtt{id} - \mathcal{B}_H)\varphi, w) = a(\varphi, w) = a_K(v, w) = 0.$$

For the second term in (3.19), we note that

$$\operatorname{supp}((\mathtt{id} - \mathcal{B}_H)(1-\eta)\varphi) \cap \operatorname{supp}(w) \subset \mathsf{N}_m(K) \cap \overline{D\setminus\mathsf{N}_{m-1}(K)} = \overline{R}.$$

Using this, (2.2), the properties of η, as well as (2.25) and (3.7), we obtain that

$$\begin{aligned} |a((\mathtt{id} - \mathcal{B}_H)(1-\eta)\varphi, w)| &\leq C_a\|(\mathtt{id} - \mathcal{B}_H)(1-\eta)\varphi\|_{\mathcal{V}(R)}\\ &\leq 2C_a(1 + \pi^{-1}(C_\eta + C_{\mathcal{B}_H}))\|\varphi\|_{\mathcal{V}(R)}, \end{aligned}$$

where we recall that $\|w\|_{\mathcal{V}} = 1$ and that D is scaled to unit size. Defining

$$C \coloneqq \big(2C_a(1 + \pi^{-1}(C_\eta + C_{\mathcal{B}_H}))/\alpha_{\mathrm{d}}\big)^2,$$

we obtain, using the previous estimates, that

$$\|\varphi\|^2_{\mathcal{V}(D\setminus\mathsf{N}_m(K))} \leq C\|\varphi\|^2_{\mathcal{V}(R)} = C\|\varphi\|^2_{\mathcal{V}(D\setminus\mathsf{N}_{m-1}(K))} - C\|\varphi\|^2_{\mathcal{V}(D\setminus\mathsf{N}_m(K))}.$$

After some algebraic manipulations, we get that

$$\|\varphi\|_{\mathcal{V}(D\setminus\mathsf{N}_m(K))} \leq \sqrt{\frac{C}{1+C}}\,\|\varphi\|_{\mathcal{V}(D\setminus\mathsf{N}_{m-1}(K))}.$$

Iterating the last inequality yields that

$$\|\varphi\|_{\mathcal{V}(D\setminus\mathsf{N}_m(K))} \leq \left(\frac{C}{1+C}\right)^{m/2}\|\varphi\|_{\mathcal{V}} = \exp(-C_{\mathrm{d}}m)\|\varphi\|_{\mathcal{V}},$$

where $C_{\mathrm{d}} \coloneqq \frac{1}{2}\log\frac{1+C}{C} > 0$. An analogous result for $\mathcal{C}^*_K$ can be proved using the same arguments. □

3.3.3 Localized corrections

The exponential decay of the element corrections shown in the previous lemma motivates their localization to patches in the coarse mesh. We introduce for all $K \in \mathcal{T}_H$ and $m \in \mathbb{N}$ local subspaces of $\mathcal{W}$ as

$$\mathcal{W}_{K,m} \coloneqq \{w \in \mathcal{W} : \ \operatorname{supp}(w) \subset \mathsf{N}_m(K)\} \tag{3.20}$$

and define the localized element correctors $\mathcal{C}_{K,m}, \mathcal{C}^*_{K,m} \colon \mathcal{V} \to \mathcal{W}_{K,m}$ such that

$$a(\mathcal{C}_{K,m}v, w) = a_K(v, w), \qquad a(w, \mathcal{C}^*_{K,m}v) = a_K(w, v) \tag{3.21}$$

is satisfied for all $v \in \mathcal{V}$ and $w \in \mathcal{W}_{K,m}$. The localized element correctors are well-defined and continuous provided that a is inf–sup stable on $\mathcal{W}_{K,m} \times \mathcal{W}_{K,m}$, i.e., there exists $\alpha_{\mathrm{fp}} > 0$ such that

$$\inf_{v\in\mathcal{W}_{K,m}} \sup_{w\in\mathcal{W}_{K,m}} \frac{|a(v,w)|}{\|v\|_{\mathcal{V}}\|w\|_{\mathcal{V}}} = \inf_{w\in\mathcal{W}_{K,m}} \sup_{v\in\mathcal{W}_{K,m}} \frac{|a(v,w)|}{\|v\|_{\mathcal{V}}\|w\|_{\mathcal{V}}} \geq \alpha_{\mathrm{fp}} \tag{3.22}$$

holds for all $K \in \mathcal{T}_H$ and $m \in \mathbb{N}$. Under this condition, the following lemma shows that the localized element correctors (3.21) exponentially approximate their global counterparts (3.15) in the operator norm.

Lemma 3.3.2 (Localization error of element corrections)**.** *For all $K \in \mathcal{T}_H$, $v \in \mathcal{V}$, and $m \in \mathbb{N}$, it holds that*

$$\|(\mathcal{C}_K - \mathcal{C}_{K,m})v\|_{\mathcal{V}} \lesssim \exp(-C_{\mathrm{d}}m)\|\mathcal{C}_K v\|_{\mathcal{V}},$$

where C_{d} is the constant from Lemma 3.3.1 and the hidden constant depends only on C_a, α_{fp}, and the shape regularity of $\mathcal{T}_H$. An analogous result holds for the difference $\mathcal{C}^*_K - \mathcal{C}^*_{K,m}$.

Proof. Note that $\varphi_m \coloneqq \mathcal{C}_{K,m} v \in \mathcal{W}_{K,m}$ can be interpreted as the Galerkin approximation to $\varphi \coloneqq \mathcal{C}_K v \in \mathcal{W}$ in the subspace $\mathcal{W}_{K,m} \subset \mathcal{W}$. Hence, Céa's lemma (see, e.g., [EG04, Lem. 2.28]) yields for all $w \in \mathcal{W}_{K,m}$ that

$$\|\varphi - \varphi_m\|_{\mathcal{V}} \leq \left(1 + \frac{C_a}{\alpha_{\mathrm{fp}}}\right) \|\varphi - w\|_{\mathcal{V}}.$$

To estimate the right-hand side, we choose $w \coloneqq (\mathtt{id} - \mathcal{B}_H)(1-\eta)\varphi \in \mathcal{W}_{K,m}$, where η is the FE cut-off function from the proof of Lemma 3.3.1. Recall that η is defined by $\eta(z) = 0$ for all $z \in \mathcal{N}_H \cap \mathtt{N}_{m-1}(K)$ and $\eta(z) = 1$ for all other nodes and that $\|\nabla \eta\|_{L^\infty(D)} \leq C_\eta H^{-1}$. Using that $\varphi \in \mathcal{W}$, which implies that $\varphi = (\mathtt{id} - \mathcal{B}_H)\varphi$, we get by (2.25) and (3.7) and Lemma 3.3.1 that

$$\begin{aligned}
\|\varphi - \varphi_m\|_{\mathcal{V}} &\leq \big(1 + \tfrac{C_a}{\alpha_{\mathrm{fp}}}\big) \|\varphi - w\|_{\mathcal{V}} \\
&= \big(1 + \tfrac{C_a}{\alpha_{\mathrm{fp}}}\big) \|(\mathtt{id} - \mathcal{B}_H)\eta\varphi\|_{\mathcal{V}(D\setminus \mathtt{N}_{m-1}(K))} \\
&\leq 2\big(1 + \tfrac{C_a}{\alpha_{\mathrm{fp}}}\big)(1 + \pi^{-1}(C_\eta + C_{\mathcal{B}_H}))\|\varphi\|_{\mathcal{V}(D\setminus \mathtt{N}_{m-1}(K))} \\
&\lesssim 2\big(1 + \tfrac{C_a}{\alpha_{\mathrm{fp}}}\big)(1 + \pi^{-1}(C_\eta + C_{\mathcal{B}_H}))\exp(-C_{\mathrm{d}} m)\|\varphi\|_{\mathcal{V}},
\end{aligned}$$

which is the assertion. Using the same arguments, an analogous result can be concluded for $\mathcal{C}_K^* - \mathcal{C}_{K,m}^*$. □

Without localization, the correctors $\mathcal{C}$ and $\mathcal{C}^*$ are equal to the sum of the element correctors $\mathcal{C}_K$ and $\mathcal{C}_K^*$, respectively, cf. (3.16). Therefore, we also define the localized correctors $\mathcal{C}_m$ and $\mathcal{C}_m^*$ as the sum of the localized element correctors $\mathcal{C}_{K,m}$ and $\mathcal{C}_{K,m}^*$, i.e.,

$$\mathcal{C}_m \coloneqq \sum_{K \in \mathcal{T}_H} \mathcal{C}_{K,m}, \qquad \mathcal{C}_m^* \coloneqq \sum_{K \in \mathcal{T}_H} \mathcal{C}_{K,m}^*. \tag{3.23}$$

The following lemma shows that these localized correctors approximate the correctors (3.1) exponentially well in the operator norm.

Lemma 3.3.3 (Localization error)**.** *For all $v \in \mathcal{V}$ and $m \in \mathbb{N}$, it holds that*

$$\|(\mathcal{C} - \mathcal{C}_m)v\|_{\mathcal{V}} \lesssim m^{d/2} \exp(-C_{\mathrm{d}} m)\|v\|_{\mathcal{V}},$$

where C_{d} is the constant from Lemma 3.3.1 and the hidden constant depends only on C_a, α_{f}, and α_{fp} as well as the quasi-uniformity and shape regularity of $\mathcal{T}_H$. An analogous result holds for the difference $\mathcal{C}^* - \mathcal{C}_m^*$.

Proof. Abbreviating $z \coloneqq (\mathcal{C} - \mathcal{C}_m)v$ and $z_K \coloneqq (\mathcal{C}_K - \mathcal{C}_{K,m})v$ for all $K \in \mathcal{T}_H$, the inf–sup stability (2.18) implies the existence of $w \in \mathcal{W}$ with $\|w\|_{\mathcal{V}} = 1$ such that

$$\alpha_{\mathrm{f}} \|z\|_{\mathcal{V}} \leq |a(z, w)| \leq \sum_{K \in \mathcal{T}_H} |a(z_K, w)|.$$

For the moment, we fix an element $K \in \mathcal{T}_H$ and define the FE cut-off function η in a similar way as in the proof of Lemma 3.3.1 by setting $\eta(z) = 0$ for all $z \in \mathcal{N}_H \cap \mathsf{N}_m(K)$ and $\eta(z) = 1$ for all other nodes.

Using that $\operatorname{supp}((\mathtt{id} - \mathcal{B}_H)\eta w) \subset \overline{D \backslash \mathsf{N}_m(K)}$ and $\operatorname{supp}(\mathcal{C}_{K,m} v) \subset \mathsf{N}_m(K)$, as well as $(\mathtt{id} - \mathcal{B}_H)(\eta w) \in \mathcal{W}$ and (3.14) and (3.15), we obtain that

$$a(z_K, (\mathtt{id} - \mathcal{B}_H)(\eta w)) = a(\mathcal{C}_K v, (\mathtt{id} - \mathcal{B}_H)(\eta w)) = a_K(v, (\mathtt{id} - \mathcal{B}_H)(\eta w)) = 0.$$

This, and the identity $w = (\mathtt{id} - \mathcal{B}_H)w$ for all $w \in \mathcal{W}$, yields that

$$a(z_K, w) = a(z_K, w - (\mathtt{id} - \mathcal{B}_H)(\eta w)) = a(z_K, (\mathtt{id} - \mathcal{B}_H)((1-\eta)w)).$$

Using that $\operatorname{supp}((\mathtt{id} - \mathcal{B}_H)((1-\eta)w)) \subset \mathsf{N}_{m+1}(K)$ as well as (2.2), (2.25), and (3.7), we obtain that

$$\left|a(z_K, (\mathtt{id} - \mathcal{B}_H)((1-\eta)w))\right| \leq 2C_a(1 + \pi^{-1}(C_\eta + C_{\mathcal{B}_H}))\|z_K\|_{\mathcal{V}}\|w\|_{\mathcal{V}(\mathsf{N}_{m+1}(K))}.$$

To show the continuity of $\mathcal{C}_K$, we use the inf–sup stability (2.18), which implies the existence of $q \in \mathcal{W}$ with $\|q\|_{\mathcal{V}} = 1$ such that

$$\alpha_{\mathrm{f}}\|\mathcal{C}_K v\|_{\mathcal{V}} \leq |a(\mathcal{C}_K v, q)| = |a_K(v, q)| \leq C_a\|v\|_{\mathcal{V}(K)},$$

where we used (3.14) and (3.15). Combining the above estimates and using Lemma 3.3.2 as well as the discrete Cauchy–Schwarz inequality, we obtain after summing over all elements that

$$\begin{aligned}
\alpha_{\mathrm{f}}\|z\|_{\mathcal{V}} &\leq \sum_{K\in\mathcal{T}_H} |a(z_K, w)| \leq C_a \sum_{K\in\mathcal{T}_H} \|z_K\|_{\mathcal{V}}\|w\|_{\mathcal{V}(\mathsf{N}_{m+1}(K))} \\
&\lesssim C_a \exp(-C_{\mathrm{d}} m) \sum_{K\in\mathcal{T}_H} \|\mathcal{C}_K v\|_{\mathcal{V}}\|w\|_{\mathcal{V}(\mathsf{N}_{m+1}(K))} \\
&\lesssim C_a^2 \alpha_{\mathrm{f}}^{-1} \exp(-C_{\mathrm{d}} m) \sum_{K\in\mathcal{T}_H} \|v\|_{\mathcal{V}(K)}\|w\|_{\mathcal{V}(\mathsf{N}_{m+1}(K))} \\
&\lesssim C_a^2 \alpha_{\mathrm{f}}^{-1} m^{d/2} \exp(-C_{\mathrm{d}} m)\|v\|_{\mathcal{V}},
\end{aligned}$$

where in the last step we used that

$$\sum_{K\in\mathcal{T}_H} \|w\|^2_{\mathcal{V}(\mathsf{N}_{m+1}(K))} \lesssim m^d\|w\|^2_{\mathcal{V}} = m^d.$$

This proves the assertion. Using the same arguments, an analogous result can be derived for the difference $\mathcal{C}^* - \mathcal{C}^*_m$. □

3.4 Practical multi-scale method

In this section, we introduce the LOD based on the considerations in the previous sections. The LOD uses localized versions of the prototypical basis functions (3.10) as its basis functions. These functions can be computed by solving local problems only, which makes the LOD feasible for practical computations.

To define the localized basis functions of the LOD, we use a custom quasi-interpolation operator, which has the same kernel as Π_H^0. This operator cures numerical pollution effects at the cost of slightly increasing the support of the LOD basis functions, see [HP22a; DHM22]. The construction of $\mathcal{P}_H$ is based on another quasi-interpolation operator defined by $\mathcal{I}_H \coloneqq \mathcal{E}_H \circ \Pi_H^0$, where $\mathcal{E}_H$ denotes an averaging operator that maps piecewise constants to the space of continuous piecewise linear functions. For nodes z that are not on the Dirichlet boundary, it is defined as

$$(\mathcal{E}_H v)(z) \coloneqq \frac{1}{\#\{K \in \mathcal{T}_H : z \in K\}} \sum_{K \in \mathcal{T}_H : z \in K} v|_K(z),$$

while for nodes on the Dirichlet boundary we set $(\mathcal{E}_H v)(z) \coloneqq 0$. The operator $\mathcal{E}_H$ is well known from the theory of domain decomposition methods, see, e.g., [Osw93; Bre94]. Using the bubble operator $\mathcal{B}_H$, we can locally manipulate the operator $\mathcal{I}_H$ so that its kernel coincides with the kernel of Π_H^0. More precisely, we define $\mathcal{P}_H$ for any $v \in L^2(D)$ as

$$\mathcal{P}_H v \coloneqq \mathcal{I}_H v + \mathcal{B}_H(v - \mathcal{I}_H v). \tag{3.24}$$

Since the operator $\mathcal{I}_H$ is quasi-local in the sense that it extends the support of a function by only one layer of elements, the same property also holds for $\mathcal{P}_H$. Furthermore, the operator $\mathcal{P}_H$ is a projection (i.e., $\mathcal{P}_H^2 = \mathcal{P}_H$) and satisfies that

$$\|\mathcal{P}_H v\|_{\mathcal{V}(K)} \leq C_{\mathcal{P}_H} \|v\|_{\mathcal{V}(\mathtt{N}(K))} \tag{3.25}$$

for all $K \in \mathcal{T}_H$ and $v \in \mathcal{V}$, where $C_{\mathcal{P}_H} > 0$ depends only on the quasi-uniformity and shape regularity of $\mathcal{T}_H$, see [AHP21, Sec. 3.4].

Given an oversampling parameter $m \in \mathbb{N}$, we define the localized problem-adapted trial and test spaces of the LOD as

$$U_{H,m}^{\mathrm{lod}} \coloneqq (\mathtt{id} - \mathcal{C}_m)\mathcal{P}_H U_H, \qquad V_{H,m}^{\mathrm{lod}} \coloneqq (\mathtt{id} - \mathcal{C}_m^*)\mathcal{P}_H U_H, \tag{3.26}$$

where, compared to (3.9), we have used the localized correctors and the additional operator $\mathcal{P}_H$. The corresponding LOD basis functions are

$$\big\{(\mathtt{id} - \mathcal{C}_m)\mathcal{P}_H b_K : K \in \mathcal{T}_H\big\}, \qquad \big\{(\mathtt{id} - \mathcal{C}_m^*)\mathcal{P}_H b_K : K \in \mathcal{T}_H\big\}. \tag{3.27}$$

These basis functions are supported on $(m+1)$-th order patches and can be computed by solving local problems on m-th order patches. For an illustration of the LOD basis functions, see Figure 3.2.

The LOD method then performs a Galerkin approach using the localized trial and test spaces defined in (3.26), i.e., it seeks $u_{H,m}^{\mathrm{lod}} \in U_{H,m}^{\mathrm{lod}}$ such that

$$a(u_{H,m}^{\mathrm{lod}}, v) = (f, v)_{L^2} \tag{3.28}$$

holds for all $v \in V_{H,m}^{\mathrm{lod}}$.

The well-posedness of the LOD approximation is guaranteed by the following lemma provided that m is chosen sufficiently large.

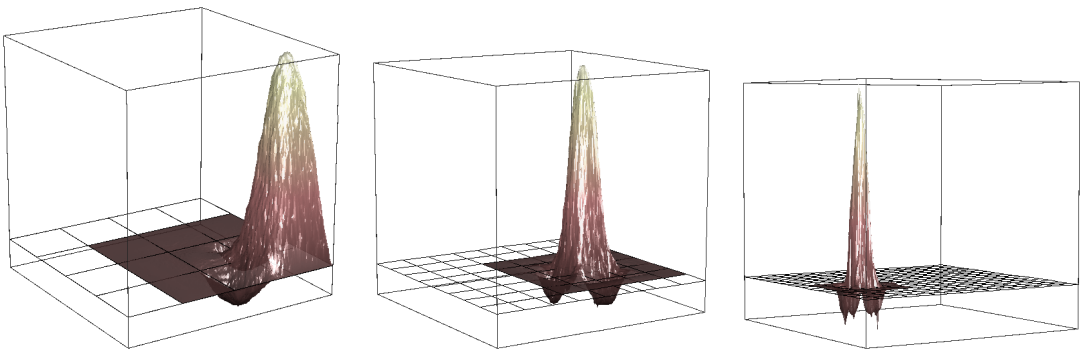

Figure 3.2: LOD basis functions for several coarse meshes and the oversampling parameter $m = 1$ for the problem considered in Section 3.6.

Theorem 3.4.1 (Inf–sup stability of the LOD)**.** *Assume that the oversampling parameter m satisfies that*

$$\alpha_{\mathrm{a}} m^{d/2} \exp(-C_{\mathrm{d}} m) \lesssim 1, \tag{3.29}$$

where C_{d} is the constant from Lemma 3.3.1 and the hidden constant depends only on C_a, α_{f}, and α_{fp} as well as the quasi-uniformity and shape regularity of $\mathcal{T}_H$. Then, the sesquilinear form a is inf–sup stable on $U_{H,m}^{\mathrm{lod}} \times V_{H,m}^{\mathrm{lod}}$, i.e., there exists $\alpha_{\mathrm{lod}} > 0$ such that

$$\inf_{v \in U_{H,m}^{\mathrm{lod}}} \sup_{w \in V_{H,m}^{\mathrm{lod}}} \frac{|a(v,w)|}{\|v\|_{\mathcal{V}} \|w\|_{\mathcal{V}}} \geq \alpha_{\mathrm{lod}} \tag{3.30}$$

holds with $\alpha_{\mathrm{lod}} \approx \alpha_{\mathrm{a}}$, where α_{a} is the constant from Lemma 2.3.1.

Proof. Given an arbitrary $v_m \in U_{H,m}^{\mathrm{lod}}$, we define $v \coloneqq (\mathtt{id} - \mathcal{C}) \mathcal{P}_H v_m$. Note that it holds $v \in U_H^{\mathrm{a}}$ due to Lemma 3.1.1. Using the inf–sup stability (2.19), we obtain that there exists $w \in V_H^{\mathrm{a}}$ such that

$$|a(v,w)| \geq \alpha_{\mathrm{a}} \|v\|_{\mathcal{V}} \|w\|_{\mathcal{V}}.$$

We define $w_m \coloneqq (\mathtt{id} - \mathcal{C}_m^*) \mathcal{P}_H w$ and note that $v_m = (\mathtt{id} - \mathcal{C}_m) \mathcal{P}_H v_m$ since the function $v_m \in U_{H,m}^{\mathrm{lod}}$ is uniquely determined by its QOIs defined in (2.13). The above identity for v_m implies that $v - v_m = (\mathcal{C}_m - \mathcal{C}) \mathcal{P}_H v_m \in \mathcal{W}$, which gives that $a(v - v_m, w) = 0$ by (3.4) since $w \in V_H^{\mathrm{a}}$. Using this, we obtain that

$$a(v_m, w_m) = a(v_m, w) + a(v_m, w_m - w) = a(v, w) + a(v_m, w_m - w).$$

The second term on the right-hand side can be bounded using Lemma 3.3.3 and (3.25) as follows:

$$\begin{aligned} \big|a(v_m, w_m - w)\big| &\leq C_a \|v_m\|_{\mathcal{V}} \|w_m - w\|_{\mathcal{V}} = C_a \|v_m\|_{\mathcal{V}} \|(\mathcal{C}^* - \mathcal{C}_m^*) \mathcal{P}_H w\|_{\mathcal{V}} \\ &\lesssim m^{d/2} \exp(-C_{\mathrm{d}} m) \|v_m\|_{\mathcal{V}} \|w\|_{\mathcal{V}}. \end{aligned}$$

Next, we estimate the $\mathcal{V}$-norms of v and w against the $\mathcal{V}$-norms of their localized counterparts and vice versa. Since $\mathcal{C}$ is a projection (which is neither the zero projection nor the identity), it has the same operator norm as its complementary projection $\mathtt{id} - \mathcal{C}$, cf. [Szy06]. Using this and (3.2) and (3.25), we obtain that

$$\|v\|_{\mathcal{V}} = \|(\mathtt{id} - \mathcal{C})\mathcal{P}_H v_m\|_{\mathcal{V}} \leq \alpha_{\mathrm{f}}^{-1} C_a \|\mathcal{P}_H v_m\|_{\mathcal{V}} \lesssim \alpha_{\mathrm{f}}^{-1} C_a \|v_m\|_{\mathcal{V}}.$$

Furthermore, using similar arguments as above, Lemma 3.3.3 and the identity $\mathcal{P}_H v = \mathcal{P}_H v_m$, which holds since $v - v_m \in \mathcal{W}$, we get that

$$\begin{aligned}\|v_m\|_{\mathcal{V}} &= \|(\mathtt{id} - \mathcal{C}_m)\mathcal{P}_H v_m\|_{\mathcal{V}} \leq \|(\mathtt{id} - \mathcal{C})\mathcal{P}_H v_m\|_{\mathcal{V}} + \|(\mathcal{C}_m - \mathcal{C})\mathcal{P}_H v_m\|_{\mathcal{V}} \\ &\lesssim \big(\alpha_{\mathrm{f}}^{-1} C_a + m^{d/2}\exp(-C_{\mathrm{d}} m)\big)\|v\|_{\mathcal{V}}.\end{aligned}$$

In total, we have that $\|v\|_{\mathcal{V}} \lesssim \|v_m\|_{\mathcal{V}}$ and $\|v_m\|_{\mathcal{V}} \lesssim \|v\|_{\mathcal{V}}$, where the constants of order one are hidden in the tilde notation. Using similar arguments, the same estimates can be proved for w and w_m. Combining the above estimates, we obtain that

$$\begin{aligned}|a(v_m, w_m)| &\geq |a(v, w)| - |a(v_m, w_m - w)| \\ &\gtrsim \alpha_{\mathrm{a}}\|v\|_{\mathcal{V}}\|w\|_{\mathcal{V}} - m^{d/2}\exp(-C_{\mathrm{d}} m)\|v_m\|_{\mathcal{V}}\|w\|_{\mathcal{V}} \\ &\gtrsim (\alpha_{\mathrm{a}} - m^{d/2}\exp(-C_{\mathrm{d}} m))\|v_m\|_{\mathcal{V}}\|w_m\|_{\mathcal{V}} \\ &\gtrsim \alpha_{\mathrm{lod}}\|v_m\|_{\mathcal{V}}\|w_m\|_{\mathcal{V}}.\end{aligned}$$

In the last estimate, we have absorbed the second term into the first term, using that m is sufficiently large, cf. (3.29). Note that the inf–sup constant α_{lod} has the same scaling as α_{a}, i.e., $\alpha_{\mathrm{lod}} \approx \alpha_{\mathrm{a}}$. □

The next theorem proves that the LOD provides optimal order approximations under minimal structural assumptions if the oversampling parameter is increased logarithmically with the mesh size.

Theorem 3.4.2 (Convergence of the LOD)**.** *For any $f \in H^k(D)$, $k \in \{0, 1\}$, the LOD approximation* (3.28) *satisfies that*

$$\|u - u_{H,m}^{\mathrm{lod}}\|_{\mathcal{V}} \lesssim H^{1+k}|f|_{H^k} + m^{d/2}\exp(-C_{\mathrm{d}} m)\|f\|_{L^2}.$$

Moreover, if $m \gtrsim \log(\frac{1}{H})$, we get that

$$\|u - u_{H,m}^{\mathrm{lod}}\|_{\mathcal{V}} \lesssim H^{1+k}\|f\|_{H^k}.$$

Note that C_{d} is the constant from Lemma 3.3.1 and that the above hidden constants depend only on C_a, α_{f}, α_{fp}, and α_{a} as well as the quasi-uniformity and shape regularity of $\mathcal{T}_H$.

Proof. Using the triangle inequality, we obtain that

$$\|u - u_{H,m}^{\mathrm{lod}}\|_{\mathcal{V}} \leq \|u - u_H^{\mathrm{a}}\|_{\mathcal{V}} + \|u_H^{\mathrm{a}} - u_{H,m}^{\mathrm{lod}}\|_{\mathcal{V}}. \tag{3.31}$$

The first term can be estimated using Lemma 2.3.3. For the second term, we apply Strang's lemma (see, e.g., [EG04, Lem. 2.25]) using that $u_{H,m}^{\mathrm{lod}} \in U_{H,m}^{\mathrm{lod}}$ can be interpreted as a non-conforming and non-consistent approximation to $u_H^{\mathrm{a}} \in U_H^{\mathrm{a}}$. We obtain that

$$\begin{aligned}&\|u_H^{\mathrm{a}} - u_{H,m}^{\mathrm{lod}}\|_{\mathcal{V}} \\ &\quad\leq \big(1 + C_a \alpha_{\mathrm{lod}}^{-1}\big) \inf_{v_m \in U_{H,m}^{\mathrm{lod}}} \|u_H^{\mathrm{a}} - v_m\|_{\mathcal{V}} + \alpha_{\mathrm{lod}}^{-1} \sup_{w_m \in V_{H,m}^{\mathrm{lod}}} \frac{|a(u_H^{\mathrm{a}}, w_m) - (f\,,\, w_m)_{L^2}|}{\|w_m\|_{\mathcal{V}}},\end{aligned}$$

where the first term can be estimated choosing $v_m \coloneqq (\mathtt{id} - \mathcal{C}_m)\mathcal{P}_H u_H^{\mathrm{a}}$. Using that $u_H^{\mathrm{a}} = (\mathtt{id} - \mathcal{C})\mathcal{P}_H u_H^{\mathrm{a}}$ and (2.19) and (3.25) and Lemma 3.3.3, we get that

$$\begin{aligned}\|u_H^{\mathrm{a}} - v_m\|_{\mathcal{V}} = \|(\mathcal{C} - \mathcal{C}_m)\mathcal{P}_H u_H^{\mathrm{a}}\|_{\mathcal{V}} &\lesssim m^{d/2} \exp(-C_{\mathrm{d}} m) \|u_H^{\mathrm{a}}\|_{\mathcal{V}} \\ &\leq \alpha_{\mathrm{a}}^{-1} m^{d/2} \exp(-C_{\mathrm{d}} m) \|f\|_{L^2}.\end{aligned}$$

For the second term, algebraic manipulations yield for all $w \in V_H^{\mathrm{a}}$ that

$$a(u_H^{\mathrm{a}}, w_m) - (f\,,\, w_m)_{L^2} = (f\,,\, w - w_m)_{L^2} - a(u_H^{\mathrm{a}}, w - w_m).$$

We choose $w \coloneqq (\mathtt{id} - \mathcal{C}^*)\mathcal{P}_H w_m$ and note that it holds $w_m = (\mathtt{id} - \mathcal{C}_m^*)\mathcal{P}_H w_m$, since the function $w_m \in V_{H,m}^{\mathrm{lod}}$ is uniquely determined by its QOIs. Using (2.2), (2.19), and (3.25) and Lemma 3.3.3, we obtain that

$$|a(u_H^{\mathrm{a}}, w_m) - (f\,,\, w_m)_{L^2}| \lesssim m^{d/2} \exp(-C_{\mathrm{d}} m)\big(1 + C_a \alpha_{\mathrm{a}}^{-1}\big) \|w_m\|_{\mathcal{V}} \|f\|_{L^2}.$$

Combining the above estimates yields the assertion. □

At first glance, this proof may seem unnecessarily complicated, since Céa's lemma (see, e.g., [EG04, Lem. 2.28]) could have been used directly. However, for the Helmholtz problem, for example, this would lead to an inf–sup constant in front of the optimal order term in the estimate of Theorem 3.4.2, which depends on the wavenumber in an undesirable way.

3.5 Fine-scale discretization

The computation of the LOD basis functions (3.27) requires the computation of localized element corrections defined in (3.21). However, this step would require the solution of (local) infinite-dimensional problems. In this section, we perform a fine-scale discretization of these corrector problems, which results in a practically computable method.

For the fine-scale discretization, we consider a fine mesh $\mathcal{T}_h$, which resolves all fine-scale features of the problem. For multi-scale problems, its mesh size h is typically much smaller than the coarse mesh size, i.e., $h \ll H$. We assume that $\mathcal{T}_h$ is obtained by refining the coarse mesh $\mathcal{T}_H$. In the following, we denote by $V_h^{\mathrm{fem}} \subset \mathcal{V}$ the $\mathcal{Q}^1$-FE space with respect to $\mathcal{T}_h$, cf. Section 2.2. We emphasize that there is great flexibility in the choice of the FE space, e.g., one could also consider higher order or adaptive FEs, cf. [Pet16; Eng+19].

A fully discrete version of the LOD is obtained by replacing the space $\mathcal{V}$ in its derivation by the finite-dimensional space V_h^{fem}. As a consequence, the computation of the element correctors (3.21) only requires computations involving the finite-dimensional spaces $\mathcal{W}_{K,m} \cap V_h^{\mathrm{fem}}$. Denoting by $\mathcal{C}_{m,h}, \mathcal{C}_{m,h}^* \colon V_h^{\mathrm{fem}} \to \mathcal{W} \cap V_h^{\mathrm{fem}}$ the fully discrete counterparts of $\mathcal{C}_m$ and $\mathcal{C}_m^*$, we define the fully discrete trial and test spaces of the LOD by

$$U_{H,m,h}^{\mathrm{lod}} \coloneqq (\mathtt{id} - \mathcal{C}_{m,h})\mathcal{P}_H U_H, \qquad V_{H,m,h}^{\mathrm{lod}} \coloneqq (\mathtt{id} - \mathcal{C}_{m,h}^*)\mathcal{P}_H U_H. \tag{3.32}$$

Here, U_H and $\mathcal{P}_H U_H$ must be subspaces of V_h^{fem}, which however is not a restriction, since the bubble function b_K corresponding to the element $K \in \mathcal{T}_H$ can be chosen as an element of $H_0^1(K) \cap V_h^{\mathrm{fem}}$. This is possible if $\mathcal{T}_h$ is obtained from $\mathcal{T}_H$ by at least one uniform (global) refinement.

The fully discrete LOD seeks $u_{H,m,h}^{\mathrm{lod}} \in U_{H,m,h}^{\mathrm{lod}}$ such that

$$a(u_{H,m,h}^{\mathrm{lod}}, v) = (f\,,\, v)_{L^2} \tag{3.33}$$

holds for all $v \in V_{H,m,h}^{\mathrm{lod}}$. If discrete versions of the inf–sup conditions (2.4), (2.18), (3.18), and (3.22) are satisfied, the results from Lemmas 3.3.1 to 3.3.3 and Theorems 3.4.1 and 3.4.2 carry over to the fully discrete setting, which ensures the well-posedness of (3.32) and (3.33). The proofs of these results are similar to the continuous setting, with the minor difference that products of functions in V_h^{fem} are generally not in V_h^{fem}, but in a higher order FE space. This technical issue can be solved using a fine-scale interpolation, see, e.g., [MP20, Sec. 4.4]. For an efficient implementation of the LOD, see [Eng+19].

Henceforth, we denote by $u_h^{\mathrm{fem}} \in V_h^{\mathrm{fem}}$ the fine-scale FE solution, which satisfies that

$$a(u_h^{\mathrm{fem}}, v) = (f\,,\, v)_{L^2} \tag{3.34}$$

for all $v \in V_h^{\mathrm{fem}}$. Note that the fine-scale FE solution is needed only for theoretical purposes, and its computation is not required for the LOD. Applying Theorem 3.4.2 in the fully discrete setting shows that the fully discrete LOD approximation converges to u_h^{fem}. Thus, the fully discrete LOD provides an accurate approximation of the solution u only if the error of the fine-scale FE approximation is small. This can be seen in the following theorem.

Theorem 3.5.1 (Convergence of the fully discrete LOD)**.** *Assume that the solution u to* (2.3) *is H^{1+r}-regular for some $r \in (0,1]$ and let $m \gtrsim \log(\frac{1}{H})$. Then,*

for any $f \in H^k(D)$, $k \in \{0,1\}$, the fully discrete LOD approximation (3.33) *satisfies that*

$$\|u - u^{\mathrm{lod}}_{H,m,h}\|_{\mathcal{V}} \lesssim h^r |u|_{H^{1+r}} + H^{1+k}\|f\|_{H^k}. \tag{3.35}$$

The hidden constant has the same dependencies as in Theorem 3.4.2 and also depends on the inf–sup constant of a on $V_h^{\mathrm{fem}} \times V_h^{\mathrm{fem}}$.

Proof. The triangle inequality yields that

$$\|u - u^{\mathrm{lod}}_{H,m,h}\|_{\mathcal{V}} \leq \|u - u_h^{\mathrm{fem}}\|_{\mathcal{V}} + \|u_h^{\mathrm{fem}} - u^{\mathrm{lod}}_{H,m,h}\|_{\mathcal{V}}.$$

Since by assumption $u \in H^{1+r}(D)$, we obtain using estimate (2.9) that

$$\|u - u_h^{\mathrm{fem}}\|_{\mathcal{V}} \lesssim h^r |u|_{H^{1+r}}.$$

For the second term, we use Theorem 3.4.2 in the fully discrete setting, where we absorb the localization error into the optimal order term using that $m \gtrsim \log(\frac{1}{H})$. We obtain that

$$\|u_h^{\mathrm{fem}} - u^{\mathrm{lod}}_{H,m,h}\|_{\mathcal{V}} \lesssim H^{1+k}\|f\|_{H^k}.$$

Combining the above estimates yields the assertion. □

3.6 Numerical experiments

This section numerically investigates the LOD using an elliptic model problem posed on the domain $D = (0,1)^2$. For this, we consider uniform Cartesian meshes of D, where the mesh size denotes the side length of the elements instead of their diameter. We impose homogeneous Dirichlet boundary conditions, i.e., $\mathcal{V} \coloneqq H_0^1(D)$. The weak formulation then seeks $u \in \mathcal{V}$ such that

$$a(u,v) \coloneqq \int_D A\nabla u \cdot \nabla v \,\mathrm{d}x = \int_D fv \,\mathrm{d}x =: F(v) \tag{3.36}$$

holds for all $v \in \mathcal{V}$. The diffusion coefficient used in the following numerical experiments is depicted in Figure 3.3. It is piecewise constant with respect to the mesh $\mathcal{T}_{2^{-7}}$ with element values chosen as realizations of independent random variables uniformly distributed in the interval $[0.01, 1]$. The source term f will be specified in the respective numerical experiments.

The natural norm for this problem is the energy norm defined by

$$\|\cdot\|_a \coloneqq \|A^{1/2}\nabla \cdot\|_{L^2}, \tag{3.37}$$

which is equivalent to the $\mathcal{V}$-norm. This can be proved using Friedrichs' inequality (recall that D is scaled to unit size) and the uniform bounds of A. It holds that A is coercive and continuous on $\mathcal{V}$ with respect to the energy norm with constants one. Thus, by the Lax–Milgram theorem (see, e.g., [Alt16, Thm. 6.2]), problem (3.36) is well-posed. Since the coercivity also holds for all subspaces of

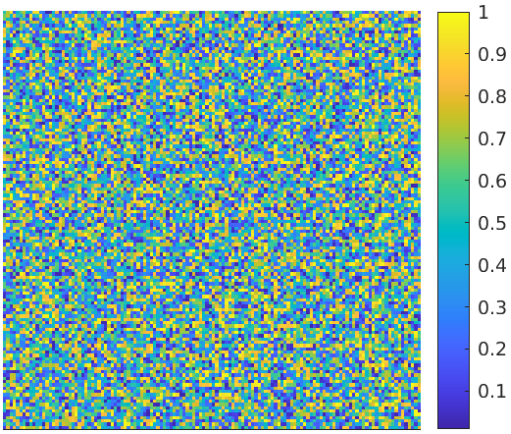

Figure 3.3: Piecewise constant coefficient A used in the numerical experiments.

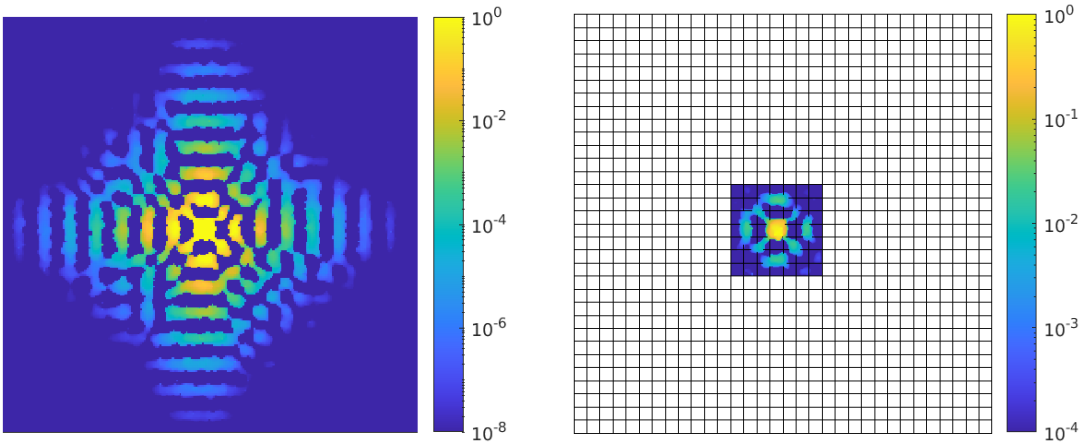

Figure 3.4: Prototypical LOD basis function (left) and corresponding localized basis function for $m = 2$ (right) for the coarse mesh $\mathcal{T}_{2^{-5}}$.

$\mathcal{V}$, all corrector problems and discrete approximations of them are well-posed, see Section 6.1 for more details.

For the discretization, we consider a coarse uniform Cartesian mesh $\mathcal{T}_H$ of the domain D and the fine Cartesian mesh $\mathcal{T}_{2^{-9}}$ obtained by uniform refinement of $\mathcal{T}_H$. The fine mesh is used for the fine-scale discretization of the LOD as described in Section 3.5. Note that henceforth, all errors are computed with respect to the FE reference solution on the same fine mesh $\mathcal{T}_{2^{-9}}$, which means that the fine-scale discretization error is not visible. Furthermore, all errors are relative errors with respect to the energy norm (3.37).

Exponential decay and localization

Figure 3.4 illustration one prototypical basis function of the LOD and its localized counterpart. Taking into account the logarithmic color scaling, one

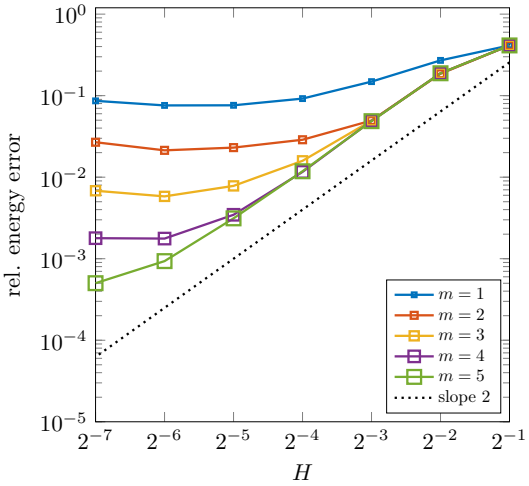

Figure 3.5: Error of the LOD as a function of H for several oversampling parameters m. The dotted line indicates the expected rate of convergence.

clearly observes the exponential decay of the prototypical LOD basis function, as predicted theoretically in Lemma 3.3.1. Furthermore, one observes that for the oversampling parameter $m = 2$ the considered localized basis function is supported on a third order patch, demonstrating the increased support of the localized basis functions due to the operator $\mathcal{P}_H$, cf. (3.27).

Optimal order convergence

For the numerical investigation of the convergence properties of the LOD, we consider the smooth source term defined as

$$f(x_1, x_2) = (x_1 + \cos(3\pi x_1)) \cdot x_2^3.$$

Provided that the oversampling parameter m is chosen sufficiently large, Figure 3.5 shows second order convergence for the LOD. Since $f \in H^1(D)$, this is consistent with the theoretical prediction in Theorem 3.4.2. Furthermore, one observes the effect of the quasi-interpolation operator $\mathcal{P}_H$ in the definition of LOD, since the numerical pollution effect observed, e.g., in [Mai21] is eliminated.

Exponential localization

To investigate the localization properties of the LOD, we consider the source term $f \equiv 1$. For this particular choice, the optimal order term in Theorem 3.4.2 vanishes since $f \in \mathcal{P}^0(\mathcal{T}_H)$, i.e., only the localization error is present. Figure 3.6 shows the exponential decay of the localization error of the LOD, which is consistent with the exponential localization properties of the LOD, see Lemma 3.3.1 and Theorem 3.4.2.

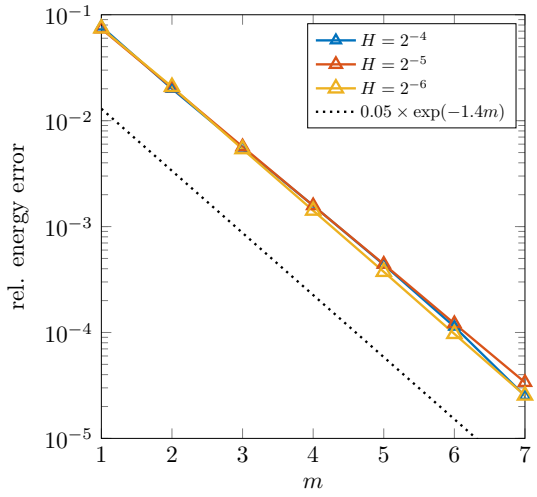

Figure 3.6: Error of the LOD as a function of m for several coarse meshes. The dotted line indicates the expected exponential decay.

4 Multi-resolution Localized Orthogonal Decomposition for Helmholtz problems

The previous chapter introduced the LOD for the reliable coarse-scale approximation of PDEs under minimal structural assumptions. In this chapter, we derive a multi-resolution variant of the LOD referred to as Multi-resolution Localized Orthogonal Decomposition (MRLOD). Given a LOD approximation on a coarse mesh, it allows one to flexibly add additional discretization levels to improve the accuracy of the approximation. The construction of the MRLOD is inspired by the framework of operator-adapted wavelets [OS19], which in turn is motivated by a game-theoretic interpretation of numerical homogenization, see [Owh15; Owh17]. We emphasize that up to now the latter approaches have mostly been applied for the numerical homogenization of elliptic problems.

The MRLOD is applicable to a large class of possibly complex-valued, non-hermitian, and indefinite problems. In the following, however, we restrict ourselves to Helmholtz problems for demonstration purposes. The numerical solution of Helmholtz problems is challenging, especially for large wavenumbers. This is due to the typically strict requirements on the mesh size of the underlying mesh, which go far beyond the minimal requirements needed to resolve the oscillatory nature of the solution. This effect is known as pollution [BS97]. Similar to other multi-scale methods [GP15; Pet16; Pet17; MAS23], the MRLOD has stabilizing properties for high-frequency Helmholtz problems. More precisely, the MRLOD is able to suppress the pollution effect, provided that the oversampling parameter is increased logarithmically with the wavenumber and that the coarsest discretization level satisfies a minimal resolution condition. Note that the suppression of the pollution effect is not a unique feature of multi-scale methods. For example, also Trefftz methods [Moi11; HMP14; HMP16] and *hp*-FEMs [MS10; MS11; MPS13] are able to cure the pollution effect under mild additional assumptions on the discretization parameters.

The MRLOD identifies hierarchical bases of the prototypical problem-adapted trial and test spaces that block-diagonalize the discrete Helmholtz operator. These basis functions are then localized using LOD techniques. To compute the localized basis functions, one solves local (coercive) sub-scale corrector problems with a relatively small effective wavenumber. Such problems can be solved efficiently using standard preconditioners, cf. [GZ19]. A special feature of the

MRLOD is that it condenses all undesirable properties of the discrete linear system (indefinite, deteriorating condition for increasing κ) to its first (comparably small) block, while all other blocks are coercive and can be solved within a few iterations of a standard iterative solver. In the following, the MRLOD is introduced for Helmholtz problems in homogeneous media. However, the theoretical results also carry over to the case of heterogeneous media provided that the underlying problem is well-posed and certain stability assumptions are satisfied, see Section 4.7 for numerical experiments. For a theoretical investigation of heterogeneous Helmholtz problems, see [ST18; GPS19; GS19].

The content and presentation of the following chapter is primarily based on the journal article

[HP22a] M. Hauck and D. Peterseim. "Multi-resolution localized orthogonal decomposition for Helmholtz problems". In: *Multiscale Model. Simul.* 20.2 (2022), pp. 657–684

4.1 Model Helmholtz problem

The Helmholtz problem models the propagation of time-harmonic acoustic waves in homogeneous media. We consider a bounded polytopal Lipschitz domain $D \subset \mathbb{R}^d$, which we assume to be scaled to unit size. Given a wavenumber $\kappa \in (\kappa_0, \infty)$ with $\kappa_0 > 0$, the Helmholtz problem on D reads

$$-\Delta u - \kappa^2 u = f \qquad \text{in } D$$

with boundary conditions of Neumann, Robin, and Dirichlet type

$$\begin{aligned} \nabla u \cdot \nu &= 0 && \text{on } \Gamma_1, \\ \nabla u \cdot \nu - i\kappa u &= 0 && \text{on } \Gamma_2, \\ u &= 0 && \text{on } \Gamma_3, \end{aligned}$$

where i denotes the imaginary unit and ν is the outer unit normal vector. Note that the second boundary condition is typically referred to as impedance boundary condition. We assume that the boundary ∂D can be decomposed into the closed boundary segments Γ_1, Γ_2, and Γ_3, i.e., $\partial D = \Gamma_1 \cup \Gamma_2 \cup \Gamma_3$ such that the intersection of the interior of the components is pairwise disjoint. We allow Γ_1 and Γ_3 to be empty, but assume a positive surface measure for Γ_2. Note that other types of boundary conditions such as perfectly matched layers could also be considered, cf. [Ber94; Ber+07].

As solution space of the Helmholtz problem, we use

$$\mathcal{V} \coloneqq \left\{ v \in H^1(D, \mathbb{C}) : \, v|_{\Gamma_3} = 0 \right\},$$

where we write $H^1(D, \mathbb{C})$ to emphasize that we consider complex-valued functions. Contrary to (2.1), we endow $\mathcal{V}$ with the Helmholtz-specific κ-dependent norm, defined as

$$\|\cdot\|_{\mathcal{V}}^2 \coloneqq \|\nabla \cdot\|_{L^2}^2 + \kappa^2 \|\cdot\|_{L^2}^2. \tag{4.1}$$

The weak formulation of the Helmholtz problem is based on the sesquilinear form $a\colon \mathcal{V} \times \mathcal{V} \to \mathbb{C}$, which is for all $v, w \in \mathcal{V}$ defined as

$$a(v,w) \coloneqq (\nabla v \,,\, \nabla w)_{L^2} - \kappa^2 (v \,,\, w)_{L^2} - i\kappa (v \,,\, w)_{L^2(\Gamma_2)}. \tag{4.2}$$

Using the multiplicative trace inequality (see, e.g., [BS08, Thm. 1.6.6]), one can show that the sesquilinear form a is continuous with respect to (4.1) with a κ-independent continuity constant C_a, cf. (2.2).

The weak formulation of the Helmholtz problem seeks $u \in \mathcal{V}$ such that

$$a(u,v) = (f \,,\, v)_{L^2} \tag{4.3}$$

holds for all $v \in \mathcal{V}$. We note that the well-posedness of this weak formulation depends on the geometry of D and the choice of boundary conditions. For example, the presence of Robin boundary conditions ensures the well-posedness of (4.3). However, the stability constant may depend on the wavenumber, i.e., for all $f \in L^2(D)$, the corresponding solution $u \in \mathcal{V}$ satisfies that

$$\|u\|_{\mathcal{V}} \leq C_{\mathrm{st}}(\kappa) \|f\|_{L^2} \tag{4.4}$$

with a κ-dependent constant $C_{\mathrm{st}} > 0$. In the following, we assume that C_{st} depends polynomially on κ, i.e., there exists $n \in \mathbb{N}_0$ such that

$$C_{\mathrm{st}}(\kappa) \lesssim \kappa^n. \tag{4.5}$$

This assumption is important for the stability and error analysis of the MR-LOD. We emphasize that (4.5) does not hold in general, since, e.g., for trapping domains counterexamples with an exponential-in-κ growth of C_{st} can be constructed, cf. [Bet+11]. Nevertheless, (4.5) can be proved under certain geometric assumptions. In [Mel95], it is proved with $n = 0$ for bounded star-shaped domains with smooth boundary or bounded convex domains. Among the known admissible setups is also the case of Lipschitz domains with pure impedance boundary conditions, i.e., $\Gamma_2 = \partial D$, see [EM12]. Another possible example are truncated exterior Dirichlet problems with a star-shaped polytopal scatterer, cf. [Het07]. Such problems arise when approximating the Sommerfeld radiation condition by truncating the unbounded exterior domain and applying impedance boundary conditions on the artificial boundary.

A direct consequence of (4.4) is the inf–sup stability of the sesquilinear form a of the Helmholtz problem, i.e.,

$$\inf_{v \in \mathcal{V}} \sup_{w \in \mathcal{V}} \frac{\Re a(v,w)}{\|v\|_{\mathcal{V}} \|w\|_{\mathcal{V}}} = \inf_{w \in \mathcal{V}} \sup_{v \in \mathcal{V}} \frac{\Re a(v,w)}{\|v\|_{\mathcal{V}} \|w\|_{\mathcal{V}}} \geq \alpha_{\mathrm{c}} \tag{4.6}$$

with $\alpha_{\mathrm{c}} = (2C_{\mathrm{st}}(\kappa)\kappa)^{-1} > 0$, see [Mel95], where $\Re$ denotes the real part of a complex number. Note that (4.6) in particular implies (2.4), since it holds that $|a(v,w)| \geq \Re a(v,w)$ for all $v, w \in \mathcal{V}$.

4.2 Multi-resolution decomposition

In this section, we perform a multi-resolution decomposition of the trial and test spaces of the LOD for the Helmholtz problem. First, we introduce a prototypical multi-resolution decomposition, which block-diagonalizes the discrete operator and thereby decouples the discretization scales. The basis functions of the prototypical multi-resolution trial and test spaces are generally globally supported and therefore not directly suitable for practical computations. In Section 4.3, we prove that they decay exponentially fast, which justifies their localization in Section 4.4.

4.2.1 Haar basis

The construction of the multi-resolution decomposition is based on a Haar basis defined with respect to a hierarchy of nested meshes. Given $L \in \mathbb{N}$, we consider the hierarchy $\{\mathcal{T}_\ell\}_{\ell=1,\dots,L}$ obtained by uniformly refining the quasi-uniform and shape regular coarse mesh $\mathcal{T}_1$, cf. Section 2.2. We denote by H_ℓ the mesh size of $\mathcal{T}_\ell$. Furthermore, we denote by $\Pi_\ell^0 \colon L^2(D) \to \mathcal{P}^0(\mathcal{T}_\ell)$ the L^2-orthogonal projection onto $\mathcal{T}_\ell$-piecewise constants, which satisfies (2.25) with the mesh size H_ℓ.

The following definition of the Haar basis is similar to [FP20]. Starting with the L^2-normalized characteristic functions of the elements of $\mathcal{T}_1$, given by

$$\mathcal{H}_1 \coloneqq \{|K|^{-1/2}\mathbf{1}_K : K \in \mathcal{T}_1\}, \tag{4.7}$$

we successively add L^2-orthogonal functions on finer meshes. For this, we define the descendants of the element $K \in \mathcal{T}_\ell$ by $\operatorname{des}(K) \coloneqq \{T \in \mathcal{T}_{\ell+1} : T \subset K\}$ and denote by $\{\phi_{K,j} : j = 1, \dots, \#\operatorname{des}(K) - 1\}$ a set of L^2-orthonormal functions in $\mathcal{P}^0(\mathcal{T}_{\ell+1} \cap \operatorname{des}(K))$ whose integrals equal zero. The latter condition ensures the L^2-orthogonality to piecewise constant functions on coarser levels. For $\ell = 1, \dots, L-1$, we consider the following sets of functions:

$$\mathcal{H}_{\ell+1} \coloneqq \bigcup_{K \in \mathcal{T}_\ell} \{\phi_{K,j} : j = 1, \dots, \#\operatorname{des}(K) - 1\}. \tag{4.8}$$

The Haar basis is then obtained as

$$\mathcal{H} \coloneqq \mathcal{H}_1 \cup \dots \cup \mathcal{H}_L. \tag{4.9}$$

By construction, $\mathcal{H}$ is an orthonormal basis of $\mathcal{P}^0(\mathcal{T}_L)$. Note that similar constructions can be performed for unstructured quadrilateral/hexahedral or simplicial meshes. For tensor-product meshes also higher order Haar basis functions can be constructed, cf. [Alp93].

Since the Haar basis functions are non-conforming with respect to $\mathcal{V}$, we need to construct $\mathcal{V}$-conforming companions. In the one-level setting, this was done by the operators $\mathcal{B}_H$ and $\mathcal{P}_H$ defined in (3.6) and (3.24). Their multi-level analogues, denoted by $\mathcal{B}_\ell$ and $\mathcal{P}_\ell$, can be defined at each level of the

hierarchy exactly as in the one-level case. Also the estimates (3.7) and (3.25) can be transferred to the multi-level setting. More precisely, for all levels, the operator $\mathcal{B}_\ell$ satisfies for all $K \in \mathcal{T}_\ell$ and $v \in L^2(D)$ that

$$\|\mathcal{B}_\ell v\|_{L^2(K)} + H_\ell \|\nabla \mathcal{B}_\ell v\|_{L^2(K)} \leq C_{\mathcal{B}_\ell} \|v\|_{L^2(K)}. \tag{4.10}$$

Furthermore, for all levels, the operator $\mathcal{P}_\ell$ satisfies that

$$\|\mathcal{P}_\ell v\|_{\mathcal{V}(K)} \leq C_{\mathcal{P}_\ell} \|v\|_{\mathcal{V}(\mathsf{N}(K))} \tag{4.11}$$

for all $K \in \mathcal{T}_\ell$ and $v \in \mathcal{V}$, where we recall that the $\mathcal{V}$-norm is now κ-dependent, cf. (4.1). The constants $\mathcal{C}_{\mathcal{B}_\ell}$ and $C_{\mathcal{P}_\ell}$ have the same dependencies as their counterparts $C_{\mathcal{B}_H}$ and $C_{\mathcal{P}_H}$ in the one-level setting.

4.2.2 Level correctors

The construction of the multi-resolution decomposition employs correctors at each level of the mesh hierarchy. At the level ℓ, these correctors are projections onto the closed subspace $\mathcal{W}_\ell \subset \mathcal{V}$ consisting of functions that cannot be resolved by the mesh $\mathcal{T}_\ell$, i.e.,

$$\mathcal{W}_\ell \coloneqq \ker \Pi^0_\ell. \tag{4.12}$$

This space is the multi-resolution analogue to $\mathcal{W}$ defined in (2.17). Using the nesting of the meshes in the hierarchy, we obtain that

$$\mathcal{W}_1 \supset \cdots \supset \mathcal{W}_L. \tag{4.13}$$

Following (3.1), we define for all levels the correctors $\mathcal{C}_\ell, \mathcal{C}^*_\ell \colon \mathcal{V} \to \mathcal{W}_\ell$ such that

$$a(\mathcal{C}_\ell v, w) = a_K(v, w), \qquad a(w, \mathcal{C}^*_\ell v) = a_K(w, v) \tag{4.14}$$

holds for all $v \in \mathcal{V}$ and $w \in \mathcal{W}_\ell$.

For the well-posedness of the corrector problems (4.14), we assume that $\mathcal{T}_1$ satisfies the following resolution condition:

$$H_1 \kappa \leq \frac{\pi}{\sqrt{2}}. \tag{4.15}$$

The following lemma proves that a is coercive on $\mathcal{W}_1 \times \mathcal{W}_1$.

Lemma 4.2.1 (Coercivity of a on $\mathcal{W}_1 \times \mathcal{W}_1$)**.** *Under the resolution condition* (4.15)*, it holds that a is coercive on $\mathcal{W}_1 \times \mathcal{W}_1$, i.e., it holds that*

$$\mathfrak{R}a(w, w) \geq \frac{1}{3} \|w\|_{\mathcal{V}}. \tag{4.16}$$

for all $w \in \mathcal{W}_1$. Furthermore, the norms $\|\cdot\|_{\mathcal{V}}$ and $\|\nabla \cdot\|_{L^2}$ are equivalent on $\mathcal{W}_1$ independently of κ.

Proof. Using (2.25) and (4.15), we obtain for all $w \in \mathcal{W}_1$ that

$$\begin{aligned}\mathfrak{R}a(w,w) &\geq \|\nabla w\|_{L^2}^2 - \kappa^2\|w\|_{L^2} = \|\nabla w\|_{L^2}^2 - \kappa^2\|(\mathtt{id} - \Pi_1^0)w\|_{L^2}^2 \\ &\geq \|\nabla w\|_{L^2}^2 - \pi^{-2}(H_1\kappa)^2\|\nabla w\|_{L^2}^2 \geq \frac{1}{2}\|\nabla w\|_{L^2}^2.\end{aligned}$$

The equivalence of the norms $\|\nabla \cdot\|_{L^2}$ and $\|\cdot\|_{\mathcal{V}}$ on $\mathcal{W}_1$ can be proved in a similar way. For all $w \in \mathcal{W}_1$, we obtain that

$$\|\nabla w\|_{L^2}^2 \leq \|w\|_{\mathcal{V}}^2 = \|\nabla w\|_{L^2}^2 + \kappa^2\|(\mathtt{id} - \Pi_1^0)w\|_{L^2}^2 \leq \frac{3}{2}\|\nabla w\|_{L^2}^2.$$

Combining both estimates yields the assertion. □

From the coercivity of a on $\mathcal{W}_1 \times \mathcal{W}_1$, the following corollary deduces the well-posedness of the corrector problems (4.14) for all levels.

Corollary 4.2.2 (Inf–sup stability of the corrector problems)**.** *If the resolution condition* (4.15) *is satisfied, it holds for all levels ℓ that the sesquilinear form a is inf–sup stable on $\mathcal{W}_\ell \times \mathcal{W}_\ell$, i.e., the condition* (2.18) *holds for $\mathcal{W}_\ell$ with the inf–sup constant*

$$\alpha_{\mathrm{f}} = \frac{1}{3}.$$

Furthermore, the inf–sup conditions (3.18) *and* (3.22) *for local subspaces of $\mathcal{W}_\ell$ hold with the inf–sup constants*

$$\alpha_{\mathrm{d}} = \alpha_{\mathrm{fp}} = \frac{1}{3}.$$

Proof. Using (4.13) and the coercivity of a on $\mathcal{W}_1 \times \mathcal{W}_1$, the coercivity of a on $\mathcal{W}_\ell \times \mathcal{W}_\ell$ follows for all levels ℓ. Since coercivity implies inf–sup stability with the inf–sup constant equal to the coercivity constant, we obtain the inf–sup stability of the real part of a. Using that $|a(v,w)| \geq \mathfrak{R}a(v,w)$ for all $v, w \in \mathcal{V}$, the first assertion follows. The second assertion, which is the inf–sup stability on certain local subspaces of $\mathcal{W}_\ell$, follows similarly.

□

4.2.3 Multi-resolution spaces

We construct the prototypical basis functions of the multi-resolution trial and test spaces by adding corrections to conforming versions of the Haar basis functions. At each level, we define the following two sets of basis functions:

$$\mathbf{B}_\ell \coloneqq \big\{(\mathtt{id} - \mathcal{C}_\ell)\mathcal{B}_\ell\phi : \ \phi \in \mathcal{H}_\ell\big\}, \qquad \mathbf{B}_\ell^* \coloneqq \big\{(\mathtt{id} - \mathcal{C}_\ell^*)\mathcal{B}_\ell\phi : \ \phi \in \mathcal{H}_\ell\big\}. \quad (4.17)$$

The prototypical multi-resolution trial and test spaces at level ℓ are then defined as the span of the above bases, i.e.,

$$U_\ell^{\mathrm{mr}} \coloneqq \operatorname{span}(\mathbf{B}_\ell), \qquad V_\ell^{\mathrm{mr}} \coloneqq \operatorname{span}(\mathbf{B}_\ell^*).$$

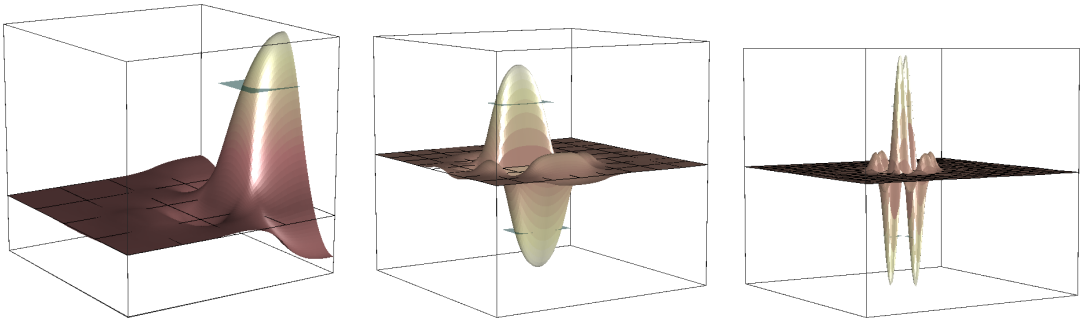

Figure 4.1: Real part of the prototypical MRLOD basis functions for the Helmholtz problem on the unit square with impedance boundary conditions and $\kappa = 4$.

For a depiction of selected basis functions, see Figure 4.1. We define the trial and test spaces of the prototypical MRLOD as the sum of the above multi-resolution spaces, i.e.,

$$U^{\mathrm{mr}} \coloneqq U_1^{\mathrm{mr}} \oplus \cdots \oplus U_L^{\mathrm{mr}}, \qquad V^{\mathrm{mr}} \coloneqq V_1^{\mathrm{mr}} \oplus \cdots \oplus V_L^{\mathrm{mr}}. \tag{4.18}$$

The multi-resolution spaces U_ℓ^{mr} and V_ℓ^{mr} and the kernels $\mathcal{W}_\ell$ satisfy certain "a-orthogonality" relations (recall that a is not an inner product). Using the nesting of the kernels (4.13) and the definition (4.17), we obtain that for all levels k and ℓ with $k \leq \ell$ it holds that

$$a(U_k^{\mathrm{mr}}, \mathcal{W}_\ell) = 0, \qquad a(\mathcal{W}_\ell, V_k^{\mathrm{mr}}) = 0. \tag{4.19}$$

These relations can be used to establish a connection to the prototypical problem-adapted approximation (2.16) on the mesh $\mathcal{T}_L$, as shown in the following lemma.

Lemma 4.2.3 (Equivalence to prototypical approximation)**.** *We denote by U_L^{a} and V_L^{a} the prototypical problem-adapted trial and test spaces with respect to the mesh $\mathcal{T}_L$ defined analogously to* (2.15)*. Then, the following identities hold:*

$$U_L^{\mathrm{a}} = U^{\mathrm{mr}}, \qquad V_L^{\mathrm{a}} = V^{\mathrm{mr}}. \tag{4.20}$$

Proof. We apply (4.19) for $\ell = L$, which shows that the spaces U^{mr} and V^{mr} satisfy $a(U^{\mathrm{mr}}, \mathcal{W}_L) = 0$ and $a(\mathcal{W}_L, V^{\mathrm{mr}}) = 0$. Using Lemma 3.1.1 and Corollary 3.1.2, we obtain the inclusions $U^{\mathrm{mr}} \subset U_L^{\mathrm{a}}$ and $V^{\mathrm{mr}} \subset V_L^{\mathrm{a}}$. Since the spaces have the same dimension, the assertion follows. □

4.2.4 Decoupling of scales

The above "a-orthogonality" relations also imply that the discrete Helmholtz operator is block-diagonal with respect to the prototypical multi-resolution test and trial spaces defined in (4.18). This is proved in the following lemma.

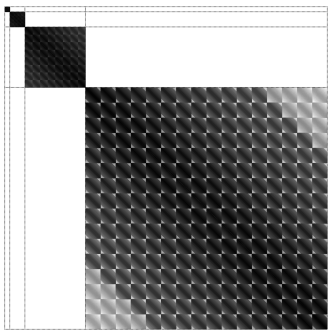

Figure 4.2: Block-diagonal discrete Helmholtz operator with respect to the trial and test spaces U^{mr} and V^{mr}. The magnitude of the matrix entries is indicated by a logarithmic color map.

Lemma 4.2.4 ("a-orthogonality" of levels)**.** *For all levels k and ℓ with $k \neq \ell$, it holds that*

$$a(U_k^{\mathrm{mr}}, V_\ell^{\mathrm{mr}}) = 0.$$

Proof. For levels k and ℓ with $k > \ell$, we first show that $U_k^{\mathrm{mr}} \subset \mathcal{W}_\ell$. Using that all $u_k \in U_k^{\mathrm{mr}}$ can be written as $u_k = (\mathtt{id} - \mathcal{C}_k)\mathcal{B}_k\phi_k$ for some $\phi_k \in \operatorname{span}(\mathcal{H}_k)$ and definition (4.14), we obtain that

$$\Pi_\ell^0(\mathtt{id} - \mathcal{C}_k)\mathcal{B}_k\phi_k = \Pi_\ell^0\Pi_k^0(\mathtt{id} - \mathcal{C}_k)\mathcal{B}_k\phi_k = \Pi_\ell^0\phi_k = 0.$$

Together with (4.19), this implies the assertion. If $k < \ell$, one can similarly show that $V_\ell^{\mathrm{mr}} \subset \mathcal{W}_k$, which again gives the assertion. □

As a consequence, computing the Galerkin approximation with respect to the trial and test spaces U^{mr} and V^{mr} boils down to solving sub-scale problems at each level of the hierarchy and adding up the sub-scale solutions. The sub-scale problem at level ℓ seeks $u_\ell^{\mathrm{mr}} \in U_\ell^{\mathrm{mr}}$ such that

$$a(u_\ell^{\mathrm{mr}}, v) = (f, v)_{L^2} \tag{4.21}$$

holds for all $v \in V_\ell^{\mathrm{mr}}$. The prototypical MRLOD approximation is then obtained by adding up these sub-scale solutions, i.e.,

$$u^{\mathrm{mr}} \coloneqq u_1^{\mathrm{mr}} + \cdots + u_L^{\mathrm{mr}} \in U^{\mathrm{mr}}. \tag{4.22}$$

For a visualization of the block-diagonal discrete Helmholtz operator, see Figure 4.2.

The following lemma proves the well-posedness of the sub-scale problems.

Lemma 4.2.5 (Inf–sup stability of the sub-scale problems)**.** *Let the resolution condition* (4.15) *be satisfied. Then, for all levels, the sesquilinear form a is inf–sup stable on $U_\ell^{\mathrm{mr}} \times V_\ell^{\mathrm{mr}}$, i.e., there exists $\alpha_{\mathrm{a},\ell} > 0$ such that*

$$\inf_{v \in U_\ell^{\mathrm{mr}}} \sup_{w \in V_\ell^{\mathrm{mr}}} \frac{\mathfrak{R}a(v, w)}{\|v\|_{\mathcal{V}}\|w\|_{\mathcal{V}}} \geq \alpha_{\mathrm{a},\ell},$$

where

$$\alpha_{\mathrm{a},\ell} \approx \begin{cases} (C_{\mathrm{st}}(\kappa)\kappa)^{-1} & \ell = 1, \\ 1 & \ell > 1. \end{cases} \tag{4.23}$$

Proof. For $\ell = 1$, the result can be proved using Lemma 2.3.1, which states that the inf–sup constant is given by $C_a^{-1}\alpha_{\mathrm{c}}\alpha_{\mathrm{f}}$. Transferred to the Helmholtz setting, this means that $\alpha_{\mathrm{a},1} \approx (C_{\mathrm{st}}(\kappa)\kappa)^{-1}$, where we used (4.6) and Corollary 4.2.2.

For $\ell > 1$, we note that any $v_\ell \in U_\ell^{\mathrm{mr}}$ can be written as $v_\ell = (\mathtt{id} - \mathcal{C}_\ell)\mathcal{B}_\ell\phi_\ell$ for some $\phi_\ell \in \operatorname{span}(\mathcal{H}_\ell)$. Defining $w_\ell \coloneqq (\mathtt{id} - \mathcal{C}_\ell^*)\mathcal{B}_\ell\phi_\ell$ and using (4.19), we obtain that

$$a(v_\ell, w_\ell) = a((\mathtt{id} - \mathcal{C}_\ell)\mathcal{B}_\ell\phi_\ell, (\mathcal{C}_\ell^* - \mathcal{C}_\ell)\mathcal{B}_\ell\phi_\ell) + a(v_\ell, v_\ell) = a(v_\ell, v_\ell).$$

Since $\ell > 1$, it holds that $v_\ell \in U_\ell^{\mathrm{mr}} \subset \mathcal{W}_1$, which can be concluded in a similar way as in the proof of Lemma 4.2.4. This allows us to apply Lemma 4.2.1, which yields that

$$\mathfrak{R}a(v_\ell, w_\ell) = \mathfrak{R}a(v_\ell, v_\ell) \geq \frac{1}{3}\|v_\ell\|_{\mathcal{V}}^2.$$

It also holds that $w_\ell \in V_\ell^{\mathrm{mr}} \subset \mathcal{W}_1$, which can be shown in a similar way as for v_ℓ. Using this, Lemma 4.2.1 and (4.19), we obtain that

$$\begin{aligned} \frac{1}{3}\|w_\ell\|_{\mathcal{V}}^2 \leq \mathfrak{R}a(w_\ell, w_\ell) &= \mathfrak{R}a((\mathcal{C}_\ell - \mathcal{C}_\ell^*)\mathcal{B}_\ell\phi_\ell, (\mathtt{id} - \mathcal{C}_\ell^*)\mathcal{B}_\ell\phi_\ell) + \mathfrak{R}a(v_\ell, w_\ell) \\ &= \mathfrak{R}a(v_\ell, w_\ell) \leq C_a\|v_\ell\|_{\mathcal{V}}\|w_\ell\|_{\mathcal{V}}. \end{aligned}$$

Combining the previous estimates yields the inf–sup stability with the inf–sup constant $\alpha_{\mathrm{a},\ell} \approx 1$ for $\ell > 1$. □

We obtain the following convergence result for the prototypical MRLOD approximation.

Corollary 4.2.6 (Convergence of the prototypical MRLOD)**.** *For any $f \in H^k(D)$, $k \in \{0, 1\}$, the prototypical MRLOD approximation* (4.22) *satisfies that*

$$\|u - u^{\mathrm{mr}}\|_{\mathcal{V}} \leq 3\pi^{-1-k}H_L^{1+k}|f|_{H^k}.$$

Proof. Since by Lemma 4.2.3, the prototypical MRLOD is equivalent to the prototypical problem-adapted approximation (2.16), we can apply Lemma 2.3.3. The desired estimate then follows by Corollary 4.2.2. □

4.3 Decay and localization

In this section, we show that the prototypical multi-resolution basis functions decay exponentially fast, which justifies their localization in Section 4.4.

For this, we apply LOD techniques at each discretization level. Note that the resolution condition (4.15) guarantees that all inf–sup conditions required by the LOD are satisfied, cf. Corollary 4.2.2. To apply the LOD in the multi-resolution setting, we first extend the definition of patches in (3.11). For all levels, we denote by $\mathsf{N}_{\ell,m}(K)$ the m-th order patch of the element $K \in \mathcal{T}_\ell$ with respect to the mesh $\mathcal{T}_\ell$. Furthermore, we adapt the definition of the element correctors in (3.15) to the multi-resolution setting. For all levels, we define for any $K \in \mathcal{T}_\ell$ the element correctors $\mathcal{C}_{K,\ell}, \mathcal{C}^*_{K,\ell} \colon \mathcal{V} \to \mathcal{W}_\ell$ so that

$$a(\mathcal{C}_{K,\ell} v, w) = a_K(v, w), \qquad a(w, \mathcal{C}^*_{K,\ell} v) = a_K(w, v) \tag{4.24}$$

holds for all $v \in \mathcal{V}$ and $w \in \mathcal{W}_\ell$. For the Helmholtz problem, the restricted sesquilinear form a_K is given by

$$a_K(v, w) \coloneqq (\nabla v \,,\, \nabla w)_{L^2(K)} - \kappa^2 (v \,,\, w)_{L^2(K)} - i\kappa (v \,,\, w)_{L^2(\partial K \cap \partial D)}.$$

The following corollary states the exponential decay of the element corrections at all levels.

Corollary 4.3.1 (Exponential decay of element corrections)**.** *If the resolution condition* (4.15) *is satisfied, there exists $C_{\mathrm{d}} > 0$ depending only on the shape regularity of $\mathcal{T}_1$, such that for all levels ℓ it holds that*

$$\|\mathcal{C}_{K,\ell} v\|_{\mathcal{V}(D \setminus \mathsf{N}_{\ell,m}(K))} \leq \exp(-C_{\mathrm{d}} m) \|\mathcal{C}_K v\|_{\mathcal{V}}$$

for all $K \in \mathcal{T}_\ell$, $v \in \mathcal{V}$, and $m \in \mathbb{N}$. An analogous result holds for $\mathcal{C}^*_{K,\ell}$.

Proof. For each level, this result can be proved similarly to Lemma 3.3.1 with the only difference that the $\mathcal{V}$-norm is now κ-dependent, cf. (4.1). To deal with this κ-dependence, one can use that for functions in $\mathcal{W}_1$ the norms $\|\cdot\|_{\mathcal{V}}$ and $\|\nabla \cdot\|_{L^2}$ are equivalent, cf. Lemma 4.2.1. The resulting constants have the same dependencies as in Lemma 3.3.1. The constant C_{d} depends only on α_{d} and the shape regularity of $\mathcal{T}_\ell$. By Corollary 4.2.2, it holds that $\alpha_{\mathrm{d}} = \frac{1}{3}$. Since the mesh hierarchy is constructed by uniform refinement, the shape regularity of $\mathcal{T}_\ell$ is the same as for $\mathcal{T}_1$. Thus, C_{d} depends only on the shape regularity of $\mathcal{T}_1$. □

Next, for all levels, we perform a localization of the element correctors $\mathcal{C}_{K,\ell}$ and $\mathcal{C}^*_{K,\ell}$ to m-th order patches in the mesh $\mathcal{T}_\ell$. For this purpose, we define local subspaces of $\mathcal{W}_\ell$ for all $K \in \mathcal{T}_\ell$ and $m \in \mathbb{N}$ as follows:

$$\mathcal{W}_{K,\ell,m} \coloneqq \{w \in \mathcal{W}_\ell : \ \operatorname{supp}(w) \subset \mathsf{N}_{\ell,m}(K)\}. \tag{4.25}$$

For all levels, we then define for any $K \in \mathcal{T}_\ell$ the localized element correctors $\mathcal{C}_{K,\ell,m}, \mathcal{C}^*_{K,\ell,m} \colon \mathcal{V} \to \mathcal{W}_{K,\ell,m}$ such that

$$a(\mathcal{C}_{K,\ell,m} v, w) = a_K(v, w), \qquad a(w, \mathcal{C}^*_{K,\ell,m} v) = a_K(w, v) \tag{4.26}$$

holds for all $v \in \mathcal{V}$ and $w \in \mathcal{W}_{K,\ell,m}$. Finally, the localized correctors at level ℓ are obtained as the sum of the localized element correctors at level ℓ, i.e.,

$$\mathcal{C}_{\ell,m} \coloneqq \sum_{K\in\mathcal{T}_\ell} \mathcal{C}_{K,\ell,m}, \qquad \mathcal{C}^*_{\ell,m} \coloneqq \sum_{K\in\mathcal{T}_\ell} \mathcal{C}^*_{K,\ell,m}.$$

The following corollary shows that the localized correctors are exponentially good approximations of their global counterparts.

Corollary 4.3.2 (Localization error)**.** *If the resolution condition* (4.15) *is satisfied, it holds for all levels ℓ that*

$$\|(\mathcal{C}_\ell - \mathcal{C}_{\ell,m})v\|_{\mathcal{V}} \lesssim m^{d/2}\exp(-C_{\mathrm{d}}m)\|v\|_{\mathcal{V}}$$

for all $v \in \mathcal{V}$ and $m \in \mathbb{N}$. The constant C_{d} is from Corollary 4.3.1 and the hidden constant depends only on the quasi-uniformity and shape regularity of $\mathcal{T}_1$. An analogous result holds for the difference $\mathcal{C}^*_\ell - \mathcal{C}^*_{\ell,m}$.

Proof. For each level, this result can be proved similarly to Lemma 3.3.3 with the only difference that the $\mathcal{V}$-norm is now κ-dependent, cf. (4.1). Similar to the proof of Corollary 4.3.1, one can deal with this κ-dependence, by using that for functions in $\mathcal{W}_1$ the norms $\|\cdot\|_{\mathcal{V}}$ and $\|\nabla\cdot\|_{L^2}$ are equivalent, cf. Lemma 4.2.1. All resulting constants have the same dependencies as in Lemma 3.3.3. The hidden constant depends only on α_{f}, α_{fp}, and the quasi-uniformity and shape regularity of $\mathcal{T}_\ell$. By Corollary 4.2.2, it holds that $\alpha_{\mathrm{f}} = \alpha_{\mathrm{fp}} = \frac{1}{3}$. The quasi-uniformity and shape regularity constants of $\mathcal{T}_\ell$ are the same as for the mesh $\mathcal{T}_1$. □

4.4 Practical multi-resolution method

In this section, we introduce the MRLOD based on the considerations in the previous sections. To solve the sub-scale problems (4.21) in practice, the MRLOD uses localized versions of the prototypical multi-resolution basis functions defined in (4.17). These localized basis functions are for all levels defined as

$$\mathbf{B}_{\ell,m} \coloneqq \big\{(\mathtt{id} - \mathcal{C}_{\ell,m})\mathcal{P}_\ell\phi : \ \phi \in \mathcal{H}_\ell\big\}, \qquad \mathbf{B}^*_{\ell,m} \coloneqq \big\{(\mathtt{id} - \mathcal{C}^*_{\ell,m})\mathcal{P}_\ell\phi : \ \phi \in \mathcal{H}_\ell\big\}. \tag{4.27}$$

For all levels, the trial and test spaces of the MRLOD are then obtained as the span of the localized basis functions defined above, i.e.,

$$U^{\mathrm{mr}}_{\ell,m} \coloneqq \operatorname{span}(\mathbf{B}_{\ell,m}), \qquad V^{\mathrm{mr}}_{\ell,m} \coloneqq \operatorname{span}(\mathbf{B}^*_{\ell,m}). \tag{4.28}$$

For a depiction of selected MRLOD basis functions, see Figure 4.3. Practical aspects regarding the computation of the basis functions (4.27) are discussed in Section 4.6.

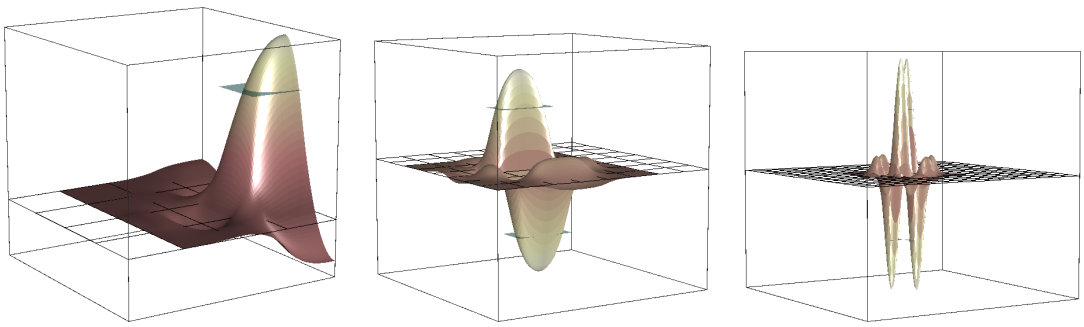

Figure 4.3: Real part of the MRLOD basis functions for the oversampling parameter $m = 1$ for the Helmholtz problem on the unit square with impedance boundary conditions and $\kappa = 4$.

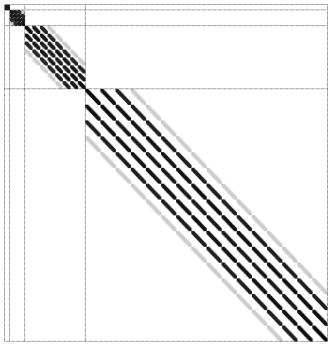

Figure 4.4: Localized discrete Helmholtz operator for $m = 1$, where we set the neglected off-diagonal blocks to zero. The magnitude of the matrix entries is indicated by a logarithmic color map.

Note that the discrete Helmholtz operator is no longer block-diagonal after localization. However, the entries of the off-diagonal blocks decay exponentially as the oversampling parameter m is increased. Thus, for a sufficiently large m, one can neglect the off-diagonal blocks without a notable loss of accuracy. As a consequence, the MRLOD first seeks, for all levels, the sub-scale solutions $u^{\mathrm{mr}}_{\ell,m} \in U^{\mathrm{mr}}_{\ell,m}$, which satisfy that

$$a(u^{\mathrm{mr}}_{\ell,m}, v) = (f, v)_{L^2} \tag{4.29}$$

for all $v \in V^{\mathrm{mr}}_{\ell,m}$. The MRLOD approximation is then obtained as the sum of these sub-scale solutions, i.e.,

$$u^{\mathrm{mr}}_{m} \coloneqq u^{\mathrm{mr}}_{1,m} + \cdots + u^{\mathrm{mr}}_{L,m}. \tag{4.30}$$

For a visualization of the localized block-diagonal discrete Helmholtz operator, see Figure 4.4.

If the oversampling parameter m is chosen large enough, the MRLOD is

sufficiently close to its prototypical counterpart so that the stability result from Lemma 4.2.5 also holds for the MRLOD. This is shown by the following theorem.

Theorem 4.4.1 (Inf–sup stability of the localized sub-scale problems)**.** *Let* (4.5) *and* (4.15) *be satisfied, as well as the oversampling condition*

$$m \gtrsim \begin{cases} \log(\kappa) & \ell = 1, \\ 1 & \ell > 1. \end{cases} \tag{4.31}$$

Then, for all levels ℓ, the sesquilinear form a is inf–sup stable on $U_{\ell,m}^{\mathrm{mr}} \times V_{\ell,m}^{\mathrm{mr}}$, i.e., there exists $\alpha_{\mathrm{mr},\ell} > 0$ such that

$$\inf_{v \in U_{\ell,m}^{\mathrm{mr}}} \sup_{w \in V_{\ell,m}^{\mathrm{mr}}} \frac{\Re a(v,w)}{\|v\|_{\mathcal{V}} \|w\|_{\mathcal{V}}} \geq \alpha_{\mathrm{mr},\ell}$$

with $\alpha_{\mathrm{mr},\ell} \approx \alpha_{\mathrm{a},\ell}$, where $\alpha_{\mathrm{a},\ell}$ is the constant from Lemma 4.2.5. Note that the hidden constants depend only on the quasi-uniformity and shape regularity of $\mathcal{T}_1$.

Proof. At each level ℓ, the inf–sup stability of a on $U_{\ell,m}^{\mathrm{mr}} \times V_{\ell,m}^{\mathrm{mr}}$ can be proved in exactly the same way as in the proof of Theorem 3.4.1. To derive the condition (4.31), we obtain, following the lines of this proof, for any $v_{\ell,m} \in U_{\ell,m}^{\mathrm{mr}}$ the existence of $w_{\ell,m} \in V_{\ell,m}^{\mathrm{mr}}$ such that

$$\Re a(v_{\ell,m}, w_{\ell,m}) \gtrsim (\alpha_{\mathrm{a},\ell} - m^{d/2} \exp(-C_{\mathrm{d}} m)) \|v_{\ell,m}\|_{\mathcal{V}} \|w_{\ell,m}\|_{\mathcal{V}}, \tag{4.32}$$

where $\alpha_{\mathrm{a},\ell}$ is defined in (4.23). The hidden constant depends only on α_{f}, α_{fp}, and the quasi-uniformity and shape regularity of $\mathcal{T}_1$. By Corollary 4.2.2, it holds that $\alpha_{\mathrm{f}} = \alpha_{\mathrm{fp}} = \frac{1}{3}$. Using the assumption (4.5), one obtains that exactly the condition (4.31) is required to absorb the second term into the first. □

Similarly, for sufficiently large oversampling parameters, also the optimal order convergence of the prototypical MRLOD, cf. Corollary 4.2.6, carries over to the localized setting. This is shown by the following theorem.

Theorem 4.4.2 (Convergence of the MRLOD)**.** *If assumptions* (4.5) *and* (4.15) *hold, then for any $f \in H^k(D)$, $k \in \{0,1\}$, the MRLOD approximation* (4.30) *satisfies that*

$$\|u - u_m^{\mathrm{mr}}\|_{\mathcal{V}} \lesssim H_L^{1+k} |f|_{H^k} + (\kappa^{2n+2} + L) m^{d/2} \exp(-C_{\mathrm{d}} m) \|f\|_{L^2}. \tag{4.33}$$

Moreover, if we treat L as a constant and if the oversampling condition

$$m \gtrsim \begin{cases} \log(\frac{\kappa}{H_L}) & \ell = 1, \\ \log(\frac{1}{H_L}) & \ell > 1, \end{cases} \tag{4.34}$$

is satisfied, we get the estimate

$$\|u - u_m^{\mathrm{mr}}\|_{\mathcal{V}} \lesssim H_L^{1+k} \|f\|_{H^k}. \tag{4.35}$$

Note that C_{d} is the constant from Corollary 4.3.1 and that the above hidden constants depend only on the quasi-uniformity and shape regularity of $\mathcal{T}_1$.

Proof. To prove the error estimate (4.33), we first add and subtract the prototypical MRLOD approximation u^{mr} defined in (4.22) and decompose u^{mr} and u_m^{mr} into their level contributions, cf. (4.22) and (4.30). Using the triangle inequality, we obtain that

$$\|u - u_m^{\mathrm{mr}}\|_{\mathcal{V}} \leq \|u - u^{\mathrm{mr}}\|_{\mathcal{V}} + \|u^{\mathrm{mr}} - u_m^{\mathrm{mr}}\|_{\mathcal{V}} \leq \|u - u^{\mathrm{mr}}\|_{\mathcal{V}} + \sum_{\ell=1}^{L} \|u_\ell^{\mathrm{mr}} - u_{\ell,m}^{\mathrm{mr}}\|_{\mathcal{V}}.$$

The first term on the right-hand side can be estimated with Corollary 4.2.6. For the second term, we proceed for each summand exactly as in the proof of Theorem 3.4.2. More precisely, we use that $u_{\ell,m}^{\mathrm{mr}} \in U_\ell^{\mathrm{mr}}$ can be viewed as a non-conforming and non-consistent approximation to $u_\ell^{\mathrm{mr}} \in U_{\ell,m}^{\mathrm{mr}}$. This allows one to apply Strang's lemma (see, e.g., [EG04, Lem. 2.25]), which yields the following estimate for the ℓ-th summand:

$$\|u_\ell^{\mathrm{mr}} - u_{\ell,m}^{\mathrm{mr}}\|_{\mathcal{V}} \lesssim \alpha_{\mathrm{a},\ell}^{-1} \alpha_{\mathrm{mr},\ell}^{-1} m^{d/2} \exp(-C_{\mathrm{d}} m) \|f\|_{L^2},$$

where we use that $\kappa \in (\kappa_0, \infty)$ for some fixed $\kappa_0 > 0$, cf. Section 4.1. The hidden constant depends only on α_{f}, α_{fp}, and the quasi-uniformity and shape regularity of $\mathcal{T}_1$. By Corollary 4.2.2, it holds that $\alpha_{\mathrm{f}} = \alpha_{\mathrm{fp}} = \frac{1}{3}$. Using the polynomial-in-κ stability assumption (4.5) and the dependence of the constants $\alpha_{\mathrm{a},\ell}$ and $\alpha_{\mathrm{mr},\ell}$ on κ as stated in Lemma 4.2.5 and Theorem 4.4.1, one obtains that $\alpha_{\mathrm{a},\ell}^{-1}\alpha_{\mathrm{mr},\ell}^{-1}$ scales like $\mathcal{O}(\kappa^{2n+2})$ for $\ell = 1$ and like $\mathcal{O}(1)$ for $\ell > 1$. Combining the above estimates gives the error bound (4.33).

Provided that the oversampling condition (4.34) is satisfied, the estimate (4.35) is a direct consequence of (4.33), if we treat L as a constant. □

4.5 Fast solvers

In this section, we study the efficient numerical solution of the localized sub-scale problems (4.29). We show that the sub-scale problems corresponding to levels $\ell > 1$ can be solved by the Generalized Minimal Residual (GMRES) method, cf. [Saa03], up to a given tolerance within a few iterations. The rather low-dimensional first sub-scale problem can be solved with a direct solver.

Subsequently, we denote the number of Haar basis functions at level ℓ by $N_\ell \coloneqq \#\mathcal{H}_\ell$. Furthermore, we denote the prototypical basis functions at level ℓ for $j = 1, \dots, N_\ell$ by $b_{\ell,j}$ and $b_{\ell,j}^*$, cf. (4.17). Similarly, we denote their localized counterparts for $j = 1, \dots, N_\ell$ by $b_{\ell,m,j}$ and $b_{\ell,m,j}^*$, cf. (4.27). The sub-scale problems (4.29) can then be rewritten as the linear system of equations

$$\mathbf{A}_{\ell,m} \mathbf{x}_{\ell,m} = \mathbf{f}_{\ell,m}, \tag{4.36}$$

where

$$\mathbf{A}_{\ell,m} \coloneqq \big(a(b_{\ell,m,k}, b_{\ell,m,j}^*)\big)_{j,k=1,\dots,N_\ell}, \qquad \mathbf{f}_{\ell,m} \coloneqq \big((f, b_{\ell,m,j}^*)_{L^2}\big)_{j=1,\dots,N_\ell}.$$

The convergence properties of the GMRES method are determined by the field of values of the considered matrix. For an invertible matrix $\mathbf{A} \in \mathbb{C}^{N\times N}$, we define the field of values by

$$\mathcal{F}(\mathbf{A}) \coloneqq \left\{ (\mathbf{A}\xi, \xi) \,:\, \xi \in \mathbb{C}^N,\ |\xi| = 1 \right\},$$

where $(\cdot,\cdot)$ denotes the Euclidean inner product on $\mathbb{C}^N$ and $|\cdot|$ denotes its induced norm. Let us consider a right-hand side $\mathbf{f} \in \mathbb{C}^N$ and denote by $\mathbf{x}^{(k)}$ the k-th GMRES iterate (without restart) applied to $\mathbf{A}\mathbf{x} = \mathbf{f}$. Then, the residuals $\mathbf{r}^{(k)} \coloneqq \mathbf{A}\mathbf{x}^{(k)} - \mathbf{f}$ converge to zero with

$$\frac{|\mathbf{r}^{(k)}|}{|\mathbf{r}^{(0)}|} \leq \left(1 - \frac{\min_{\xi\in\mathcal{F}(\mathbf{A})} |\xi|^2}{\|\mathbf{A}\|^2}\right)^{k/2}, \tag{4.37}$$

where $\|\cdot\|$ denotes the spectral norm of a matrix, cf. [LT20].

Using this convergence result, the following theorem proves the uniform convergence of the GMRES method applied to the sub-scale problems (4.29).

Theorem 4.5.1 (Uniform convergence of the GMRES)**.** *We consider the sub-scale problems* (4.29) *for* $\ell > 1$*. If* (4.15) *and* $m \gtrsim 1$ *(the hidden constant depends only on the quasi-uniformity and shape regularity of* $\mathcal{T}_1$*) is satisfied, the linear system* (4.36) *can be solved with the GMRES method up to a given relative tolerance within a fixed number of iterations depending only on the tolerance.*

Proof. Let the level $\ell > 1$ be fixed. First, we consider the prototypical setting, i.e., we prove upper and lower bounds for the field of values of the matrix

$$\mathbf{A}_\ell \coloneqq \left(a(b_{\ell,k}, b^*_{\ell,j})\right)_{j,k=1,\dots,N_\ell}.$$

Denoting by $\phi_{\ell,j}$ the Haar basis functions at the level ℓ (i.e., the elements of $\mathcal{H}_\ell$), we obtain for any $\xi \in \mathbb{C}^{N_\ell}$ the upper bound

$$\begin{aligned}
|\,(\mathbf{A}_\ell\xi,\xi)\,| &= \left| a\left(\sum_{j=1}^{N_\ell} \xi_j b_{\ell,j}, \sum_{j=1}^{N_l} \xi_j b^*_{\ell,j}\right)\right| = \left| a\left(\sum_{j=1}^{N_\ell} \xi_j b_{\ell,j}, \sum_{j=1}^{N_\ell} \xi_j b_{\ell,j}\right)\right| \\
&\lesssim \left\| \sum_{j=1}^{N_\ell} \xi_j b_{\ell,j} \right\|^2_{\mathcal{V}} = \left\| (\mathtt{id} - \mathcal{C}_\ell)\left(\sum_{j=1}^{N_\ell} \xi_j \mathcal{B}_\ell \phi_{\ell,j}\right)\right\|^2_{\mathcal{V}} \\
&\lesssim \left\| \sum_{j=1}^{N_\ell} \xi_j \mathcal{B}_\ell \phi_{\ell,j} \right\|^2_{\mathcal{V}} = \kappa^2 \left\| \sum_{j=1}^{N_\ell} \xi_j \mathcal{B}_\ell \phi_{\ell,j} \right\|^2_{L^2} + \left\| \nabla\left(\sum_{j=1}^{N_\ell} \xi_j \mathcal{B}_\ell \phi_{\ell,j}\right)\right\|^2_{L^2} \\
&\lesssim \frac{(H_\ell\kappa)^2 + 1}{H_\ell^2} \left\| \sum_{j=1}^{N_\ell} \xi_j \phi_{\ell,j} \right\|^2_{L^2} \lesssim \frac{1}{H_\ell^2} |\xi|^2,
\end{aligned}$$

where we used (2.2), (4.10), (4.15), and (4.19) and the continuity of $\mathtt{id} - \mathcal{C}_\ell$, which holds due to Corollary 4.2.2 and the fact that $\mathcal{C}_\ell$ and $\mathtt{id} - \mathcal{C}_\ell$ have the

same operator norms, cf. [Szy06]. Using similar arguments, as well as (2.25) and Lemma 4.2.1, we obtain the lower bound

$$\begin{aligned}
|\left(\mathbf{A}_\ell \xi, \xi\right)| &= \left| a\left(\sum_{j=1}^{N_\ell} \xi_j b_{\ell,j}, \sum_{j=1}^{N_l} \xi_j b^*_{\ell,j}\right)\right| = \left| a\left(\sum_{j=1}^{N_\ell} \xi_j b_{\ell,j}, \sum_{j=1}^{N_l} \xi_j b_{\ell,j}\right)\right| \\
&\gtrsim \left\| \nabla \left(\sum_{j=1}^{N_l} \xi_j b_{\ell,j}\right)\right\|^2_{L^2} \gtrsim \frac{1}{H_\ell^2} \left\| (\mathtt{id} - \Pi^0_{\ell-1}) \left(\sum_{j=1}^{N_l} \xi_j b_{\ell,j}\right)\right\|^2_{L^2} \\
&= \frac{1}{H_\ell^2} \left\| \sum_{j=1}^{N_l} \xi_j b_{\ell,j}\right\|^2_{L^2} \geq \frac{1}{H_\ell^2} \left\| \sum_{j=1}^{N_l} \xi_j \Pi^0_\ell b_{\ell,j}\right\|^2_{L^2} \\
&= \frac{1}{H_\ell^2} \left\| \sum_{j=1}^{N_l} \xi_j \phi_{\ell,j}\right\|^2_{L^2} = \frac{1}{H_\ell^2} |\xi|^2.
\end{aligned}$$

The next step is to transfer the field of values bound for the prototypical approximation to the localized setting. Using (4.19), we obtain that

$$\begin{aligned}
(\mathbf{A}_{\ell,m} \xi, \xi) &= a\left(\sum_{j=1}^{N_\ell} \xi_j b_{\ell,m,j}, \sum_{j=1}^{N_l} \xi_j b^*_{\ell,m,j}\right) \\
&= a\left(\sum_{j=1}^{N_\ell} \xi_j b_{\ell,j}, \sum_{j=1}^{N_l} \xi_j b_{\ell,j}\right) + a\left(\sum_{j=1}^{N_\ell} \xi_j (b_{\ell,m,j} - b_{\ell,j}), \sum_{j=1}^{N_l} \xi_j b^*_{\ell,m,j}\right).
\end{aligned}$$

For the first term, we apply the field of values bounds for the prototypical approximation. In the following, we show that the second term is exponentially small. Using (2.2), (4.10), (4.11), and (4.15) and Corollary 4.3.2, we obtain that

$$\begin{aligned}
&\left| a\left(\sum_{j=1}^{N_\ell} \xi_j (b_{\ell,m,j} - b_{\ell,j}), \sum_{j=1}^{N_l} \xi_j b^*_{\ell,m,j}\right)\right| \\
&\quad \lesssim \left\| (\mathcal{C}_{\ell,m} - \mathcal{C}_\ell) \left(\sum_{j=1}^{N_\ell} \xi_j \mathcal{P}_\ell \mathcal{B}_\ell \phi_{\ell,j}\right)\right\|_{\mathcal{V}} \left\| \left(\mathtt{id} - \mathcal{C}^*_{\ell,m}\right) \left(\sum_{j=1}^{N_\ell} \xi_j \mathcal{P}_\ell \mathcal{B}_\ell \phi_{\ell,j}\right)\right\|_{\mathcal{V}} \\
&\quad \lesssim m^{d/2} \exp(-C_{\mathrm{d}} m) \left\| \mathcal{P}_\ell \left(\sum_{j=1}^{N_\ell} \xi_j \mathcal{B}_\ell \phi_{\ell,j}\right)\right\|^2_{\mathcal{V}} \\
&\quad \lesssim m^{d/2} \exp(-C_{\mathrm{d}} m) \left(\kappa^2 \left\| \sum_{j=1}^{N_\ell} \xi_j \mathcal{B}_\ell \phi_{\ell,j}\right\|^2_{L^2} + \left\| \nabla \left(\sum_{j=1}^{N_\ell} \xi_j \mathcal{B}_\ell \phi_{\ell,j}\right)\right\|^2_{L^2}\right) \\
&\quad \lesssim m^{d/2} \exp(-C_{\mathrm{d}} m) \frac{((H_\ell \kappa)^2 + 1)}{H_\ell^2} \left\| \sum_{j=1}^{N_\ell} \xi_j \phi_{\ell,j}\right\|^2_{L^2} \\
&\quad \lesssim \frac{m^{d/2} \exp(-C_{\mathrm{d}} m)}{H_\ell^2} |\xi|^2.
\end{aligned}$$

In the estimate above, we also used the continuity of $\mathtt{id} - \mathcal{C}^*_{\ell,m}$, which can be proved using Corollary 4.3.2 and the continuity of $\mathtt{id} - \mathcal{C}^*_\ell$. Note that the continuity of $\mathtt{id} - \mathcal{C}^*_\ell$ can be shown similarly as described above using Corollary 4.2.2 and the fact that $\mathcal{C}^*_\ell$ and $\mathtt{id} - \mathcal{C}^*_\ell$ have the same operator norms, cf. [Szy06].

Combining the previous estimates, we obtain that

$$\frac{\min_{\xi \in \mathcal{F}(\mathbf{A}_{\ell,m})} |\xi|^2}{\max_{\xi \in \mathcal{F}(\mathbf{A}_{\ell,m})} |\xi|^2} \gtrsim \frac{1 - m^{d/2} \exp(-C_{\mathrm{d}} m)}{1 + m^{d/2} \exp(-C_{\mathrm{d}} m)} |\xi|^2.$$

Using the oversampling condition $m \gtrsim 1$, we further get that

$$0 < C < \frac{1}{4} \frac{\min_{\xi \in \mathcal{F}(\mathbf{A}_{\ell,m})} |\xi|^2}{\max_{\xi \in \mathcal{F}(\mathbf{A}_{\ell,m})} |\xi|^2} \leq \frac{\min_{\xi \in \mathcal{F}(\mathbf{A}_{\ell,m})} |\xi|^2}{\|\mathbf{A}_{\ell,m}\|^2} < 1,$$

where we applied the inequality

$$\max_{\xi \in \mathcal{F}(\mathbf{A}^m_\ell)} |\xi| \leq \|\mathbf{A}^m_\ell\| \leq 2 \max_{\xi \in \mathcal{F}(\mathbf{A}^m_\ell)} |\xi|,$$

see [HJ90, Ch. 1]. The constant C depends only on the quasi-uniformity and shape regularity of $\mathcal{T}_1$ and, in particular, is independent of κ. Applying the GMRES convergence result (4.37), yields the assertion. □

4.6 Implementation aspects

In this section we discuss aspects related to the practical implementation of the MRLOD. First, we note that all the element corrector problems (4.26) are independent of each other and thus can be solved in parallel. Furthermore, since the coefficient κ of the Helmholtz problem is constant in space (and thus in particular periodic with respect to $\mathcal{T}_L$), only the solution to $\mathcal{O}(m^d)$ corrector problems is required at each level. The solution to the other problems can be obtained by translation, cf. [GP15]. Moreover, using the properties of the Helmholtz sesquilinear form, one can show that $\mathcal{C}^*_{K,\ell,m} v = \overline{\mathcal{C}_{K,\ell,m} \overline{v}}$ holds for all $v \in \mathcal{V}$, cf. [Pet16]. Note that such an identity is well known for the solution operator of Helmholtz problems, see, e.g., [MS11, Lem. 3.1]. Using this identity, we can show that for any $\phi \in \mathcal{H}_\ell$ it holds that

$$(\mathtt{id} - \mathcal{C}^*_{\ell,m}) \mathcal{P}_\ell \phi = \overline{(\mathtt{id} - \mathcal{C}_{\ell,m}) \mathcal{P}_\ell \phi},$$

where we used that $\overline{\mathcal{P}_\ell \phi} = \mathcal{P}_\ell \phi$. A direct consequence of this identity is that only one of the two sets of basis functions in (4.27) needs to be computed, and the other one can be obtained by complex conjugation.

Another important aspect is the fine-scale discretization of the MRLOD, which can be done similarly as described in Section 3.5. For this, we replace the space $\mathcal{V}$ in the derivation of the MRLOD by its fine-scale FE counterpart V_h^{fem}

defined with respect to the fine mesh $\mathcal{T}_h$ obtained by refining $\mathcal{T}_L$. For a reliable MRLOD approximation, the fine-scale FEM solution must be an accurate approximation of the continuous solution, cf. Theorem 3.5.1. For the $\mathcal{Q}^1$-FEM, a classical assumption that guarantees stability and convergence is that $\kappa^2 h$ is sufficiently small, see [Mel95]. This assumption is much stronger than the requirement needed to resolve the oscillations of the solution, which is known as the pollution effect. Note that for the Helmholtz problem it may be particularly useful to use *hp*-FEMs for the fine-scale discretization, as these methods are able to achieve stability and convergence under more moderate assumptions on the discretization parameters, cf. [MS10; MS11; MPS13]. However, this is not done here, since the focus lies on the construction of the MRLOD and the efficient solution of the coarse system matrix rather than the fine-scale discretization.

In Lemma 4.2.1 it was shown that all corrector problems are coercive. However, this has no real practical benefit, since the explicit construction of the spaces $\mathcal{W}_\ell$ and their local counterparts $\mathcal{W}_{K,\ell,m}$ is difficult. It is more practicable to use a saddle-point formulation of the corrector problems with $\mathcal{O}(m^d)$ constraints enforcing that the solution is in $\mathcal{W}_{K,\ell,m}$, see, e.g., [Eng+19] and [MP20, Ch. 7]. Due to the small number of constraints, one typically computes the Schur complement of the saddle point problem explicitly by solving $\mathcal{O}(m^d)$ local Helmholtz problems on each patch. Since the patches have at most a diameter of the order $\mathcal{O}(mH_1)$, the effective wavenumber of the patch problems is at most $\mathcal{O}(m)$ by (4.15). For such Helmholtz problems there are effective preconditioners, see for example the review article [GZ19].

4.7 Numerical experiments

This section numerically studies the MRLOD for Helmholtz problems. We consider uniform Cartesian meshes of the domain D, where the mesh size denotes the side length of the elements instead of their diameter. Note that for simplicity, we use the same oversampling parameter on all levels. The fine-scale discretization of the MRLOD is performed similarly as described in Sections 3.5 and 4.6. It is based on a fine Cartesian mesh $\mathcal{T}_h$ obtained by uniform refinement of the finest mesh in the hierarchy $\mathcal{T}_L$. Henceforth, unless otherwise stated, all errors are relative errors with respect to the κ-dependent norm (4.1) computed with the fine-scale FE solution as the reference solution.

Optimal order convergence

First, we numerically study the convergence properties of the MRLOD in dependence of the wavenumber κ. We consider the domain $D = (0,1)^2$ with homogeneous impedance boundary conditions, i.e. $\Gamma_2 = \partial D$. For consistency reasons, we use the same source term as in Section 3.6, namely:

$$f(x_1, x_2) = (x_1 + \cos(3\pi x_1)) \cdot x_2^3.$$

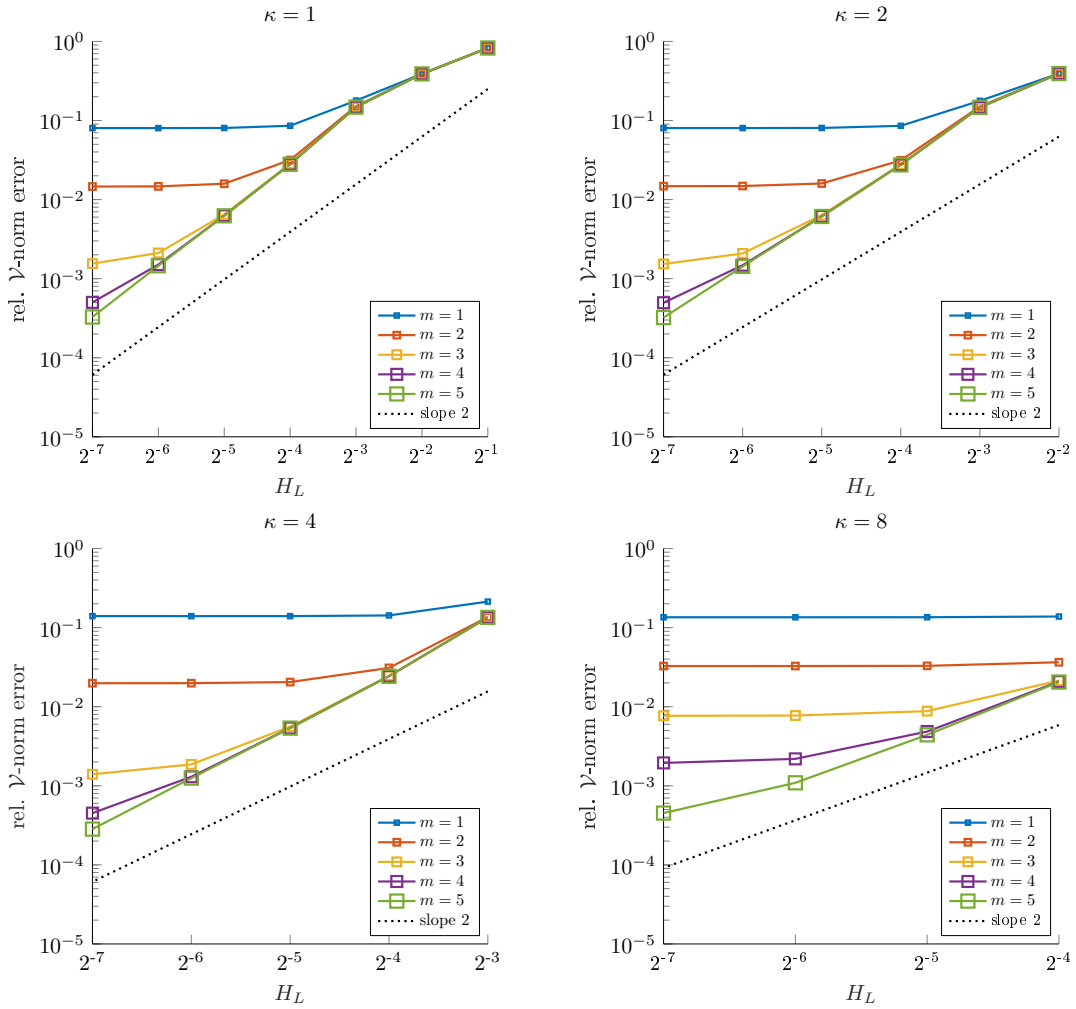

Figure 4.5: Error of the MRLOD as a function of H_L for several oversampling parameters m and wavenumbers κ. The dotted line indicates the expected rate of convergence.

For $\kappa = 2^j$, $j = 0, \dots, 3$, we consider the hierarchy of meshes obtained by uniformly refining the uniform Cartesian mesh $\mathcal{T}_1$ with $H_1 = 2^{-1}\kappa^{-1}$. We note that the κ-dependent choice of the mesh size H_1 satisfies the resolution condition (4.15). For the fine-scale discretization we use the Cartesian mesh $\mathcal{T}_{2^{-9}}$.

Figure 4.5 shows the convergence of the MRLOD as successively finer mesh levels are added to the hierarchy. The finest considered mesh has the mesh size $H_L = 2^{-7}$. If the oversampling parameter m is chosen sufficiently large, one observes convergence of second order. Recalling that $f \in H^1(D)$, this is consistent with the theoretical prediction in Theorem 4.4.2. For small m and comparably large κ, one observes that the error of the MRLOD remains of order one as finer mesh levels are added to the hierarchy. The reason for this effect is that m may not satisfy the condition (4.31). Therefore, convergence cannot

Table 4.1: Properties of the sub-scale problems (4.36) and GMRES iterations needed for reaching a relative residual of 10^{-6}.

ℓ	1	2	3	4	5
H_ℓ	2^{-5}	2^{-6}	2^{-7}	2^{-8}	2^{-9}
$\#\mathcal{H}_\ell$	240	720	2880	11520	46080
$\mathrm{cond}_2(\mathbf{A}_{\ell,2})$	198	23	17	16	16
iterations	176	21	17	16	15

be expected.

Uniform number of GMRES iterations

Next, we numerically investigate the number of GMRES iterations needed to solve the sub-scale problems (4.29) up to a given tolerance. We consider the domain $D = (0,1)^2 \backslash S$ with the scatterer $S = [\frac{3}{8}, \frac{5}{8}]^2$. At the boundary of S, we impose homogeneous Dirichlet boundary conditions, i.e., $\Gamma_3 = \partial S$. Furthermore, at the remaining boundary $\partial D \backslash \partial S$, we impose homogeneous impedance boundary conditions, i.e., $\Gamma_2 = \partial D \backslash \partial S$. For this numerical experiment, we choose $\kappa = 2^5$ and consider the source term

$$f(x) = \begin{cases} 10^4 \times \exp\left(\frac{1}{1-\frac{|x-x_0|^2}{r^2}}\right) & \text{if } |x - x_0| < r, \\ 0 & \text{else,} \end{cases} \tag{4.38}$$

where $r = \frac{1}{20}$ and $x_0 = (\frac{1}{8}, \frac{1}{8})$. The hierarchy of meshes used is specified in Table 4.1. We choose the oversampling parameter $m = 2$ and use the Cartesian mesh $\mathcal{T}_{2^{-12}}$ for the fine-scale discretization. To avoid excessive memory consumption, we restart the GMRES method every 50 iterations. The GMRES method terminates if a relative residual of 10^{-6} is reached.

Table 4.1 shows the number of GMRES iterations needed to solve the sub-scale problems (4.36) up to the prescribed accuracy. The uniform boundedness of the number of iterations for $\ell > 1$ is in line with the theoretical prediction in Theorem 4.5.1. The high number of iterations for $\ell = 1$ shows that the GMRES method performs poorly when applied to the first level. Note that the poor performance of the GMRES for the first sub-scale problem is strongly related to the unfavorable scaling of the corresponding inf–sup constant in κ, see Theorem 4.4.1. Therefore, it is recommended to solve this relatively small linear system with a direct solver. The spectral condition numbers of the sub-scale problems (4.36), which are typically a good indicator of the convergence behavior of iterative solvers, support the above observations.

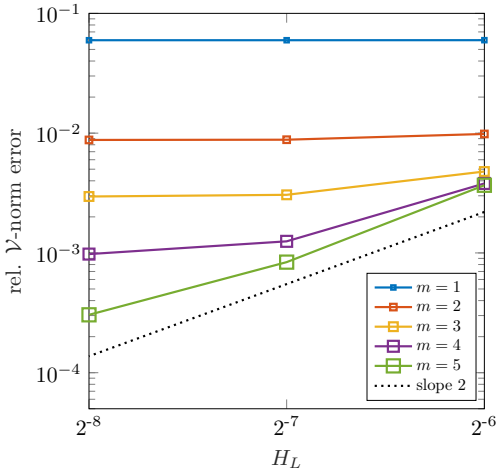

Figure 4.6: Error of the MRLOD as a function of H_L for several oversampling parameters m. The dotted line indicates the expected rate of convergence.

High-frequency Helmholtz problem

In the next numerical experiment, we again consider the domain $D = (0,1)^2$, but this time with the relatively large wavenumber $\kappa = 2^6$. We impose homogeneous impedance boundary conditions on the whole boundary, i.e., $\Gamma_2 = \partial D$. As source term, we use the one defined in (4.38) with $r = \frac{1}{8}$ and $x_0 = (\frac{1}{2}, \frac{1}{2})^T$. The hierarchy of meshes used in this experiment is obtained by uniform refinement of the uniform Cartesian mesh $\mathcal{T}_1$ with $H_1 = 2^{-6}$. The finest considered mesh in the hierarchy has the mesh size $H_L = 2^{-8}$. For the fine-scale discretization, we employ the Cartesian mesh $\mathcal{T}_{2^{-10}}$.

Provided that the oversampling parameter m is chosen sufficiently large, Figure 4.6 shows second order convergence for the MRLOD as finer levels are added to the hierarchy of meshes. This is again consistent with the theoretical predictions in Theorem 4.4.2.

Heterogeneous media

This numerical example shall illustrate that the MRLOD is also applicable to heterogeneous Helmholtz problems of the form

$$-\nabla \cdot (A\nabla u) - \kappa^2 u = f,$$

where A is a coefficient with uniform upper and lower bounds that describes the properties of the medium at hand. We consider the domain $D = (0,1)^2$ with homogeneous impedance boundary conditions, i.e., $\Gamma_2 := \partial D$. For the definition of the coefficient A, we define for $j \in \mathbb{Z}^2$ and $\epsilon = 2^{-7}$ the following inclusions:

$$S_\epsilon^j := \epsilon\Big(j + \big(\tfrac{1}{4}, \tfrac{3}{4}\big)^2\Big).$$

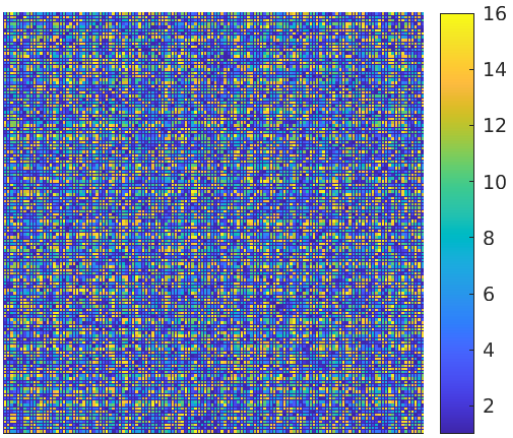

Figure 4.7: Heterogeneous coefficient A used in the numerical experiment.

For all inclusions contained in D, the coefficient A then takes constant values that are obtained as realizations of independent and uniformly distributed random variables in the interval $[1, 16]$. Elsewhere, the coefficient A is set to 1. For a visualization of A, see Figure 4.7. We remark that, since $A|_{\partial D} = 1$, the coefficient is compatible with the impedance boundary conditions introduced in Section 4.1. In the heterogeneous setting, one typically uses the norm

$$\|\cdot\|_{\mathcal{V}}^2 = \|A^{1/2}\nabla\cdot\|_{L^2}^2 + \kappa^2\|\cdot\|_{L^2}^2 \tag{4.39}$$

instead of the one defined in (4.1). This norm is henceforth used for the error computation. We choose $\kappa = 2^4$ and use the source term defined in (4.38) with $r = \frac{1}{8}$ and $x_0 = (\frac{1}{2}, \frac{1}{2})^T$. Note that the above choice of A results in a lower effective wavenumber of the problem inside the inclusions. We use a hierarchy of meshes obtained by uniform refinement of the uniform Cartesian mesh $\mathcal{T}_1$ with $H_1 = 2^{-4}$. The finest considered mesh in the hierarchy is the Cartesian mesh with the mesh size $H_L = 2^{-7}$. For the fine-scale discretization we use the Cartesian mesh $\mathcal{T}_{2^{-9}}$.

Quantitatively, the convergence behavior in Figure 4.8 is similar to that in the previous numerical experiments, i.e., one observes second order convergence provided that the oversampling parameter is chosen sufficiently large. This demonstrates the applicability of the MRLOD to heterogeneous Helmholtz problems.

Note that we have not addressed the well-posedness and the polynomial-in-κ stability of the considered heterogeneous Helmholtz problem, cf. (4.5) and (4.6). These properties are necessary for the theoretical results of the MRLOD to hold also in the heterogeneous setting. We refer to [ST18; GPS19; GS19] for a theoretical investigation of heterogeneous Helmholtz problems.

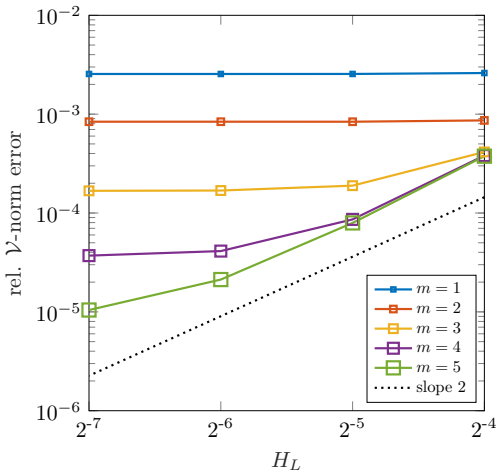

Figure 4.8: Error of the MRLOD as a function of H_L for several oversampling parameters m. The dotted line indicates the expected rate of convergence.

5 Super-Localized Orthogonal Decomposition

In Chapter 3, we have introduced the LOD, which constructs its problem-adapted basis functions by solving local sub-scale correction problems. Equivalently, the LOD basis functions can be obtained as solutions to local constraint energy minimization problems, where the constraints impose a Kronecker delta condition on the QOIs of the basis functions, cf. [OS19; Mai21]. The constraints on the QOIs cause the LOD basis functions to decay exponentially fast.

In this chapter, we will introduce a novel localization approach, which we refer to as Super-Localized Orthogonal Decomposition (SLOD). The idea of the SLOD is to drop the constraints on the QOIs of the basis functions and to enforce their decay in a more direct way. Given an element and its m-th order patch, the SLOD identifies a local FE source term whose response decays rapidly under the local solution operator. The decay is enforced by minimizing the conormal derivative of the response at the patch boundary. The SLOD performs this procedure for all elements and uses the resulting local responses as its basis functions. In practice, one observes that the localization error of the SLOD decays super-exponentially as the oversampling parameter m is increased, i.e., it behaves like $\exp(-Cm^{d/(d-1)})$, where $C > 0$ is a constant and d denotes the spatial dimension. In one dimension, the localization error is zero, and thus the SLOD provides a truly local basis, see Figure 2.5. The super-exponential localization properties of the SLOD represent a significant improvement over other state-of-the-art localization techniques, such as the LOD with exponential localization properties, cf. Theorem 3.4.2. However, a rigorous proof of the super-exponential localization property is still open, and we can only provide a justification using a conjecture related to spectral geometry. Nevertheless, using LOD techniques, one can prove that the novel localization approach yields at least exponentially decaying localization errors. The main advantages of the novel localization strategy are its lower computational cost for the basis computation due to the considerably smaller supports of the basis functions and a sparser coarse system matrix.

For the LOD, the Kronecker delta property of the basis functions with respect to the QOIs ensures the stability of the basis. For the SLOD, however, we drop these constraints for better localization properties. As a consequence, we are no longer able to ensure the stability of the basis a priori. This issue is resolved in Chapter 6, where we combine the SLOD with a partition of unity approach and thereby enforce the basis stability. In the following, we introduce the SLOD in

the general setting from Chapter 2.

The content and presentation of the following chapter is primarily based on the journal and preprint articles

[HP22b] M. Hauck and D. Peterseim. "Super-localization of elliptic multiscale problems". In: *Math. Comp.* 92.341 (2022), pp. 981–1003

[FHP21] P. Freese, M. Hauck, and D. Peterseim. "Super-localized orthogonal decomposition for high-frequency Helmholtz problems". In: *arXiv preprint 2112.11368* (2021)

5.1 Localized spaces and operators

Before we present the novel localization approach of the SLOD, we introduce some notation and preliminaries. As usual, localization is based on the concept of patches. In the following, we fix the element $K \in \mathcal{T}_H$ and abbreviate its m-th order patch by $S \coloneqq \mathsf{N}_m(K)$. We denote the space of $\mathcal{T}_H$-piecewise constants restricted to S by $\mathcal{P}^0(S)$. Furthermore, we denote by $\Pi^0_{H,S}\colon L^2(S) \to \mathcal{P}^0(S)$ the $L^2(S)$-orthogonal projection onto $\mathcal{P}^0(S)$. Recalling that $\mathcal{V}(S) \coloneqq \mathcal{V}|_S$, we define the sesquilinear form $a_S\colon \mathcal{V}(S) \times \mathcal{V}(S) \to \mathbb{C}$ by restricting the integrals in the definition of a to S. Similar to (3.14), we require that a_S is continuous, i.e., it holds that

$$|a_S(v,w)| \leq C_a \|v\|_{\mathcal{V}(S)} \|w\|_{\mathcal{V}(S)} \tag{5.1}$$

for all $v, w \in \mathcal{V}(S)$. Since the constant C_a is typically the same as the constant in (2.2), we will not introduce a new constant for simplicity. The novel localization approach uses local versions of the solution operators $\mathcal{L}$ and $\mathcal{L}^*$. We define the local solution space by

$$\mathcal{V}_S \coloneqq \{v \in \mathcal{V}(S) : \ v|_{\partial S \setminus \partial D} = 0\} \tag{5.2}$$

whose boundary conditions are chosen such that an extension by zero yields a conforming subspace of $\mathcal{V}$. The local solution operator and its adjoint counterpart are then defined by $\mathcal{L}^*_S\colon \mathcal{V}_S^* \to \mathcal{V}_S$, $F_S \mapsto u_S$ and $\mathcal{L}^*_S\colon \mathcal{V}_S^* \to \mathcal{V}_S$, $F_S \mapsto w_S$, respectively, where u_S and w_S satisfy for all $v \in \mathcal{V}_S$ that

$$a_S(u_S, v) = F_S(v), \qquad \overline{a_S(v, w_S)} = F_S(v). \tag{5.3}$$

To ensure that the operators $\mathcal{L}_S$ and $\mathcal{L}^*_S$ are well-defined and continuous, we assume that a_S is inf–sup stable on $\mathcal{V}_S \times \mathcal{V}_S$, i.e., there exists $\alpha_{\mathrm{p}} > 0$ such that

$$\inf_{v \in \mathcal{V}_S} \sup_{w \in \mathcal{V}_S} \frac{|a_S(v,w)|}{\|v\|_{\mathcal{V}} \|w\|_{\mathcal{V}}} = \inf_{w \in \mathcal{V}_S} \sup_{v \in \mathcal{V}_S} \frac{|a_S(v,w)|}{\|v\|_{\mathcal{V}} \|w\|_{\mathcal{V}}} \geq \alpha_{\mathrm{p}}. \tag{5.4}$$

While for coercive problems this condition follows immediately since $\mathcal{V}_S \subset \mathcal{V}$, it must be proved separately for indefinite problems. The following remark discusses the validity of the condition (5.4) for Helmholtz problems.

Remark 5.1.1 (Local inf–sup stability for the Helmholtz problem)**.** For the Helmholtz problem introduced in Section 4.1, the inf–sup stability (5.4) can be shown under the resolution condition $\kappa H m \lesssim 1$, which is a slightly stronger condition than (4.15). The proof requires Friedrichs' inequality for functions in $\mathcal{V}_S$, i.e., for all $v \in \mathcal{V}_S$ it holds that

$$\|v\|_{L^2(S)} \leq C_{\mathrm{F}} \operatorname{diam}(S) \|\nabla v\|_{L^2(S)},$$

cf. [FHP21, Rem. 4.1]. Using this inequality and the above resolution condition, we obtain for all $v \in \mathcal{V}_S$ that

$$\mathfrak{R}a(v,v) = \|\nabla v\|^2_{L^2(S)} - \kappa^2 \|v\|^2_{L^2(S)} \gtrsim (1 - C_{\mathrm{F}}^2 \kappa^2 H^2 m^2) \|\nabla v\|^2_{L^2(S)} \gtrsim \|\nabla v\|^2_{L^2(S)}$$

Recalling the definition of the κ-dependent Helmholtz norm in (4.1), one can show that the norms $\|\cdot\|_{\mathcal{V}(S)}$ and $\|\nabla \cdot\|_{L^2(S)}$ are equivalent on $\mathcal{V}_S$, i.e., for all $v \in \mathcal{V}_S$ it holds that

$$\|v\|^2_{\mathcal{V}(S)} \lesssim (1 + C_{\mathrm{F}}^2 \kappa^2 H^2 m^2) \|\nabla v\|^2_{L^2(S)} \lesssim \|\nabla v\|^2_{L^2(S)} \leq \|v\|^2_{\mathcal{V}(S)}.$$

Combining the previous estimates shows the coercivity of a on $\mathcal{V}_S \times \mathcal{V}_S$, which implies the inf–sup condition (5.4).

5.2 Localization approach

For the derivation of the SLOD basis functions, we make the assumption that the patch S does not coincide with the whole domain D. Henceforth, we only present the derivation of the basis functions of the trial space, noting that the basis functions of the test space can be derived analogously. For the basis function of the trial space, which corresponds to the element K, we make the ansatz

$$\varphi \coloneqq \mathcal{L} g, \tag{5.5}$$

where $g \in \mathcal{P}^0(S)$ is a $L^2(S)$-normalized source term to be determined subsequently. Here, g is implicitly extended by zero and embedded in $\mathcal{V}^*$ such that it is compatible with the solution operator $\mathcal{L}\colon \mathcal{V}^* \to \mathcal{V}$. We note that instead of a piecewise constant source term, one could equivalently consider a linear combination of $\{q_T : T \subset S\}$, which are the QOIs defined in (2.13).

A local approximation $\psi \in \mathcal{V}_S$ of the generally global function φ can be obtained by using the local solution operator instead of the global one, i.e.,

$$\psi = \mathcal{L}_S g. \tag{5.6}$$

Note that the local function ψ is in general a poor approximation of the global function φ. However, by an appropriate choice of g, one can obtain highly accurate approximations in the $\mathcal{V}$-norm. Following classical textbooks (see,

e.g., [LM72]), we define the local trace operator restricted to the boundary segment $\Sigma \coloneqq \partial S \backslash \partial D$ by

$$\operatorname{tr}_\Sigma \colon \mathcal{V}(S) \to X \coloneqq \operatorname{im}(\operatorname{tr}_\Sigma) \subset H^{1/2}(\Sigma). \tag{5.7}$$

Furthermore, we denote by $\operatorname{tr}_\Sigma^{-1} \colon X \to \mathcal{V}(S)$ the operator-harmonic extension, which defines a continuous right-inverse of tr_Σ. Given $w \in X$, it satisfies the boundary condition $\operatorname{tr}_\Sigma \operatorname{tr}_\Sigma^{-1} w = w$ and is (adjoint) operator-harmonic in the sense that

$$a_S(v, \operatorname{tr}_\Sigma^{-1} w) = 0 \tag{5.8}$$

holds for all $v \in \mathcal{V}_S$. The well-posedness of $\operatorname{tr}_\Sigma^{-1}$ follows by (5.1) and (5.4).

Given the trace and extension operators, we can conclude from (5.6) and (5.8) that it holds

$$a(\psi, v) = a_S(\psi, v) = a_S(\psi, v - \operatorname{tr}_\Sigma^{-1} \operatorname{tr}_\Sigma\, v) = (g, v - \operatorname{tr}_\Sigma^{-1} \operatorname{tr}_\Sigma\, v)_{L^2(S)}$$

for all $v \in \mathcal{V}$, using that $(v - \operatorname{tr}_\Sigma^{-1} \operatorname{tr}_\Sigma v)|_S \in \mathcal{V}_S$ for any $v \in \mathcal{V}$. We emphasize that we do not distinguish between functions in $\mathcal{V}_S$ and their $\mathcal{V}$-conforming extensions by zero. The previous identity, (5.5), and $\operatorname{supp}(g) \subset S$ yield for any $v \in \mathcal{V}$ the crucial observation

$$a(\varphi - \psi, v) = (g, v)_{L^2(S)} - a(\psi, v) = (g, \operatorname{tr}_\Sigma^{-1} \operatorname{tr}_\Sigma\, v)_{L^2(S)}, \tag{5.9}$$

which rephrases the smallness of the localization error as the (almost) $L^2(S)$-orthogonality of g to the space

$$Y \coloneqq \operatorname{tr}_\Sigma^{-1} X \subset \mathcal{V}(S). \tag{5.10}$$

The space Y is the space of (adjoint) operator-harmonic functions on S, which satisfy the global boundary conditions of the considered problem at $\partial S \cap \partial D$. We emphasize that (5.9) coincides with the (negative) conormal derivative of ψ, which is an element of X^*, where X^* denotes the anti-dual space of X. This means that the smallness of the localization error is also equivalent to a small X^*-norm of the conormal derivative of ψ at the patch boundary segment Σ.

For an optimal choice of g, we perform a singular value decompsition (SVD) of the operator $\Pi^0_{H,S}|_Y$. Since this operator has finite rank less or equal to $R \coloneqq \dim \mathcal{P}^0(S)$, its SVD is given by

$$\Pi^0_{H,S}|_Y\, v = \sum_{k=1}^{R} \sigma_k (v, w_k)_{\mathcal{V}(S)}\, q_k \tag{5.11}$$

with the singular values $\sigma_1 \geq \cdots \geq \sigma_R \geq 0$, the $L^2(S)$-orthonormal left singular vectors $q_1 \ldots, q_R$, and the $\mathcal{V}(S)$-orthonormal right singular vectors $w_1 \ldots, w_R$. The left singular vector q_R corresponding to the smallest singular value σ_R satisfies

$$q_R \in \operatorname*{arg\,min}_{g \in \mathcal{P}^0(S) \colon \|g\|_{L^2(S)} = 1} \; \sup_{v \in Y \colon \|v\|_{\mathcal{V}(S)} = 1} |(g, v)_{L^2(S)}|. \tag{5.12}$$

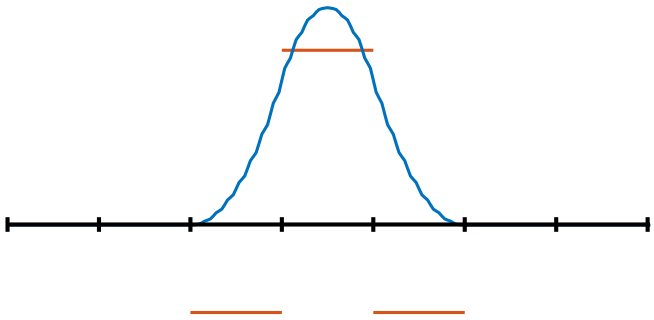

Figure 5.1: SLOD basis function and corresponding local source term for the oversampling parameter $m = 1$ for the problem (2.11).

In this sense, the choice $g \coloneqq q_R$ is optimal and we define

$$\sigma_K = \sigma_K(H, m) \coloneqq \sigma_R = \sup_{v \in Y\colon \|v\|_{\mathcal{V}(S)}=1} |(g\,,\, v)_{L^2(S)}|. \tag{5.13}$$

The value of σ_K is used in the remainder as a measure of the orthogonality between g and Y. It coincides with the X^*-norm of the conormal derivative of ψ up to a constant, which may depend on the geometry of the patch.

In one dimension, the trace space X is at most two-dimensional, which implies that the space Y is also at most two-dimensional. Therefore, already for $m = 1$, one can choose a local source term $g \in \mathcal{P}^0(S)$, which is $L^2(S)$-orthogonal to Y, i.e., we obtain a truly local basis function. This basis function and its local source term are shown in Figure 5.1. Truly local means that φ coincides with its localized version ψ. Note that for the Poisson problem, the constructed basis coincides with the quadratic B-splines [PT95, Ch. 2].

The one-dimensional case also demonstrates the possible non-uniqueness of the smallest singular value of the operator $\Pi^0_{H,S}|_Y$, which implies the non-uniqueness of solutions to the problem (5.12). For $m \geq 2$, a simple counting argument shows that there are multiple optimal choices of g. In higher dimensions, the problem manifests itself rather in clusters of small singular values, which may appear for large m and certain patch configurations near the boundary. For a practical solution to this problem, see Section 5.5.

Above, we presented the derivation of the basis functions of the trial space. The basis function of the test space can be constructed similarly by replacing the operators $\mathcal{L}$ and $\mathcal{L}_S$ in (5.5) and (5.6) by their adjoint counterparts $\mathcal{L}^*$ and $\mathcal{L}^*_S$, respectively. Furthermore, instead of the extension (5.8), one has to consider the extension defined by swapping arguments in (5.8). The resulting source term, global basis function, and localized counterpart are denoted by g^*, φ^*, and ψ^*, respectively. We denote by σ^*_K the counterpart of (5.13), which measures the orthogonality of the source term g^* on the space Y^*. Here, the space Y^* denotes the counterpart of (5.10), which is defined as the image of the

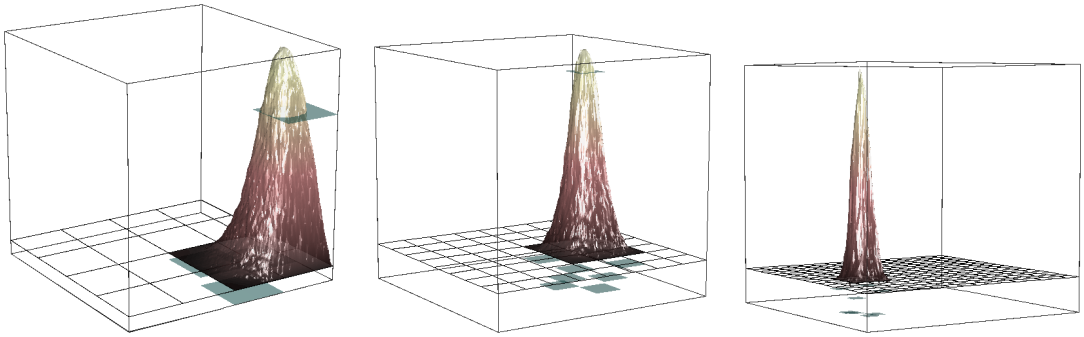

Figure 5.2: SLOD basis functions and the corresponding local source terms for the oversampling parameter $m = 1$ for the problem (3.36).

extension with swapped arguments. For a visualization of selected SLOD basis functions in two dimensions, see Figure 5.2.

5.3 Practical multi-scale method

In this section, we use the novel localization strategy presented in the previous section to transform the prototypical method (2.16) into a practically feasible method. In the following, the element $K \in \mathcal{T}_H$ is not fixed but variable and therefore has to be included in the notation. For the trial space, we denote the local source term, the global basis function, and its localized counterpart associated with the element K by $g_{K,m}$, $\varphi_{K,m}$, and $\psi_{K,m}$. Similarly, we write $g^*_{K,m}, \varphi^*_{K,m}$, and $\psi^*_{K,m}$ for the test space.

We define the trial and test spaces of the SLOD as the span of the respective localized basis functions, i.e.,

$$U^{\mathrm{slod}}_{H,m} \coloneqq \operatorname{span}\{\psi_{K,m} : K \in \mathcal{T}_H\}, \qquad V^{\mathrm{slod}}_{H,m} \coloneqq \operatorname{span}\{\psi^*_{K,m} : K \in \mathcal{T}_H\}.$$

The SLOD then seeks the Galerkin approximation with respect to the above trial and test spaces, i.e., it seeks $u^{\mathrm{slod}}_{H,m} \in U^{\mathrm{slod}}_{H,m}$ such that

$$a(u^{\mathrm{slod}}_{H,m}, v) = (f\,,\, v)_{L^2} \tag{5.14}$$

holds for all $v \in V^{\mathrm{slod}}_{H,m}$.

Alternatively, using the fact that the SLOD basis functions are localized responses of the local source terms, we can define a collocation-type SLOD approximation, which we also denote by $u^{\mathrm{slod}}_{H,m}$, as

$$u^{\mathrm{slod}}_{H,m} = \sum_{K \in \mathcal{T}_H} c_K \, \psi_{K,m}, \tag{5.15}$$

where the $(c_K)_{K \in \mathcal{T}_H}$ are the coefficients of the expansion of $\Pi^0_H f$ in terms of the local source terms $g_{K,m}$. Thus, the collocation variant requires only the basis

functions and local source terms of the trial space of the SLOD. Note that this variant is related to collocation in the sense that it enforces the PDE to hold on average (up to localization errors) in each element of $\mathcal{T}_H$. Similar to the Galerkin method, this variant only requires the solution of a linear system of equations at the coarse scale. The collocation version, however, has the advantage that the assembly of the system matrix requires only the coarse functions $g_{K,m}$ and no inner products between the $\psi_{K,m}$ and $\psi^*_{K,m}$ need to be computed.

A minimal requirement for the stability and convergence of both SLOD variants is that the two sets of local source terms

$$\{g_{K,m} : K \in \mathcal{T}_H\}, \qquad \{g^*_{K,m} : K \in \mathcal{T}_H\} \tag{5.16}$$

are Riesz bases of $\mathcal{P}^0(\mathcal{T}_H)$, i.e., they span the space of piecewise constants in a stable way. Numerically, this can by ensured a posteriori as outlined in Section 5.5. For the subsequent stability and error analysis, we assume that there exists a constant $C_{\mathrm{r}} > 0$ depending polynomially on H^{-1} and m such that

$$C_{\mathrm{r}}^{-1}(H,m) \sum_{K\in\mathcal{T}_H} |c_K|^2 \leq \Big\| \sum_{K\in\mathcal{T}_H} c_K g_{K,m} \Big\|^2_{L^2} \leq C_{\mathrm{r}}(H,m) \sum_{K\in\mathcal{T}_H} |c_K|^2 \tag{5.17}$$

holds for all $(c_K)_{K\in\mathcal{T}_H}$. Similarly, we assume that the estimate holds for $g_{K,m}$ replaced by $g^*_{K,m}$.

The subsequent stability and error analysis of the SLOD is explicit in the quantity σ defined by

$$\sigma = \sigma(H,m) \coloneqq \max_{K\in\mathcal{T}_H} \max\big\{\sigma_K, \sigma^*_K\big\}, \tag{5.18}$$

where σ_K and σ^*_K measure the orthogonality of the source terms $g_{K,m}$ and $g^*_{K,m}$ on the spaces Y and Y^*, respectively, cf. (5.13). The quantity σ decays rapidly as the oversampling parameter m is increased, see Section 5.4 for a study of the decay of σ.

The following theorem proves the inf–sup stability of the sesquilinear form a on $U^{\mathrm{slod}}_{H,m} \times V^{\mathrm{slod}}_{H,m}$, if m is chosen large enough. This implies the well-posedness of the Galerkin variant of the SLOD. The proof that the collocation variant of the SLOD is well-posed is very similar and will be omitted.

Theorem 5.3.1 (Inf–sup stability of the SLOD)**.** *Assume that the basis stability assumption* (5.17) *holds and that m is chosen sufficiently large so that*

$$\varepsilon(H,m) \coloneqq H^{-1} m^{d/2} C_{\mathrm{r}}^{1/2}(H,m)\sigma(H,m) \lesssim 1, \tag{5.19}$$

where the hidden constant depends only on C_a, α_{c}, α_{f}, and α_{p} and the quasi-uniformity and shape regularity of $\mathcal{T}_H$. Then, the sesquilinear form a is inf–sup stable on $U^{\mathrm{slod}}_{H,m} \times V^{\mathrm{slod}}_{H,m}$, i.e., there exists $\alpha_{\mathrm{slod}} > 0$ such that

$$\inf_{v\in U^{\mathrm{slod}}_{H,m}} \sup_{w\in V^{\mathrm{slod}}_{H,m}} \frac{|a(v,w)|}{\|v\|_{\mathcal{V}}\|w\|_{\mathcal{V}}} \geq \alpha_{\mathrm{slod}} \tag{5.20}$$

with $\alpha_{\mathrm{slod}} \approx \alpha_{\mathrm{a}}$, where α_{a} is the constant from Lemma 2.3.1.

Proof. We consider the following mapping between the prototypical problem-adapted trial space U_H^{a} defined in (2.15) and the SLOD trial space $U_{H,m}^{\mathrm{slod}}$:

$$\iota\colon U_H^{\mathrm{a}} \to U_{H,m}^{\mathrm{slod}}, \quad v \coloneqq \sum_{K\in\mathcal{T}_H} c_K\varphi_{K,m} \mapsto \sum_{K\in\mathcal{T}_H} c_K\psi_{K,m} =: v_m.$$

For proving the continuity of ι, we first apply the triangle inequality, which yields that

$$\|v_m\|_{\mathcal{V}} \leq \|v\|_{\mathcal{V}} + \|v - v_m\|_{\mathcal{V}}.$$

To estimate the second term, we derive a local preliminary result. We fix the patch $S = \mathsf{N}_m(K)$ and denote $\Sigma = \partial S \backslash \partial D$. Using (5.13), we obtain for any $w \in \mathcal{V}(S)$ that

$$|(g_{K,m}\,,\, \operatorname{tr}_\Sigma^{-1}\operatorname{tr}_\Sigma w)_{L^2(S)}| \leq \sigma_K(H,m)\|\operatorname{tr}_\Sigma^{-1}\operatorname{tr}_\Sigma w\|_{\mathcal{V}(S)}. \tag{5.21}$$

The $\mathcal{V}(S)$-norm on the right-hand side can be estimated using the decomposition $\operatorname{tr}_\Sigma^{-1}\operatorname{tr}_\Sigma w = w + w_0$, where $w_0 \in \mathcal{V}_S$ satisfies that $a_S(w_0,z) = -a_S(w,z)$ for all $z \in \mathcal{V}_S$. To estimate w_0, we use the continuity of a_S, cf. (5.1), and the inf–sup condition (5.4). This ensures that there exists $z \in \mathcal{V}_S$ with $\|z\|_{\mathcal{V}(S)} = 1$ such that

$$\alpha_{\mathrm{p}}\|w_0\|_{\mathcal{V}(S)} \leq |a_S(w_0,z)| = |a_S(w,z)| \leq C_a\|w\|_{\mathcal{V}(S)}. \tag{5.22}$$

Combining the estimates yields the desired local preliminary result

$$|(g_{K,m}\,,\, \operatorname{tr}_\Sigma^{-1}\operatorname{tr}_\Sigma w)_{L^2(S)}| \leq \sigma_K(H,m)(1+\alpha_{\mathrm{p}}^{-1}C_a)\|w\|_{\mathcal{V}(S)}. \tag{5.23}$$

The inf–sup stability of the continuous problem (2.4) yields the existence of $w \in \mathcal{V}$ with $\|w\|_{\mathcal{V}} = 1$ such that

$$\alpha_{\mathrm{c}}\|v - v_m\|_{\mathcal{V}} \leq |a(v-v_m,w)| \leq \sigma(H,m)(1+\alpha_{\mathrm{p}}^{-1}C_a)\sum_{K\in\mathcal{T}_H}|c_K|\|w\|_{\mathcal{V}(\mathsf{N}_m(K))},$$

where we used (5.9) and the local preliminary result (5.23).

Furthermore, we observe that by (3.7), we get for all $p \in \mathcal{P}^0(\mathcal{T}_H)$ that

$$\|p\|_{L^2} = \sup_{v\in\mathcal{V}} \frac{(p\,,\,v)_{L^2}}{\|v\|_{L^2}} \leq C_{\mathcal{B}_H}H^{-1}\sup_{v\in\mathcal{V}}\frac{(p\,,\,\mathcal{B}_H v)_{L^2}}{\|\mathcal{B}_H v\|_{\mathcal{V}}} \leq C_{\mathcal{B}_H}H^{-1}\|p\|_{\mathcal{V}^*}. \tag{5.24}$$

Another observation, which will be used in the following, is that due to the finite overlap of the patches and $\|w\|_{\mathcal{V}} = 1$, it holds that

$$\sum_{K\in\mathcal{T}_H}\|w\|^2_{\mathcal{V}(\mathsf{N}_m(K))} \lesssim m^d\|w\|^2_{\mathcal{V}} = m^d. \tag{5.25}$$

Using the discrete Cauchy–Schwarz inequality, the Riesz basis assumption (5.17) as well as (2.2), (5.24), and (5.25), we obtain that

$$\begin{aligned}\alpha_{\mathrm{c}}\|v - v_m\|_{\mathcal{V}} &\lesssim (1+\alpha_{\mathrm{p}}^{-1}C_a)m^{d/2}\sigma(H,m)\sqrt{\sum_{K\in\mathcal{T}_H}|c_K|^2}\\ &\leq (1+\alpha_{\mathrm{p}}^{-1}C_a)m^{d/2}C_{\mathrm{r}}^{1/2}(H,m)\sigma(H,m)\Big\|\sum_{K\in\mathcal{T}_H}c_K g_{K,m}\Big\|_{L^2}\\ &\leq (1+\alpha_{\mathrm{p}}^{-1}C_a)C_a C_{\mathcal{B}_H}H^{-1}m^{d/2}C_{\mathrm{r}}^{1/2}(H,m)\sigma(H,m)\|v\|_{\mathcal{V}}.\end{aligned}$$

Using the assumption (5.19), we can then conclude the continuity of ι, i.e., $\|v_m\|_{\mathcal{V}} \lesssim \|v\|_{\mathcal{V}}$. The continuity of ι^{-1}, i.e., $\|v\|_{\mathcal{V}} \lesssim \|v_m\|_{\mathcal{V}}$, can be proved similarly. Note that the same estimates can also be shown for

$$\iota^*\colon V_H^{\mathrm{a}} \to V_{H,m}^{\mathrm{slod}}, \quad w \coloneqq \sum_{K\in\mathcal{T}_H} c_K\varphi_{K,m}^* \mapsto \sum_{K\in\mathcal{T}_H} c_K\psi_{K,m}^* =: w_m$$

and its inverse.

Next, we prove the inf–sup condition (5.20) using the inf–sup stability of the prototypical method (2.19). We consider a fixed but arbitrary $v_m \in U_{H,m}^{\mathrm{slod}}$ and define $v \coloneqq \iota^{-1}v_m \in U_H^{\mathrm{a}}$. We then set $w_m \coloneqq \iota^* w \in V_{H,m}^{\mathrm{slod}}$, where $w \in V_H^{\mathrm{a}}$ is chosen such that

$$|a(v,w)| \geq \alpha_{\mathrm{a}}\|v\|_{\mathcal{V}}\|w\|_{\mathcal{V}},$$

cf. (2.19). Elementary algebraic manipulations and the reverse triangle inequality yield that

$$|a(v_m,w_m)| \geq |a(v,w)| - |a(v_m-v,w)| - |a(v_m,w_m-w)|.$$

Next, we estimate the terms on the right-hand side separately. For the first term, it follows from the continuity of ι and ι^* that

$$|a(v,w)| \geq \alpha_{\mathrm{a}}\|v\|_{\mathcal{V}}\|w\|_{\mathcal{V}} \gtrsim \alpha_{\mathrm{a}}\|v_m\|_{\mathcal{V}}\|w_m\|_{\mathcal{V}}.$$

For the second term, one obtains using (5.19) that

$$|a(v_m-v,w)| \leq C_a\|v_m-v\|_{\mathcal{V}}\|w\|_{\mathcal{V}} \lesssim \varepsilon(H,m)\|v_m\|_{\mathcal{V}}\|w_m\|_{\mathcal{V}}.$$

The third term can be estimated in the same way. Using condition (5.19), we can absorb the second and third terms into the first term. This gives the desired inf–sup stability of the SLOD with $\alpha_{\mathrm{slod}} \approx \alpha_{\mathrm{a}}$. □

The following theorem gives an error estimate for the Galerkin variant of the SLOD. Note that an analogous result can be proved for the collocation variant of the SLOD using very similar arguments.

Theorem 5.3.2 (Convergence of the SLOD)**.** *For any $f \in H^k(D)$, $k \in \{0,1\}$, the SLOD approximation* (5.14) *satisfies that*

$$\|u - u_{H,m}^{\mathrm{slod}}\|_{\mathcal{V}} \lesssim H^{1+k}|f|_{H^k} + \varepsilon(H,m)\|f\|_{L^2}$$

with ε defined in (5.19)*. The hidden constant depends only on C_a, α_{c}, α_{f}, and α_{p} and the quasi-uniformity and shape regularity of $\mathcal{T}_H$.*

Proof. In this proof, we use the notation introduced in the proof of Theorem 5.3.1. We begin estimating the approximation error of the SLOD with the triangle inequality as follows:

$$\|u - u_{H,m}^{\mathrm{slod}}\|_{\mathcal{V}} \leq \|u - u_H^{\mathrm{a}}\|_{\mathcal{V}} + \|u_H^{\mathrm{a}} - u_{H,m}^{\mathrm{slod}}\|_{\mathcal{V}}.$$

The first term can be estimated using Lemma 2.3.3. For the second term, we apply Strang's lemma (see, e.g., [EG04, Lem. 2.25]) using that $u_{H,m}^{\mathrm{slod}} \in U_{H,m}^{\mathrm{slod}}$ can be interpreted as non-conforming and non-consistent approximation to $u_H^{\mathrm{a}} \in U_H^{\mathrm{a}}$. This yields that

$$\begin{aligned}\|u_H^{\mathrm{a}} - u_{H,m}^{\mathrm{slod}}\|_{\mathcal{V}} \leq \big(1 + C_a\alpha_{\mathrm{slod}}^{-1}\big) \inf_{v_m \in U_{H,m}^{\mathrm{slod}}} \|u_H^{\mathrm{a}} - v_m\|_{\mathcal{V}} \\ + \alpha_{\mathrm{slod}}^{-1} \sup_{w_m \in V_{H,m}^{\mathrm{slod}}} \frac{|a(u_H^{\mathrm{a}}, w_m) - (f\,,\, w_m)_{L^2}|}{\|w_m\|_{\mathcal{V}}}.\end{aligned}$$

The first term can be estimated by choosing $v_m \coloneqq \iota u_H^{\mathrm{a}}$. Using the same arguments as in the proof of Theorem 5.3.1 and the inf–sup stability (2.19), we obtain that

$$\|u_H^{\mathrm{a}} - \iota u_H^{\mathrm{a}}\|_{\mathcal{V}} \lesssim \varepsilon(H,m)\|u_H^{\mathrm{a}}\|_{\mathcal{V}} \leq \alpha_{\mathrm{a}}^{-1}\varepsilon(H,m)\|f\|_{L^2}.$$

For the second term, we perform algebraic manipulations, which yields for all $w \in V_H^{\mathrm{a}}$ that

$$a(u_H^{\mathrm{a}}, w_m) - (f\,,\, w_m)_{L^2} = (f\,,\, w - w_m)_{L^2} - a(u_H^{\mathrm{a}}, w - w_m).$$

Choosing $w \coloneqq (\iota^*)^{-1}w_m$, we obtain using again the arguments from the proof of Theorem 5.3.1 and the inf–sup stability (2.19) that

$$|a(u_H^{\mathrm{a}}, w_m) - (f\,,\, w_m)_{L^2}| \lesssim \varepsilon(H,m)\|f\|_{L^2}\|w_m\|_{\mathcal{V}} + C_a\alpha_{\mathrm{a}}^{-1}\varepsilon(H,m)\|f\|_{L^2}\|w_m\|_{\mathcal{V}}.$$

Combining the estimates finishes the proof. □

5.4 Decay of localization error

In this section we study the decay of σ defined in (5.18), which determines the localization error of the SLOD. It appears in the assumptions and estimates in Theorems 5.3.1 and 5.3.2 and is therefore essential for the stability and convergence of the SLOD. We first give a justification for the super-exponential decay of σ for diffusion-type PDEs based on a connection to spectral geometry. Furthermore, we present a pessimistic exponential decay result for σ, which can be rigorously proved using LOD arguments.

5.4.1 Super-exponential decay

In the following justification of the super-exponential decay, we restrict ourselves to diffusion-type PDEs. Note that we will only mention the main results and refer to [HP22b, Sec. 7] for more details. The presented justification is based on a connection between the decay of σ and the decay of Steklov eigenfunctions. Denoting $\Sigma \coloneqq \partial S \backslash \partial D$, the local Steklov eigenvalue problem on the patch $S \coloneqq \mathsf{N}_m(K)$ seeks eigenpairs $(\phi, \lambda) \in \mathcal{V}(S) \times \mathbb{R}$ such that

$$a_S(\phi, v) = \lambda(\phi\,,\, v)_{L^2(\Sigma)} \tag{5.26}$$

holds for all $v \in \mathcal{V}(S)$, where ϕ denotes the Steklov eigenfunction and λ the corresponding eigenvalue. All eigenvalues of (5.26) are non-negative and it holds that the Steklov eigenfunctions $\{\phi_k : k \in \mathbb{N}_0\}$ form a basis of the space Y defined in (5.10), cf. [Auc05]. We assume that the eigenfunctions are ordered so that the corresponding eigenvalues are non-increasing. For large indices, the oscillatory nature and the operator-harmonicity, cf. (5.26), lead to a strong decay of the eigenfunctions in the interior of the patch. For some special cases this has been made rigorous, see for example [HL01; PST15; GT16]. These works, however, require smoothness (or in some cases even analyticity) of the domain and the coefficient. In [HL01] a conjecture on the decay of Steklov eigenfunctions in the interior of a domain was formulated. Using a relaxed version of this conjecture for the decay of the element averages of the Steklov eigenfunctions, one can show that σ defined in (5.18) decays super-exponentially as m is increased, i.e.,

$$\sigma(H, m) \leq C_{\mathrm{s}}(H, m) \exp\big(-Cm^{\frac{d}{d-1}}\big) \tag{5.27}$$

with $C_{\mathrm{s}} > 0$ depending at most polynomially on H^{-1} and m and $C > 0$ independent of H and m, cf. [HP22b, Thm. 7.3]. We remark that, in one dimension, the fraction $\frac{d}{d-1}$ in (5.27) can be interpreted as infinity, which is consistent with the existence of a local basis in one dimension, see Section 5.2.

For a numerical investigation of the super-exponential decay in two dimensions, we refer to Figure 5.3. It can be observed that the distance between the dashed horizontal lines becomes larger as m is increased, especially between the oversampling parameters 3 and 4, which indicates a presumably super-exponential decay of σ. For a more detailed numerical study of the super-exponential decay, we refer to the numerical experiments in Section 5.6.

Remark 5.4.1 (Oversampling condition)**.** This remark specifies the choice of the oversampling parameter m needed to ensure the stability and optimal order convergence of the SLOD, cf. Theorems 5.3.1 and 5.3.2. Assuming the Riesz stability of the local source terms (5.17) and the validity of the super-exponential decay result (5.27), we obtain the oversampling condition $m \gtrsim (\log \frac{1}{H})^{(d-1)/d}$, which is a significant improvement compared to the oversampling condition $m \gtrsim \log(\frac{1}{H})$ for the LOD, cf. Theorem 3.4.2. For Helmholtz problems, stability

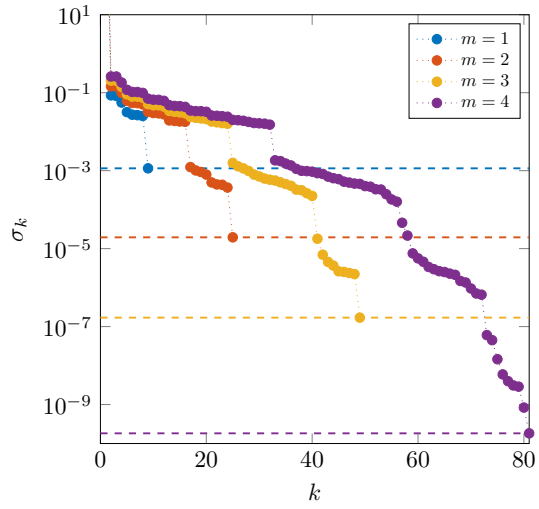

Figure 5.3: Singular values of the operators $\Pi^0_{H,S}|_Y$ for the patches $S = \mathsf{N}_m(K)$ for several values of m and fixed $K \in \mathcal{T}_H$ for problem (3.36). The dashed horizontal lines indicate the smallest singular value, which determines the value of σ defined in (5.18).

and optimal order convergence of the SLOD can be ensured under the oversampling condition $m \gtrsim (\log \frac{\kappa}{H})^{(d-1)/d}$, while the corresponding condition for the LOD is $m \gtrsim \log(\frac{\kappa}{H})$, cf. Theorem 4.4.2.

5.4.2 Pessimistic exponential decay

Next, we prove a pessimistic exponential decay result, which is based on LOD techniques. More precisely, we construct local basis functions and corresponding local source terms satisfying (5.17) for which σ decays exponentially in the oversampling parameter. As basis functions of the trial and test space corresponding to the element $K \in \mathcal{T}_H$, we choose

$$\psi_{K,m} \coloneqq (\mathtt{id} - \mathcal{C}_m) b_K, \qquad \psi^*_{K,m} \coloneqq (\mathtt{id} - \mathcal{C}^*_m) b_K, \tag{5.28}$$

where $\mathcal{C}_m$ and $\mathcal{C}^*_m$ denote the localized correction operators defined in (3.23) and $b_K \in H^1_0(K)$ is the bubble function associated with the element K, cf. (3.5). This choice is similar to that of the LOD basis functions (3.27), but without the additional quasi-interpolation operator $\mathcal{P}_H$. We assume that the inf–sup condition (3.22) holds in order for (5.28) to be well-defined.

The following lemma shows that the basis functions (5.28) have local piecewise constant source terms $g_{K,m}$ and $g^*_{K,m}$, which decay exponentially fast. To prove the decay, we apply LOD theory locally, treating the patch $S \coloneqq \mathsf{N}_m(K)$ as the whole domain. This requires a local version of the inf–sup condition (3.18). In the following, the corresponding inf–sup constant is denoted by α_{dp}.

Lemma 5.4.2 (Properties of the LOD source terms)**.** *The LOD basis functions $\psi_{K,m}$ and $\psi^*_{K,m}$ defined in* (5.28) *have the local source terms $g_{K,m}$, $g^*_{K,m} \in \mathcal{P}^0(S)$, i.e.,*

$$\psi_{K,m} = \mathcal{L}_S g_{K,m}, \qquad \psi^*_{K,m} = \mathcal{L}^*_S g^*_{K,m}. \tag{5.29}$$

Moreover, denoting $S = \mathsf{N}_m(K)$, the source terms decay exponentially fast, i.e., it holds for all $l \in \mathbb{N}$ that

$$\|g_{K,m}\|_{L^2(S\setminus \mathsf{N}_l(K))} \lesssim H^{-1} \exp(-C_{\mathrm{dl}} l) \|g_{K,m}\|_{L^2(S)}, \tag{5.30}$$

where $C_{\mathrm{dl}} > 0$ depends only on C_a, α_{dp}, and the shape regularity of $\mathcal{T}_H$ and the hidden constant depends only on C_a, α_{p}, α_{fp}, and the shape regularity of $\mathcal{T}_H$. An analogous result holds for $g^*_{K,m}$.

Proof. We fix the patch $S = \mathsf{N}_m(K)$ and, if not explicitly required, drop the indices K and m. We denote the local space of fine-scale functions by $\mathcal{W}_S \coloneqq \mathcal{W}_{K,m}|_S \subset \mathcal{V}_S$, where $\mathcal{W}_{K,m}$ is defined in (3.20). Furthermore, we define the local correction operators $\mathcal{C}_S$, $\mathcal{C}^*_S \colon \mathcal{V}_S \to \mathcal{W}_S$ such that

$$a_S(\mathcal{C}_S v, w) = a_S(v, w), \qquad a_S(w, \mathcal{C}^*_S v) = a_S(w, v) \tag{5.31}$$

holds for all $v \in \mathcal{V}_S$ and $w \in \mathcal{W}_S$. These operators are well-posed due to the inf–sup condition (3.22). Using that $b_K \in H^1_0(K)$, we can rewrite the basis functions (5.28) as follows:

$$\psi = (\mathtt{id} - \mathcal{C}_S) b_K, \qquad \psi^* = (\mathtt{id} - \mathcal{C}^*_S) b_K. \tag{5.32}$$

For proving the identity (5.29), we use a saddle point characterization of the of the LOD basis functions ψ and ψ^* (see, e.g., [Mai21, Eq. (4.5)]), i.e., the pair $(\psi, \lambda) \in \mathcal{V}_S \times \mathcal{P}^0(S)$, with λ denoting a Lagrange multiplier, solves

$$\begin{pmatrix} \mathcal{A}_S & \mathcal{J}^*_{H,S} \\ \mathcal{J}_{H,S} & 0 \end{pmatrix} \begin{pmatrix} \psi \\ \lambda \end{pmatrix} = \begin{pmatrix} 0 \\ \mathbf{1}_K \end{pmatrix}, \tag{5.33}$$

where $\mathcal{A}_S \colon \mathcal{V}_S \to \mathcal{V}^*_S$, $v \mapsto a_S(v, \cdot)$ and $\mathcal{J}_{H,S} \colon \mathcal{V}_S \to \mathcal{P}^0(S), u \mapsto \Pi^0_{H,S} u$. Its adjoint $\mathcal{J}^*_{H,S} \colon \mathcal{P}^0(S) \to \mathcal{V}^*_S$ is defined such that

$$\langle \mathcal{J}^*_{H,S} p, v \rangle_{\mathcal{V}^*_S \times \mathcal{V}_S} \coloneqq (p\,,\, v)_{L^2(S)}$$

holds for all $p \in \mathcal{P}^0(S)$ and $v \in \mathcal{V}_S$. To prove that the Schur complement $\mathcal{S}_{H,S} \colon \mathcal{P}^0(S) \to \mathcal{P}^0(S)$, $p \mapsto (\mathcal{J}_{H,S} \mathcal{L}_S \mathcal{J}^*_{H,S}) p$ is invertible, we note that

$$\begin{aligned} (\mathcal{S}_{H,S} p\,,\, q)_{L^2(S)} &= \langle \mathcal{L}_S \mathcal{J}^*_{H,S} p,\, \mathcal{J}^*_{H,S} q \rangle_{\mathcal{V}_S \times \mathcal{V}^*_S} = \langle \mathcal{L}_S \mathcal{J}^*_{H,S} p,\, \mathcal{A}^*_S \mathcal{L}^*_S \mathcal{J}^*_{H,S} q \rangle_{\mathcal{V}_S \times \mathcal{V}^*_S} \\ &= \overline{a_S(\mathcal{L}_S \mathcal{J}^*_{H,S} p, \mathcal{L}^*_S \mathcal{J}^*_{H,S} q)} \end{aligned}$$

holds for all $p, q \in \mathcal{P}^0(S)$, where $\mathcal{A}^*_S \colon \mathcal{V}_S \to \mathcal{V}^*_S$, $v \mapsto \overline{a_S(\cdot, v)}$ denotes the adjoint operator of $\mathcal{A}_S$. Using (5.4) and the inf–sup stability of a_S on $\mathcal{W}_S \times \mathcal{W}_S$,

cf. (3.22), one can apply Lemma 2.3.1 in the local setting. This yields the inf–sup stability of a_S on $\mathcal{L}_S\mathcal{J}_{H,S}^*\mathcal{P}^0(S) \times \mathcal{L}_S^*\mathcal{J}_{H,S}^*\mathcal{P}^0(S)$ with the inf–sup constant $\alpha_{\mathrm{ap}} \coloneqq C_a^{-1}\alpha_{\mathrm{p}}\alpha_{\mathrm{fp}} > 0$. Thus, for all $p \in L^2(S)$, there exists $q \in L^2(S)$ such that

$$\begin{aligned}|(\mathcal{S}_{H,S}p\,,\,q)_{L^2(S)}| &= |a_S(\mathcal{L}_S\mathcal{J}_{H,S}^*p, \mathcal{L}_S^*\mathcal{J}_{H,S}^*q)| \geq \alpha_{\mathrm{ap}}\|\mathcal{L}_S\mathcal{J}_{H,S}^*p\|_{\mathcal{V}(S)}\|\mathcal{L}_S^*\mathcal{J}_{H,S}^*q\|_{\mathcal{V}(S)} \\ &\geq \alpha_{\mathrm{ap}}C_a^{-2}\|\mathcal{J}_{H,S}^*p\|_{\mathcal{V}_S^*}\|\mathcal{J}_{H,S}^*q\|_{\mathcal{V}_S^*},\end{aligned}$$

where we used the continuity of a_S, cf. (5.1).

Denoting by $\mathcal{B}_{H,S}$ the restriction of $\mathcal{B}_H$ defined in (3.6) to functions in $L^2(S)$, we further obtain that

$$\begin{aligned}\|\mathcal{J}_{H,S}^*p\|_{\mathcal{V}_S^*} &\geq \sup_{v\in\mathcal{V}_S}\frac{(\mathcal{J}_{H,S}^*p\,,\,\mathcal{B}_{H,S}v)_{L^2(S)}}{\|\mathcal{B}_{H,S}v\|_{\mathcal{V}(S)}} \geq C_{\mathcal{B}_H}^{-1}H\sup_{v\in\mathcal{V}_S}\frac{(\mathcal{J}_{H,S}^*p\,,\,\mathcal{B}_{H,S}v)_{L^2(S)}}{\|v\|_{L^2(S)}} \\ &= C_{\mathcal{B}_H}^{-1}H\|p\|_{L^2(S)}.\end{aligned}$$

Combining the previous estimates proves the inf–sup stability of $\mathcal{S}_{H,S}$. The continuity of $\mathcal{S}_{H,S}$ can be proved as follows:

$$\begin{aligned}|(\mathcal{S}_{H,S}p\,,\,q)_{L^2(S)}| &= |a_S(\mathcal{L}_S\mathcal{J}_{H,S}^*p, \mathcal{L}_S^*\mathcal{J}_{H,S}^*q)| \leq C_a\alpha_{\mathrm{p}}^{-2}\|\mathcal{J}_{H,S}^*p\|_{\mathcal{V}_S^*}\|\mathcal{J}_{H,S}^*q\|_{\mathcal{V}_S^*} \\ &\leq C_a\alpha_{\mathrm{p}}^{-2}\|p\|_{L^2(S)}\|q\|_{L^2(S)}.\end{aligned} \tag{5.34}$$

From the inf–sup stability and the continuity of $\mathcal{S}_{H,S}$, we can conclude that $\mathcal{S}_{H,S}^{-1}$ exists and that it is continuous satisfying that

$$\|\mathcal{S}_{H,S}^{-1}p\|_{L^2(S)} \leq \alpha_{\mathrm{ap}}^{-1}C_a^2C_{\mathcal{B}_H}^2H^{-2}\|p\|_{L^2(S)} \tag{5.35}$$

for all $p \in \mathcal{P}^0(S)$. Using the identity

$$\mathcal{A}_S\psi = \mathcal{J}_{H,S}^*\mathcal{S}_{H,S}^{-1}\mathbf{1}_K,$$

which can be derived from (5.33), we obtain the assertion (5.29) with the local source term $g = g_{K,m} = \mathcal{S}_{H,S}^{-1}\mathbf{1}_K$.

To prove the decay result (5.30), we establish a connection of the operator $\mathcal{S}_{H,S}^{-1}$ to the operators $\mathcal{C}_S$ and $\mathcal{C}_S^*$. We obtain that

$$\begin{aligned}(\mathcal{S}_{H,S}^{-1}p\,,\,q)_{L^2(S)} &= \langle\mathcal{A}_S\mathcal{L}_S\mathcal{J}_{H,S}^*\mathcal{S}_{H,S}^{-1}p, (\mathtt{id}-\mathcal{C}_S^*)\mathcal{B}_{H,S}q\rangle_{\mathcal{V}_S^*\times\mathcal{V}_S} \\ &= a_S((\mathtt{id}-\mathcal{C}_S)\mathcal{B}_{H,S}p, (\mathtt{id}-\mathcal{C}_S^*)\mathcal{B}_{H,S}q)\end{aligned}$$

holds for all $p, q \in \mathcal{P}^0(S)$, where we used that q and $(\mathtt{id}-\mathcal{C}_S^*)\mathcal{B}_{H,S}q$ have the same element averages and the identity $(\mathtt{id}-\mathcal{C}_S)\mathcal{B}_{H,S}p = \mathcal{L}_S\mathcal{J}_{H,S}^*\mathcal{S}_{H,S}^{-1}p$.

Defining $\tilde{g} \coloneqq g\mathbf{1}_{S\setminus\mathsf{N}_l(K)}$, we obtain that

$$\|g\|_{L^2(S\setminus\mathsf{N}_l(K))}^2 = (\mathcal{S}_{H,S}^{-1}\,\mathbf{1}_K\,,\,\tilde{g})_{L^2(S)} = a_S((\mathtt{id}-\mathcal{C}_S)b_K, (\mathtt{id}-\mathcal{C}_S^*)\mathcal{B}_{H,S}\tilde{g}),$$

which allows one to use LOD theory for proving the decay of g. Since the remainder of this proof is based on fairly standard LOD cut-off arguments, we only sketch the main ideas. Let us introduce the FE cut-off function η, which is uniquely defined as follows: we set η to one for all nodes contained in the $\lfloor l/2 \rfloor$-th order patch of K and to zero for all other nodes. We obtain that

$$\begin{aligned} &a_S((\mathtt{id} - \mathcal{C}_S)b_K, (\mathtt{id} - \mathcal{C}_S^*)\mathcal{B}_{H,S}\tilde{g}) \\ &\quad = a_S(\eta(\mathtt{id} - \mathcal{C}_S)b_K, \eta(\mathtt{id} - \mathcal{C}_S^*)\mathcal{B}_{H,S}\tilde{g}) + a_S(\eta(\mathtt{id} - \mathcal{C}_S)b_K, \tilde{\eta}(\mathtt{id} - \mathcal{C}_S^*)\mathcal{B}_{H,S}\tilde{g}) \\ &\quad + a_S(\tilde{\eta}(\mathtt{id} - \mathcal{C}_S)b_K, \eta(\mathtt{id} - \mathcal{C}_S^*)\mathcal{B}_{H,S}\tilde{g}) + a_S(\tilde{\eta}(\mathtt{id} - \mathcal{C}_S)b_K, \tilde{\eta}(\mathtt{id} - \mathcal{C}_S^*)\mathcal{B}_{H,S}\tilde{g}), \end{aligned}$$

where $\tilde{\eta} \coloneqq 1 - \eta$. By slightly adapting the proof of Lemma 3.3.1, one can show the following global decay result: for any $v \in \mathcal{V}$, it holds that

$$\|(\mathtt{id} - \mathcal{C})v\|_{\mathcal{V}(D \setminus \mathtt{N}_m(\mathrm{supp}(v)))} \leq \exp(-C_{\mathrm{d}} m)\|(\mathtt{id} - \mathcal{C})v\|_{\mathcal{V}} \tag{5.36}$$

for all $m \in \mathbb{N}$, see for example [Mai20, Rem. 3.3.2]. An analogous result holds for $\mathtt{id} - \mathcal{C}^*$. Treating the patch S as the entire domain, this result can be applied to the operators $\mathtt{id} - \mathcal{C}_S$ and $\mathtt{id} - \mathcal{C}_S^*$. Using (2.2), (2.25), (3.7), (5.1), and (5.36), the first of the four terms above can be estimated as follows:

$$|a_S(\eta(\mathtt{id} - \mathcal{C}_S)b_K, \eta(\mathtt{id} - \mathcal{C}_S^*)\mathcal{B}_{H,S}\tilde{g})| \lesssim H^{-1} \exp(-C_{\mathrm{dl}} l)\|\mathbf{1}_K\|_{L^2(K)}\|\tilde{g}\|_{L^2(S)}$$

with the decay rate $C_{\mathrm{dl}} > 0$ depending only on C_a, α_{dp}, and the shape regularity of $\mathcal{T}_H$, cf. Lemma 3.3.1. Furthermore, using (5.34), we obtain that

$$\|\mathbf{1}_K\|_{L^2(S)} = \|\mathcal{S}_{H,S} g\|_{L^2(S)} \leq C_a \alpha_{\mathrm{p}}^{-2} \|g\|_{L^2(S)}.$$

Note that all other terms can be estimated using similar arguments. Combining all estimates yields that

$$\|g\|_{L^2(S \setminus \mathtt{N}_l(K))} \lesssim H^{-1} \exp(-C_{\mathrm{dl}} l)\|g\|_{L^2(S)},$$

which is the desired exponential decay result for g, cf. (5.30). For ψ^* and g^*, the results (5.29) and (5.30) can be shown similarly. □

Using the results from the previous lemma, the following theorem shows that the local LOD source terms (5.29) are Riesz stable in the sense of (5.17) and that the quantity σ defined in (5.18) decays at least exponentially.

Theorem 5.4.3 (Stability and exponential decay of the LOD basis)**.** *Provided that m is chosen such that*

$$m \gtrsim \log(\tfrac{1}{H}), \tag{5.37}$$

the local LOD source terms satisfy that

$$H^4 \sum_{K \in \mathcal{T}_H} |c_K|^2 \lesssim \Big\| \sum_{K \in \mathcal{T}_H} c_K \frac{g_{K,m}}{\|g_{K,m}\|_{L^2}} \Big\|_{L^2}^2 \lesssim H^{-4} \sum_{K \in \mathcal{T}_H} |c_K|^2 \tag{5.38}$$

for all $(c_K)_{K\in\mathcal{T}_H}$*. An analogous result holds for the source terms* $g^*_{K,m}$*. Furthermore, considering normalized versions of* $g_{K,m}$ *and* $g^*_{K,m}$*, the quantity* σ *defined in* (5.13) *can be estimated as follows:*

$$\sigma(H,m) \lesssim H^{-1}\exp(-C_{\mathrm{dl}}m) \tag{5.39}$$

with C_{dl} *from Lemma 5.4.2. Note that the hidden constants may depend on* C_a*,* α_{c}*,* α_{f}*,* α_{p}*, and* α_{fp} *as well as the shape regularity of* $\mathcal{T}_H$*.*

Proof. We start with the proof of (5.39). For this, we fix an element $K \in \mathcal{T}_H$ and abbreviate $S \coloneqq \mathsf{N}_m(K)$. In the following, we drop the indices K and m, in case they are not explicitly needed. Denoting $\Sigma \coloneqq \partial S\backslash\partial D$ and using that $\mathrm{tr}_\Sigma^{-1}\,\mathrm{tr}_\Sigma\, v = v$ for all $v \in Y$ and $Y \subset \mathcal{V}(S)$, we obtain that

$$\sigma_K(H,m) \leq \frac{1}{\|g\|_{L^2(S)}} \sup_{v\in\mathcal{V}(S)\colon \|v\|_{\mathcal{V}(S)}=1} |(g\,,\,\mathrm{tr}_\Sigma^{-1}\,\mathrm{tr}_\Sigma\, v)_{L^2(S)}|, \tag{5.40}$$

where we account for possibly non-normalized g by dividing by its norm. Let us locally on S define the FE cut-off function η by setting its nodal values to one for all nodes at Σ and to zero for all other nodes. By the definition of η, it holds that $\mathrm{tr}_\Sigma\, v = \mathrm{tr}_\Sigma\, \eta v$ for all $v \in \mathcal{V}(S)$, which implies that

$$(g\,,\,\mathrm{tr}_\Sigma^{-1}\,\mathrm{tr}_\Sigma\, v)_{L^2(S)} = (g\,,\,\eta v)_{L^2(S)} - a_S(\psi,\eta v). \tag{5.41}$$

For estimating the first term, we employ Lemma 5.4.2, which yields that

$$|(g\,,\,\eta v)_{L^2(S)}| \leq \|g\|_{L^2(S\backslash\mathsf{N}_{m-1}(K))}\|v\|_{L^2(S)} \lesssim H^{-1}\exp(-C_{\mathrm{dl}}m)\|g\|_{L^2(S)}\|v\|_{\mathcal{V}(S)}.$$

To estimate the second term on the right-hand side of (5.41), we apply the decay result (5.36) locally on the patch S and use the inf–sup stability (5.4). We obtain that

$$\begin{aligned}
|a_S(\psi,\eta v)| &\leq C_a\|\psi\|_{\mathcal{V}(S\backslash\mathsf{N}_{m-1}(K))}\|\eta v\|_{\mathcal{V}(S)}\\
&\lesssim C_a H^{-1}\exp(-C_{\mathrm{dl}}m)\|\psi\|_{\mathcal{V}(S)}\|v\|_{\mathcal{V}(S)}\\
&\leq C_a\alpha_{\mathrm{p}}^{-1}H^{-1}\exp(-C_{\mathrm{dl}}m)\|g\|_{L^2(S)}\|v\|_{\mathcal{V}(S)}.
\end{aligned}$$

The same result can be shown for ψ^* and g^*. Taking the maximum over all elements yields the assertion (5.39).

For proving the Riesz property (5.38), we first note that the prototypical (non-localized) LOD basis functions and their corresponding global source terms can be obtained for all $K \in \mathcal{T}_H$ as

$$\varphi_K \coloneqq \mathcal{L}\mathcal{J}_H^* g_K, \qquad g_K \coloneqq \mathcal{S}_H^{-1}\mathbf{1}_K,$$

where the operators $\mathcal{S}_H \coloneqq \mathcal{J}_H\mathcal{L}\mathcal{J}_H^*$, $\mathcal{L}$, and $\mathcal{J}_H$ are the global counterparts of the operators used in the proof of Lemma 5.4.2. Adapting (5.34) and (5.35) to the global setting yields for all $p \in \mathcal{P}^0(\mathcal{T}_H)$ that

$$\|\mathcal{S}_H p\|_{L^2} \leq C_a\alpha_{\mathrm{c}}^{-2}\|p\|_{L^2}, \tag{5.42}$$

$$\|\mathcal{S}_H^{-1} p\|_{L^2} \leq \alpha_{\mathrm{a}}^{-1}C_a^2 C_{\mathcal{B}_H}^2 H^{-2}\|p\|_{L^2}. \tag{5.43}$$

Second, we estimate the difference between g_K and $g_{K,m}$, where $g_{K,m}$ denotes the local source term of the localized LOD basis function $\psi_{K,m}$. For this, we use the following decay result: for all $K \in \mathcal{T}_H$ and $m \in \mathbb{N}$, it holds that

$$\|\varphi_K - \psi_{K,m}\|_{\mathcal{V}} \lesssim \exp(-C_{\mathrm{d}} m)\|\psi_{K,m}\|_{\mathcal{V}},$$

which can be proved using that $(\mathcal{C}_K - \mathcal{C}_{K,m})v = (\mathcal{C}_K - \mathcal{C}_{K,m})(\mathtt{id} - \mathcal{C}_{K,m})v$ for all $v \in \mathcal{V}$ and by applying Lemma 3.3.2. Using this decay result and the local supports of $g_{K,m}$ and $\psi_{K,m}$, we obtain that

$$\begin{aligned}
\|g_K - g_{K,m}\|_{L^2}^2 &= (g_K - g_{K,m}\,,\, \mathcal{B}_H(g_K - g_{K,m}))_{L^2} \\
&= a(\varphi_K, \mathcal{B}_H(g_K - g_{K,m})) - a_S(\psi_{K,m}, \mathcal{B}_H|_S(g_K - g_{K,m})) \\
&= a(\varphi_K - \psi_{K,m}, \mathcal{B}_H(g_K - g_{K,m})) \\
&\leq C_a C_{\mathcal{B}_H} H^{-1} \|\varphi_K - \psi_{K,m}\|_{\mathcal{V}} \|g_K - g_{K,m}\|_{L^2} \\
&\lesssim \alpha_{\mathrm{p}}^{-1} C_a C_{\mathcal{B}_H} H^{-1} \exp(-C_{\mathrm{d}} m) \|g_{K,m}\|_{L^2} \|g_K - g_{K,m}\|_{L^2},
\end{aligned}$$

where we used that (3.7), (5.1), and (5.4) and the abbreviation $S = \mathsf{N}_m(K)$. It directly follows that

$$\|g_K - g_{K,m}\|_{L^2} \lesssim H^{-1} \exp(-C_{\mathrm{d}} m)\|g_{K,m}\|_{L^2}. \tag{5.44}$$

Third, using the continuity estimates for $\mathcal{S}_H^{-1}$ and $\mathcal{S}_H$ in (5.42) and (5.43), one can show the desired Riesz property for the normalized global source terms g_K. We obtain the following upper bound:

$$\left\| \sum_{K \in \mathcal{T}_H} c_K \frac{g_K}{\|g_K\|_{L^2}} \right\|_{L^2} = \left\| \mathcal{S}_H^{-1} \sum_{K \in \mathcal{T}_H} \frac{c_K}{\|g_K\|_{L^2}} \mathbf{1}_K \right\|_{L^2} \lesssim H^{-2} \sqrt{\sum_{K \in \mathcal{T}_H} |c_K|^2},$$

where we used that

$$\|\mathbf{1}_K\|_{L^2} = \|\mathcal{S}_H g_K\|_{L^2} \lesssim \|g_K\|_{L^2}.$$

The lower bound in (5.38) can be obtained similarly.

Finally, we can estimate the difference between the normalized global source terms g_K and the normalized local source terms $g_{K,m}$ as follows:

$$\begin{aligned}
&\left\| \frac{g_K}{\|g_K\|_{L^2}} - \frac{g_{K,m}}{\|g_{K,m}\|_{L^2}} \right\|_{L^2} \\
&\quad = \left\| \frac{g_K(\|g_{K,m}\|_{L^2} - \|g_K\|_{L^2}) + \|g_K\|_{L^2}(g_K - g_{K,m})}{\|g_K\|_{L^2}\|g_{K,m}\|_{L^2}} \right\|_{L^2} \\
&\quad \lesssim H^{-1} \exp(-C_{\mathrm{d}} m),
\end{aligned}$$

where we used (5.44). We finally obtain that

$$\left\| \sum_{K \in \mathcal{T}_H} c_K \left(\frac{g_K}{\|g_K\|_{L^2}} - \frac{g_{K,m}}{\|g_{K,m}\|_{L^2}} \right) \right\|_{L^2} \lesssim H^{-1-d/2} \exp(-C_{\mathrm{d}} m) \sqrt{\sum_{K \in \mathcal{T}_H} |c_K|^2}.$$

Using the oversampling condition $m \gtrsim \log(\frac{1}{H})$, cf. (5.37), the second inequality in (5.38) can be obtained by combining the previous estimates. Note that the first inequality in (5.38) can be proved using very similar arguments. Altogether, we obtain the Riesz stability of the source terms $g_{K,m}$. An analogous Riesz stability estimate can be derived for the source terms $g^*_{K,m}$. □

Remark 5.4.4 (Pessimistic oversampling condition)**.** The oversampling condition from Remark 5.4.1 is based on the super-exponential decay result (5.27), which can be observed numerically (see Section 5.6), but has not yet been rigorously proved. Instead of (5.27), we can also use the rigorous exponential decay result (5.39) to derive the pessimistic oversampling condition $m \gtrsim \log(\frac{1}{H})$. For the Helmholtz problem, one obtains the pessimistic oversampling condition $m \gtrsim \log(\frac{\kappa}{H})$. Both conditions are the same as for the LOD, cf. Theorems 3.4.2 and 4.4.2. The numerical experiments in Section 5.6 show that these conditions are pessimistic and that the conditions from Remark 5.4.1 seems to be more accurate. We emphasize that regardless of the oversampling, the Riesz stability (5.17) is still an assumption. For a method with the same super-exponential localization properties as the SLOD, but without stability assumptions on the basis, see Chapter 6.

5.5 Practical implementation

In this section we discuss aspects regarding the practical implementation of the SLOD. A practical implementation of the SLOD requires, on the one hand, that the source terms $g_{K,m}$ and $g^*_{K,m}$ can be computed with minimal communication between the patches. On the other hand, the sets $\{g_{K,m} : K \in \mathcal{T}_H\}$ and $\{g^*_{K,m} : K \in \mathcal{T}_H\}$ need to be Riesz stable bases of $\mathcal{P}^0(\mathcal{T}_H)$ in the sense of (5.17). In the following, we will first demonstrate that the choice of the basis functions in (5.12) can violate the Riesz stability (5.17) and then present an algorithm to overcome such stability issues.

For illustration purposes, we consider an elliptic model problem as in (3.36). It is posed on the domain $D = (0,1)^2$, which is equipped with the uniform Cartesian mesh $\mathcal{T}_H$. For the oversampling parameter $m = 2$, the patches corresponding to the elements with positions[1] $(1,1)$, $(1,2)$, and $(2,1)$ are contained in the patch corresponding to the element with position $(2,2)$. This nesting is problematic since, for example, the basis function corresponding to the element $(2,2)$ almost coincides with the basis functions corresponding to the element $(1,1)$, see Figure 5.4. To solve this problem, we consider only the (largest) patch of the element $(2,2)$. On this patch, we compute four basis functions corresponding to the source terms associated with the four smallest singular values on the

[1]The position is a vector in $\{1,\dots,H^{-1}\}^2$, where the first and second components determine the location in the x- and y-directions, respectively. The numbering is such that $(1,1)$ is the bottom left element.

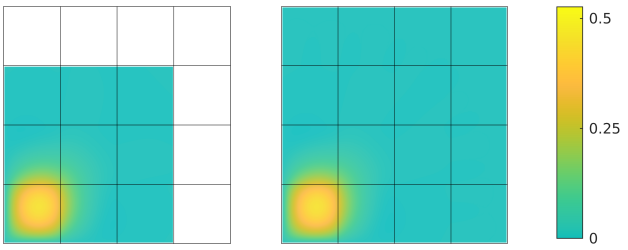

Figure 5.4: Instable choice of the SLOD basis functions corresponding to elements $(1,1)$ (left) and $(2,2)$ (right) for problem (3.36).

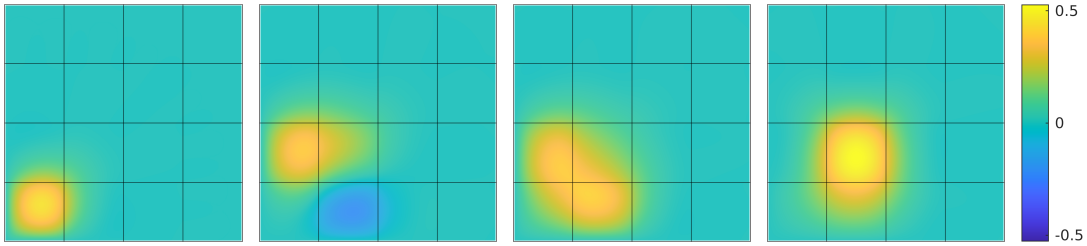

Figure 5.5: Stable choice of the SLOD basis functions corresponding to the source terms for the four smallest singular values (singular values increase from left to right) on the patch of element $(2,2)$.

patch. For a visualization of these four basis functions, see Figure 5.5. The elements $(1,1)$, $(1,2)$, and $(2,1)$ are no longer considered. By construction, this strategy yields four linearly independent basis functions. The span of these four functions contains the basis functions one would intuitively expect for the four elements.

The previously described procedure can be easily generalized. The first step is to identify groups of patches for which the basis functions are computed simultaneously. This can be done as follows: All patches $\mathsf{N}_m(K)$ for which the element K has a distance of at least m element layers to ∂D can be considered separately. Patches for which K has a distance of exactly $m-1$ element layers to ∂D are considered to be representatives of a corresponding group of patches. All remaining patches $\mathsf{N}_m(K)$ (K has a distance of less than $m-1$ layers to ∂D) are then uniquely assigned to these groups such that the patch is contained in the representative patch of the group. We can then apply the localization approach from Section 5.2 to the representative patches, selecting on each patch as many basis functions as patches are contained in the respective group of patches.

For the fine-scale discretization of the SLOD, we use a fine mesh $\mathcal{T}_h$ obtained by uniform refinement of the coarse mesh $\mathcal{T}_H$ and replace all infinite-dimensional spaces by their finite-dimensional fine-scale FE counterparts. This can be done in a similar way as for the LOD in Section 3.5. Following this procedure, we obtain a discrete approximation of the space Y of locally operator-harmonic functions on the patch S, by applying the discrete operator-harmonic extension

operator (with respect to S) to fine-scale boundary hat functions supported on $\partial S \backslash \partial D$. In practice, this is quite computationally expensive, and one rather uses a sampling approach similar to [BS18; Che+20]. More precisely, we sample fine-scale Dirichlet boundary data with nodal values independently and uniformly distributed in the interval $[-1, 1]$. Numerical experiments suggest that it is sufficient to choose the number of samples proportional to the number of coarse elements in the patch (we use a factor of five in the numerical experiments). Note that the space Y can alternatively be approximated by harmonic polynomials [BL11] or Steklov-type eigenfunctions [MSD22].

For the numerical realization of the SVD in (5.11), we note that suitable weighting matrices are required to guarantee that the right (resp. left) singular vectors are $\mathcal{V}(S)$-orthogonal (resp. $L^2(S)$-orthogonal). The computation of these weighting matrices requires the inversion and square root of a matrix whose size is proportional to the number of coarse elements in the considered patch, cf. [HP22b, App. B]. In practice, the effect of the weighting matrices on the choice of the SLOD basis functions is hardly noticeable. Therefore, for the numerical experiments in Section 5.6, the weighting matrices are omitted in the implementation of the SLOD.

5.6 Numerical experiments

This section numerically studies the SLOD for elliptic model problems and Helmholtz-type problems. We consider uniform Cartesian meshes of the domain D, where the mesh size denotes the side length of the elements instead of their diameter. The SLOD is implemented as described in Section 5.5, taking into account the remarks on the stable basis selection and the fine-scale discretization. We emphasize that, similar to Section 3.5 for the LOD, we expect the theoretical results of the SLOD to remain valid in the fully discrete setting.

Elliptic model problem

We first study the SLOD for an elliptic model problem. In the following, all errors are relative errors with respect to the energy norm defined in (3.37). The errors are computed using the fine-scale FE solution as the reference solution.

Optimal order convergence

To numerically study the optimal order convergence properties of the SLOD, we consider the elliptic model problem from Section 3.6. It is posed on the domain $D = (0, 1)^2$ and uses homogeneous Dirichlet boundary conditions. The coefficient is piecewise constant with respect to the mesh $\mathcal{T}_{2^{-7}}$, where the element values are realizations of independent uniformly distributed random variables in the interval $[0.01, 1]$, see Figure 3.3. For the fine-scale discretization we use

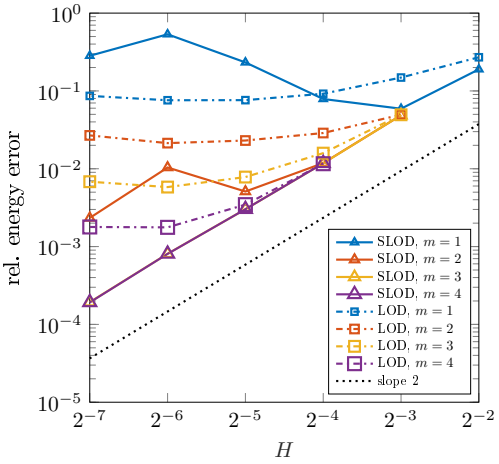

Figure 5.6: Errors of the SLOD and LOD as functions of H for several oversampling parameters m. The dotted line indicates the expected rate of convergence.

the mesh $\mathcal{T}_{2^{-9}}$. We consider the smooth source term defined by

$$f(x_1, x_2) = (x_1 + \cos(3\pi x_1)) \cdot x_2^3, \tag{5.45}$$

which, for the sake of consistency, is the same as for the numerical study of the LOD and MRLOD in Sections 3.6 and 4.7.

Provided that the oversampling parameter m is chosen sufficiently large, Figure 5.6 shows second order convergence for the SLOD. Note that in Figure 5.6 the yellow and orange lines are difficult to see because they are partially behind the purple line. Since $f \in H^1(D)$, the second order convergence is consistent with the theoretical prediction in Theorem 5.3.2. It can be observed that the SLOD requires much smaller oversampling parameters than the LOD to achieve the same accuracy. However, for the parameters $m = 1, 2$, it is clearly visible that the SLOD suffers from numerical pollution. To obtain optimal order convergence, the oversampling parameter needs to be coupled to the mesh size as described in Remark 5.4.1. For the LOD, numerical pollution can be avoided by using basis functions with slightly enlarged supports, cf. Chapter 3. More precisely, we use LOD basis functions with a support of $m + 1$ element layers around the respective elements. Note that the second order convergence may be difficult to see for the LOD, because only pairs of H and m are considered for which no patch coincides with the entire domain. This means that the convergence curves corresponding to large values of m may not start at the coarsest mesh, but at an intermediate one.

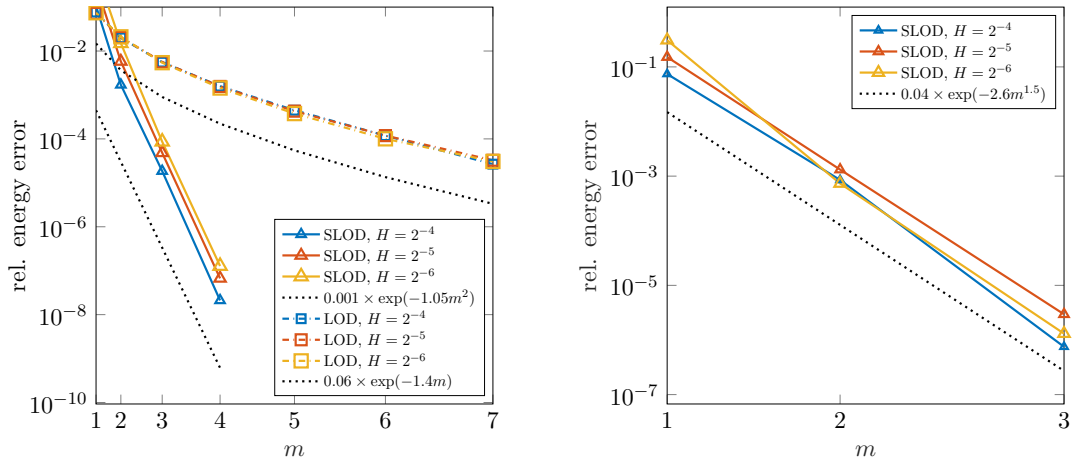

Figure 5.7: Errors of the SLOD and LOD as functions of H for several oversampling parameters m. The dotted line indicates the expected rate of convergence.

Super-exponential localization

Next, we want to numerically verify the super-exponential decay rates of the localization error as stated in (5.27). Since the decay rate depends on the spatial dimension of the PDE, we will consider elliptic problems posed on $D = (0,1)^d$ for $d \in \{2,3\}$. For the two-dimensional problem, we consider the coefficient from the previous numerical experiment, while for the three-dimensional problem, we consider the periodic coefficient

$$A(x_1,x_2,x_3) = \frac{1}{100} + \frac{99}{200}\Big(\prod_{i=1}^{3} \sin(2^8 \pi x_i) + 1\Big).$$

Both coefficients have the same upper and lower bounds of 0.01 and 1. We use homogeneous Dirichlet boundary conditions and consider the source term $f \equiv 1$ for which the optimal error term in Theorem 5.3.2 is zero and only the localization error is present. For the fine-scale discretization, we again use the mesh $\mathcal{T}_{2^{-9}}$. Exploiting the periodicity of the coefficient for the three-dimensional problem allows one to consider only $\mathcal{O}(m^d)$ patch problems, while the basis functions and local source terms corresponding to the remaining patches can be obtained by translation. This drastically reduces the computational cost of the SLOD. Furthermore, to avoid the costly assembly of the SLOD stiffness matrix, we use the collocation variant of the SLOD defined in (5.15) for the three-dimensional problem.

Figure 5.7 shows the expected super-exponential decay rates of the localization errors of the SLOD, cf. (5.27). Note that for the two-dimensional experiment, we have also included the localization errors of the LOD, which decay exponentially in m, cf. Theorem 3.4.2. It is clearly visible that the localization

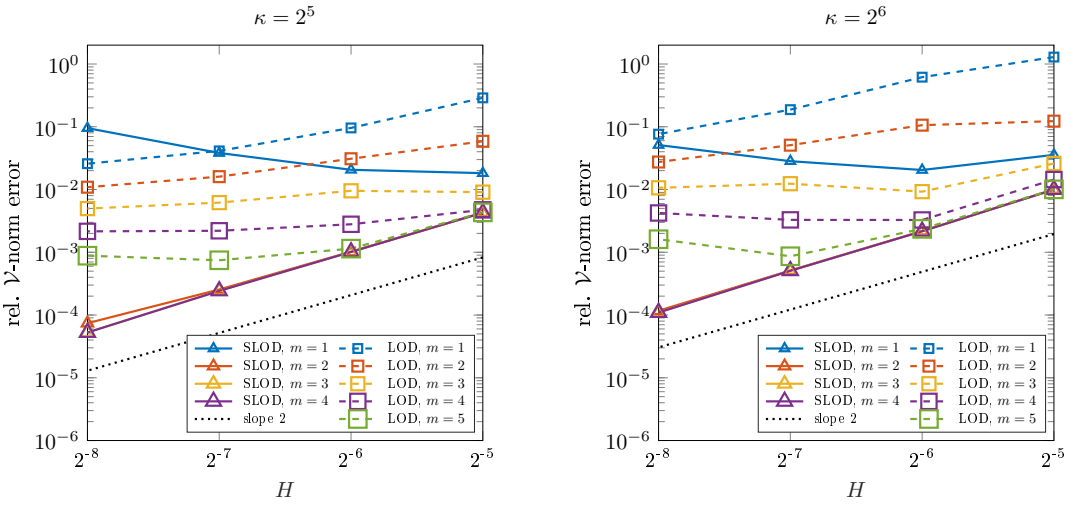

Figure 5.8: Errors of the SLOD and LOD as functions of H for several oversampling parameters m and $\kappa = 2^5, 2^6$. The dotted line indicates the expected rate of convergence.

errors of the SLOD are of a different magnitude compared to those of the LOD. Very large values of m are required for the LOD to match the localization errors of the SLOD. Note that for the three-dimensional problem, the fine-scale FE solution uses $2^{3\times 9} \approx 130$M degrees of freedom to resolve the coefficient. Using numerical homogenization, we are able to reduce this number significantly (e.g., to $2^{3\times 4} \approx 4$K for $H = 2^{-4}$) and still get a reliable approximation.

Helmholtz problem

Second, we numerically study the SLOD for Helmholtz problems. For a brief introduction to Helmholtz problems and some theoretical background, we refer to Section 4.1. The natural norm for Helmholtz problems is the wavenumber-dependent norm defined in (4.1). Subsequently, all errors are relative errors with respect to this norm. We compute the errors using the fine-scale FE solution as the reference solution.

Optimal order convergence

To numerically investigate the optimal order convergence of the SLOD for the Helmholtz problem, we consider the domain $D = (0,1)^2$ and impose homogeneous impedance boundary conditions (i.e., $\Gamma_2 = \partial D$). We use the source term given in (5.45) and use the mesh $\mathcal{T}_{2^{-10}}$ for the fine-scale discretization. Figure 5.8 shows convergence of second order for the SLOD provided that the oversampling parameter is chosen sufficiently large. One observes that already for the oversampling parameter $m = 2$, the SLOD yields better approximations

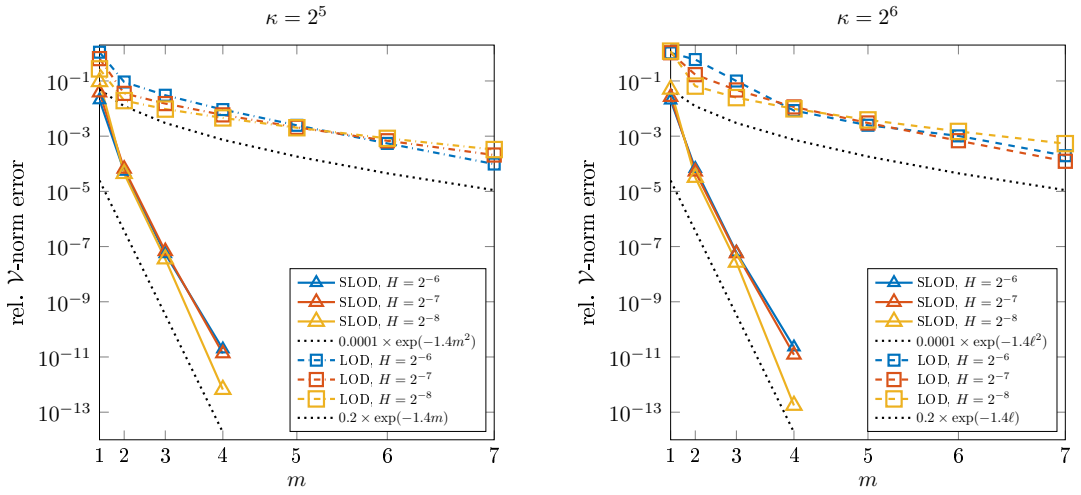

Figure 5.9: Errors of the SLOD and LOD as functions of H for several oversampling parameters m and $\kappa = 2^5$ and 2^6. The dotted line indicates the expected rate of decay.

than the LOD for $m = 5$, which underlines the high potential of the SLOD.

Super-exponential localization

To numerically verify the localization properties of the SLOD for the Helmholtz problem, we use the same setting as in the previous numerical experiment, but with the source term $f \equiv 1$. Recall that for this source term, only the localization error in Theorem 5.3.2 is present. Figure 5.9 shows the expected super-exponential decay of the localization error of the SLOD also for the Helmholtz problem. The localization errors of the SLOD are several orders of magnitude smaller than those of the LOD.

High-contrast heterogeneous media

Next, we apply the SLOD to a Helmholtz problem in heterogeneous media, namely $-\nabla \cdot (A_\varepsilon \nabla u) - \kappa^2 u = f$ on the domain $D = (0,1)^2$ with homogeneous impedance boundary conditions (i.e., $\Gamma_2 = \partial D$). For a given $0 < \varepsilon \ll 1$, the coefficient A_ε is defined such that it takes the value ε^2 inside some periodically aligned inclusions of size $\varepsilon/2$ and the value 1 elsewhere, see Figure 5.10 for a depiction of the coefficient. For $\varepsilon = 2^{-4}$ and $\kappa = 9$, a particular interaction between the wavenumber and the periodic structure of the inclusions leads to a negative effective wavenumber in homogenization theory, which triggers an exponential decay of the modulus of the Helmholtz solution in the bulk domain. This physically interesting effect is caused by so-called Mie resonances in the inclusions, cf. [PV20]. As source term, we use the one defined in (4.38) with

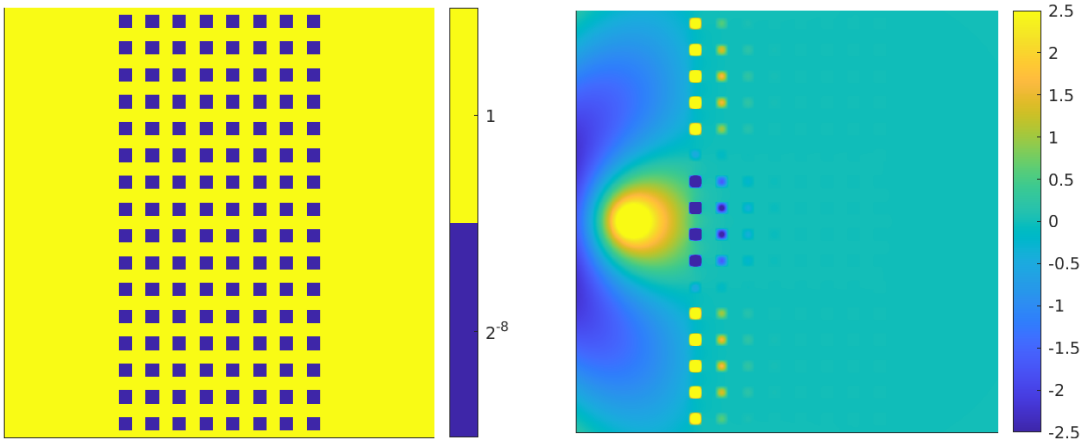

Figure 5.10: Heterogeneous coefficient $A_{2^{-4}}$ (left) and real part of the corresponding SLOD solution (right) for $\kappa = 9$, $m = 2$, and $H = 2^{-6}$.

$x_0 = (\frac{1}{8}, \frac{1}{2})^T$ and $r = \frac{1}{20}$.

We consider the parameters $H = 2^{-6}$ and $m = 2$. For a visualization of the corresponding SLOD solution, see Figure 5.10. Note that the color map is truncated to $[-2.5, 2.5]$ for illustration purposes. With respect to the weighted norm defined in (4.39), the SLOD approximation achieves a relative error of 3.3×10^{-3}. To achieve a similar accuracy, the LOD needs an oversampling parameter of at least $m = 4$.

Perfectly matched layer boundary condition

A perfectly matched layer (PML) is an artificial absorbing layer that can be used to truncate wave propagation problems on the full space to bounded computational domains. Compared to impedance boundary conditions, which often serve the same purpose, PMLs are able to avoid spurious reflections at the artificial boundary of the computational domain, cf. [Ber94; GLS21]. In this numerical experiment, we aim to demonstrate that the SLOD can be easily combined with PMLs. For this, we consider the domain $D = (0, 1)^2$ and the source term defined in (4.38) with $x_0 = (\frac{1}{2}, \frac{1}{2})^T$ and $r = \frac{1}{20}$. For the implementation of the PML, we adapt [Ber+07] to the present setting. We use the mesh $\mathcal{T}_H$ with $H = 2^{-7}$ and divide the domain D into a physical domain $D_{\mathrm{F}} \coloneqq (4H, 1 - 4H)^2$ and the absorbing layer $D_{\mathrm{A}} \coloneqq D \backslash D_{\mathrm{F}}$. For this configuration, the absorbing layer has a width of $4H$. The (unbounded) absorbing function in x-direction is given by

$$\rho_x(x) = \begin{cases} \frac{\mathrm{i}}{\kappa}\left(\frac{1}{-x} + \frac{1}{4H}\right) & \text{if } 0 < x \leq 4H, \\ \frac{\mathrm{i}}{\kappa}\left(\frac{1}{1-x} - \frac{1}{4H}\right) & \text{if } 1 - 4H \leq x < 1. \end{cases}$$

In y-direction, the absorbing function is chosen analogously. As usual for PMLs, we impose homogeneous Dirichlet boundary conditions on ∂D. We refer to [Ber+07, Sec. 3] for the weak formulation of the Helmholtz problem with PML

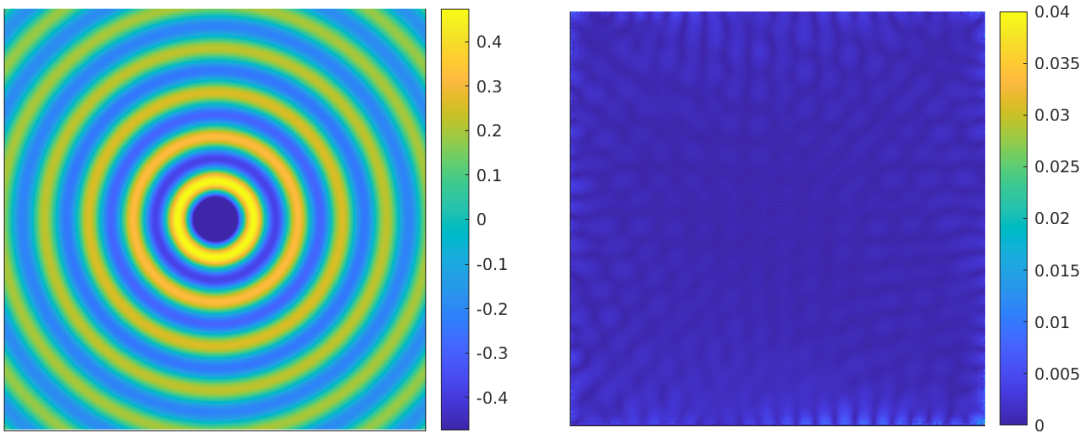

Figure 5.11: Real part of the PML-SLOD solution (left) and absolute value of the difference between the PML-SLOD solution and the reference solution (right) for $\kappa = 2^6$, $m = 2$, and $H = 2^{-7}$. Both plots only show the physical domain D_{F}.

boundary conditions. The PML-SLOD solution is then obtained by applying the SLOD to this problem and by restricting the resulting solution to the physical domain D_{F}. Using the mesh $\mathcal{T}_{2^{-10}}$ for the fine-scale discretization, we obtain, e.g., for $\kappa = 2^6$ and $m = 2$, a relative error of 6.5×10^{-3} with respect to the restricted $\mathcal{V}$-norm. For a visualization of the PML-SLOD solution and its error, see Figure 5.11. Note that for the plot of the solution, we truncated the color map to $[-0.45, 0.45]$.

6 Super-Localized Generalized Finite Element Method

The SLOD introduced in the previous chapter is an enhancement of the LOD with better localization properties. However, the main disadvantage of the SLOD is that the stability of its basis cannot be guaranteed a priori. For example, for high-contrast channeled coefficients or convection-dominated regimes, these basis stability issues may degrade the approximation quality of the method. For a numerical demonstration of this effect, see Section 6.5. This chapter introduces the Super-Localized Generalized Finite Element Method (SL-GFEM), which, in order to overcome these basis stability issues, combines the SLOD with a partition of unity (PU) approach, cf. [MB96; BM97]. More precisely, locally on nodal patches, we apply the respective local solution operator to classical FE source terms. Multiplying these spaces with the corresponding PU functions yields local ansatz spaces with a low effective dimension. By solving local spectral problems, we compute corresponding low-dimensional optimal approximation spaces. The global problem-adapted approximation space of the SL-GFEM is then obtained by gluing together these low-dimensional approximation spaces with a PU.

Compared to the MS-GFEM [BL11; EGH13; MSD22], the SL-GFEM has the major advantage that its local spectral problems are posed in a space spanned by a few deterministic snapshots. Thus, random sampling strategies can be avoided. Moreover, the local spectral problems are easily solvable, due to their typically low dimension. From an application point of view, the SL-GFEM is conceptually simple and straightforward to implement. Furthermore, by adjusting the polynomial degree of the FE source terms, one can easily construct higher order versions of the method. Similar to the higher order LOD [Mai21; DHM22], one obtains higher order convergence rates by exploiting only the regularity of the source term.

In this chapter, we prove that the SL-GFEM possesses the advantageous localization and convergence properties of the SLOD, which can be quantified a posteriori. Building on the well-understood theoretical foundation of the LOD, we additionally perform a pessimistic a priori error analysis proving that the SL-GFEM at least recovers the convergence and localization properties of the LOD. For the higher order versions of the method, we observe that increasing the polynomial degree alone significantly improves the localization properties. The implementation of the SL-GFEM is done using the `Python`-library `gridlod` [HK17] and supports the computation on large parallel clusters. We stress that

although the SL-GFEM is introduced for elliptic problems only, an extension to non-symmetric and indefinite problems such as the Helmholtz problem seems possible.

The content and presentation of the following chapter is primarily based on the preprint article

[Fre+22a] P. Freese, M. Hauck, T. Keil, and D. Peterseim. "A super-localized generalized finite element method". In: *arXiv preprint 2211.09461* (2022)

6.1 Elliptic model problem

On the bounded polytopal Lipschitz domain $D \subset \mathbb{R}^d$, which is assumed to be scaled to unit size, we consider the following linear diffusion-type PDE with homogeneous Dirichlet boundary conditions:

$$\begin{aligned} -\operatorname{div}(A\nabla u) &= f && \text{in } D, \\ u &= 0 && \text{on } \partial D. \end{aligned} \tag{6.1}$$

The matrix-valued diffusion coefficient $A \in L^\infty(D, \mathbb{R}^{d\times d})$ is assumed to be symmetric and positive definite almost everywhere. This means that there exist constants α, β with $0 < \alpha \leq \beta < \infty$ such that

$$\alpha|\xi|^2 \leq (A(x)\xi)\cdot\xi \leq \beta|\xi|^2 \tag{6.2}$$

holds for almost all $x \in D$ and all $\xi \in \mathbb{R}^d$ with $|\cdot|$ denoting the Euclidean norm of $\mathbb{R}^d$. The weak formulation of (6.1) uses the solution space $\mathcal{V} \coloneqq H^1_0(D)$ and the bilinear form $a\colon \mathcal{V}\times\mathcal{V} \to \mathbb{R}$, which is defined as

$$a(v,w) \coloneqq \int_D (A\nabla v)\cdot\nabla w \,\mathrm{d}x.$$

Friedrichs' inequality (see, e.g., [Alt16, Thm. 6.7]), the symmetry of a, and condition (6.2) ensure that the bilinear form a is an inner product on $\mathcal{V}$. Its induced norm is the energy norm defined by $\|\cdot\|_a \coloneqq \sqrt{a(\cdot,\cdot)}$. We denote by $\|\cdot\|_{a,S}$ the restriction of the energy norm to the subdomain $S \subset D$. Applying Friedrichs' inequality and using (6.2), we obtain the equivalence of the energy norm to the H^1-norm.

Given a source term $f \in L^2(D)$, the weak formulation of (6.1) seeks $u \in \mathcal{V}$ such that

$$a(u,v) = (f,v)_{L^2} \tag{6.3}$$

holds for all $v \in \mathcal{V}$. The well-posedness of (6.3) follows from the fact that a is coercive and continuous with constants one with respect to the energy norm, i.e., it holds that

$$a(v,v) \geq \|v\|_a^2, \qquad a(v,w) \leq \|v\|_a\|w\|_a$$

for all $v, w \in \mathcal{V}$. This directly follows form the definition of the energy norm and the Cauchy–Schwarz inequality. Note that the coercivity in fact holds with an equality. Applying the Lax–Milgram theorem (see, e.g., [Alt16, Thm. 6.2]) then yields the well-posedness of the problem (6.3). We emphasize that the coercivity of the bilinear form a on $\mathcal{V}$ also implies the coercivity of a for all subspaces of $\mathcal{V}$. In particular, this means that all corrector problems and conforming discretizations of the problem (6.3) are well-posed.

6.2 Derivation of multi-scale method

The SL-GFEM can be classified as PU method, cf. [MB96; BM97], since its global approximation space is obtained by gluing together local approximation spaces by means of a PU. For the construction of the local approximation spaces, we first introduce discontinuous FE spaces and conforming companion spaces.

6.2.1 Higher order discontinuous finite element spaces

The local approximation spaces of the SL-GFEM are obtained by applying the local solution operator to discontinuous FE spaces. Denoting by $p \in \mathbb{N}_0$ a fixed but arbitrary polynomial degree, we define the space of piecewise polynomials of degree at most p with respect to $\mathcal{T}_H$ as

$$\mathcal{P}(\mathcal{T}_H) \coloneqq \big\{v \in L^2(D) : v|_K \text{ is a polynomial of coordinate degree} \leq p,\ K \in \mathcal{T}_H\big\}.$$

Furthermore, we denote the restriction of $\mathcal{P}(\mathcal{T}_H)$ to a union of elements S by

$$\mathcal{P}(S) \coloneqq \{v|_S :\ v \in \mathcal{P}(\mathcal{T}_H)\}.$$

For any $K \in \mathcal{T}_H$, one can characterize the space $\mathcal{P}(K)$ in terms of a suitable orthonormal basis $\{\theta_{K,j} :\ j = 1, \dots, J\}$, where $J \coloneqq \dim \mathcal{P}(K)$. An example for such an orthonormal basis are L^2-normalized shifted tensor-product Legendre polynomials. A local orthonormal basis of $\mathcal{P}(\mathcal{T}_H)$ is given by

$$\{\theta_{K,j} :\ K \in \mathcal{T}_H,\ j = 1, \dots, J\}.$$

Henceforth, let us denote by $\Pi_H \colon L^2(D) \to \mathcal{P}(\mathcal{T}_H)$ the L^2-orthogonal projection, which is for any $v \in L^2(D)$ and $K \in \mathcal{T}_H$ locally defined such that

$$(\Pi_H v, w)_{L^2(K)} = (v, w)_{L^2(K)} \tag{6.4}$$

holds for all $w \in \mathcal{P}(K)$. By definition, the L^2-projection is locally L^2-stable. Furthermore, there exists $C_{\mathrm{ap}} > 0$ only depending on the polynomial degree p and the shape regularity of $\mathcal{T}_H$ such that, for all $K \in \mathcal{T}_H$ and $v \in H^k(K)$ with $k \leq p + 1$, it holds that

$$\|v - \Pi_H v\|_{L^2(K)} \leq C_{\mathrm{ap}} H^k |v|_{H^k(K)}, \tag{6.5}$$

where $|\cdot|_{H^k(K)}$ denotes the $H^k(K)$-seminorm, cf. [DPE11, Lem. 1.58]. We define the broken Sobolev space $H^k(\mathcal{T}_H)$ for $k \in \mathbb{N}_0$ by

$$H^k(\mathcal{T}_H) \coloneqq \big\{v \in L^2(D) : \, v|_K \in H^k(K), \; K \in \mathcal{T}_H\big\}.$$

This space can be equipped with the seminorm

$$|\cdot|^2_{H^k(\mathcal{T}_H)} \coloneqq \sum_{K\in\mathcal{T}_H} |\cdot|^2_{H^k(K)}.$$

Note that for $k = 0$, it holds that $H^0(\mathcal{T}_H) = L^2(D)$ and $|\cdot|_{H^0} = \|\cdot\|_{L^2}$.

Since $\mathcal{P}(\mathcal{T}_H)$ is non-conforming with respect to $\mathcal{V}$, we define, similarly to Section 3.2, local conforming companions of the functions in $\mathcal{P}(\mathcal{T}_H)$. Given a basis function $\theta_{K,j}$ of $\mathcal{P}(\mathcal{T}_H)$, we consider an associated bubble function $b_{K,j} \in H^1_0(K)$ such that $\Pi_H b_{K,j} = \theta_{K,j}$, which satisfies an estimate similar to (3.5) (the constant is now also p-dependent). An existence result for such bubble functions can be found in [Mai21, Cor. 3.6]. Note that an explicit characterization of the bubble functions is not required, since they are used for theoretical purposes only. Similar to (3.6), we can then define the following bubble operator:

$$\mathcal{B}_H \colon L^2(D) \to \mathcal{V}, \qquad v \mapsto \sum_{\substack{K\in\mathcal{T}_H\\ j=1,\dots,J}} \int_K v\theta_{K,j} \,\mathrm{d}x \; b_{K,j}. \tag{6.6}$$

Note that the operator $\mathcal{B}_H$ is constructed such that its kernel coincides with the kernel of Π_H, i.e., $\ker \mathcal{B}_H = \ker \Pi_H$. Furthermore, for all $v \in L^2(K)$ and $K \in \mathcal{T}_H$, it holds that

$$\|\mathcal{B}_H v\|_{L^2(K)} + H\|\nabla \mathcal{B}_H v\|_{L^2(K)} \leq C_{\mathcal{B}_H}\|v\|_{L^2(K)}, \tag{6.7}$$

where the constant $C_{\mathcal{B}_H} > 0$ depends only on the shape regularity of $\mathcal{T}_H$ and the polynomial degree p, cf. [Mai21, Cor. 3.6]. This estimate is the higher order analogue to (3.7).

6.2.2 Partition of unity

We denote by Λ_z the continuous $\mathcal{T}_H$-piecewise bilinear hat function associated with the node $z \in \mathcal{N}_H$, i.e., it holds that $\Lambda_z(y) = \delta_{yz}$ for all $y \in \mathcal{N}_H$, where δ denotes the Kronecker symbol. Here, we denoted by $\mathcal{N}_H$ the set of all (interior and boundary) nodes of $\mathcal{T}_H$. The SL-GFEM uses the hat functions

$$\{\Lambda_z : \, z \in \mathcal{N}_H\}$$

as PU functions. The hat functions satisfy the PU property $\sum_{z\in\mathcal{N}_H} \Lambda_z \equiv 1$ and have an L^∞-norm of one. Their gradients satisfy for all $z \in \mathcal{N}_H$ that

$$\|\nabla \Lambda_z\|_{L^\infty} \leq C_\Lambda H^{-1}, \tag{6.8}$$

where the constant $C_\Lambda > 0$ only depends on the shape regularity of $\mathcal{T}_H$. Denoting $S_z \coloneqq \operatorname{supp} \Lambda_z$, the shape regularity of $\mathcal{T}_H$ also implies that the maximal number of overlapping supports $\{S_z : z \in \mathcal{N}_H\}$ is uniformly bounded. More precisely, the number

$$C_{\mathrm{ol}} \coloneqq \max_{K \in \mathcal{T}_H} \#\{z \in \mathcal{N}_H : K \subset S_z\} \tag{6.9}$$

is bounded uniformly as the coarse mesh is refined.

6.2.3 Local approximation spaces

Denoting by $S_z^m \coloneqq \mathsf{N}_m(S_z)$ the m-th order patch of S_z, cf. (3.11), the local approximation space corresponding to node $z \in \mathcal{N}_H$ is defined by restricting

$$V_{H,m,z} \coloneqq \operatorname{span}\big\{\mathcal{L}_{S_z^m} q : q \in \mathcal{P}(S_z^m)\big\} \subset H_0^1(S_z^m) \tag{6.10}$$

to S_z, where $\mathcal{L}_{S_z^m}$ denotes the local solution operator on S_z^m, cf. (5.3). Due to the oversampling, the restricted space has a low effective dimension. This holds also true after multiplication with the hat function Λ_z when gluing the local approximation spaces together. Therefore, we investigate the optimal approximation of $\Lambda_z V_{H,m,z}$ by n-dimensional subspaces $Q(n) \subset H_0^1(S_z)$. Given the subspace $Q(n)$, the worst-case best approximation error is defined as

$$\sup_{v \in V_{H,m,z}} \inf_{w \in Q(n)} \frac{\|\Lambda_z v - w\|_{a,S_z}}{\|v\|_{a,S_z^m}}.$$

The minimal worst-case best approximation error is known as Kolmogorov n-width, cf. [Pin85], and is defined as

$$d_z^n(H,m) \coloneqq \inf_{Q(n) \subset H_0^1(S_z)} \sup_{v \in V_{H,m,z}} \inf_{w \in Q(n)} \frac{\|\Lambda_z v - w\|_{a,S_z}}{\|v\|_{a,S_z^m}}. \tag{6.11}$$

In fact, there exists a corresponding optimal local approximation space of dimension n, which we compute explicitly in the following. For this, we solve the low-dimensional eigenvalue problem, which seeks eigenpairs $(v,\lambda) \in V_{H,m,z} \times \mathbb{R}$ such that it holds

$$a_{S_z}(\Lambda_z v, \Lambda_z w) = \lambda\, a_{S_z^m}(v,w) \tag{6.12}$$

for all $w \in V_{H,m,z}$. This eigenvalue problem has $N \coloneqq \dim V_{H,m,z}$ eigenfunctions denoted by $\{v_i : i = 1,\dots,N\}$, where we assume an ordering such that the corresponding eigenvalues satisfy $\lambda_1 \geq \lambda_2 \geq \cdots \geq \lambda_N \geq 0$. Defining

$$V_{H,m,z}^n \coloneqq \operatorname{span}\{v_i : i = 1,\dots,n\},$$

the optimal local approximation space of dimension n is given by $\Lambda_z V_{H,m,z}^n$.

6.2.4 Global approximation space

The global approximation space of the SL-GFEM is obtained by gluing together the above local approximation spaces using the PU, i.e.,

$$V_{H,m,n}^{\mathrm{gfem}} \coloneqq \sum_{z \in \mathcal{N}_H} \Lambda_z V_{H,m,z}^n.$$

For measuring the overall error when approximating $\Lambda_z V_{H,m,z}$ by spaces of dimension n, we introduce the quantity d^n defined by

$$d^n(H,m) \coloneqq \max_{z \in \mathcal{N}_H} d_z^n(H,m). \tag{6.13}$$

The SL-GFEM approximation $u_{H,m,n}^{\mathrm{gfem}} \in V_{H,m,n}^{\mathrm{gfem}}$ is then defined such that

$$a(u_{H,m,n}^{\mathrm{gfem}}, v) = (f\,,\, v)_{L^2} \tag{6.14}$$

holds for all $v \in V_{H,m,n}^{\mathrm{gfem}}$. The following two sections are devoted to the theoretical investigation of the SL-GFEM. In Section 6.3 we present an a posteriori error analysis based on SLOD techniques, while in Section 6.4, we present a priori error bounds using LOD arguments.

6.3 A posteriori error analysis

The subsequent a posteriori error analysis of the SL-GFEM is based on a connection to a higher order variant of the SLOD, which we will derive in the following. We emphasize that this higher order variant serves theoretical purposes only and therefore is not implemented in practice. The higher order SLOD is conceptually very similar to the SLOD from Chapter 5 with the main difference that $J \coloneqq \dim \mathcal{P}(K)$ basis functions are constructed per mesh element instead of one for the SLOD.

For the derivation of these basis functions, we fix an element $K \in \mathcal{T}_H$ and denote its m-th order patch by $S \coloneqq \mathsf{N}_m(K)$. For the sake of readability, we drop all fixed indices. For the indices $j = 1, \dots, J$, we construct the prototypical (global) basis functions associated to the element K by the ansatz $\varphi_j \coloneqq \mathcal{L} g_j$ and denote their localized counterparts by $\psi_j \coloneqq \mathcal{L}_S g_j$. Here, $\mathcal{L}$ (resp. $\mathcal{L}_S$) denotes the global (resp. local) solution operator, cf. (2.14) and (5.3). The source terms $g_j \in \mathcal{P}(S)$ are henceforth determined such that the localization error is minimal. Denoting $\Sigma \coloneqq \partial S \backslash \partial D$, we recall the definitions of the operators $\mathrm{tr}_\Sigma \colon \mathcal{V}(S) \to X \subset H^{1/2}(\Sigma)$ and $\mathrm{tr}_\Sigma^{-1} \colon X \to \mathcal{V}(S)$ in (5.7) and (5.8), where $\mathcal{V}(S) = \mathcal{V}|_S$. Transferring identity (5.9) to the higher order setting, we obtain that the smallness of the localization error is equivalent to the (almost) $L^2(S)$-orthogonality of g_j to the space $Y \coloneqq \mathrm{tr}_\Sigma^{-1} X \subset \mathcal{V}(S)$. Similar to (5.11), we perform a SVD of the operator $\Pi_{H,S}|_Y$, where $\Pi_{H,S}$ denotes the restriction of Π_H

to the local subspace $\mathcal{P}(S)$. The local source terms g_j are then obtained as the left singular vectors corresponding to the J smallest singular values. More precisely with the notation from (5.11) and $R \coloneqq \dim \mathcal{P}(S)$, we choose the source terms g_j for $j = 1, \dots, J$ as

$$g_j \coloneqq q_{R-J+j}. \tag{6.15}$$

We emphasize that, by the definition of the SVD, the source terms g_j are L^2-normalized. For all $j = 1, \dots, J$, we obtain that

$$\sup_{v \in Y \colon \|v\|_{\mathcal{V}(S)}=1} (g_j \, , \, v)_{L^2(S)} \leq \sigma_{R-J+1},$$

cf. (5.13). Similar to (5.18), the localization error of the higher order SLOD is determined by the quantity σ defined as

$$\sigma(H, m) \coloneqq \max_{K \in \mathcal{T}_H} \sigma_K(H, m), \qquad \sigma_K(H, m) \coloneqq \sigma_{R-J+1}. \tag{6.16}$$

Note that the dependence of σ on the (fixed) polynomial degree p is not made explicit here.

Numerically, one observes that σ decays rapidly as the oversampling parameter m or the polynomial degree p are increased. For a study of the decay of σ in m, see Sections 5.4 and 5.6. There, for $p = 0$, numerical experiments have been performed that suggest a super-exponential decay of σ in m. Pessimistic exponential decay results for the case $p = 0$ were proved in Theorem 5.4.3. Note that also for $p > 0$, numerical experiments indicate a super-exponential decay of σ as m is increased. Conversely, for fixed m, a rapid decay of σ in p can be observed numerically, cf. Figure 6.1.

Since in the remainder the element $K \in \mathcal{T}_H$ is not fixed but variable, it needs to be included in the notation. Let us denote the source term, the global basis function, and its localized counterpart corresponding to the element K by $g_{K,m,j}, \varphi_{K,m,j}$, and $\psi_{K,m,j}$, respectively. For the error analysis of the SLGFEM we use the collocation variant of the higher order SLOD, cf. (5.15). Its approximation is defined as

$$u_{H,m}^{\text{slod}} \coloneqq \sum_{K \in \mathcal{T}_H} c_{K,j} \, \psi_{K,m,j}, \tag{6.17}$$

where the $(c_{K,j})_{K \in \mathcal{T}_H, j=1,\dots,J}$ are the coefficients of the expansion of $\Pi_H f$ in terms of the local source terms

$$\{g_{K,m,j} : \, K \in \mathcal{T}_H, \, j = 1, \dots, J\}. \tag{6.18}$$

We emphasize that, in order to obtain a reasonable approximation, the local source terms and the corresponding basis functions need to be chosen in a stable way. Similar to (5.17), we assume that the local source terms (6.18) form a Riesz

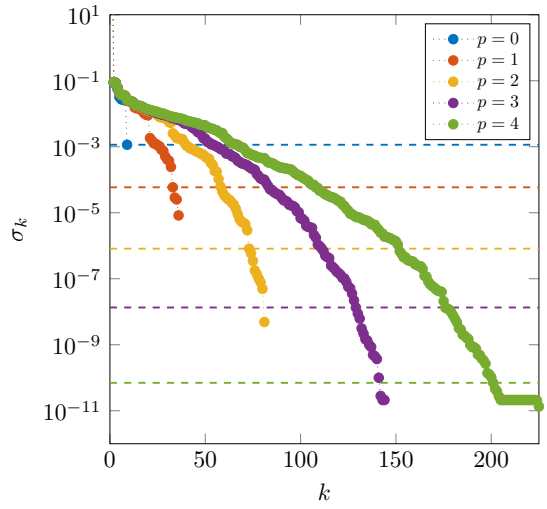

Figure 6.1: Singular values of the operator $\Pi_{H,S}|_Y$ for a fixed patch S with $m = 1$ and several values of p for problem (3.36). The dashed horizontal lines indicate the singular values σ_{R-J+1}, which determine the value of σ defined in (6.16).

basis of $\mathcal{P}(\mathcal{T}_H)$, i.e., there exists $C_{\mathrm{r}}(H,m) > 0$ depending polynomially on H^{-1} and m such that

$$C_{\mathrm{r}}^{-1}(H,m) \sum_{\substack{K\in\mathcal{T}_H \\ j=1,\dots,J}} c_{K,j}^2 \leq \Big\| \sum_{\substack{K\in\mathcal{T}_H \\ j=1,\dots,J}} c_{K,j} g_{K,m,j} \Big\|_{L^2}^2 \leq C_{\mathrm{r}}(H,m) \sum_{\substack{K\in\mathcal{T}_H \\ j=1,\dots,J}} c_{K,j}^2. \tag{6.19}$$

holds for all $(c_{K,j})_{K\in\mathcal{T}_H, j=1,\dots,J}$.

The following theorem provides an a posteriori error bound for the SL-GFEM based on the higher order SLOD. This bound includes the local optimal approximation error d^n defined in (6.13), which can be bounded using Theorem 6.3.2.

Theorem 6.3.1 (A posteriori error bound for the SL-GFEM)**.** *For any $f \in H^s(\mathcal{T}_H)$, $s \in \mathbb{N}_0$, the SL-GFEM approximation* (6.14) *satisfies for $k := \min\{s, p+1\}$ that*

$$\begin{aligned} &\|u - u_{H,m,n}^{\mathrm{gfem}}\|_a \\ &\quad \lesssim H^{1+k}|f|_{H^k(\mathcal{T}_H)} + m^{d+1} C_{\mathrm{r}}^{1/2}(H,m)\big(\sigma(H,m) + H d^n(H,m)\big)\|f\|_{L^2}, \end{aligned}$$

where the hidden constant only depends on α, β, p, and the quasi-uniformity and shape regularity of $\mathcal{T}_H$.

Proof. Applying Céa's lemma (see, e.g., [EG04, Lem. 2.28]) yields that

$$\|u - u_{H,m,n}^{\mathrm{gfem}}\|_a \leq \|u - v\|_a \tag{6.20}$$

for any $v \in V^{\mathrm{gfem}}_{H,m,n}$. We denote by $u^{\mathrm{slod}}_{H,l}$ the solution of the higher order collocation variant of the SLOD for the oversampling parameter $l \coloneqq \lfloor m/2 \rfloor$, i.e.,

$$u^{\mathrm{slod}}_{H,l} \coloneqq \sum_{\substack{K\in\mathcal{T}_H \\ j=1,\dots,J}} c_{K,j}\psi_{K,l,j}, \tag{6.21}$$

where the $(c_{K,j})_{K\in\mathcal{T}_H,j=1,\dots,J}$ are the coefficients of the expansion of $\Pi_H f$ in terms of the local source terms $\{g_{K,l,j} : K \in \mathcal{T}_H, j = 1,\dots,J\}$, cf. (6.17). Adding and subtracting $u^{\mathrm{slod}}_{H,l}$ in (6.20) and employing the triangle inequality yields that

$$\|u - u^{\mathrm{gfem}}_{H,m,n}\|_a \leq \|u - u^{\mathrm{slod}}_{H,l}\|_a + \|u^{\mathrm{slod}}_{H,l} - v\|_a. \tag{6.22}$$

The first term is the error of the collocation variant of the higher order SLOD. Using the approximation property (6.5) of the L^2-projection, it is not difficult to derive a higher order version of Theorem 5.3.2, i.e.,

$$\|u - u^{\mathrm{slod}}_{H,l}\|_a \lesssim H^{1+k}|f|_{H^k(\mathcal{T}_H)} + C_{\mathrm{r}}^{1/2}(H,l)l^{d/2}\sigma(H,l)\|f\|_{L^2},$$

which gives the desired bound for the first term in (6.22).

For the second term in (6.22), we choose $v \in V^{\mathrm{gfem}}_{H,m,n}$ as the sum of functions $v^n_z \in V^n_{H,m,z}$ to be specified later, i.e.,

$$v = \sum_{z\in\mathcal{N}_H} \Lambda_z v^n_z.$$

Using the PU property of the hat functions $\sum_{z\in\mathcal{N}_H}\Lambda_z \equiv 1$, we obtain that

$$\|u^{\mathrm{slod}}_{H,l} - v\|^2_a = \Big\| \sum_{z\in\mathcal{N}_H} \Lambda_z(u^{\mathrm{slod}}_{H,l} - v^n_z)\Big\|^2_a \leq C_{\mathrm{ol}} \sum_{z\in\mathcal{N}_H} \|\Lambda_z(u^{\mathrm{slod}}_{H,l} - v^n_z)\|^2_{a,S_z},$$

where C_{ol} is defined in (6.9) and denotes the maximal number of overlapping supports S_z. For each $z \in \mathcal{N}_H$, locally on S_z, we replace $u^{\mathrm{slod}}_{H,l}$ with $u^{\mathrm{slod}}_{H,l,z}$ defined by

$$u^{\mathrm{slod}}_{H,l,z} \coloneqq \sum_{\substack{K\subset S^l_z \\ j=1,\dots,J}} c_{K,j}\psi_{K,l,j} \in H^1_0(S^m_z),$$

where the coefficients $c_{K,j}$ are defined in (6.21). As approximation to $u^{\mathrm{slod}}_{H,l,z}$ in the space $V_{H,m,z}$, cf (6.10), we use

$$v_z \coloneqq \sum_{\substack{K\subset S^l_z \\ j=1,\dots,J}} c_{K,j}\hat{\psi}_{K,l,j} \in V_{H,m,z},$$

where $\hat{\psi}_{K,l,j} \coloneqq \mathcal{L}_{S^m_z} g_{K,l,j} \in V_{H,m,z}$. Note that the difference between $\psi_{K,l,j}$ and $\hat{\psi}_{K,l,j}$ is the local domain, where the local solution operator is applied to

the common local source term $g_{K,l,j}$. Due to the rapid decay of $\psi_{K,l,j}$, the function $\hat{\psi}_{K,l,j}$ is a good approximation to $\psi_{K,l,j}$. We choose $v_z^n \in V_{H,m,z}^n$ as the not necessarily unique element minimizing $\|\Lambda_z v_z - \Lambda_z v_z^n\|_{a,S_z^m}$.

Abbreviating

$$e_z^1 \coloneqq u_{H,l,z}^{\mathrm{slod}} - v_z, \qquad e_z^2 \coloneqq v_z - v_z^n$$

and performing the local replacement mentioned above, we obtain that

$$\|\Lambda_z(u_{H,l}^{\mathrm{slod}} - v_z^n)\|_{a,S_z}^2 \leq 2\big(\|\Lambda_z e_z^1\|_{a,S_z}^2 + \|\Lambda_z e_z^2\|_{a,S_z}^2\big), \tag{6.23}$$

where we added and subtracted v_z and employed the triangle inequality. Using the product rule and (6.8), we get for the first term on the right-hand side of (6.23) that

$$\|\Lambda_z e_z^1\|_{a,S_z}^2 \leq 2\beta\big(C_\Lambda^2 H^{-2}\|e_z^1\|_{L^2(S_z)}^2 + \|\nabla e_z^1\|_{L^2(S_z)}^2\big). \tag{6.24}$$

Noting that by $e_z^1 \in H_0^1(S_z^m)$, we can apply Friedrichs' inequality on S_z^m with $\operatorname{diam}(S_z^m) \lesssim mH$ to estimate the first term in (6.24). We obtain that

$$\|e_z^1\|_{L^2(S_z)}^2 \leq \|e_z^1\|_{L^2(S_z^m)}^2 \lesssim m^2 H^2 \|\nabla e_z^1\|_{L^2(S_z^m)}^2. \tag{6.25}$$

For the second term in (6.24), we use the trivial estimate

$$\|\nabla e_z^1\|_{L^2(S_z)}^2 \leq \|\nabla e_z^1\|_{L^2(S_z^m)}^2,$$

which implies that in order to bound (6.24), it is sufficient to estimate the term $\|\nabla e_z^1\|_{L^2(S_z^m)}$. Denoting $\Sigma \coloneqq \partial S_K^l \backslash \partial D$, where $S_K^l \coloneqq \mathsf{N}_l(K)$, we obtain, similar to the proof of Theorem 5.3.1, for all $v \in \mathcal{V}(S_K^l)$ the following continuity estimate

$$\|\operatorname{tr}_\Sigma^{-1}\operatorname{tr}_\Sigma v\|_{\mathcal{V}(S_K^l)} \leq (1+\alpha^{-1}\beta)\|v\|_{\mathcal{V}(S_K^l)}.$$

Using this estimate, one can show that

$$(g_{K,l,j}\,,\,\operatorname{tr}_\Sigma^{-1}\operatorname{tr}_\Sigma e_z^1)_{L^2(S_K^l)} \leq (1+\alpha^{-1}\beta)\sigma(H,l)\|e_z^1\|_{\mathcal{V}(S_K^l)}. \tag{6.26}$$

By (5.9) and (6.26), the discrete Cauchy–Schwarz inequality, the finite overlap of the patches S_K^l, and Friedrichs' inequality, we obtain that

$$\begin{aligned}
\alpha\|\nabla e_z^1\|_{L^2(S_z^m)}^2 &\leq \sum_{\substack{K\subset S_z^l\\ j=1,\dots,J}} c_{K,j}\, a(\psi_{K,l,j} - \hat{\psi}_{K,l,j}, e_z^1) \\
&\leq (1+\alpha^{-1}\beta)\sigma(H,l) \sum_{\substack{K\subset S_z^l\\ j=1,\dots,J}} |c_{K,j}|\|e_z^1\|_{\mathcal{V}(S_K^l)} \\
&\lesssim (1+\alpha^{-1}\beta)\sigma(H,l) l^{d/2} J^{1/2} \sqrt{\sum_{\substack{K\subset S_z^l\\ j=1,\dots,J}} c_{K,j}^2}\, \|\nabla e_z^1\|_{L^2(S_z^m)}.
\end{aligned}$$

Combining the previous estimate with (6.24) and (6.25) yields a bound for the first term in (6.23).

To estimate the second term in (6.23), we use the definition of the Kolmogorov n-width in (6.11), Friedrichs' inequality on the patch S_z^m with $\operatorname{diam}(S_z^m) \lesssim mH$, the discrete Cauchy–Schwarz inequality, and that the source terms $g_{K,l,j}$ are L^2-normalized. We obtain that

$$\begin{aligned}
\|\Lambda_z e_z^2\|_{a,S_z} &\leq d^n(H,m)\|v_z\|_{a,S_z^m} = d^n(H,m)\left\|\mathcal{L}_{S_z^m} \sum_{\substack{K\subset S_z^l \\ j=1,\dots,J}} c_{K,j} g_{K,l,j}\right\|_{a,S_z^m} \\
&\lesssim d^n(H,m)\alpha^{-1/2} mH \left\| \sum_{\substack{K\subset S_z^l \\ j=1,\dots,J}} c_{K,j} g_{K,l,j}\right\|_{L^2(S_z^m)} \\
&\lesssim d^n(H,m)\alpha^{-1/2} mH\, l^{d/2} J^{1/2} \sqrt{\sum_{\substack{K\subset S_z^l \\ j=1,\dots,J}} c_{K,j}^2}.
\end{aligned}$$

The desired a posteriori error estimate of the SL-GFEM can then be concluded by combining all previous estimates and utilizing that

$$\sum_{z\in\mathcal{N}_H} \sum_{\substack{K\subset S_z^l \\ j=1,\dots,J}} c_{K,j}^2 \lesssim m^d \sum_{\substack{K\in\mathcal{T}_H \\ j=1,\dots,J}} c_{K,j}^2 \lesssim C_{\mathrm{r}}(H,m) m^d \|f\|_{L^2}^2,$$

where we used (6.19), the fact that the $(c_{K,j})_{K\in\mathcal{T}_H,\, j=1,\dots,J}$ are the coefficients of the expansion of $\Pi_H f$ in terms of the local source terms, cf. (6.17), and the L^2-stability of Π_H. Finally, for the sake of readability, we replace $l = \lfloor m/2 \rfloor$ with m. Using (5.27), this may introduce additional constants that change the decay rate of σ by a constant factor. □

Subsequently, we derive a bound for the local approximation error d^n that appears in the error bound from Theorem 6.3.1. To do this, we locally use the higher order SLOD to construct basis functions of the spaces $V_{H,m,z}$ defined in (6.10). For a fixed node $z \in \mathcal{N}_H$, we treat the patch S_z^m as the whole domain and locally apply the higher order SLOD. For $l = 1, \dots, m-1$, this results in the basis functions

$$\{\tilde{\varphi}_{K,l,j} \coloneqq \mathcal{L}_{S_z^m} \tilde{g}_{K,l,j} : \ K \subset S_z^m,\, j = 1, \dots, J\} \tag{6.27}$$

with the source terms $\tilde{g}_{K,l,j} \in \mathcal{P}(\tilde{S}_K^l)$, where $\tilde{S}_K^l \coloneqq S_K^l \cap S_z^m$ and l denotes the local oversampling parameter. Here, we denote $S_K^l \coloneqq \mathsf{N}_l(K)$ and use a tilde to emphasize that the basis functions and source terms are, in general, not the same as their counterparts in the global setting. The corresponding localized basis functions are given by

$$\{\tilde{\psi}_{K,l,j} \coloneqq \mathcal{L}_{\tilde{S}_K^l} \tilde{g}_{K,l,j} : \ K \subset S_z^m,\, j = 1, \dots, J\}, \tag{6.28}$$

which are also in general different to their counterparts in the global setting.

Similarly as before, we need to measure for all $K \subset S_z^m$ the orthogonality of the source terms $\{\tilde{g}_{K,l,j} : j = 1, \dots, J\}$ on the corresponding space of operator-harmonic functions, cf. (6.16). Denoting $\Sigma \coloneqq \partial \tilde{S}_K^l \backslash \partial S_z^m$, this space of operator-harmonic functions is in the local setting given by

$$\operatorname{tr}_\Sigma^{-1} \operatorname{tr}_\Sigma \left(H_0^1(S_z^m)|_{\tilde{S}_K^l} \right). \tag{6.29}$$

Furthermore, similar to (5.11) and (6.16), we denote the singular values of Π_H restricted to (6.29) by $\tilde{\sigma}_1 \geq \tilde{\sigma}_2 \geq \cdots \geq \tilde{\sigma}_K \geq 0$ and define

$$\tilde{\sigma}(H, m, l) \coloneqq \max_{z \in \mathcal{N}_H} \max_{K \in \mathcal{T}_H} \tilde{\sigma}_{z,K}, \qquad \tilde{\sigma}_{z,K} \coloneqq \tilde{\sigma}_{R-J+1}.$$

Note that the quantity $\tilde{\sigma}$ is strongly related to its counterpart σ from (6.16). For fixed H and m, one observes a rapid decay of $\tilde{\sigma}$ as the local oversampling parameter l is increased (the parameter l in the local setting plays the role of m in the global setting), cf. Figures 5.3 and 6.1.

In order to ensure the stability of the local basis, we need to require a local variant of (6.19), i.e., we assume that for all patches S_z^m the set

$$\{\tilde{g}_{K,l,j} : K \subset S_z^m, j = 1, \dots, J\}$$

is a Riesz basis of $\mathcal{P}(S_z^m)$, i.e., there is $\tilde{C}_{\mathrm{r}}(H, m, l) > 0$ depending polynomially on H^{-1}, m, and l such that for all $z \in \mathcal{N}_H$ it holds that

$$\tilde{C}_{\mathrm{r}}^{-1}(H, m, l) \sum_{\substack{K \subset S_z^m \\ j=1,\dots,J}} c_{K,j}^2 \leq \left\| \sum_{\substack{K \subset S_z^m \\ j=1,\dots,J}} c_{K,j} \tilde{g}_{K,l,j} \right\|_{L^2(S_z^m)}^2 \leq \tilde{C}_{\mathrm{r}}(H, m, l) \sum_{\substack{K \subset S_z^m \\ j=1,\dots,J}} c_{K,j}^2 \tag{6.30}$$

for all $(c_{K,j})_{K \subset S_z^m, j=1,\dots,J}$.

The following theorem gives a bound of the local approximation error d^n that appears in the error bound of Theorem 6.3.1 using the local higher order SLOD construction introduced above.

Theorem 6.3.2 (Bound on d^n)**.** *The Kolmogorov n-width defined in* (6.13) *can be estimated for $l = 1, \dots, m-1$ as*

$$d^n(H, m) \lesssim m\, l^{d/2} H^{-1} \tilde{C}_{\mathrm{r}}^{1/2}(H, m, l) \tilde{\sigma}(H, m, l),$$

where $n \approx l^d$. The hidden constant only depends on α, β, p, and the quasi-uniformity and shape regularity of $\mathcal{T}_H$.

Proof. For the proof, we fix the node $z \in \mathcal{N}_H$ and the oversampling parameter m. As an approximation space $Q(n)$ of dimension $n \approx l^d$, we choose

$$Q(n) \coloneqq \operatorname{span}\{\Lambda_z \tilde{\psi}_{K,l,j} : K \subset S_z^l, j = 1, \dots, J\}$$

with the basis functions defined in (6.28). To approximate $v_z \in V_{H,m,z}$, we choose the element $w_z \in Q(n)$ as

$$w_z = \Lambda_z \sum_{\substack{K \subset S_z^l \\ j=1,\dots,J}} c_{K,j} \tilde{\psi}_{K,l,j},$$

where the $c_{K,j}$ are the coefficients of the expansion of v_z in terms of the basis functions $\tilde{\varphi}_{K,l,j}$ defined in (6.27). Note that by (6.30), the coefficients $c_{K,j}$ are uniquely determined. We can estimate the spectral approximation error (6.11) using the definitions of v_z and w_z as follows:

$$\begin{aligned} d_z^n(H,m) &= \inf_{Q(n) \subset H_0^1(S_z)} \sup_{v_z \in V_{H,m,z}} \inf_{w_z \in Q(n)} \frac{\|\Lambda_z v_z - w_z\|_{a,S_z}}{\|v_z\|_{a,S_z^m}} \\ &\leq \sup_{v_z \in V_{H,m,z}} \frac{\|\Lambda_z v_z - w_z\|_{a,S_z}}{\|v_z\|_{a,S_z^m}}. \end{aligned} \tag{6.31}$$

Denoting

$$e_z := \sum_{\substack{K \subset S_z^l \\ j=1,\dots,J}} c_{K,j} \big(\tilde{\varphi}_{K,l,j} - \tilde{\psi}_{K,l,j} \big) \in H_0^1(S_z^m)$$

and using the product rule, the triangle inequality, and (6.8), we obtain for the numerator in (6.31) that

$$\beta^{-1/2} \|\Lambda_z v_z - w_z\|_{a,S_z} \leq \|\nabla(\Lambda_z e_z)\|_{L^2(S_z^m)} \leq \big(C_\Lambda H^{-1} \|e_z\|_{L^2(S_z^m)} + \|\nabla e_z\|_{L^2(S_z^m)} \big).$$

Applying Friedrichs' inequality on the patch S_z^m with $\operatorname{diam}(S_z^m) \lesssim mH$, we can bound the first term against the second term, i.e.,

$$\|e_z\|_{L^2(S_z^m)} \lesssim mH \|\nabla e_z\|_{L^2(S_z^m)}.$$

Note that the estimate (6.26) can be transferred to the local setting with $\tilde{\sigma}$ instead of σ. Using the finite overlap of the patches $\tilde{S}_K^l$, the discrete Cauchy–Schwarz inequality, and Friedrichs' inequality on S_z^m, we obtain that

$$\begin{aligned} \alpha \|\nabla e_z\|_{L^2(S_z^m)}^2 &\leq \sum_{\substack{K \subset S_z^l \\ j=1,\dots,J}} c_{K,j} a(\tilde{\varphi}_{K,l,j} - \tilde{\psi}_{K,l,j}, e_z) \\ &\leq (1 + \alpha^{-1}\beta) \tilde{\sigma}(H,m,l) \sum_{\substack{K \subset S_z^l \\ j=1,\dots,J}} c_{K,j} \|e_z\|_{H^1(\tilde{S}_K^l)} \\ &\lesssim (1 + \alpha^{-1}\beta) l^{d/2} \tilde{\sigma}(H,m,l) \sqrt{\sum_{\substack{K \subset S_z^l \\ j=1,\dots,J}} c_{K,j}^2} \|\nabla e_z\|_{L^2(S_z^m)}. \end{aligned}$$

Adding the remaining coefficients $c_{K,j}$ from the expansion of v_z in terms of the $\tilde{\varphi}_{K,l,j}$ and employing the local Riesz stability (6.30) yields that

$$\begin{aligned}\tilde{C}_{\mathrm{r}}^{-1}(H,m,l)\sum_{\substack{K\subset S_z^m\\ j=1,\dots,J}} c_{K,j}^2 &\leq \Big\| \sum_{\substack{K\subset S_z^m\\ j=1,\dots,J}} c_{K,j}\tilde{g}_{K,l,j}\Big\|^2_{L^2(S_z^m)}\\ &\leq C_{\mathcal{B}_H}^2 H^{-2}\Big\| \sum_{\substack{K\subset S_z^m\\ j=1,\dots,J}} c_{K,j}\tilde{g}_{K,l,j}\Big\|^2_{H^{-1}(S_z^m)}\\ &\leq C_{\mathcal{B}_H}^2\beta H^{-2}\|v_z\|^2_{a,S_z^m},\end{aligned}$$

where we used that by (6.6) and (6.7), it holds for all $q\in\mathcal{P}(S_z^m)$ that

$$\begin{aligned}\|q\|_{L^2(S_z^m)} &= \sup_{v\in H_0^1(S_z^m)}\frac{(q\,,\,v)_{L^2(S_z^m)}}{\|v\|_{L^2(S_z^m)}} \leq C_{\mathcal{B}_H}H^{-1}\sup_{v\in H_0^1(S_z^m)}\frac{(q\,,\,\mathcal{B}_H v)_{L^2(S_z^m)}}{\|\nabla\mathcal{B}_H v\|_{L^2(S_z^m)}}\\ &\leq C_{\mathcal{B}_H}H^{-1}\|q\|_{H^{-1}(S_z^m)}.\end{aligned}$$

Combining the above estimates gives the assertion. □

Remark 6.3.3 (Choice of parameters)**.** This remark specifies how to choose the oversampling parameter m and the dimension of the local optimal approximation spaces n in order to preserve the optimal order convergence in Theorem 6.3.1. For m, the super-exponential decay (5.27) implies the condition $m\gtrsim(\log\frac{1}{H})^{(d-1)/d}$. Using Theorem 6.3.2 and that $\tilde{\sigma}$ has similar decay properties as σ, we obtain for n the condition $n\gtrsim(\log\frac{1}{H})^{d-1}$. Note that these choices require the validity of (5.27), (6.19), and (6.30). For a (pessimistic) choice of parameters that holds without additional assumptions, see Remark 6.4.4 below.

6.4 (Pessimistic) a priori error analysis

This section presents an a priori error analysis of the SL-GFEM based on a higher order variant of the LOD that we derive below. Note that the exponential localization properties of the LOD do not match the practically observed super-exponential localization properties of the SLOD, cf. (5.27). Nevertheless, the LOD construction has the decisive advantage that the stability of the basis is guaranteed by construction and that its exponential localization properties can be rigorously proved. This allows an a priori analysis without assumptions on the stability of the basis and without conjectures on the decay of singular values, cf. (5.27), (6.19), and (6.30).

The construction of the higher order LOD is similar to that of the LOD in Chapter 3 with the main difference that a different fine-scale space $\mathcal{W}$ is used. More precisely, instead of (2.17), we define $\mathcal{W}$ as the kernel of the higher order L^2-orthogonal projection (6.4), i.e.,

$$\mathcal{W} := \ker\Pi_H. \tag{6.32}$$

The constructions of the corrector $\mathcal{C}$, the element correctors $\mathcal{C}_K$, the localized element correctors $\mathcal{C}_{K,m}$, and the localized corrector $\mathcal{C}_m$, cf. (3.1), (3.15), (3.21), and (3.23), can be performed analogously for the higher order fine-scale space defined above. The basis functions of the higher order LOD are obtained by adding localized corrections to the bubble functions from Section 6.2.1, i.e.,

$$V_{H,m}^{\mathrm{lod}} \coloneqq \operatorname{span}\{(\mathtt{id} - \mathcal{C}_m) b_{K,j} : K \in \mathcal{T}_H,\, j = 1, \dots, J\}.$$

The approximation $u_{H,m}^{\mathrm{lod}} \in V_{H,m}^{\mathrm{lod}}$ of the higher order LOD is then defined such that it holds

$$a(u_{H,m}^{\mathrm{lod}}, v) = (f\,,\, v)_{L^2}. \tag{6.33}$$

for all $v \in V_{H,m}^{\mathrm{lod}}$.

The following theorem gives an a priori error estimate for the SL-GFEM based on the higher order LOD. Numerical experiments in Section 6.5 suggest that the derived bound is pessimistic. However, compared to Theorem 6.3.1, it does not rely on additional assumptions or conjectures.

Theorem 6.4.1 (A priori error bound for the SL-GFEM)**.** *For any $f \in H^s(\mathcal{T}_H)$, $s \in \mathbb{N}_0$, the SL-GFEM approximation* (6.14) *satisfies for $k \coloneqq \min\{s, p+1\}$ that*

$$\|u - u_{H,m,n}^{\mathrm{gfem}}\|_a \lesssim H^{1+k} |f|_{H^k(\mathcal{T}_H)} + m^{d/2} H^{-1} \big(m^{d/2} \exp(-C_{\mathrm{d}} m) + d^n(H, m)\big) \|f\|_{L^2},$$

where the decay rate $C_{\mathrm{d}} > 0$ depends only on α, β, p, and the shape regularity of $\mathcal{T}_H$. The hidden constant has the same dependencies as C_{d} and additionally depends on the quasi-uniformity of $\mathcal{T}_H$.

Proof. We apply Céa's lemma, which gives for any $v \in V_{H,m,n}^{\mathrm{gfem}}$ that

$$\|u - u_{H,m,n}^{\mathrm{gfem}}\|_a \leq \|u - v\|_a. \tag{6.34}$$

For the oversampling parameter $l \coloneqq \lfloor m/2 \rfloor$, we define the approximation

$$u_{H,l}^{\mathrm{lod}} \coloneqq (\mathtt{id} - \mathcal{C}_l) \mathcal{B}_H u,$$

which is not the higher order LOD solution (6.33) but has the same approximation properties. This is an observation used in many proofs showing the convergence of the LOD method, see, e.g., [Mai21, Thm. 4.4]. Adding and subtracting $u_{H,l}^{\mathrm{lod}}$ in (6.34) and using the triangle inequality yields that

$$\|u - u_{H,m,n}^{\mathrm{gfem}}\|_a \leq \|u - u_{H,l}^{\mathrm{lod}}\|_a + \|u_{H,l}^{\mathrm{lod}} - v\|_a. \tag{6.35}$$

The approximation properties of $u_{H,l}^{\mathrm{lod}}$ mentioned above yield for the first term in (6.35) that

$$\|u - u_{H,l}^{\mathrm{lod}}\|_a \lesssim H^{1+k} |f|_{H^k(\mathcal{T}_H)} + l^{d/2} H^{-1} \exp(-C_{\mathrm{d}} l) \|f\|_{L^2}$$

with the decay rate $C_{\mathrm{d}} > 0$. Note that C_{d} is not equal to, but has the same dependencies as the decay rate in Lemma 3.3.1, and additionally depends on the polynomial degree p.

To estimate the second term in (6.35), we choose $v \in V_{H,m,n}^{\mathrm{gfem}}$ as the sum of functions $v_z^n \in V_{H,m,z}^n$ to be specified later, i.e.,

$$v = \sum_{z \in \mathcal{N}_H} \Lambda_z v_z^n.$$

Using the PU property of the hat functions $\sum_{z \in \mathcal{N}_H} \Lambda_z \equiv 1$, we then obtain that

$$\|u_{H,l}^{\mathrm{lod}} - v\|_a^2 = \Big\| \sum_{z \in \mathcal{N}_H} \Lambda_z (u_{H,l}^{\mathrm{lod}} - v_z^n) \Big\|_a^2 \leq C_{\mathrm{ol}} \sum_{z \in \mathcal{N}_H} \|\Lambda_z (u_{H,l}^{\mathrm{lod}} - v_z^n)\|_{a,S_z}^2,$$

where C_{ol} defined in (6.9) denotes the maximal number of overlapping supports S_z. For any $z \in \mathcal{N}_H$, we can replace $u_{H,l}^{\mathrm{lod}}$ locally on S_z with

$$u_{H,l,z}^{\mathrm{lod}} \coloneqq (\mathtt{id} - \mathcal{C}_l)(\mathcal{B}_H u|_{S_z^l}).$$

Hence, we define $v_z^n \in V_{H,m,z}^n$ as the (not necessarily unique) element minimizing the expression $\|\Lambda_z v_z - \Lambda_z v_z^n\|_{a,S_z^m}$, where

$$v_z \coloneqq (\mathtt{id} - \tilde{\mathcal{C}}_{z,m})(\mathcal{B}_H u|_{S_z^l})$$

is an approximation to $u_{H,l,z}^{\mathrm{lod}}$. Denoting $\mathcal{W}_{z,m} \coloneqq \{v \in \mathcal{W} : \operatorname{supp}(v) \subset S_z^m\}$, we define the corrector $\tilde{\mathcal{C}}_{z,m} \colon \mathcal{V} \to \mathcal{W}_{z,m}$ used above such that

$$a_{S_z^m}(\tilde{\mathcal{C}}_{z,m} v, w) = a_{S_z^m}(v, w) \tag{6.36}$$

holds for all $w \in \mathcal{W}_{z,m}$. Note that it holds $v_z \in V_{H,m,z}$, which is a non-trivial observation that can be concluded from Lemma 3.1.1.

Abbreviating

$$e_z^1 \coloneqq u_{H,l,z}^{\mathrm{lod}} - v_z, \qquad e_z^2 \coloneqq v_z - v_z^n,$$

we obtain after performing the local replacement mentioned above that

$$\|\Lambda_z (u_{H,l}^{\mathrm{lod}} - v_z^n)\|_{a,S_z}^2 \leq 2\big(\|\Lambda_z e_z^1\|_{a,S_z}^2 + \|\Lambda_z e_z^2\|_{a,S_z}^2\big). \tag{6.37}$$

Similar to (6.24), in order to bound the first term in (6.37), it suffices to bound $\|e_z^1\|_{L^2(S_z)}$ and $\|\nabla e_z^1\|_{L^2(S_z)}$. It holds that

$$e_z^1 = (\mathcal{C}_l - \tilde{\mathcal{C}}_{z,m})(\mathcal{B}_H u|_{S_z^l}) \in \mathcal{W}_{z,m},$$

which in particular implies that e_z^1 has vanishing element averages. Therefore, we obtain by Poincaré's inequality, cf. (2.25), that

$$\|e_z^1\|_{L^2(S_z)}^2 \lesssim H^2 \|\nabla e_z^1\|_{L^2(S_z)}^2.$$

Hence, it is sufficient to estimate $\|\nabla e_z^2\|_{L^2(S_z)}$ to obtain a bound for the first term in (6.37). Given a function that is supported on S_z^l (e.g., $\mathcal{B}_H u|_{S_z^l}$) the correction operator $\mathcal{C}_l$ coincides with the localization of $\tilde{\mathcal{C}}_{z,m}$ to l-th order patches. Thus, we can apply a higher order version of the localization error estimate from Lemma 3.3.3, here in the oversampling parameter l. Using (6.7), it follows that

$$\begin{aligned}\|\nabla e_z^1\|_{L^2(S_z)}^2 &\leq \|\nabla(\mathcal{C}_l - \tilde{\mathcal{C}}_{z,m})(\mathcal{B}_H u|_{S_z^l})\|_{L^2(S_z^m)}^2 \lesssim l^d \exp(-C_{\mathrm{d}} l)^2 \|\nabla(\mathcal{B}_H u|_{S_z^l})\|_{L^2(S_z^m)}^2 \\ &\leq C_{\mathcal{B}_H}^2 H^{-2} l^d \exp(-C_{\mathrm{d}} l)^2 \|u\|_{L^2(S_z^l)}^2.\end{aligned}$$

For the second term in (6.37), we obtain by the definition of the Kolmogorov n-width, the stability of $\mathtt{id} - \tilde{\mathcal{C}}_{z,m}$ (recall that by [Szy06], the operators $\tilde{\mathcal{C}}_{z,m}$ and $\mathtt{id} - \tilde{\mathcal{C}}_{z,m}$ have the same operator norms), and (6.7) that

$$\begin{aligned}\|\Lambda_z e_z^2\|_{a,S_z} &\leq d^n(H,m)\|v_z\|_{a,S_z^m} \leq \beta^{1/2} d^n(H,m)\|\nabla(\mathcal{B}_H u|_{S_z^l})\|_{L^2(S_z^m)} \\ &\leq C_{\mathcal{B}_H} H^{-1} \beta d^n(H,m)\|u\|_{L^2(S_z^l)}.\end{aligned}$$

We note that by Friedrichs' inequality (recall that D is scaled to unit size), it holds that

$$\|u\|_{L^2} \lesssim \|\nabla u\|_{L^2} \lesssim \alpha^{-1}\|f\|_{L^2}.$$

Combining the previous estimates, using the finite overlap of the patches S_z^l and replacing $l = \lfloor m/2 \rfloor$ with m, which introduces additional constants and changes the exponential decay rate C_{d} by a constant factor, the assertion follows. □

Remark 6.4.2 (Numerical pollution)**.** In the error estimate of Theorem 6.4.1, there is a factor of H^{-1} in front of the localization and local approximation error. In the proof, this factor is caused by the use of the operator $\mathcal{B}_H$ and the corresponding estimate (6.7). Indeed, numerical experiments confirm the presence of numerical pollution, see Section 6.5. For the LOD, we were able to avoid such pollution by using a quasi-interpolation operator, cf. Chapter 3. Note that such techniques are not directly applicable to the SL-GFEM, due to difficulties arising from the combination of the PU approach and the quasi-locality of the operator. Nevertheless, using a more sophisticated construction of the local approximation spaces (6.10), it may be possible to eliminate the pollution also for the SL-GFEM.

The following theorem gives an a priori bound of d^n that is fully explicit in H and m. This is the analogue of Theorem 6.3.2, which does not rely on any additional assumptions or conjectures. Numerical experiments suggest that this estimate is pessimistic.

Theorem 6.4.3 (Bound of d^n)**.** *The Kolmogorov n-width defined in* (6.13) *can be estimated for $l = 1, \dots, m-1$ as*

$$d^n(H,m) \lesssim m l^{d/2} \exp(-C_{\mathrm{d}} l),$$

where $n \approx l^d$. The constant C_{d} is the same as in Theorem 6.4.1 and the hidden constant depends only on α, β, p, and the quasi-uniformity and shape regularity of $\mathcal{T}_H$.

Proof. We consider a fixed node $z \in \mathcal{N}_H$ and oversampling parameter m. Using Lemma 3.1.1, it can be shown that for any $v \in V_{H,m,z}$ it holds that

$$v = (\mathtt{id} - \tilde{\mathcal{C}}_{z,m})\mathcal{B}_H v,$$

where $\tilde{\mathcal{C}}_{z,m}$ denotes the correction operator defined in (6.36). Furthermore, we define the localized correction operator $\tilde{\mathcal{C}}_l \coloneqq \sum_{K \subset S_z^m} \tilde{\mathcal{C}}_{K,l}$ with respect to the patch S_z^m. Here, denoting $\tilde{\mathcal{W}}_{K,l} \coloneqq \{v \in \mathcal{W} : \ \operatorname{supp}(v) \subset S_K^l \cap S_z^m\}$, the element correctors $\tilde{\mathcal{C}}_{K,l} \colon H_0^1(S_z^m) \to \tilde{\mathcal{W}}_{K,l}$ are defined such that

$$a_{S_z^m}(\tilde{\mathcal{C}}_{K,l} v, w) = a_K(v, w)$$

holds for all $w \in \tilde{\mathcal{W}}_{K,l}$.

As an approximation space $Q(n)$ of dimension $n \approx l^d$, we choose

$$Q(n) \coloneqq \operatorname{span}\{\Lambda_z(\mathtt{id} - \tilde{\mathcal{C}}_l) b_{K,j} : \ K \subset S_z^l,\ j = 1, \dots, J\}$$

and as approximation $w_z \in Q(n)$ of the function $v_z \in V_{H,m,z}$, we employ

$$w_z = \Lambda_z(\mathtt{id} - \tilde{\mathcal{C}}_l)(\mathcal{B}_H v_z|_{S_z^l}).$$

Using the approximation space $Q(n)$ and the above defined choice of w_z, we can bound the Kolmogorov n-width as follows:

$$\begin{aligned} d_z^n(H, m) &= \inf_{Q(n) \subset H_0^1(S_z)} \sup_{v_z \in V_{H,m,z}} \inf_{w_z \in Q(n)} \frac{\|\Lambda_z v_z - w_z\|_{a,S_z}}{\|v_z\|_{a,S_z^m}} \\ &\leq \sup_{v_z \in V_{H,m,z}} \frac{\|\Lambda_z v_z - w_z\|_{a,S_z}}{\|v_z\|_{a,S_z^m}}. \end{aligned}$$

Abbreviating

$$e_z \coloneqq (\tilde{\mathcal{C}}_l - \tilde{\mathcal{C}}_{z,m})\mathcal{B}_H v_z,$$

we can estimate the numerator using (6.8) and

$$\Lambda_z(\mathtt{id} - \tilde{\mathcal{C}}_l)(\mathcal{B}_H v_z|_{S_z^l}) = \Lambda_z(\mathtt{id} - \tilde{\mathcal{C}}_l)\mathcal{B}_H v_z,$$

since

$$\beta^{-1/2}\|\Lambda_z v_z - w_z\|_{a,S_z} \leq \|\nabla \Lambda_z e_z\|_{L^2(S_z)} \leq \big(C_\Lambda H^{-1}\|e_z\|_{L^2(S_z)} + \|\nabla e_z\|_{L^2(S_z)}\big).$$

It holds that $e_z \in \mathcal{W}_{z,m}$, which implies that e_z^1 has vanishing element averages. Thus, by Poincaré's inequality, cf. (2.25), we get that

$$\|e_z\|_{L^2(S_z)} \lesssim H\|\nabla e_z\|_{L^2(S_z)}.$$

Applying a localization error estimate similar to Lemma 3.3.3 to show that $\tilde{\mathcal{C}}_l$ approximates $\tilde{\mathcal{C}}_{z,m}$ exponentially well and using (6.7) as well as Friedrichs' inequality on the patch S_z^m with $\operatorname{diam}(S_z^m) \lesssim mH$, we get that

$$\begin{aligned}\|\Lambda_z v_z - w_z\|_{a,S_z} &\leq \beta^{1/2}(C_\Lambda + 1)\|\nabla e_z\|_{L^2(S_z^m)} \\ &\lesssim \beta^{1/2}(C_\Lambda + 1) l^{d/2} \exp(-C_{\mathrm{d}} l)\|\nabla \mathcal{B}_H v\|_{L^2(S_z^m)} \\ &\lesssim C_{\mathcal{B}_H} m\, l^{d/2} \alpha^{-1/2} \beta^{1/2}(C_\Lambda + 1) \exp(-C_{\mathrm{d}} l)\|v_z\|_{a,S_z^m}.\end{aligned}$$

After combining the previous estimates, the assertion follows. □

Remark 6.4.4 (Pessimistic choice of parameters)**.** This remark specifies how to choose the oversampling parameter m and the dimension of the local optimal approximating spaces n in order to guarantee optimal order convergence in Theorem 6.4.1. For m, we obtain the oversampling condition $m \gtrsim \log(\frac{1}{H})$, which is the same as for the LOD, cf. Theorem 3.4.2. Furthermore, by Theorem 6.4.3 we get for the dimension of the local approximation spaces that $n \gtrsim (\log \frac{1}{H})^d$. We emphasize that these choices of m and n guarantee, without any assumptions or conjectures, optimal order convergence of the SL-GFEM. However, numerical experiments suggest that these conditions are pessimistic. The choices from Remark 6.3.3 seem to be more accurate in practice.

6.5 Numerical experiments

This section is devoted to the numerical study of the SL-GFEM. Similar to the LOD in Section 3.5 and the SLOD in Section 5.5, we need to perform a fine-scale discretization of the SL-GFEM in order to obtain a practical implementation. Denoting by $\mathcal{T}_h$ a fine mesh obtained by uniform refinement of $\mathcal{T}_H$, we replace the infinite-dimensional space $\mathcal{V}$ in the definition of the SL-GFEM by its finite-dimensional fine-scale FE counterpart with respect to $\mathcal{T}_h$. Similar to Section 3.5 for the LOD, we expect that the theoretical results of the SL-GFEM remain valid in the fully discrete setting. The SL-GFEM is implemented in the `Python` library `gridlod` [HK17]. The source code can be found at [Fre+22b]. Note that, similar to the LOD and SLOD, all patch problems can be solved independently. The implementation takes advantage of this by solving all local patch problems in parallel. Note that the provided implementation supports computation on large parallel clusters.

In all numerical experiments we consider the domain $D = (0,1)^2$ equipped with uniform Cartesian meshes $\mathcal{T}_H$, where the mesh size denotes the side length of the elements instead of their diameter. For the fine-scale discretization, we use the uniform Cartesian mesh $\mathcal{T}_{2^{-10}}$, which resolves all fine-scale features of the considered coefficients. In the following, all errors are relative errors with respect to the energy norm. The fine-scale FE solution is used as the reference solution for the error computation.

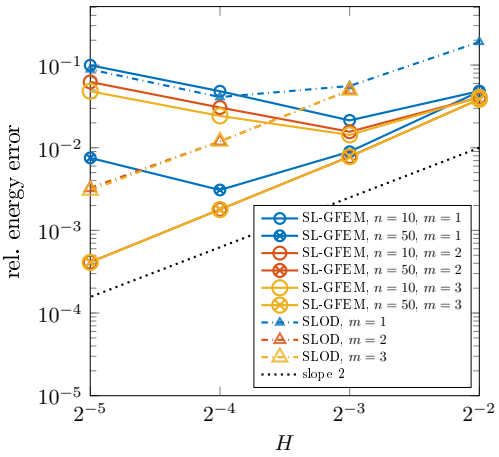

Figure 6.2: Errors of the SL-GFEM and SLOD for multiple choices of n and m as functions of H. The dotted line indicates the expected rate of convergence.

Optimal order convergence

To numerically verify the optimal order convergence properties of the SL-GFEM, we consider an elliptic model problem posed on the domain $D = (0, 1)^2$ with homogeneous Dirichlet boundary conditions. The considered coefficient A is piecewise constant with respect to the mesh $\mathcal{T}_{2^{-8}}$ and has element values, which are realizations of independent uniformly distributed random variables in the interval $[1, 100]$, see Figure 3.3 for a depiction of a similar coefficient. Similar to the previous chapters, we use the smooth source term defined by

$$f(x_1, x_2) = (x_1 + \cos(3\pi x_1)) \cdot x_2^3. \tag{6.38}$$

In Figure 6.2, we observe second order convergence of the SL-GFEM provided that the dimension of the local approximation space n and the oversampling parameter m are chosen sufficiently large. Recalling that $f \in H^1(D)$, this is in line with the theoretical predictions in Theorems 6.3.1 and 6.4.1. Note that, similar to the SLOD, also the SL-GFEM shows numerical pollution for fixed values of m and n. The presence of pollution has already been predicted by Theorem 6.4.1, see also Remark 6.4.2. To obtain optimal order approximations, the parameters m and n need to be increased with the mesh size H, see Remarks 6.3.3 and 6.4.4. Notably, the errors of the SL-GFEM are smaller by nearly one order of magnitude compared to the errors of the SLOD. Since this effect only appears for non-trivial coefficients A, it is most likely related to the contrast of the coefficient. More numerical experiments investigating the contrast dependence can be found in the remainder of this section.

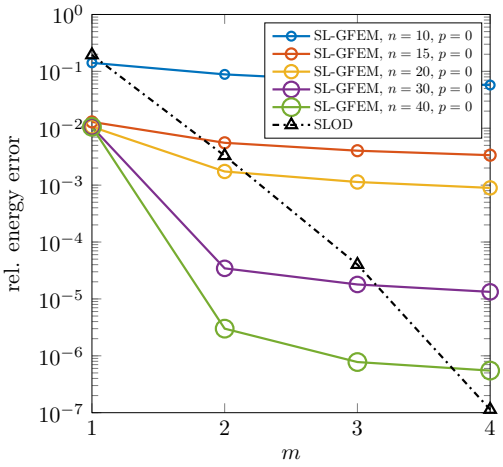

Figure 6.3: Error of the SL-GFEM for multiple choices of n as a function of m for the fixed coarse mesh $\mathcal{T}_{2^{-5}}$. As reference, also the respective errors of the SLOD are shown.

Super-exponential localization

In this numerical experiment, we investigate the localization properties of the SL-GFEM. For this, we use the same setting as in the previous numerical experiment, but this time with the source term $f \equiv 1$. As a result of this choice, the optimal order term in Theorems 6.3.1 and 6.4.1 vanishes and only the localization error and the approximation error d^n are present. Figure 6.3 shows a rapid decay of the localization error in m and n, which is in line with Theorems 6.3.1 and 6.4.1. Note that the parameter m determines the theoretically achievable error, while n determines the actual error within the range of achievable errors. For the SLOD, the super-exponential decay of the localization error can be observed, cf. (5.27). It can be observed that the SL-GFEM is able to achieve localization errors similar in magnitude to that of the SLOD, provided that n is chosen sufficiently large.

High-contrast channeled coefficients

One of the major challenges for multi-scale methods is their sensitivity to high-contrast channeled coefficients. To study the contrast dependence of the SL-GFEM, we consider for a given $\gamma > 0$ the coefficient A_γ, which is constructed by adding four channels of conductivity γ to the coefficient used in the previous numerical experiments. For an illustration of the coefficient, we refer to Figure 6.4. In this numerical experiment we again study the localization of the SL-GFEM and therefore consider the same setup as in the previous localization experiment. Figure 6.5 shows that the SL-GFEM is largely unaffected by large values of γ. In contrast, for the SLOD, the best practical realization known until

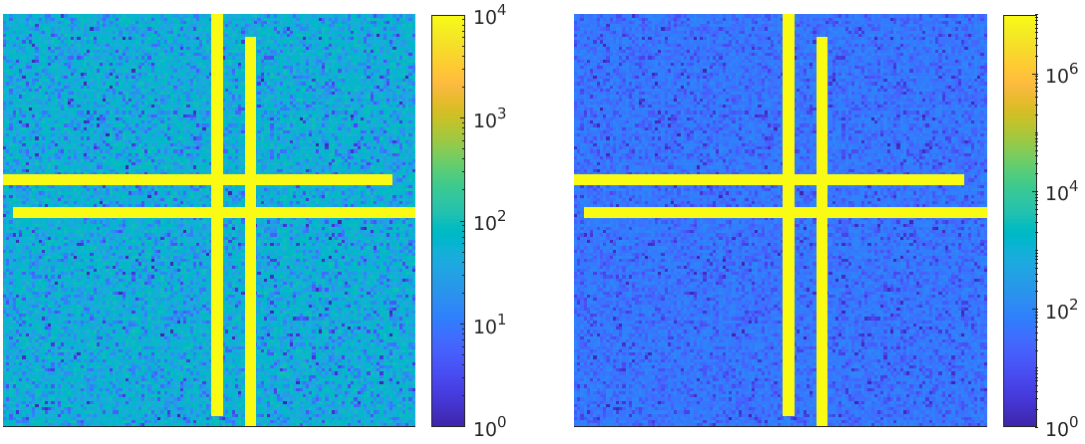

Figure 6.4: Coefficients A_{10^4} (left) and A_{10^7} (right) with a maximum contrast of 10^4 and 10^7, respectively. Some of the channels touch the boundary, while others stop before.

now (cf. Section 5.5) yields a basis with deteriorating stability as γ is increased. This corresponds to growing constants in (5.17) or (6.19) and (6.30) and explains the worse performance of the SLOD for $\gamma = 10^7$ compared to $\gamma = 10^4$. Notably, compared to Section 6.5, the SL-GFEM does not require a higher dimension of the local approximation spaces n in order to retain a good approximation quality, suggesting that the choice of n is not affected by the contrast.

Higher order polynomials

One key benefit of the proposed method is its flexibility with regard to the choice of polynomial degree, i.e., the construction of higher order methods is straightforward. While the previous numerical experiments have investigated the performance of the SL-GFEM for the polynomial degree $p = 0$, this experiment also considers higher polynomial degrees. We use the setup from the first numerical experiment with the non-polynomial source term (6.38). Figure 6.6 shows that, for n and m sufficiently large, the SL-GFEM of degree p converges with an order of $p+2$. Recalling that f is sufficiently smooth, this is in line with the theoretical predictions in Theorems 6.3.1 and 6.4.1. Note that the choice of n needs to be adapted to p. More precisely, we observe that n needs to be increased linearly with p. Also an adaptive choice of n based on the size of the eigenvalues of problem (6.12) seems possible.

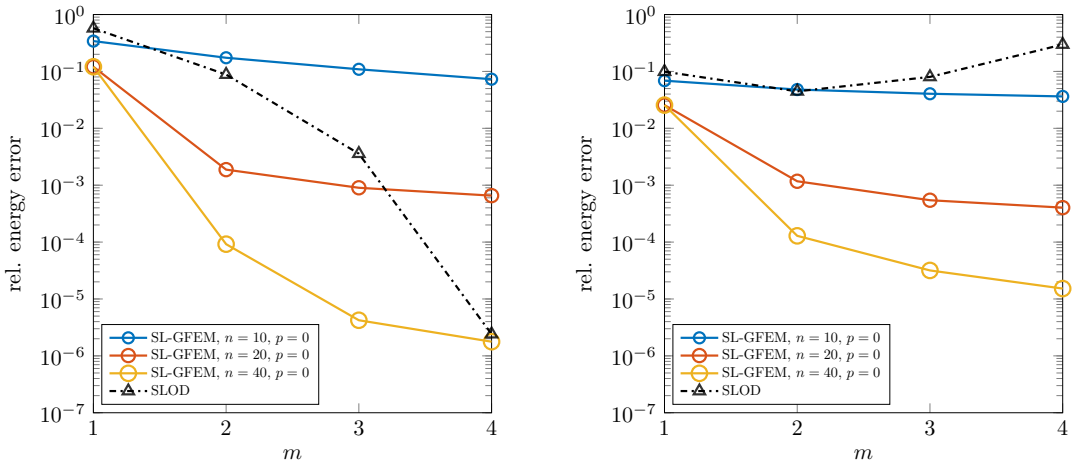

Figure 6.5: Errors of the SL-GFEM and SLOD as functions of m for the fixed coarse mesh $\mathcal{T}_{2^{-5}}$. As coefficients, we use the high-contrast channeled coefficients A_{10^4} (left) and A_{10^7} (right).

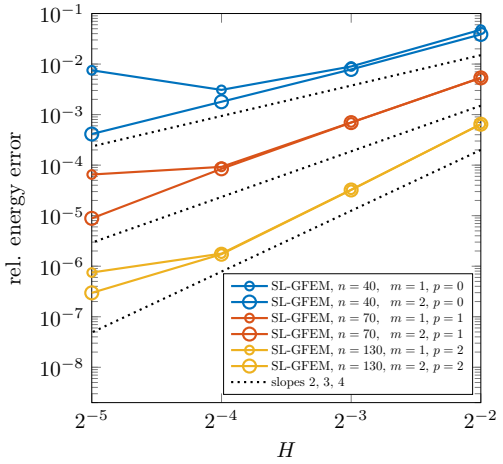

Figure 6.6: Error of the higher order SL-GFEM for $p = 0, 1, 2$ as a function of H for multiple choices of n and m. The dotted lines indicate the respective expected orders of convergence.

7 Reduced Basis Super-Localized Orthogonal Decomposition for reaction–convection–diffusion problems

Given a parameter-dependent PDE, reduced basis (RB) methods are a remarkable tool for computing approximations for arbitrary parameter values at low computational cost, see, e.g., the textbooks [QMN15; HRS16]. As approximation space, RB methods use a typically low-dimensional space spanned by global snapshots of the problem under consideration. For any parameter value, the approximation is then obtained by performing a Galerkin approach in this snapshot space. The online complexity of RB methods typically depends mainly on the dimension of the snapshot space.

However, for parameter-dependent multiscale PDEs, RB methods based on global snapshot computations can easily become intractable. To overcome such limitations, this chapter introduces the Reduced Basis Super-Localized Orthogonal Decomposition (RB-SLOD), using the reaction–convection–diffusion problem with parameter-dependent multi-scale coefficients as a model problem. For any given parameter value, the RB-SLOD allows one to quickly generate coarse-scale models of the considered problem. These coarse-scale models accurately capture the effective behavior of the problem and thus provide reliable approximations even in underresolved regimes. Due to their typically small dimension, the coarse-scale models can be solved at low computational cost.

The RB-SLOD is a combination of the SLOD from Chapter 5 with the RB method. More specifically, we use the RB to accelerate the typically expensive (local) SLOD basis computation, while we use the SLOD to efficiently compress the PDE operator into a coarse-scale model. Note that the unique localization properties of the SLOD allow one to perform the snapshot computation of the RB on particularly small patches, which is key to the low offline and online complexity of the algorithm. A major strength of the RB-SLOD is that it is affected only by the parameters appearing in the PDE operator and not by parametric, possibly non-affine, source terms. For such source terms, classical RB approaches require appropriate interpolation methods such as the empirical interpolation method [Bar+04], which adds to the overall computational cost.

The ability of the RB-SLOD to tackle challenging parametric multi-scale

PDEs is due to its local snapshot computation. We emphasize that a local snapshot computation can also be achieved by domain decomposition approaches or other multi-scale methods. Approaches based on domain decomposition include the Reduced Basis Element method [MR02; KOH11; APQ16; HKP12; IQR12], the Localized Reduced Basis Multiscale method [Alb+12; OS15], and the Arbitrary Local Modifications method [Buh+17]. Other approaches that use multi-scale methods to localize the snapshot computation include the RB-MsFEM [HZZ15], the RB-HMM [AB12; AB13], and the RB-LOD [AH15; KR21]. For an overview of localized model reduction techniques for parametric PDEs, see [Buh+21].

The content and presentation of the following chapter is primarily based on the preprint article

[BHP22] F. Bonizzoni, M. Hauck, and D. Peterseim. "A reduced basis super-localized orthogonal decomposition for reaction–convection–diffusion problems". In: *arXiv preprint 2211.15221* (2022)

7.1 Parametric reaction–convection–diffusion problem

Let $D \subset \mathbb{R}^d$ be a bounded polytopal Lipschitz domain, which is assumed to be scaled to unit size. Furthermore, let $\mathcal{M} \subset \mathbb{R}^p$, $p \in \mathbb{N}$ be a compact parameter set with parameters denoted by μ. We consider a parametric reaction–convection–diffusion problem posed on D with parameters from $\mathcal{M}$, i.e.,

$$-\operatorname{div}(A_\mu \nabla u_\mu) + c_\mu \cdot \nabla u_\mu + r_\mu u_\mu = f, \tag{7.1}$$

where r_μ, c_μ, and A_μ denote the reaction, convection, and diffusion coefficients, respectively and $f \in L^2(D)$ is a parameter-independent source term. We assume that $r_\mu \in L^\infty(D)$ and $c_\mu \in L^\infty(D, \mathbb{R}^d)$ with L^∞-norms bounded uniformly in the parameter μ. Furthermore, we assume that the diffusion coefficient $A_\mu \in L^\infty(D, \mathbb{R}^{d\times d})$ is symmetric and uniformly positive definite, i.e., there exist parameter-independent constants λ, Λ with $0 < \lambda \leq \Lambda < \infty$ such that

$$\lambda|\xi|^2 \leq \xi \cdot (A_\mu(x)\xi) \leq \Lambda|\xi|^2 \tag{7.2}$$

holds for almost all $x \in D$ and all $\mu \in \mathcal{M}$ and $\xi \in \mathbb{R}^d$, where $|\cdot|$ denotes the Euclidean norm of $\mathbb{R}^d$.

For the well-posedness of the problem (7.1), we need to impose suitable boundary conditions. We consider a decomposition of the boundary ∂D into the closed boundary segments Γ_1, Γ_2, and Γ_3, i.e., $\partial D = \Gamma_1 \cup \Gamma_2 \cup \Gamma_3$, where the intersection of the interior of the components is pairwise disjoint. Given this decomposition,

we impose the mixed boundary conditions

$$\begin{aligned} (A_\mu \nabla u_\mu) \cdot \nu &= 0 && \text{on } \Gamma_1, \\ (A_\mu \nabla u_\mu) \cdot \nu + d_\mu u &= 0 && \text{on } \Gamma_2, \\ u_\mu &= 0 && \text{on } \Gamma_3, \end{aligned} \tag{7.3}$$

where ν denotes the outer unit normal vector and $d_\mu \in L^\infty(\Gamma_2)$ is a non-negative function with L^∞-norm uniformly bounded in μ.

As solution space of the above reaction–convection–diffusion problem, we use

$$\mathcal{V} \coloneqq \{v \in H^1(D) : \, v|_{\Gamma_3} = 0\}.$$

We equip $\mathcal{V}$ with the standard H^1-inner product and the corresponding induced norm, denoted by $(\cdot\,,\,\cdot)_{\mathcal{V}}$ and $\|\cdot\|_{\mathcal{V}}$, respectively, cf. (2.1). For fixed parameter values $\mu \in \mathcal{M}$, the weak formulation of (7.1) with the boundary conditions (7.3) seeks $u_\mu \in \mathcal{V}$ such that

$$a_\mu(u_\mu, v) = (f\,,\, v)_{L^2} \tag{7.4}$$

holds for all $v \in \mathcal{V}$, where the bilinear form $a_\mu \colon \mathcal{V} \times \mathcal{V} \to \mathbb{R}$ is given by

$$a_\mu(u, v) \coloneqq (A_\mu \nabla u\,,\, \nabla v)_{L^2} + (c_\mu \cdot \nabla u\,,\, v)_{L^2} + (r_\mu u\,,\, v)_{L^2} + (d_\mu u\,,\, v)_{L^2(\Gamma_2)}.$$

Under standard assumptions on the coefficients d_μ, r_μ, and c_μ (see, e.g., the textbook [KA03, Ch. 3.2]), one can prove the uniform coercivity and continuity of the bilinear form a_μ, i.e., there exist parameter-independent constants α, β with $0 < \alpha \leq \beta < \infty$ such that

$$a_\mu(v, v) \geq \alpha \|v\|_{\mathcal{V}}^2, \qquad a_\mu(v, w) \leq \beta \|v\|_{\mathcal{V}} \|w\|_{\mathcal{V}} \tag{7.5}$$

holds for all $v, w \in \mathcal{V}$. If these conditions hold, the well-posedness of (7.4) for any parameter value follows directly using the Lax–Milgram theorem (see, e.g., [Alt16, Thm. 6.2]).

As usual in the RB context, we assume that the bilinear form a_μ can be affinely decomposed into $Q \in \mathbb{N}$ terms as follows:

$$a_\mu(u, v) = \sum_{q=1}^{Q} \theta_q(\mu) b_q(u, v) \tag{7.6}$$

with parameter-independent continuous bilinear forms $b_q \colon \mathcal{V} \times \mathcal{V} \to \mathbb{R}$ and measurable functions $\theta_q \colon \mathcal{M} \to \mathbb{R}$. Note that theoretically there are no restrictions on the number of summands Q in (7.6). However, for RB methods, there are typically practical limitations on Q and smoothness requirements with respect to μ, see, e.g., [QMN15, Ch. 5]. In fact, for large Q or lack of smoothness, the offline phase of RB methods (including the RB-SLOD) becomes increasingly expensive due to the large amount of precomputation required. In such cases, RB approaches may not be worthwhile.

Note that if an affine decomposition of a_μ is not available, one can use the empirical interpolation method [Bar+04] to compute affine approximations of the PDE coefficients d_μ, r_μ, c_μ, and A_μ. The RB-SLOD can then be applied to these approximated coefficients. Note that the number of terms in such approximate affine decompositions depends on the smoothness of the coefficient with respect to μ, i.e., for a given accuracy, smoother coefficients can be approximated by sums of fewer terms.

Let us recall some notation that we will use frequently in the remainder of this chapter. In the following, we denote by $\mathcal{V}'$ the dual space of $\mathcal{V}$ (recall that we only consider real functions). For a fixed parameter $\mu \in \mathcal{M}$, we further denote by $\mathcal{L}_\mu \colon \mathcal{V}' \to \mathcal{V}$ the solution operator associated with the problem (7.4), cf. (2.14). Furthermore, for subsets $S \subset D$ we denote by $a_{S,\mu}(\cdot,\cdot)$, $b_{S,q}(\cdot,\cdot)$, $(\cdot\,,\cdot)_{\mathcal{V}(S)}$, and $\|\cdot\|_{\mathcal{V}(S)}$ the restrictions of $a_\mu(\cdot,\cdot)$, $b_q(\cdot,\cdot)$, $(\cdot\,,\cdot)_{\mathcal{V}}$, and $\|\cdot\|_{\mathcal{V}}$ to S, cf. Section 2.1. Recalling the definition of the local solution space $\mathcal{V}_S$ in (5.2), we define for any parameter value the local solution operator $\mathcal{L}_{S,\mu} \colon \mathcal{V}_S' \to \mathcal{V}_S$ analogously to (5.3). Here, $\mathcal{V}_S'$ denotes the dual space of $\mathcal{V}_S$.

7.2 Reinterpretation of prototypical approximation

This section motivates the definition of the prototypical operator-adapted approximation spaces in Chapter 2 by a RB approach in the source term. We fix the parameter $\mu \in \mathcal{M}$ and consider the source term $f_\vartheta \in H^s(D)$, $s \in [0,1]$ depending on another parameter ϑ. Besides its H^s-regularity, the source term f_ϑ can be a general parameter-dependent function, which depends on ϑ in a non-smooth and non-affine way. For non-affine source terms, one typically computes an approximate affine decomposition using appropriate interpolation techniques, e.g., the empirical interpolation method, cf. [Bar+04]. Note that sophisticated interpolation methods such as the empirical interpolation method may be ineffective here due to the lack of smoothness. The L^2-orthogonal projection onto $\mathcal{T}_H$-piecewise constants denoted by $\Pi_H^0 \colon L^2(D) \to \mathcal{P}^0(\mathcal{T}_H)$, cf. (2.23), has optimal approximation properties for general H^s-regular functions. Therefore, we use the following approximate affine decomposition:

$$\Pi_H^0 f_\vartheta = \sum_{K \in \mathcal{T}_H} (\Pi_H^0 f_\vartheta)|_K \, \mathbf{1}_K.$$

The general parameter dependence of f_ϑ motivates to choose the RB space as $\mathcal{L}_\mu \mathcal{P}^0(\mathcal{T}_H)$, which is exactly the prototypical operator-adapted trial space from Chapter 2, cf. (2.15). This space is not adapted to the parameter dependence of f_ϑ and therefore suited for approximating all H^s-regular source terms. Since one can only expect an algebraic decay of the approximation error in the number of basis functions, cf. Lemma 2.3.3, the dimension of the above RB space

is typically large. Moreover, its canonical basis functions $\{\mathcal{L}_\mu \mathbf{1}_K : K \in \mathcal{T}_H\}$ are non-local and decay very slowly, cf. Figure 2.2. Therefore, such approaches are infeasible in practice without modification.

In the following, we will again concentrate on parameter-dependent PDE operators and omit the parameter dependence in the source term. The next section presents a variant of the SLOD that can be used to localize the basis computation, thereby deriving a practical method.

7.3 Super-Localized Orthogonal Decomposition revisited

For a fixed parameter value $\mu \in \mathcal{M}$, this section introduces a variant of the SLOD that will prove particularly useful in the RB context. This variant will be used in Section 7.4 as the basis for deriving the RB-SLOD.

First, we introduce some preliminaries regarding the explicit computation of norms associated with traces and conormal derivatives. For this, we fix the element $K \in \mathcal{T}_H$ and abbreviate its m-th order patch by $S \coloneqq \mathsf{N}_m(K)$. We assume that the patch S does not coincide with the whole domain D. Denoting $\Sigma \coloneqq \partial S \backslash \partial D$, we recall the definition of the trace operator tr_Σ and its image X from (5.7). As a subspace of $H^{1/2}(\Sigma)$, we can endow X with the norm

$$\|w\|_X \coloneqq \inf\{\|v\|_{\mathcal{V}(S)} : v \in \mathcal{V}(S),\ \mathrm{tr}_\Sigma v = w\}. \tag{7.7}$$

Note that, by the definition of the X-norm, the operator tr_Σ is continuous independent of the patch geometry, i.e., it holds that

$$\|\mathrm{tr}_\Sigma v\|_X \leq \|v\|_{\mathcal{V}(S)} \tag{7.8}$$

for all $v \in \mathcal{V}(S)$. The X-norm of a function $w \in X$ can be computed explicitly by generalizing the textbook result from [BF91, Ch. III.1, Eq. (1.5)]. One can prove the identity $\|u_w\|_{\mathcal{V}(S)} = \|w\|_X$, where $u_w \in \mathcal{V}(S)$ is the weak solution to the following boundary value problem:

$$\begin{cases} -\Delta u_w + u_w = 0 & \text{in } S, \\ u_w = w & \text{on } \Sigma, \\ \nabla u_w \cdot \nu = 0 & \text{on } \partial S \cap (\Gamma_1 \cup \Gamma_2), \\ u_w = 0 & \text{on } \partial S \cap \Gamma_3. \end{cases}$$

The proof of this result is rather standard and can be found in [BHP22, Lem. 3.1]. A direct consequence of this result is that the right-inverse of tr_Σ defined by $\mathrm{tr}_\Sigma^{-1} \colon X \to \mathcal{V}(S)$, $\mathrm{tr}_\Sigma^{-1} w \coloneqq u_w$ is continuous with

$$\|\mathrm{tr}_\Sigma^{-1} w\|_{\mathcal{V}(S)} = \|w\|_X \tag{7.9}$$

for all $w \in X$. Furthermore, this representation of the X-norm allows one to explicitly compute the X'-norm of a functional $q \in X'$. Generalizing the textbook result [BF91, Ch. III.1, Eq. (1.8)], we obtain that

$$\|u_q\|_{\mathcal{V}(S)} = \|q\|_{X'}, \tag{7.10}$$

where $u_q \in \mathcal{V}(S)$ is the weak solution to the following boundary value problem:

$$\begin{cases} -\Delta u_q + u_q = 0 & \text{in } S, \\ \nabla u_q \cdot \nu = q & \text{on } \Sigma, \\ \nabla u_q \cdot \nu = 0 & \text{on } \partial S \cap (\Gamma_1 \cup \Gamma_2), \\ u_q = 0 & \text{on } \partial S \cap \Gamma_3. \end{cases} \tag{7.11}$$

The proof of this result again uses rather standard arguments and can be found in [BHP22, Lem. 3.2].

In the remainder of this section, we use the tools introduced above to derive the proposed variant of the SLOD. Since we consider a fixed element $K \in \mathcal{T}_H$, we drop all fixed indices if they are not explicitly needed. Similar to Section 5.2, the global SLOD basis function φ associated with the fixed element K is given by the ansatz $\varphi = \mathcal{L}_\mu g$, where $g \in \mathcal{P}^0(S)$ is an L^2-normalized local source term to be determined, cf. (5.5). The corresponding localized basis function ψ is obtained by replacing the global solution operator by the local one, i.e., $\psi \coloneqq \mathcal{L}_{S,\mu} g \in \mathcal{V}_S$, cf. (5.6).

The conormal derivative of ψ at the boundary segment Σ is a functional in X', which is defined for all $w \in X$ by

$$\langle A_\mu \nabla \psi \cdot \nu, w \rangle_{X' \times X} = a_{S,\mu}(\psi, \operatorname{tr}_\Sigma^{-1} w) - (g\,,\, \operatorname{tr}_\Sigma^{-1} w)_{L^2(S)}, \tag{7.12}$$

where $\langle \cdot, \cdot \rangle_{X' \times X}$ denotes the duality pairing. Note that the conormal derivative is independent of the choice of the extension operator $\operatorname{tr}_\Sigma^{-1}$. There is a close relation between the conormal derivative of ψ and the size of the localization error. More precisely, it holds that

$$a_\mu(\psi - \varphi, v) = a_{S,\mu}(\psi, v) - (g, v)_{L^2(S)} = \langle A_\mu \nabla \psi \cdot \nu, \operatorname{tr}_\Sigma v|_S \rangle_{X' \times X} \tag{7.13}$$

for all $v \in \mathcal{V}$. For the sake of notation, we introduce the operator $\mathcal{R}$, which maps g to the function u_q solving (7.11) for $q = A_\mu \nabla \psi \cdot \nu \in X'$ (recall that $\psi = \mathcal{L}_{S,\mu} g \in \mathcal{V}_S$), i.e.,

$$\mathcal{R} \colon \mathcal{P}^0(S) \to \mathcal{V}(S),\ g \mapsto u_q. \tag{7.14}$$

We choose the local source term g as the solution to the minimization problem

$$g \in \operatorname*{arg\,min}_{p \in \mathcal{P}^0(S)} \frac{\|\mathcal{R} p\|^2_{\mathcal{V}(S)}}{\|p\|^2_{L^2(S)}}, \tag{7.15}$$

which, by (7.10) and (7.13), guarantees a small localization error. Regarding the possible non-uniqueness of the choice (7.15), we refer to Section 5.2, where this was discussed for the SLOD.

Remark 7.3.1 (Comparison to the SLOD from Chapter 5)**.** In this remark we use the notation from Section 5.2, i.e., tr_Σ^{-1} denotes the local operator-harmonic extension defined in (5.8). Then, the choice (7.15) for g can be rewritten as the solution to the following minimization problem:

$$\operatorname*{arg\,min}_{g\in\mathcal{P}^0(S)\colon \|g\|_{L^2(S)}=1} \sup_{w\in X\colon \|w\|_X=1} |(g, \mathrm{tr}_\Sigma^{-1} w)_{L^2(S)}|.$$

This alternative characterization allows one to see the subtle difference to the choice (5.12) of the SLOD from Chapter 5. While there the supremum was taken over local operator-harmonic functions, here the supremum is taken over traces. Although one can identify traces with operator-harmonic functions and vice versa, the difference lies in the norms being considered, which are equivalent but not the same.

Note that solving the problem (7.15) is equivalent to computing the eigenvector corresponding to the smallest eigenvalue of the generalized eigenvalue problem

$$\mathbf{C}\mathbf{x} = \lambda \mathbf{D}\mathbf{x}. \tag{7.16}$$

Denoting by J the number of coarse elements in S, the matrices $\mathbf{C}$, $\mathbf{D} \in \mathbb{R}^{J\times J}$ are defined by

$$\mathbf{C}_{ij} = (\mathcal{R}\mathbf{1}_{K_j}\,,\, \mathcal{R}\mathbf{1}_{K_i})_{\mathcal{V}(S)}, \qquad \mathbf{D}_{ij} \coloneqq (\mathbf{1}_{K_j}\,,\, \mathbf{1}_{K_i})_{L^2(S)},$$

where $\{K_j : j = 1, \dots J\}$ is some numbering of the coarse elements in S.

Similar to (5.18), we measure the localization error when replacing φ with its local counterpart ψ using the local error indicator

$$\sigma_{K,\mu} = \sigma_{K,\mu}(H, m) \coloneqq \|\mathcal{R}g\|_{\mathcal{V}(S)}.$$

It coincides with the X'-norm of the conormal derivative of ψ. Taking the maximum over all elements, we get the following error indicator for the overall localization error of the method:

$$\sigma_\mu = \sigma_\mu(H, m) \coloneqq \max_{K\in\mathcal{T}_H} \sigma_{K,\mu}. \tag{7.17}$$

We emphasize that the decay results in Section 5.4 also apply to σ_μ. This means that we practically observe a super-exponential decay of σ_μ in m and that we can prove an exponential decay in m, cf. (5.27) and (5.39). In the following, we denote the local source term, the global basis function, and its localized counterpart associated with the element K by $g_{K,m,\mu}$, $\varphi_{K,m,\mu}$, and $\psi_{K,m,\mu}$. The proposed SLOD variant uses the collocation ansatz of (5.15), i.e., denoting by $(c_K)_{K\in\mathcal{T}_H}$ the coefficients of the expansion of $\Pi_H^0 f$ in terms of the basis functions $g_{K,m,\mu}$, we define its approximation as

$$u_{H,m,\mu}^{\mathrm{slod}} = \sum_{K\in\mathcal{T}_H} c_K\, \psi_{K,m,\mu}. \tag{7.18}$$

Since no inner products between basis functions need to be computed, the assembly of the coarse system is very cheap. This makes the collocation approach well suited for RB applications.

7.4 Reduced Basis Super-Localized Orthogonal Decomposition

This section introduces the RB-SLOD, which combines the SLOD variant presented in the previous section with a RB approach. For any parameter value, the RB-SLOD is able to quickly generate accurate coarse scale models of the parametric multi-scale PDE under consideration. The RB-SLOD algorithm consists of an offline phase and an online phase. The offline phase is run only once and performs precomputations that are used in the online phase to quickly compute the RB-SLOD approximations.

7.4.1 Offline phase

We now return to the local perspective and consider the element $K \in \mathcal{T}_H$ with its patch $S \coloneqq \mathsf{N}_m(K)$. Given a parameter $\mu \in \mathcal{M}$, most of the computational time for computing the SLOD basis function ψ and its associated local source term g is spent on computing the set

$$\{\chi_{T,\mu} : T \subset S\},$$

where for all elements $T \subset S$, we define

$$\chi_{T,\mu} \coloneqq \mathcal{L}_{S,\mu}\mathbf{1}_T. \tag{7.19}$$

We derive a RB approach to obtain approximations of $\chi_{T,\mu}$ that can be evaluated quickly. From now on we also fix the element $T \subset S$ and omit the corresponding subscript for better readability.

Initialization

In RB approaches, one usually first selects a training set of parameters, denoted by $\mathcal{M}^{\mathrm{tr}} \subset \mathcal{M}$, of prescribed size $M \in \mathbb{N}$. Possible options for selecting its elements are random sampling approaches or structured grids. We also initialize the sets of RB parameters $\mathcal{M}^{\mathrm{rb}}$ and functions $\mathcal{W}^{\mathrm{rb}}$, which will be used later to store iteratively selected important parameter and function pairs. For a pseudocode implementation, see Algorithm 1.

Error estimation

Suppose we have already chosen the following sets of RB parameters and corresponding RB functions:

$$\mathcal{M}^{\mathrm{rb}} = \{\mu_1, \dots, \mu_L\}, \qquad \mathcal{W}^{\mathrm{rb}} = \{\chi_{\mu_1}, \dots, \chi_{\mu_L}\}.$$

Algorithm 1 Offline – Initialization with starting parameters.

1: $\mathcal{M}^{\mathrm{tr}} \leftarrow \{\mu_1, \dots, \mu_M\}$ with selected parameters from $\mathcal{M}$
2: $\mathcal{M}^{\mathrm{rb}} \leftarrow \{\mu_1\}$
3: $\mathcal{W}^{\mathrm{rb}} \leftarrow \{\chi_{\mu_1}\}$ with $\chi_{\mu_1} \coloneqq \mathcal{L}_{S,\mu_1}\mathbf{1}_T$

Given a new parameter $\mu \in \mathcal{M}^{\mathrm{tr}} \backslash \mathcal{M}^{\mathrm{rb}}$, we then need to

1. compute an approximation χ_μ^{rb} to $\chi_\mu = \mathcal{L}_{S,\mu}\mathbf{1}_T$ in the span of $\mathcal{W}^{\mathrm{rb}}$ and
2. efficiently estimate the corresponding approximation error.

An approximation of χ_μ is obtained by computing the Galerkin projection onto the span of $\mathcal{W}^{\mathrm{rb}}$, i.e., we seek $\chi_\mu^{\mathrm{rb}} = \sum_{l=1}^{L} c_l \chi_{\mu_l} \in \operatorname{span} \mathcal{W}^{\mathrm{rb}}$ such that

$$a_{S,\mu}(\chi_\mu^{\mathrm{rb}}, w) = a_{S,\mu}(\chi_\mu, w) = (\mathbf{1}_T\,,\, w)_{L^2(S)} \tag{7.20}$$

holds for all $w \in \operatorname{span} \mathcal{W}^{\mathrm{rb}}$. By choosing the elements of $\mathcal{W}^{\mathrm{rb}}$ as test functions in (7.20), we get a small linear system with the unknowns $(c_l)_{l=1}^{L}$. Note that χ_μ itself is not needed to compute the approximation.

To estimate the error made when approximating χ_μ by χ_μ^{rb}, we use the Riesz representation $\tau_\mu \in \mathcal{V}_S$ of the residual functional, which satisfies

$$(\tau_\mu\,,\, w)_{\mathcal{V}(S)} = a_{S,\mu}(\chi_\mu^{\mathrm{rb}}, w) - (\mathbf{1}_T\,,\, w)_{L^2(S)} \tag{7.21}$$

for all $w \in \mathcal{V}_S$. We then define the a posteriori error estimator

$$\Delta_\mu \coloneqq \|\tau_\mu\|_{\mathcal{V}(S)}, \tag{7.22}$$

which is proved to be reliable and efficient in the following lemma.

Lemma 7.4.1 (Reliability and efficiency of the estimator)**.** *For any parameter $\mu \in \mathcal{M}^{\mathrm{tr}} \backslash \mathcal{M}^{\mathrm{rb}}$, the RB error can be bounded from below and above by Δ_μ, i.e., it holds that*

$$\beta^{-1}\Delta_\mu \leq \|\chi_\mu - \chi_\mu^{\mathrm{rb}}\|_{\mathcal{V}(S)} \leq \alpha^{-1}\Delta_\mu.$$

Proof. We define $e \coloneqq \chi_\mu - \chi_\mu^{\mathrm{rb}}$. Using (7.5) and (7.21) together with $\mathcal{V}_S \subset \mathcal{V}$, we obtain that

$$\|\tau_\mu\|_{\mathcal{V}(S)}^2 = a_{S,\mu}(\chi_\mu^{\mathrm{rb}}, \tau_\mu) - (\mathbf{1}_T\,,\, \tau_\mu)_{L^2(S)} = -a_{S,\mu}(e, \tau_\mu) \leq \beta \|e\|_{\mathcal{V}(S)} \|\tau_\mu\|_{\mathcal{V}(S)},$$

which, after dividing by $\|\tau_\mu\|_{\mathcal{V}(S)}$, implies the first inequality. Similarly, we get for the second inequality that

$$\alpha\|e\|_{\mathcal{V}(S)}^2 \leq a_{S,\mu}(e,e) = (\mathbf{1}_T\,,\, e)_{L^2(S)} - a_{S,\mu}(\chi_\mu^{\mathrm{rb}}, e) \leq \|\tau_\mu\|_{\mathcal{V}(S)} \|e\|_{\mathcal{V}(S)}. \qquad \square$$

Using the affine decomposition (7.6) and recalling that $\chi_\mu^{\mathrm{rb}} = \sum_{l=1}^{L} c_l \chi_{\mu_l}$, the a posteriori error estimator can be computed efficiently as

$$\tau_\mu = \sum_{q=1}^{Q} \theta_q(\mu) \sum_{l=1}^{L} c_l s_{q,l} - p, \tag{7.23}$$

where the $s_{q,l} \in \mathcal{V}_S$ are defined such that

$$(s_{q,l}\,,\, w)_{\mathcal{V}(S)} = b_{S,q}(\chi_{T,\mu_l}, w) \tag{7.24}$$

holds for all $w \in \mathcal{V}_S$, and $p \in \mathcal{V}_S$ is defined such that it holds

$$(p\,,\, w)_{\mathcal{V}(S)} = (\mathbf{1}_T\,,\, w)_{L^2(S)} \tag{7.25}$$

for all $w \in \mathcal{V}_S$.

Denoting for any q the sets that store the functions $\{s_{q,l} : l = 1, \dots, L\}$ by $\mathcal{S}_q$, we can initialize the Riesz representations as shown in Algorithm 2.

Algorithm 2 Offline – Initialization of Riesz representations.

1: **for** $q = 1, \dots, Q$ **do**
2: $\quad \mathcal{S}_q \leftarrow \{s_{q,1}\}$ with $s_{q,1}$ solving (7.24)
3: **end for**
4: compute p by (7.25)

Greedy search

The greedy search algorithm iterates through the parameters $\mu \in \mathcal{M}^{\mathrm{tr}} \backslash \mathcal{M}^{\mathrm{rb}}$ and, for each μ, estimates the error made when approximating χ_μ by χ_μ^{rb} using the error estimator Δ_μ from (7.22). It selects the parameter μ for which the estimator is largest and adds it to the set $\mathcal{M}^{\mathrm{rb}}$. We also compute the corresponding function χ_μ by (7.19) and add it to the set $\mathcal{W}^{\mathrm{rb}}$. For numerical stability reasons, we perform an orthogonalization with respect to $(\cdot\,,\,\cdot)_{\mathcal{V}(S)}$ using a Gram–Schmidt-type algorithm. Note that due to the typically small size of $\mathcal{W}^{\mathrm{rb}}$, numerical stability issues of the Gram–Schmidt algorithm are not noticeable in practice. Given a tolerance $\mathsf{tol} > 0$, this procedure is then repeated until the training error satisfies the relative stopping criterion

$$\mathsf{trerr}(L) \coloneqq \frac{\max_{\mu \in \mathcal{M}^{\mathrm{tr}}} \Delta_\mu}{\|p\|_{\mathcal{V}(S)}} \leq \mathsf{tol} \tag{7.26}$$

with p defined in (7.25). Note that it is justified to use p instead of χ_μ since

$$\|p\|_{\mathcal{V}(S)} = \|\mathbf{1}_T\|_{\mathcal{V}_S'} \approx \|\chi_\mu\|_{\mathcal{V}(S)},$$

Algorithm 3 Offline – Greedy search.

1: **while** $\frac{\max_{\mu\in\mathcal{M}^{\mathrm{tr}}} \Delta_\mu}{\|p\|_{\mathcal{V}(S)}} > \mathsf{tol}$ **do**
2: $L \leftarrow \#\mathcal{M}^{\mathrm{rb}}$
3: // compute error estimators
4: **for** $\mu \in \mathcal{M}^{\mathrm{tr}} \backslash \mathcal{M}^{\mathrm{rb}}$ **do**
5: compute χ_μ^{rb} by (7.20)
6: compute τ_μ by (7.23)
7: $\Delta_\mu \leftarrow \|\tau_\mu\|_{\mathcal{V}(S)}$ by (7.22)
8: **end for**
9: // select element with largest estimator
10: $\mu_{L+1} \leftarrow \operatorname{argmax}_{\mu\in\mathcal{M}^{\mathrm{tr}}\backslash\mathcal{M}^{\mathrm{rb}}} \Delta_\mu$
11: $\mathcal{M}^{\mathrm{rb}} \leftarrow \mathcal{M}^{\mathrm{rb}} \cup \mu_{L+1}$
12: compute $\chi_{\mu_{L+1}}$ by (7.19)
13: $\mathcal{W}^{\mathrm{rb}} \leftarrow \mathcal{W}^{\mathrm{rb}} \cup \{\chi_{\mu_{L+1}}\}$
14: // update Riesz representations
15: **for** $q = 1, \dots, Q$ **do**
16: $\mathcal{S}_q \leftarrow \mathcal{S}_q \cup \{s_{q,L+1}\}$ with $s_{q,L+1}$ by (7.24)
17: **end for**
18: **end while**

which means that both quantities have the same scaling in H. Note that the hidden constants only depend on α and β. Algorithm 3 shows an implementation of the greedy search in pseudocode.

Note that the computation of χ_μ^{rb} in Line 5 of Algorithm 3 can be accelerated using the affine decomposition (7.6). After selecting an element μ_{L+1}, adding it to $\mathcal{M}^{\mathrm{rb}}$, and computing $\chi_{\mu_{L+1}}$, one can precompute the inner products

$$(\mathbf{1}_T\,,\,\chi_{\mu_{L+1}})_{L^2(S)}, \qquad b_{S,q}(\chi_{\mu_l}, \chi_{\mu_{L+1}})$$

for all $q = 1, \dots, Q$ and $l = 1, \dots, L$. Such precomputations are essential since the training set $\mathcal{M}^{\mathrm{tr}}$ is typically large and the small linear system (7.20) in Line 5 must therefore be solved many times. By precomputation, we are able to reduce the complexity of Line 5 to polynomial complexity in J, where J is the number of coarse elements in S.

In practice, provided that the bilinear form a_μ depends smoothly on the parameter μ, one typically observes a (sub-)exponential decay of the training error (7.26), i.e., there exist $\gamma > 0$ and a constant $C > 0$, such that

$$\mathsf{trerr}(L) \lesssim \exp(-CL^\gamma) \tag{7.27}$$

holds for all $L \in \mathbb{N}$. For a numerical demonstration of the decay, see Section 7.6. The theoretical derivation of such explicit decay rates is difficult, see, e.g., [Buf+12; AH15; OR16] for some theoretical results.

Note that the above computations need to be repeated for all $T \subset \mathsf{N}_m(K)$ and all $K \in \mathcal{T}_H$, which can be done in parallel. Hence, the final output of the offline phase is a collection of sets of RB functions $\mathcal{W}^{\mathrm{rb}}$.

7.4.2 Online phase

Given an arbitrary parameter value $\mu \in \mathcal{M}$, the online phase quickly computes approximate SLOD basis functions and corresponding approximate local source terms using the computations performed in the offline phase. The RB-SLOD approximation is then obtained by solving a sparse coarse linear system.

Basis computation

Next, we use the RB techniques introduced above to construct a rapidly computable approximation of the SLOD basis function ψ corresponding to the element K. This approximation, denoted by ψ^{rb}, is given by

$$\psi^{\mathrm{rb}} \coloneqq \sum_{T \subset S} c_T \chi^{\mathrm{rb}}_{T,\mu}, \tag{7.28}$$

where we denote by $\chi^{\mathrm{rb}}_{T,\mu}$ the RB approximation of $\chi_{T,\mu}$, cf. (7.20). To determine the coefficients $(c_T)_{T \subset S}$ above, we will use an approach similar to (7.15). Note, however, that due to the RB approximation, ψ^{rb} in general does not have an L^2-regular source term with respect to the local PDE operator. Since the L^2-regularity is necessary to define a conormal derivative in the sense of (7.12), a straightforward application of the approach of Section 7.3 is not possible.

We denote by g^{rb} an analogue to the non-existent local source term. It can be defined as

$$g^{\mathrm{rb}} \coloneqq \sum_{T \subset S} c_T \mathbf{1}_T, \tag{7.29}$$

where the coefficients are the same as in (7.28). Recalling the definition of the extension operator $\mathrm{tr}_\Sigma^{-1} \colon \mathcal{V}(S) \to X$ in (5.7), we can define an analogue to the conormal derivative of ψ^{rb} for all $w \in X$ as follows:

$$\langle A_\mu \nabla \psi^{\mathrm{rb}} \cdot \nu, w \rangle_{X' \times X} \coloneqq a_{S,\mu}(\psi^{\mathrm{rb}}, \mathrm{tr}_\Sigma^{-1} w) - (g^{\mathrm{rb}}, \mathrm{tr}_\Sigma^{-1} w)_{L^2(S)}. \tag{7.30}$$

This functional is an element of X' which, unlike (7.12), depends on the choice of the extension operator, i.e., for two different extension operators, the respective functionals in general do not coincide. However, we will prove that the X'-norm of their difference is bounded by the tolerance of the greedy search algorithm (7.26); see the proof of Theorem 7.5.1. Hence, the functionals corresponding to different extension operators (almost) coincide for small tolerances.

We introduce the operator $\mathcal{R}^{\mathrm{rb}}$, which maps g^{rb} to $u_q \in \mathcal{V}(S)$ solving (7.11) for $q = A_\mu \nabla \psi^{\mathrm{rb}} \cdot \nu \in X'$, i.e.,

$$\mathcal{R}^{\mathrm{rb}} \colon \mathcal{P}^0(S) \to \mathcal{V}(S).$$

Similar to (7.15), we then choose the local source term g^{rb} as the solution to the minimization problem

$$g^{\mathrm{rb}} \in \operatorname*{arg\,min}_{p \in \mathcal{P}^0(S)} \frac{\|\mathcal{R}^{\mathrm{rb}} p\|^2_{\mathcal{V}(S)}}{\|p\|^2_{L^2(S)}}, \tag{7.31}$$

where we again refer to Section 5.2 regarding possible non-uniqueness issues.

Note that the above problem is again equivalent to a low-dimensional eigenvalue problem similar to (7.16). The low-dimensional matrices in the eigenvalue problem can be quickly assembled using a suitable approximation of the X' norm. Such approximations are discussed in Section 7.4.3. We refer to Figure 7.5 for a illustration of g^{rb} and ψ^{rb} for different parameter choices.

The above basis computation needs to be repeated for all $K \in \mathcal{T}_H$. For an implementation of the basis computation in pseudocode, see Algorithm 4. The

Algorithm 4 Online – RB-SLOD basis computation.

$\mathcal{B}, \mathcal{G} \leftarrow \{\}$
for $K \in \mathcal{T}_H$ **do**
    // compute RB approximations
    for $T \subset \mathsf{N}_m(K)$ **do**
        compute $\chi^{\mathrm{rb}}_{T,\mu}$ by (7.20)
    end for
    // compute and save basis functions
    compute $g^{\mathrm{rb}}_{K,m,\mu}$ by (7.31)
    $\mathcal{G} \leftarrow \mathcal{G} \cup \{g^{\mathrm{rb}}_{K,m,\mu}\}$
    obtain $\psi^{\mathrm{rb}}_{K,m,\mu}$ by (7.28) with coefficients from (7.29)
    $\mathcal{B} \leftarrow \mathcal{B} \cup \{\psi^{\mathrm{rb}}_{K,m,\mu}\}$
end for

algorithm collects the RB-SLOD basis functions and the corresponding local source terms in the sets $\mathcal{B}$ and $\mathcal{G}$. This information will be used during the coarse solve for the computation of the RB-SLOD approximation.

Coarse solve

In the following, $\psi^{\mathrm{rb}}_{K,m,\mu} \in \mathcal{B}$ and $g^{\mathrm{rb}}_{K,m,\mu} \in \mathcal{G}$ denote the RB approximations of the basis function and local source term corresponding to the element $K \in \mathcal{T}_H$, cf. (7.28) and (7.31). For the RB-SLOD approximation we use the collocation ansatz of (5.15), i.e., denoting by $(c_K)_{K \in \mathcal{T}_H}$ the coefficients of the expansion of $\Pi^0_H f$ in terms of the local source terms $g^{\mathrm{rb}}_{K,m,\mu}$, we define

$$u^{\mathrm{rb}}_{H,m,\mu} \coloneqq \sum_{K \in \mathcal{T}_H} c_K \psi^{\mathrm{rb}}_{K,m,\mu}. \tag{7.32}$$

In Algorithm 5 we denote by $\mathbf{G} \in \mathbb{R}^{\#\mathcal{T}_H \times \#\mathcal{T}_H}$ the matrix whose columns are the element values of the $\mathcal{T}_H$-piecewise constant functions in $\mathcal{G}$. Furthermore, $\mathbf{f}$

denotes the load vector with the element values of $\Pi_H^0 f$ as entries. Note that due to the collocation ansatz, no inner products between basis functions need to be computed in Algorithm 5.

Algorithm 5 Online – Coarse solve.

1: assemble $\mathbf{G}$ from $\mathcal{G}$
2: compute $\mathbf{f}$
3: solve $\mathbf{c} = \mathbf{G}\backslash\mathbf{f}$
4: compute $u_{H,m,\mu}^{\mathrm{rb}}$ by (7.32) with the coefficients $(\mathbf{c}_i)_{i=1,\dots,\#\mathcal{T}_H}$

It is noteworthy that the source term f first appears in Algorithm 5, i.e., the offline phase and the basis computation are completely independent of f. This feature makes the RB-SLOD method suitable for applications where the solution for different source terms is of interest. In particular, parameter-dependent and possibly non-affine source terms do not pose any further difficulties. In the implementation, the source term parameters only affect the coarse solve, and the actual RB approach is independent of these parameters, see also Section 7.2 and the numerical example in Section 7.6.

7.4.3 Practical implementation

For the practical implementation, we note that the RB-SLOD inherits the basis stability issues of the SLOD. Consequently, the practical implementation of the SLOD presented in Section 5.5, which solves these stability issues, can also be used for the RB-SLOD.

Furthermore, to discretize the infinite-dimensional patch problems (7.19), (7.21), (7.24), and (7.25), we need to perform a fine-scale discretization. Similarly to Section 3.5, we consider the fine mesh $\mathcal{T}_h$ obtained by uniform refinement of $\mathcal{T}_H$ and replace the infinite-dimensional space $\mathcal{V}$ in the definition of the RB-SLOD by its finite-dimensional fine-scale FE counterpart with respect to $\mathcal{T}_h$. Consequently, the above patch problems are posed in local finite-dimensional subspaces of the global fine-scale FE space.

Practical basis computation

We denote by ψ_h^{rb} the fully discrete RB-SLOD basis function associated with the element $K \in \mathcal{T}_H$. It is a linear combination of the fully discrete RB approximations $\{\chi_{T,\mu,h}^{\mathrm{rb}} : T \subset S\}$, cf. (7.28). The local source term $g_h^{\mathrm{rb}} \in \mathcal{P}^0(S)$ is defined analogously to (7.29). Exploiting the fact that the conormal derivative of ψ_h^{rb} exists in the $L^2(\partial S)$ sense, one can derive alternative choices to (7.31) with reduced computational cost.

For example, instead of minimizing the X'-norm of (7.30), one may minimize the $L^2(\Sigma)$-norm of the conormal derivative $(A_\mu \nabla \psi_h^{\mathrm{rb}} \cdot \nu)|_\Sigma$. Here, one may also omit the diffusion tensor, i.e., we minimize the normal derivative $(\nabla \psi_h^{\mathrm{rb}} \cdot \nu)|_\Sigma$

instead of the conormal derivative $(A_\mu \nabla \psi_h^{\mathrm{rb}} \cdot \nu)|_\Sigma$. This is justified since, by (7.2), a small norm of the normal derivative implies a small norm of the conormal derivative. In the practical implementation, we choose g_h^{rb} as the solution to the minimization problem

$$g_h^{\mathrm{rb}} \in \operatorname*{arg\,min}_{p \in \mathcal{P}^0(S)} \frac{\|\mathcal{R}_h^{\mathrm{rb}} p\|_{L^2(\Sigma)}^2}{\|p\|_{L^2(S)}^2}, \tag{7.33}$$

where $\mathcal{R}_h^{\mathrm{rb}} \colon \mathcal{P}^0(S) \to L^2(\Sigma)$ denotes the operator mapping g_h^{rb} to the normal derivative $(\nabla \psi_h^{\mathrm{rb}} \cdot \nu)|_\Sigma$ of the fully discrete RB-SLOD basis function. Such an approach has for example been used in [BFP22] for convection-dominated diffusion problems.

In practice, one solves (7.33) by considering the equivalent generalized eigenvalue problem $\mathbf{C}\mathbf{x} = \lambda \mathbf{D}\mathbf{x}$ given in (7.16), where $\mathcal{R}$ is replaced by $\mathcal{R}_h^{\mathrm{rb}}$. Note that the assembly of the matrix $\mathbf{C}$ can be drastically accelerated by precomputing the following four-dimensional array in the offline phase:

$$(\nabla \chi_{T_j,\mu_n} \cdot \nu \,,\, \nabla \chi_{T_i,\mu_l} \cdot \nu)_{L^2(\Sigma)},$$

where $l = 1, \dots, L_i$, $n = 1, \dots, L_j$, and $i, j = 1, \dots, J$. Here, L_i and L_j denote the cardinality of the parameter sets $\mathcal{M}^{\mathrm{rb}}$ corresponding to the elements T_i and T_j and J denotes the number of coarse elements in S. Note that the matrix $\mathbf{D}$ is parameter-independent and thus only needs to be assembled once.

Complexity

Due to the precomputations in the offline phase, no (local or global) fine-scale solves are needed in the online phase. More precisely, the only fine-scale operations in the online phase are (i) the addition of (local) fine-scale functions in the computation of the RB-SLOD basis (see Algorithm 4, Line 5 and 10) and (ii) the addition of the RB-SLOD basis functions using the coefficients computed by solving a coarse linear system (see Algorithm 5, Line 4).

Note that if one is only interested in the coarse QOIs of the solution, fine-scale operations can be completely avoided in the online phase. For this, one additionally computes the element averages of the fine-scale functions in Algorithm 3, Line 12 in the offline phase. This information can then be used in the online phase to compute the element averages of the SLOD basis functions without fine-scale operations. By adding up the element averages of the SLOD basis functions using the same coefficients as in Algorithm 5, Line 4, one obtains a $\mathcal{T}_H$ piecewise constant approximation to the solution without performing any fine-scale operations in the online phase.

7.5 Error analysis

This section presents an a posteriori error analysis of the RB-SLOD. Similar to the SLOD in (5.17), we have to assume also for the RB-SLOD that the set $\{g^{\mathrm{rb}}_{K,m,\mu} : K \in \mathcal{T}_H\}$ is a Riesz stable basis of $\mathcal{P}^0(\mathcal{T}_H)$. This assumption guarantees the well-posedness and stability of the method. In practice, the Riesz stability can be ensured a posteriori as described in Section 5.5. For the following error analysis we assume that there exists $C_\mu > 0$ depending polynomially on H^{-1} and m such that

$$C_\mu^{-1}(H,m) \sum_{K\in\mathcal{T}_H} c_K^2 \leq \Big\| \sum_{K\in\mathcal{T}_H} c_K g^{\mathrm{rb}}_{K,m,\mu} \Big\|^2_{L^2} \leq C_\mu(H,m) \sum_{K\in\mathcal{T}_H} c_K^2 \tag{7.34}$$

holds for all $(c_K)_{K\in\mathcal{T}_H}$.

The following theorem gives an a posteriori error estimate for the RB-SLOD. It differs from the one for the SLOD in Theorem 5.3.2 since it additionally takes into account the RB error and therefore includes a term depending on the tolerance of the greedy search algorithm.

Theorem 7.5.1 (Convergence of the RB-SLOD)**.** *For any $f \in H^k(D)$, $k \in \{0,1\}$, the RB-SLOD approximation* (7.32) *satisfies that*

$$\|u_\mu - u^{\mathrm{rb}}_{H,m,\mu}\|_{\mathcal{V}} \lesssim \big(H^{1+k}|f|_{H^k} + C_\mu^{1/2}(H,m)m^{d/2}(\sigma_\mu(H,m) + \mathsf{tol}\, m^{d/2})\|f\|_{L^2}\big),$$

where the hidden constant depends on α, β, and the quasi-uniformity and shape regularity of $\mathcal{T}_H$.

Proof. Let $\mu \in \mathcal{M}^{\mathrm{tr}}$ be arbitrary but fixed. We first add and subtract the function $\tilde{u}_\mu \coloneqq \mathcal{L}_\mu \Pi^0_H f \in \mathcal{V}_{H,\mu}$ and apply the triangle inequality to obtain that

$$\|u_\mu - u^{\mathrm{rb}}_{H,m,\mu}\|_{\mathcal{V}} \leq \|u_\mu - \tilde{u}_\mu\|_{\mathcal{V}} + \|u^{\mathrm{rb}}_{H,m,\mu} - \tilde{u}_\mu\|_{\mathcal{V}}.$$

For the first term, one can show using the definition of $\tilde{u}_\mu$, (7.5), and (2.25) that

$$\begin{aligned}\alpha\|u_\mu - \tilde{u}_\mu\|_{\mathcal{V}} &\leq \sup_{v\in\mathcal{V}} \frac{a_\mu(u_\mu - \tilde{u}_\mu, v)}{\|v\|_{\mathcal{V}}} = \sup_{v\in\mathcal{V}} \frac{(f - \Pi^0_H f\,,\, v - \Pi^0_H v)_{L^2}}{\|v\|_{\mathcal{V}}} \\ &\lesssim \pi^{-1} H \|f - \Pi^0_H f\|_{L^2}.\end{aligned}$$

For the second term, we define

$$\tilde{\varphi}_{K,m,\mu} \coloneqq \mathcal{L}_\mu g^{\mathrm{rb}}_{K,m,\mu}$$

and denote by $(c_K)_{K\in\mathcal{T}_H}$ the coefficients of the expansion of $\Pi^0_H f$ in terms of the source terms $g^{\mathrm{rb}}_{K,m,\mu}$. Using these coefficients, $\tilde{u}_\mu$ can be expanded as

$$\tilde{u}_\mu = \sum_{K\subset S} c_K \tilde{\varphi}_{K,m,\mu}.$$

Abbreviating $e \coloneqq u^{\mathrm{rb}}_{H,m,\mu} - \tilde{u}_\mu$, using (7.5) and the definition of the collocation solution (7.32), we obtain that

$$\alpha \|e\|^2_{\mathcal{V}} \leq a_\mu(e,e) = \sum_{K \in \mathcal{T}_H} c_K a_\mu(\psi^{\mathrm{rb}}_{K,m,\mu} - \tilde{\varphi}_{K,m,\mu}, e). \tag{7.35}$$

Next, we consider one fixed summand corresponding to an element $K \in \mathcal{T}_H$ and abbreviate $S \coloneqq \mathsf{N}_m(K)$. We omit the fixed indices K, m, and μ of the functions $\tilde{\varphi}_{K,m,\mu}$ and $\psi^{\mathrm{rb}}_{K,m,\mu}$ and denote the trace and extension operators with respect to $\Sigma = \partial S \backslash \partial D$ by tr_Σ and tr_Σ^{-1}, respectively, cf. (7.8) and (7.9). Defining $\tilde{\psi} \coloneqq \mathcal{L}_{S,\mu} g^{\mathrm{rb}}$ and using (7.30) and $e - \mathrm{tr}_\Sigma^{-1} \mathrm{tr}_\Sigma e \in \mathcal{V}_S$ yields that

$$\begin{aligned} a_\mu(\psi^{\mathrm{rb}} - \tilde{\varphi}, e) &= a_\mu(\psi^{\mathrm{rb}}, e) - (g^{\mathrm{rb}}\,,\, e)_{L^2(S)} \\ &= a_{S,\mu}(\psi^{\mathrm{rb}}, \mathrm{tr}_\Sigma^{-1}\mathrm{tr}_\Sigma e) - (g^{\mathrm{rb}}\,,\, \mathrm{tr}_\Sigma^{-1}\mathrm{tr}_\Sigma e)_{L^2(S)} + a_{S,\mu}(\psi^{\mathrm{rb}} - \tilde{\psi}, e - \mathrm{tr}_\Sigma^{-1}\mathrm{tr}_\Sigma e) \\ &= \langle A_\mu \nabla \psi^{\mathrm{rb}} \cdot \nu, \mathrm{tr}_\Sigma e \rangle_{X' \times X} + a_{S,\mu}(\psi^{\mathrm{rb}} - \tilde{\psi}, e - \mathrm{tr}_\Sigma^{-1}\mathrm{tr}_\Sigma e). \end{aligned} \tag{7.36}$$

For the bound of the first term in (7.36), we denote by $g \in \mathcal{P}^0(S)$ the L^2-normalized SLOD source term from (7.15). We define

$$\hat{\psi}^{\mathrm{rb}} \coloneqq \sum_{T \subset S} g|_T \chi^{\mathrm{rb}}_{T,\mu}, \qquad \psi \coloneqq \mathcal{L}_{S,\mu} g$$

with $\chi^{\mathrm{rb}}_{T,\mu}$ defined in (7.20). Using (7.10), the definition of the conormal derivative (7.13), the definitions of g^{rb} and σ_μ in (5.18) and (7.31), respectively, as well as (7.5) and the continuity of tr_Σ^{-1} in (7.9), we obtain that

$$\begin{aligned} \|A_\mu \nabla \psi^{\mathrm{rb}} \cdot \nu\|_{X'} = \|\mathcal{R}^{\mathrm{rb}} g^{\mathrm{rb}}\|_{\mathcal{V}(S)} &\leq \|\mathcal{R}^{\mathrm{rb}} g\,\|_{\mathcal{V}(S)} \\ &= \sup_{w \in X\,:\,\|w\|_X = 1} |a_\mu(\hat{\psi}^{\mathrm{rb}}, \mathrm{tr}_\Sigma^{-1} w) - (g\,,\, \mathrm{tr}_\Sigma^{-1} w)_{L^2(S)}| \\ &\leq \|A_\mu \nabla \psi \cdot \nu\|_{X'} + \sup_{w \in X\,:\,\|w\|_X = 1} |a_\mu(\hat{\psi}^{\mathrm{rb}} - \psi, \mathrm{tr}_\Sigma^{-1} w)| \\ &\leq \sigma_\mu(H,m) + \beta \,\|\hat{\psi}^{\mathrm{rb}} - \psi\|_{\mathcal{V}(S)}. \end{aligned} \tag{7.37}$$

Using that the norm of p in (7.26) can be bounded as

$$\|p\|_{\mathcal{V}(S)} = \|\mathbf{1}_T\|_{\mathcal{V}_S'} \leq \|\mathbf{1}_T\|_{L^2(S)},$$

we obtain for the second term in (7.37) that

$$\begin{aligned} \|\hat{\psi}^{\mathrm{rb}} - \psi\|_{\mathcal{V}(S)} &\leq \sum_{T \subset S} |g|_T| \|\chi^{\mathrm{rb}}_{T,\mu} - \chi_{T,\mu}\|_{\mathcal{V}(S)} \leq \alpha^{-1} \mathsf{tol} \sum_{T \subset S} g|_T \|\mathbf{1}_T\|_{L^2(S)} \\ &\lesssim \alpha^{-1} \mathsf{tol}\, m^{d/2}. \end{aligned} \tag{7.38}$$

Here, we used that the number of elements in S is bounded by m^d, Lemma 7.4.1, the stopping criterion (7.26), the discrete Cauchy–Schwarz inequality, and the normalization condition $\|g\|_{L^2(S)} = 1$.

For the second term in (7.36), we obtain using the continuity of tr_Σ and tr_Σ^{-1} in (7.8) and (7.9) that

$$\begin{aligned} a_{S,\mu}(\psi^{\mathrm{rb}} - \tilde{\psi}, e - \mathrm{tr}_\Sigma^{-1}\,\mathrm{tr}_\Sigma\, e) &\leq \beta \|\psi^{\mathrm{rb}} - \tilde{\psi}\|_{\mathcal{V}(S)} \|e - \mathrm{tr}_\Sigma^{-1}\,\mathrm{tr}_\Sigma\, e\|_{\mathcal{V}(S)} \\ &\leq 2\beta \|\psi^{\mathrm{rb}} - \tilde{\psi}\|_{\mathcal{V}(S)} \|e\|_{\mathcal{V}(S)}. \end{aligned}$$

Here, the first norm on the right-hand side can be estimated similarly to (7.38) by

$$\|\psi^{\mathrm{rb}} - \tilde{\psi}\|_{\mathcal{V}(S)} \lesssim \alpha^{-1}\mathsf{tol}\, m^{d/2}$$

using that $\|g^{\mathrm{rb}}\|_{L^2(S)} = 1$.

Finally, using the above estimates, we are able to return to estimate (7.35). Summing over all elements $K \in \mathcal{T}_H$, using (2.24) and (7.34), and the finite overlap of the patches $\mathsf{N}_m(K)$, we obtain that

$$\begin{aligned} \alpha\|e\|_{\mathcal{V}}^2 &\leq \sum_{K\in\mathcal{T}_H} c_K a_\mu(\psi_{K,m,\mu}^{\mathrm{rb}} - \tilde{\varphi}_{K,m,\mu}, e) \\ &\lesssim m^{d/2}\big(\sigma_\mu(H,m) + \mathsf{tol}\,\beta\alpha^{-1}m^{d/2}\big)\sqrt{\sum_{K\in\mathcal{T}_H} c_K^2}\,\|e\|_{\mathcal{V}} \\ &\lesssim C_\mu^{1/2}(H,m) m^{d/2}\big(\sigma_\mu(H,m) + \mathsf{tol}\,\beta\alpha^{-1}m^{d/2}\big)\|f\|_{L^2}\|e\|_{\mathcal{V}}. \end{aligned}$$

The assertion follows immediately. □

Remark 7.5.2 (Choice of parameters)**.** This remark specifies how to choose the oversampling parameter m and the number L of elements in $\mathcal{M}^{\mathrm{rb}}$ to preserve the optimal orders of convergence in Theorem 7.5.1. For the choice of m, the super-exponential decay result (5.27) implies the oversampling condition $m \gtrsim (\log \frac{1}{H})^{(d-1)/d}$. Furthermore, for the choice of L, we recall that the training error of the greedy search algorithm, defined in (7.26), decays (sub-)exponentially in L, cf. (7.27). This yields the condition $L \gtrsim (\log \frac{m}{H})^{1/\gamma}$, where γ denotes the exponent of L in the sub-exponential decay.

7.6 Numerical experiments

This section numerically investigates the RB-SLOD for a parametric elliptic model problem and a parametric reaction–convection–diffusion problem. We consider uniform Cartesian meshes of the domain $D = (0,1)^2$, where the mesh size denotes the side length of the elements instead of their diameter. The RB-SLOD is implemented as described in Section 7.4.3 taking into account the remarks on the practical basis computation and the fine-scale discretization. We emphasize that, similar to Section 3.5 for the LOD, we expect the theoretical results of the RB-SLOD to remain valid in the fully discrete setting.

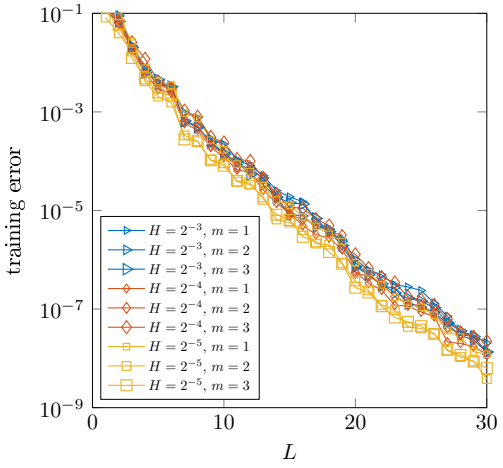

Figure 7.1: Training error as a function of the size L of $\mathcal{M}^{\mathrm{rb}}$ for different patch configurations.

Parametric elliptic model problem

The first numerical experiment is taken from [AH15, Sec. 4.1]. It considers a parametric diffusion problem with homogeneous Dirichlet boundary conditions. Its anisotropic multi-scale diffusion tensor exhibits oscillations on various scales with the smallest being 2^{-6} (see the reference for the exact definition of the coefficient). The bilinear form of the problem admits an affine decomposition as in (7.6) with $Q = 4$ terms, where the parameter space is $\mathcal{M} = [0, 5]$. As training set $\mathcal{M}^{\mathrm{tr}}$, we use 100 equidistantly distributed points. For the fine-scale discretization we consider the uniform Cartesian mesh $\mathcal{T}_{2^{-8}}$. In the following, all errors are relative errors with respect to the energy norm defined in (3.37), which are computed using the fine-scale FE solution as the reference solution.

Decay of training error

To demonstrate the decay of the training error (7.26) in the greedy search algorithm, we consider representative patches $\mathsf{N}_m(K)$ in the coarse mesh $\mathcal{T}_H$ for different mesh sizes H and oversampling parameters m. Figure 7.1 shows the sub-exponential decay of the training error for several patch configurations as the number L of elements in $\mathcal{M}^{\mathrm{rb}}$ is increased, which is consistent with the prediction (7.27). Note that the discretization parameters H and m have only a small effect on the size of the training error. Given the discretization parameters H and m and a tolerance tol, one can use Figure 7.1 to estimate the size of the sets $\mathcal{M}^{\mathrm{rb}}$ needed to achieve the given tolerance.

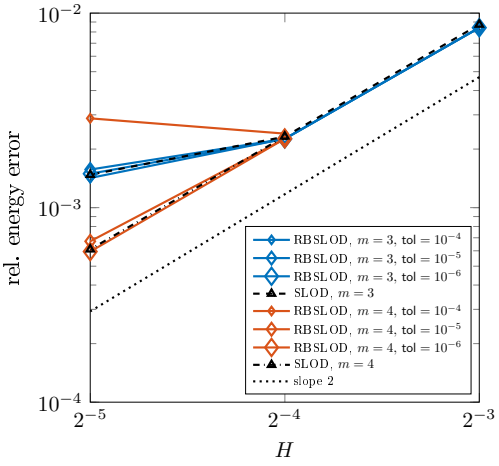

Figure 7.2: Errors of the RB-SLOD and SLOD as functions of H for several oversampling parameters m and tolerances tol for the elliptic problem. The dotted line indicates the expected rate of convergence.

Optimal order convergence

To numerically verify the optimal order convergence properties of the RB-SLOD, we consider the above parametric elliptic model problem with the source term

$$f(x_1, x_2) = (x_1 + \cos(3\pi x_1)) \cdot x_2^3, \tag{7.39}$$

which, for consistency, is the same as in the convergence experiments in the previous chapters. We compute the RB-SLOD solution for the parameter $\mu \approx 2.129$, which is not contained in the training set $\mathcal{M}^{\text{tr}}$. Provided that the oversampling parameter m is chosen sufficiently large, Figure 7.2 shows second order convergence of the RB-SLOD. Recalling that $f \in H^1(D)$, this is consistent with the theoretical prediction in Theorem 7.5.1. Furthermore, one observes the expected behavior that the RB-SLOD error curve approaches the SLOD error curve as tol is decreased. Note that in this numerical experiment we use slightly larger oversampling parameters than in the numerical experiments for the SLOD in Section 5.6. This is consistent with the general observation that the collocation variant of the SLOD (used for the construction of the RB-SLOD) requires slightly larger oversampling parameters to achieve the same accuracy as the Galerkin variant of the SLOD.

Super-exponential localization

In this numerical experiment we consider the same problem as in the previous numerical experiment, but with the source term $f \equiv 1$. Note that for such source terms, only the localization error and the RB error are present in Theorem 7.5.1, and the optimal order term vanishes. We emphasize that the basis functions of

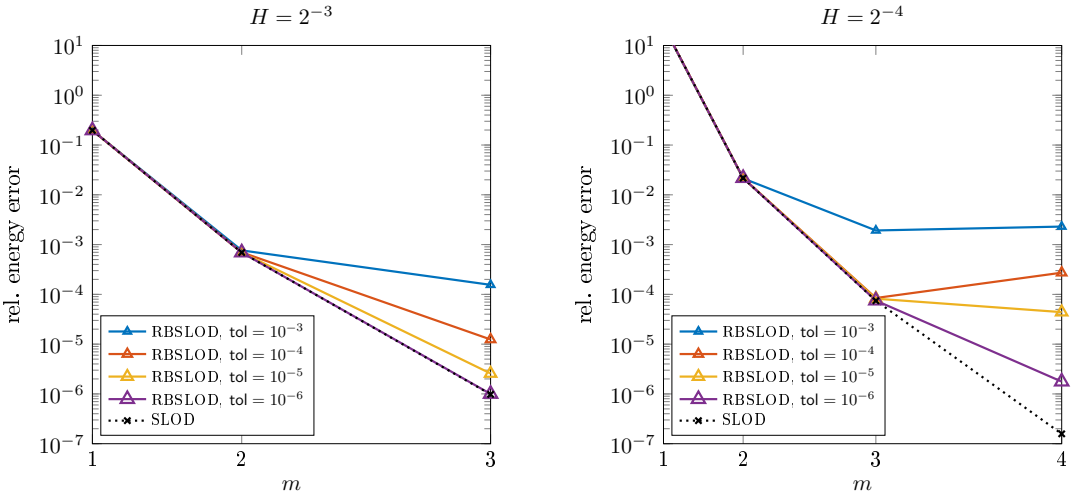

Figure 7.3: Errors of the RB-SLOD and SLOD as functions of m for several tolerances tol for $H = 2^{-3}$ (left) and $H = 2^{-4}$ (right) for the elliptic problem.

the RB-SLOD are independent of the actual source term f. Thus, we can use the same basis functions as in the previous numerical experiment and only need to repeat the cheap coarse solve in Algorithm 5, Line 3. In Figure 7.3 one can observe the super-exponential decay of the localization error, provided that tol is chosen sufficiently small, cf. Section 5.4. In the left plot of Figure 7.3, the error curve of the SLOD is reached for the tolerance $\mathsf{tol} = 10^{-6}$, whereas in the right plot of Figure 7.3, an even smaller tolerance would have been necessary. In general, one can observe that the error curve of the RB-SLOD approaches the error curve of the SLOD as tol is decreased. Note that in the left plot in Figure 7.3 only oversampling parameters m less than or equal to 3 are considered. This is due to the assumption in the construction of the RB-SLOD that no patch coincides with the entire domain.

Note that a direct comparison of the RB-SLOD with the RB-LOD from [AH15] is difficult. For the only source term $f \equiv 1$ considered in [AH15], the RB-SLOD is unbeatable, since only the localization error and the RB error are present. In contrast, the RB-LOD also has a spatial approximation error due to a different construction of the approximation space. Therefore, it seems reasonable to compare the size of the errors of the RB-SLOD for the non-polynomial source term (7.39) with the one of the RB-LOD for the constant source term. It can be observed that for the same magnitude of errors, the RB-SLOD requires considerably smaller oversampling parameters than the RB-SLOD. For example, given $H = 2^{-4}$, both methods achieve a relative error of the order of 10^{-2} with $m = 2$ for the RB-SLOD (2.04×10^{-2}) and $m = 4$ for the RB-LOD (2.83×10^{-2}, cf. [AH15, Tbl. 1]). This allows a sparser coarse system of equations and a more localized computation of the basis functions.

Parametric mass transfer with non-affine source

Next, we consider a parametric reaction–convection–diffusion problem taken from [QMN15, Ch. 8.4]. The parameters in the problem determine the magnitude of the diffusion, the direction of the convection, and the shape of the non-affine Gaussian source term. The corresponding five-dimensional parameter vector $\mu \in \mathbb{R}^5$ has the components $\mu_1 \in [0.01, 0.1]$, $\mu_2 \in [0, 2\pi)$, $\mu_3, \mu_4, \in [0.25, 0.75]$, and $\mu_5 \in [0.1, 0.25]$. The strong formulation of the problem under consideration is

$$\begin{aligned} -\mu_1 \Delta u - b_\mu \cdot \nabla u + u &= f_\mu && \text{in } D \coloneqq (0,1)^2, \\ \mu_1 \nabla u \cdot \nu &= 0 && \text{on } \partial D \end{aligned}$$

with

$$b_\mu = (\cos(\mu_2), \sin(\mu_2))^T$$

and

$$f_\mu(x_1, x_2) = \exp\left(- \frac{(x_1 - \mu_3)^2 + (x_2 - \mu_4)^2}{\mu_5^2} \right).$$

This problem is challenging for several reasons. First, the nature of the problem is strongly dependent on the magnitude of the diffusion μ_1, i.e., the proposed RB method must be able to handle both the diffusion-dominated and the convection-dominated regime simultaneously. Second, the parameter space is relatively high-dimensional, which typically makes RB methods quite expensive. Third, the chosen source term does not admit an affine decomposition, which prevents the straightforward application of standard RB approaches and typically requires additional tools, such as the empirical interpolation method [Bar+04], at additional computational cost.

For such numerical examples the RB-SLOD has the decisive advantage that it has a built-in RB approach in the source term, cf. Section 7.2. More specifically, the source term parameters are only important for the coarse solve in Algorithm 5 and can be ignored in the actual RB approach in Section 7.4.1. In addition, since the considered coefficients are constant in space (and therefore in particular periodic with respect to $\mathcal{T}_H$), only $\mathcal{O}(m^d)$ patches need to be considered for the computations. The remaining patches can be handled by translation, which drastically reduces the computational cost. Furthermore, in the implementation we use a training set $\mathcal{M}^{\text{tr}}$ of 400 points on a Cartesian grid of the two-dimensional parameter set $\mathcal{M} = [0.01, 0.1] \times [0.2\pi]$, where we ignore the parameters coming from the source term. For the fine-scale discretization of the patch problems we use the grid $\mathcal{T}_{2^{-8}}$.

Decay of training error

In this numerical experiment, we investigate the training error (7.26) for the above reaction–convection–diffusion problem. In Figure 7.4 we observe a fast decay of the training error as the number L of elements in $\mathcal{M}^{\text{rb}}$ is increased. However, compared to Figure 7.1, the magnitude of the training errors is sig-

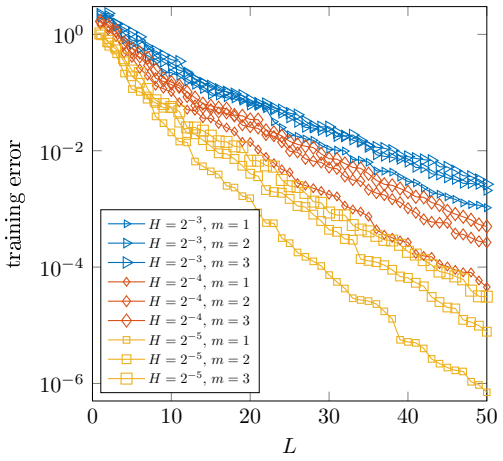

Figure 7.4: Training error as a function of the size L of $\mathcal{M}^{\mathrm{rb}}$ for different patch configurations.

nificantly larger due to the more complicated nature of the underlying problem. Note that for this numerical example, the magnitude of the error depends on the choice of H and m in the sense that for patches with a large diameter, also the training error is large.

Numerical results and illustration of basis functions

Consider the coarse mesh with mesh size $H = 2^{-4}$ and oversampling parameter $m = 2$. For this choice of discretization parameters, the largest patches occupy at most 10% of the total domain volume and the maximum number of elements in the sets $\mathcal{M}^{\mathrm{rb}}$ is 34. In Figure 7.5 we plot a RB-SLOD basis function $\psi^{\mathrm{rb}}_{K,m}$ and the corresponding source term $g^{\mathrm{rb}}_{K,m}$ for three different parameter values of μ_1 and μ_2. Note that the basis functions are independent of the parameters μ_3, μ_4, and μ_5 of the source term f_μ.

Figure 7.6 shows the RB-SLOD solutions and the absolute value of the difference between the RB-SLOD solutions and the fine-scale FE reference solutions for the same parameter pairs as in Figure 7.5. The remaining parameters μ_3, μ_4, and μ_5 are randomly chosen. Note that all plots in the same row have the same color scale. From left to right, the relative $\mathcal{V}$-norm errors are 5.62×10^{-2}, 4.53×10^{-2}, and 6.29×10^{-2}. For this numerical experiment, a direct comparison to [QMN15, Ch. 8.4] is again difficult. There, the parameters μ_1 and μ_5 are fixed, which simplifies the resulting problem. In particular, the nature of the problem no longer depends on the choice of the parameters (the magnitude of the diffusion μ_1 is fixed). We emphasize that the RB-SLOD is able to avoid the additional difficulties with non-affine source terms f that classical RB approaches have, cf. [Bar+04].

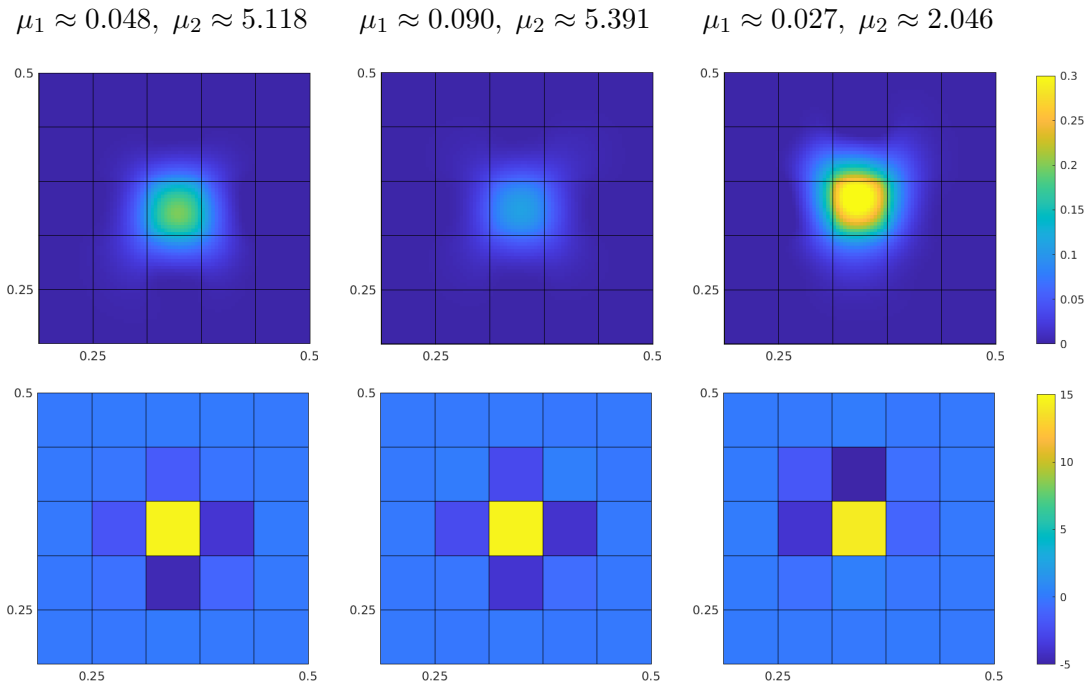

Figure 7.5: RB-SLOD basis functions (top) and the corresponding local source terms (bottom) for three different parameter pairs.

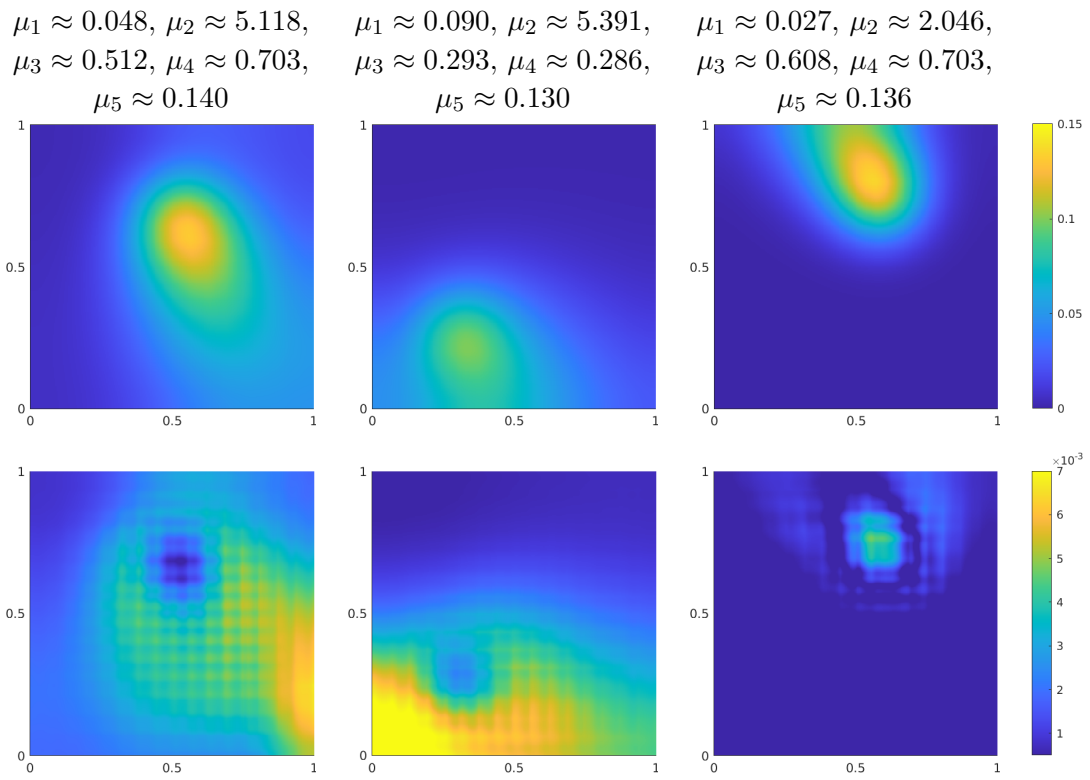

Figure 7.6: RB-SLOD solutions (top) and the absolute value of the errors (bottom) for three different parameter choices.

8 Conclusion and Outlook

8.1 Conclusion

In this thesis, we have presented recent advances in the field of LOD-based numerical homogenization. As a starting point, we first introduced the LOD in a general setting and showed that the LOD is able to achieve optimal approximation orders without having to globally resolve the underlying coefficients. The LOD approach was then extended to the multi-resolution setting by the MRLOD, where we uses the Helmholtz problem as a model problem. The MRLOD allows one to improve the accuracy of an existing LOD approximation by adding additional discretization levels. We have presented a rigorous wavenumber-explicit stability and error analysis of the method showing its pollution-free optimal order convergence properties under mild assumptions on the discretization parameters, see Theorems 4.4.1 and 4.4.2. The resulting coarse system matrix of the MRLOD is block-diagonal, and all but the first small block can be solved with a standard iterative solver within a few iterations, see Theorem 4.5.1.

Moreover, we have introduced the SLOD, a novel LOD-based numerical homogenization method that identifies basis functions which are significantly more local than those of the LOD. As a result, the computational cost of the basis computation is lower and the coarse system matrix is sparser. These properties are a consequence of the practically observed super-exponential decay of the localization error, see Section 5.4. While a proof of the super-exponential decay of the localization error is still open, we have proved that the localization error decays at least exponentially using LOD arguments, see Theorem 5.4.3. In a general setting, we have also performed a rigorous stability and error analysis of the SLOD, where the stability of the basis is quantified a posteriori, see Theorems 5.3.1 and 5.3.2.

For high-contrast channeled coefficients, for example, the SLOD may suffer from basis stability issues, resulting in a degradation of its approximation quality, see Section 6.5. To overcome this problem, we combined the SLOD with a partition of unity approach, resulting in the SL-GFEM. From an application point of view, the SL-GFEM is conceptually simple and easy to implement. We have provided a rigorous a posteriori and a priori error analysis of the SL-GFEM showing that its approximation quality is at least as good as that of the SLOD, see Theorem 6.3.1, and at the same time not worse than that of the LOD, see Theorem 6.4.1. Furthermore, we have derived higher order versions of the SL-GFEM that achieve higher order convergence rates using only the

regularity of the source term. Finally, we introduced the RB-SLOD, which is a local RB technique for parameter-dependent multi-scale problems. This method integrates an RB approach into the SLOD framework, allowing for the efficient generation of accurate coarse-scale models of the problem. An a posteriori error analysis of the RB-SLOD, in the spirit of that of the SLOD, is presented in Theorem 7.5.1. Due to the unique localization properties of the SLOD, the RB snapshot computation can be performed on particularly small patches, resulting in a relatively low offline and online complexity of the method.

8.2 Outlook

The work presented in this thesis provides many opportunities for future research. One important open point is the proof of the super-localization property of the SLOD, see Section 5.4. This may be done using techniques related to spectral geometry, which however usually require strong assumptions on the regularity of the coefficients and the boundary, cf. [HL01; PST15; GT16].

Another possible follow-up is the combination of the SLOD with a multi-resolution approach similar to the MRLOD. However, in order to obtain a decoupling of scales, additional constraints must be placed on the basis functions, which could potentially affect their localization properties.

A further future project is the extension of the SL-GFEM to Helmholtz problems. Based on previous experience with the LOD and the SLOD for Helmholtz problems, no major challenges are expected. Moreover, the SL-GFEM could be combined with a multi-resolution approach to improve the accuracy of the approximation while keeping the size of the subdomains fixed.

Given the effectiveness of the SLOD in treating Helmholtz problems, it may be worthwhile to explore its applicability to other time-harmonic wave propagation problems, such as elastic wave propagation and Maxwell-type problems.

List of Symbols

b_K	bubble function associated to element K	25
$\mathcal{B}_H$	bubble operator w.r.t. $\mathcal{T}_H$	25
$\mathcal{B}_\ell$	bubble operator w.r.t. $\mathcal{T}_\ell$	44
$\mathcal{C}$, $\mathcal{C}^*$	corrector	24
$\mathcal{C}_K$, $\mathcal{C}_K^*$	element corrector	27
$\mathcal{C}_{K,m}$, $\mathcal{C}_{K,m}^*$	localized element corrector	29
$\mathcal{C}_m$, $\mathcal{C}_m^*$	localized corrector	30
$\mathcal{C}_\ell$, $\mathcal{C}_\ell^*$	corrector at level ℓ	45
$\mathcal{C}_{K,\ell}$, $\mathcal{C}_{K,\ell}^*$	element corrector at level ℓ	50
$\mathcal{C}_{K,\ell,m}$, $\mathcal{C}_{K,\ell,m}^*$	localized element corrector at level ℓ	50
$\mathcal{C}_{\ell,m}$, $\mathcal{C}_{\ell,m}^*$	localized corrector at level ℓ	51
d	spatial dimension	11
D	physical domain	11
$\|\cdot\|_a$	energy norm w.r.t. the sesquilinear form a	37
$\approx$	equal up to a constant	9
$\gtrsim$	greater than or equal to up to a constant	9
h	fine mesh size	36
H	coarse mesh size	13
H_ℓ	mesh size at level ℓ	44
$\mathcal{H}$	Haar basis w.r.t. $\{\mathcal{T}_\ell\}_{\ell=1,\dots,L}$	44
`id`	identity operator	24
im	image of a linear operator	24
κ	wavenumber	42
ker	kernel of a linear operator	17
ℓ	level parameter	44
Λ_z	hat function associated with node $z \in \mathcal{N}_H$	94
$\lesssim$	less than or equal to up to a constant	9
m	localization/oversampling parameter	26
μ	parameter value	116
$\mathcal{M}$	parameter set	116
$\mathcal{M}^{\mathrm{tr}}$	training set	122
$\mathcal{M}^{\mathrm{rb}}$	reduced basis parameter set	122
N_m	m-th order patch w.r.t. $\mathcal{T}_H$	26
$\mathsf{N}_{\ell,m}$	m-th order patch w.r.t. $\mathcal{T}_\ell$	50
$\mathcal{N}_H$	set of all (interior and boundary) nodes of $\mathcal{T}_H$	13

p	fixed polynomial degree	93
$\mathcal{P}_H$	quasi-interpolation with the same kernel as Π_H^0	32
$\mathcal{P}_\ell$	quasi-interpolation with the same kernel as Π_ℓ^0	44
Π_H^0	L^2-projection onto $\mathcal{T}_H$-piecewise constants	18
Π_ℓ^0	L^2-projection onto $\mathcal{T}_\ell$-piecewise constants	44
Π_H	L^2-projection onto $\mathcal{T}_H$-piecewise polynomials	93
q_K	QOI defined as element average over K	16
$\mathfrak{R}$	real part of a complex number	43
σ	measure for the localization error of the SLOD	71
$g_{K,m}$,$g_{K,m}^*$	local source terms of the SLOD trial/test space	70
$\varphi_{K,m}$,$\varphi_{K,m}^*$	global responses of local SLOD source terms	70
$\psi_{K,m}$,$\psi_{K,m}^*$	SLOD basis function of the trial/test space	70
supp	support of a function	12
$\mathcal{T}_H$	coarse mesh	13
$\mathcal{T}_\ell$	mesh at level ℓ	44
tr_Σ	local trace operator	68
tr_Σ^{-1}	local operator-harmonic extension	68
U_H^{a},V_H^{a}	prototypical problem-adapted trial/test space	16
$U_{H,m}^{\mathrm{lod}}$,$V_{H,m}^{\mathrm{lod}}$	LOD trial/test space	32
$U_{\ell,m}^{\mathrm{mr}}$,$V_{\ell,m}^{\mathrm{mr}}$	MRLOD trial/test space at level ℓ	51
$U_{H,m}^{\mathrm{slod}}$,$V_{H,m}^{\mathrm{slod}}$	SLOD trial/test space	70
$V_{H,m,n}^{\mathrm{gfem}}$	SL-GFEM trial and test space	96
$\mathcal{V}$	H^1-space with possibly prescribed zero traces	12
$\mathcal{V}(S)$	restriction of $\mathcal{V}$ to $S \subset D$	12
$\mathcal{V}_S$	$\mathcal{V}$-conforming subspace of $\mathcal{V}(S)$	66
V_H^{fem}	$\mathcal{V}$-conforming first order coarse FE space	13
V_h^{fem}	$\mathcal{V}$-conforming first order fine FE space	36
$(\cdot\,,\cdot)_{\mathcal{V}}$	H^1-inner product restricted to $\mathcal{V}$	12
$\|\cdot\|_{\mathcal{V}}$	H^1-norm restricted to $\mathcal{V}$	12
$\mathcal{W}$	fine-scale space w.r.t. $\mathcal{T}_H$	16
$\mathcal{W}^{\mathrm{rb}}$	reduced basis functions	122
$\mathcal{W}_\ell$	fine-scale space w.r.t. $\mathcal{T}_\ell$	45
X	local trace space	68
Y	space of locally operator-harmonic functions	68

Acronyms

ALB	Adaptive Local Basis	4
FE	finite element	4
FEM	finite element method	1
GMRES	Generalized Minimal Residual	54
GMsFEM	Generalized Multiscale Finite Element Method	5
HMM	Heterogeneous Multiscale Method	3
LOD	Localized Orthogonal Decomposition	4
MRLOD	Multi-resolution Localized Orthogonal Decomposition	7
MS-GFEM	Multiscale Spectral Generalized Finite Element Method	5
MsFEM	Multiscale Finite Element Method	3
PDE	partial differential equation	1
PML	perfectly matched layer	89
PU	partition of unity	5
QOI	quantity of interest	16
RB	reduced basis	6
RB-SLOD	Reduced Basis Super-Localized Orthogonal Decomposition	8
RPS	Rough Polyharmonic Splines	4
SL-GFEM	Super-Localized Generalized Finite Element Method	8
SLOD	Super-Localized Orthogonal Decomposition	8
SVD	singular value decompsition	68
VMM	Variational Multiscale Method	3

Bibliography

[AB12] A. Abdulle and Y. Bai. "Reduced basis finite element heterogeneous multiscale method for high-order discretizations of elliptic homogenization problems". In: *J. Comput. Phys.* 231.21 (2012), pp. 7014–7036.

[AB13] A. Abdulle and Y. Bai. "Adaptive reduced basis finite element heterogeneous multiscale method". In: *Comput. Methods Appl. Mech. Engrg.* 257 (2013), pp. 203–220.

[AB96] G. Allaire and M. Briane. "Multiscale convergence and reiterated homogenisation". In: *Proc. Roy. Soc. Edinburgh Sect. A* 126.2 (1996), pp. 297–342.

[Abd05] A. Abdulle. "On a priori error analysis of fully discrete heterogeneous multiscale FEM". In: *Multiscale Model. Simul.* 4.2 (2005), pp. 447–459.

[Abd+12] A. Abdulle, W. E, B. Engquist, and E. Vanden-Eijnden. "The heterogeneous multiscale method". In: *Acta Numer.* 21 (2012), pp. 1–87.

[AH15] A. Abdulle and P. Henning. "A reduced basis localized orthogonal decomposition". In: *J. Comput. Phys.* 295 (2015), pp. 379–401.

[AHP21] R. Altmann, P. Henning, and D. Peterseim. "Numerical homogenization beyond scale separation". In: *Acta Numer.* 30 (2021), pp. 1–86.

[Alb+12] F. Albrecht, B. Haasdonk, S. Kaulmann, and M. Ohlberger. "The localized reduced basis multiscale method". In: *Proceedings of Algoritmy*. 2012, pp. 393–403.

[All92] G. Allaire. "Homogenization and two-scale convergence". In: *SIAM J. Math. Anal.* 23.6 (1992), pp. 1482–1518.

[Alp93] B. Alpert. "A class of bases in L^2 for the sparse representations of integral operators". In: *SIAM J. Math. Anal.* 24 (1993), pp. 246–262.

[Alt16] H. W. Alt. *Linear Functional Analysis*. Springer London, 2016.

[APQ16] P. F. Antonietti, P. Pacciarini, and A. Quarteroni. "A discontinuous Galerkin reduced basis element method for elliptic problems". In: *ESAIM: Math. Model. Numer. Anal.* 50.2 (2016), pp. 337–360.

[Auc05] G. Auchmuty. "Steklov eigenproblems and the representation of solutions of elliptic boundary value problems". In: *Numer. Funct. Anal. Optim.* 25.3-4 (2005), pp. 321–348.

[Bab+20] I. Babuška, R. Lipton, P. Sinz, and M. Stuebner. "Multiscale spectral GFEM and optimal oversampling". In: *Comput. Methods Appl. Mech. Eng.* 364 (2020), p. 112960.

[Bab71] I. Babuška. "Error-bounds for finite element method". In: *Numer. Math.* 16 (1971), pp. 322–333.

[Bar+04] M. Barrault, Y. Maday, N.-C. Nguyen, and A. T. Patera. "An 'empirical interpolation method': application to efficient reduced-basis discretization of partial differential equations". In: *C. R. Math. Acad. Sci. Paris* Ser. I 339 (2004), pp. 667–672.

[BD98] A. Braides and A. Defranceschi. *Homogenization of Multiple Integrals*. Oxford Lecture Mathematics. Clarendon Press, 1998.

[Beb03] M. Bebendorf. "A note on the Poincaré inequality for convex domains". In: *Z. Anal. Anwendungen* 22.4 (2003), pp. 751–756.

[Ber+07] A. Bermúdez, L. Hervella-Nieto, A. Prieto, and R. Rodríguez. "An optimal perfectly matched layer with unbounded absorbing function for time-harmonic acoustic scattering problems". In: *J. Comput. Phys.* 223.2 (2007), pp. 469–488.

[Ber94] J.-P. Berenger. "A perfectly matched layer for the absorption of electromagnetic waves". In: *J. Comput. Phys.* 114.2 (1994), pp. 185–200.

[Bet+11] T. Betcke, S. N. Chandler-Wilde, I. G. Graham, S. Langdon, and M. Lindner. "Condition number estimates for combined potential integral operators in acoustics and their boundary element discretisation". In: *Numer. Methods Partial Diff. Equations* 27.1 (2011), pp. 31–69.

[BF91] F. Brezzi and M. Fortin. *Mixed and Hybrid Finite Element Methods*. Vol. 15. Springer Series in Computational Mathematics. Springer, 1991.

[BFP22] F. Bonizzoni, P. Freese, and D. Peterseim. "Super-localized orthogonal decomposition for convection-dominated diffusion problems". In: *arXiv preprint 2206.01975* (2022).

[BG22] D. Brown and D. Gallistl. "Multiscale sub-grid correction method for time-harmonic high-frequency elastodynamics with wave number explicit bounds". In: *Comput. Methods Appl. Math.* 23.1 (2022), pp. 65–82.

[BH82] A. N. Brooks and T. J. R. Hughes. "Streamline upwind/Petrov-Galerkin formulations for convection dominated flows with particular emphasis on the incompressible Navier-Stokes equations". In: *Comput. Methods Appl. Mech. Engrg.* 32.1-3 (1982), pp. 199–259.

[BHL14] I. Babuška, X. Huang, and R. P. Lipton. "Machine computation using the exponentially convergent multiscale spectral generalized finite element method". In: *ESAIM: Math. Model. Numer. Anal.* 48 (2014), pp. 493–515.

[BHP22] F. Bonizzoni, M. Hauck, and D. Peterseim. "A reduced basis super-localized orthogonal decomposition for reaction–convection–diffusion problems". In: *arXiv preprint 2211.15221* (2022).

[BL11] I. Babuška and R. Lipton. "Optimal local approximation spaces for generalized finite element methods with application to multiscale problems". In: *Multiscale Model. Simul.* 9.1 (2011), pp. 373–406.

[BM97] I. Babuška and J. M. Melenk. "The partition of unity method". In: *Int. J. Numer. Methods Eng.* 40.4 (1997), pp. 727–758.

[BMP93] C. Bernardi, Y. Maday, and A. T. Patera. "Domain decomposition by the mortar element method". In: *Asymptotic and Numerical Methods for Partial Differential Equations with Critical Parameters*. Springer Netherlands, 1993, pp. 269–286.

[BO00] I. Babuška and J. E. Osborn. "Can a finite element method perform arbitrarily badly?" In: *Math. Comp.* 69.230 (2000), pp. 443–462.

[BO83] I. Babuška and J. E. Osborn. "Generalized finite element methods: their performance and their relation to mixed methods". In: *SIAM J. Numer. Anal.* 20 (1983), pp. 510–536.

[BR94] F. Brezzi and A. Russo. "Choosing bubbles for advection-diffusion problems". In: *Math. Models Methods Appl. Sci.* 4.4 (1994), pp. 571–587.

[Bre94] S. C. Brenner. "Two-level additive Schwarz preconditioners for non-conforming finite elements". In: *Domain Decomposition Methods in Scientific and Engineering Computing*. Vol. 180. Contemp. Math. Amer. Math. Soc., Providence, RI, 1994, pp. 9–14.

[Bre+97] F. Brezzi, L. P. Franca, T. J. R. Hughes, and A. Russo. "$b = \int g$". In: *Comput. Methods Appl. Mech. Engrg.* 145.3-4 (1997), pp. 329–339.

[Bre+99] F. Brezzi, T. J. R. Hughes, L. D. Marini, A. Russo, and E. Süli. "A priori error analysis of residual-free bubbles for advection–diffusion problems". In: *SIAM J. Numer. Anal.* 36.6 (1999), pp. 1933–1948.

[BS07] N. Banthia and M. Sappakittipakorn. "Toughness enhancement in steel fiber reinforced concrete through fiber hybridization". In: *Cem. Concr. Res.* 37.9 (2007), pp. 1366–1372.

[BS08] S. C. Brenner and L. R. Scott. *The Mathematical Theory of Finite Element Methods*. Third. Vol. 15. Texts in Applied Mathematics. Springer New York, 2008.

[BS18] A. Buhr and K. Smetana. "Randomized local model order reduction". In: *SIAM J. Sci. Comput.* 40.4 (2018), A2120–A2151.

[BS97] I. M. Babuška and S. A. Sauter. "Is the pollution effect of the FEM avoidable for the Helmholtz equation considering high wave numbers?" In: *SIAM J. Numer. Anal.* 34.6 (1997), pp. 2392–2423.

[Buf+12] A. Buffa, Y. Maday, A. T. Patera, C. Prud'homme, and G. Turinici. "A priori convergence of the greedy algorithm for the parametrized reduced basis". In: *ESAIM: Math. Model. Numer. Anal.* 46 (2012), pp. 595–603.

[Buh+17] A. Buhr, C. Engwer, M. Ohlberger, and S. Rave. "ArbiLoMod, a simulation technique designed for arbitrary local modifications". In: *SIAM J. Sci. Comput.* 39.4 (2017), A1435–A1465.

[Buh+21] A. Buhr, L. Iapichino, M. Ohlberger, S. Rave, F. Schindler, and K. Smetana. "Localized model reduction for parameterized problems". In: *Snapshot-Based Methods and Algorithms*. Ed. by P. Benner, S. Grivet-Talocia, A. Quarteroni, G. Rozza, W. Schilders, and L. Sileira. Vol. 3. Model Order Reduction. De Gruyter Berlin, 2021.

[Cal+16] V. M. Calo, Y. Efendiev, J. Galvis, and G. Li. "Randomized oversampling for generalized multiscale finite element methods". In: *Multiscale Model. Simul.* 14.1 (2016), pp. 482–501.

[CDG02] D. Cioranescu, A. Damlamian, and G. Griso. "Periodic unfolding and homogenization". In: *C. R. Math. Acad. Sci. Paris* 335.1 (2002), pp. 99–104.

[CEL18] E. T. Chung, Y. Efendiev, and W. T. Leung. "Constraint energy minimizing generalized multiscale finite element method". In: *Comput. Methods Appl. Mech. Eng.* 339 (2018), pp. 298–319.

[CEL19] E. Chung, Y. Efendiev, and W. T. Leung. "Generalized multiscale finite element methods with energy minimizing oversampling". In: *Internat. J. Numer. Methods Engrg.* 117.3 (2019), pp. 316–343.

[Che+20] K. Chen, Q. Li, J. Lu, and S. J. Wright. "Randomized sampling for basis function construction in generalized finite element methods". In: *Multiscale Model. Simul.* 18.2 (2020), pp. 1153–1177.

[CL18] L. Chamoin and F. Legoll. "A posteriori error estimation and adaptive strategy for the control of MsFEM computations". In: *Comput. Methods Appl. Mech. Eng.* 336 (2018), pp. 1–38.

[Dem06] L. Demkowicz. *Babuška ↔ Brezzi*. Tech. rep. Texas Institute for Computational and Applied Mathematics, The University of Texas at Austin, 2006.

[DG75] E. De Giorgi. "Sulla convergenza di alcune successioni d'integrali del tipo dell'area". In: *Rend. Mat. (6)* 8 (1975), pp. 277–294.

[DHM22] Z. Dong, M. Hauck, and R. Maier. "An improved high-order method for elliptic multiscale problems". In: *arXiv preprint 2211.02484 (to appear in SIAM J. Numer. Anal.)* (2022).

[DPE11] D. Di Pietro and A. Ern. *Mathematical Aspects of Discontinuous Galerkin Methods*. Mathématiques et Applications. Springer Berlin Heidelberg, 2011.

[EE03] W. E and B. Engquist. "The heterogeneous multiscale methods". In: *Commun. Math. Sci.* 1.1 (2003), pp. 87–132.

[EG04] A. Ern and J.-L. Guermond. *Theory and Practice of Finite Elements*. Vol. 159. Applied Mathematical Sciences. Springer New York, 2004, pp. xiv+524.

[EG17] A. Ern and J.-L. Guermond. "Finite element quasi-interpolation and best approximation". In: *ESAIM: Math. Model. Numer. Anal.* 51.4 (2017), pp. 1367–1385.

[EGH13] Y. Efendiev, J. Galvis, and T. Y. Hou. "Generalized multiscale finite element methods (GMsFEM)". In: *J. Comput. Phys.* 251 (2013), 116–135.

[EM12] S. Esterhazy and J. M. Melenk. "On stability of discretizations of the Helmholtz equation". In: *Numerical analysis of multiscale problems*. Vol. 83. Lecture Notes in Computational Science and Engineering. Springer Berlin Heidelberg, 2012, pp. 285–324.

[Eng+19] C. Engwer, P. Henning, A. Målqvist, and D. Peterseim. "Efficient implementation of the localized orthogonal decomposition method". In: *Comput. Methods Appl. Mech. Engrg.* 350 (2019), pp. 123–153.

[EP04] A. L. Efros and A. L. Pokrovsky. "Dielectric photonic crystal as medium with negative electric permittivity and magnetic permeability". In: *Solid State Commun.* 129.10 (2004), pp. 643–647.

[Eva10] L. C. Evans. *Partial Differential Equations*. Second. Vol. 19. Graduate Studies in Mathematics. Amer. Math. Soc., Providence, RI, 2010.

[FHP21] P. Freese, M. Hauck, and D. Peterseim. "Super-localized orthogonal decomposition for high-frequency Helmholtz problems". In: *arXiv preprint 2112.11368* (2021).

[FL96] S.-Y. Fu and B. Lauke. "Effects of fiber length and fiber orientation distributions on the tensile strength of short-fiber-reinforced polymers". In: *Compos. Sci. Technol.* 56.10 (1996), pp. 1179–1190.

[FNS98] L. Franca, A. Nesliturk, and M. Stynes. "On the stability of residual-free bubbles for convection-diffusion problems and their approximation by a two-level finite element method". In: *Comput. Methods Appl. Mech. Eng.* 166.1 (1998), pp. 35–49.

[FP20] M. Feischl and D. Peterseim. "Sparse compression of expected solution operators". In: *SIAM J. Numer. Anal.* 58.6 (2020), pp. 3144–3164.

[Fre+22a] P. Freese, M. Hauck, T. Keil, and D. Peterseim. "A super-localized generalized finite element method". In: *arXiv preprint 2211.09461* (2022).

[Fre+22b] P. Freese, M. Hauck, T. Keil, and D. Peterseim. *Software for "A super-localized generalized finite element method".* `https://doi.org/10.5281/zenodo.7326579`. 2022.

[GGS12] L. Grasedyck, I. Greff, and S. Sauter. "The AL basis for the solution of elliptic problems in heterogeneous media". In: *Multiscale Model. Simul.* 10.1 (2012), pp. 245–258.

[Glo12] A. Gloria. "Numerical homogenization: survey, new results, and perspectives". In: *ESAIM: Proc.* 37 (2012), pp. 50–116.

[GLS21] J. Galkowski, D. Lafontaine, and E. A. Spence. "Local absorbing boundary conditions on fixed domains give order-one errors for high-frequency waves". In: *arXiv preprint 2101.02154* (2021).

[GP15] D. Gallistl and D. Peterseim. "Stable multiscale Petrov-Galerkin finite element method for high frequency acoustic scattering". In: *Comput. Methods Appl. Mech. Engrg.* 295 (2015), pp. 1–17.

[GPS19] I. G. Graham, O. R. Pembery, and E. A. Spence. "The Helmholtz equation in heterogeneous media: A priori bounds, well-posedness, and resonances". In: *J. Differ. Equ.* 266.6 (2019), pp. 2869–2923.

[GS19] I. G. Graham and S. A. Sauter. "Stability and error analysis for the Helmholtz equation with variable coefficients". In: *Math. Comp. 89 (2020), 105-138* (2019).

[GT16] J. Galkowski and J. Toth. "Pointwise bounds for Steklov eigenfunctions". In: *J. Geom. Anal.* 29 (2016).

[GZ19] M. J. Gander and H. Zhang. "A class of iterative solvers for the Helmholtz equation: factorizations, sweeping preconditioners, source transfer, single layer potentials, polarized traces, and optimized Schwarz methods". In: *SIAM Rev.* 61.1 (2019), pp. 3–76.

[Hel97] R. Helmig. *Multiphase Flow and Transport Processes in the Subsurface: A Contribution to the Modeling of Hydrosystems*. Springer Berlin Heidelberg, 1997.

[Het07] U. Hetmaniuk. "Stability estimates for a class of Helmholtz problems". In: *Commun. Math. Sci.* 5 (2007).

[HJ90] R. A. Horn and C. R. Johnson. *Matrix Analysis*. Cambridge University Press, 1990.

[HK17] F. Hellmann and T. Keil. *gridlod*. GitHub repository `https://github.com/fredrikhellman/gridlod`. 2017.

[HKP12] D. B. P. Huynh, D. J. Knezevic, and A. T. Patera. "A static condensation reduced basis element method: approximation and a posteriori error estimation". In: *ESAIM: Math. Model. Numer. Anal.* 47.1 (2012), pp. 213–251.

[HL01] P. Hislop and C. Lutzer. "Spectral asymptotics of the Dirichlet-to-Neumann map on multiply connected domains in $\mathbb{R}^{d}$". In: *Inverse Probl.* 17 (2001), pp. 1717–1741.

[HM14] P. Henning and A. Målqvist. "Localized orthogonal decomposition techniques for boundary value problems". In: *SIAM J. Sci. Comput.* 36.4 (2014), A1609–A1634.

[HM22] M. Hauck and A. Målqvist. "Super-localization of spatial network models". In: *arXiv preprint 2210.07860* (2022).

[HMA86] T. Hughes, M. Mallet, and M. Akira. "A new finite element formulation for computational fluid dynamics: II. Beyond SUPG". In: *Comput. Methods Appl. Mech. Eng.* 54.3 (1986), pp. 341–355.

[HMP14] R. Hiptmair, A. Moiola, and I. Perugia. "Trefftz discontinuous Galerkin methods for acoustic scattering on locally refined meshes". In: *Appl. Numer. Math.* 79 (2014), 79–91.

[HMP16] R. Hiptmair, A. Moiola, and I. Perugia. "A survey of Trefftz methods for the Helmholtz equation". In: vol. 114. Springer International Publishing, 2016, pp. 237–278.

[Hoa08] V. H. Hoang. "Sparse finite element method for periodic multiscale nonlinear monotone problems". In: *Multiscale Model. Simul.* 7.3 (2008), pp. 1042–1072.

[HOS14] P. Henning, M. Ohlberger, and B. Schweizer. "An adaptive multiscale finite element method". In: *Multiscale Model. Simul.* 12.3 (2014), pp. 1078–1107.

[HP13] P. Henning and D. Peterseim. "Oversampling for the multiscale finite element method". In: *Multiscale Model. Simul.* 11.4 (2013), pp. 1149–1175.

[HP22a] M. Hauck and D. Peterseim. "Multi-resolution localized orthogonal decomposition for Helmholtz problems". In: *Multiscale Model. Simul.* 20.2 (2022), pp. 657–684.

[HP22b] M. Hauck and D. Peterseim. "Super-localization of elliptic multiscale problems". In: *Math. Comp.* 92.341 (2022), pp. 981–1003.

[HRS16] J. S. Hesthaven, G. Rozza, and B. Stamm. *Certified Reduced Basis Methods for Parametrized Partial Differential Equations*. Vol. 590. SpringerBriefs in Mathematics. Springer, 2016.

[HS05] V. H. Hoang and C. Schwab. "High-dimensional finite elements for elliptic problems with multiple scales". In: *Multiscale Model. Simul.* 3.1 (2005), pp. 168–194.

[HS07] T. J. R. Hughes and G. Sangalli. "Variational multiscale analysis: the fine-scale Green's function, projection, optimization, localization, and stabilized methods". In: *SIAM J. Numer. Anal.* 45.2 (2007), pp. 539–557.

[HS11] H. Harbrecht and C. Schwab. "Sparse tensor finite elements for elliptic multiple scale problems". In: *Comput. Methods Appl. Mech. Engrg.* 200.45-46 (2011), pp. 3100–3110.

[Hug87] T. J. R. Hughes. "Recent progress in the development and understanding of SUPG methods with special reference to the compressible Euler and Navier-Stokes equations". In: *Int. J. Numer. Methods Fluids* 7.11 (1987), pp. 1261–1275.

[Hug95] T. J. R. Hughes. "Multiscale phenomena: Green's functions, the Dirichlet-to-Neumann formulation, subgrid scale models, bubbles and the origins of stabilized methods". In: *Comput. Methods Appl. Mech. Engrg.* 127.1-4 (1995), pp. 387–401.

[Hug+98] T. J. R. Hughes, G. R. Feijóo, L. Mazzei, and J.-B. Quincy. "The variational multiscale method—a paradigm for computational mechanics". In: *Comput. Methods Appl. Mech. Engrg.* 166.1-2 (1998), pp. 3–24.

[HW97] T. Y. Hou and X.-H. Wu. "A multiscale finite element method for elliptic problems in composite materials and porous media". In: *J. Comput. Phys.* 134.1 (1997), pp. 169–189.

[HWC99] T. Y. Hou, X.-H. Wu, and Z. Cai. "Convergence of a multiscale finite element method for elliptic problems with rapidly oscillating coefficients". In: *Math. Comp.* 68.227 (1999), pp. 913–943.

[HWZ04] T. Y. Hou, X.-H. Wu, and Y. Zhang. "Removing the cell resonance error in the multiscale finite element method via a Petrov-Galerkin formulation". In: *Commun. Math. Sci.* 2.2 (2004), pp. 185–205.

[HZZ15] J. S. Hesthaven, S. Zhang, and X. Zhu. "Reduced basis multiscale finite element methods for elliptic problems". In: *Multiscale Model. Simul.* 13.1 (2015), pp. 316–337.

[IB95] F. Ihlenburg and I. Babuška. "Dispersion analysis and error estimation of Galerkin finite element methods for the Helmholtz equation". In: *Int. J. Numer. Methods Eng.* 38.22 (1995), pp. 3745–3774.

[IQR12] L. Iapichino, A. Quarteroni, and G. Rozza. "A reduced basis hybrid method for the coupling of parametrized domains represented by fluidic networks". In: *Comput. Methods Appl. Mech. Eng.* 221-222 (2012), pp. 63–82.

[KA03] P. Knabner and L. Angermann. *Numerical Methods for Elliptic and Parabolic Partial Differential Equations*. Texts in Applied Mathematics. Springer International Publishing, 2003.

[KOH11] S. Kaulmann, M. Ohlberger, and B. Haasdonk. "A new local reduced basis discontinuous Galerkin approach for heterogeneous multiscale problems". In: *Comptes Rendus Math.* 349.23 (2011), pp. 1233–1238.

[KPY18] R. Kornhuber, D. Peterseim, and H. Yserentant. "An analysis of a class of variational multiscale methods based on subspace decomposition". In: *Math. Comp.* 87.314 (2018), pp. 2765–2774.

[KR21] T. Keil and S. Rave. "An online efficient two-scale reduced basis approach for the localized orthogonal decomposition". In: *arXiv preprint 2111.08643* (2021).

[KY16] R. Kornhuber and H. Yserentant. "Numerical homogenization of elliptic multiscale problems by subspace decomposition". In: *Multiscale Model. Simul.* 14.3 (2016), pp. 1017–1036.

[Lau+21] P. Lauff, P. Pugacheva, M. Rutzen, U. Weiß, O. Fischer, D. Volkmer, M. A. Peter, and C. U. Grosse. "Evaluation of the behavior of carbon short fiber reinforced concrete (CSFRC) based on a multi-sensory experimental investigation and a numerical multiscale approach". In: *Materials* 14.22 (2021).

[LBLL13] C. Le Bris, F. Legoll, and A. Lozinski. "MsFEM à la Crouzeix-Raviart for highly oscillatory elliptic problems". In: *Chin. Ann. Math. Ser. B* 34.1 (2013), pp. 113–138.

[LBLL14] C. Le Bris, F. Legoll, and A. Lozinski. "An MsFEM type approach for perforated domains". In: *Multiscale Model. Simul.* 12.3 (2014), pp. 1046–1077.

[Leg+22] F. Legoll, P.-L. Rothé, C. L. Bris, and U. Hetmaniuk. "An Ms-FEM approach enriched using Legendre polynomials". In: *Multiscale Model. Simul.* 20.2 (2022), pp. 798–834.

[LM05] M. G. Larson and A. Målqvist. "Adaptive variational multiscale methods based on a posteriori error estimation: duality techniques for elliptic problems". In: *Multiscale Methods in Science and Engineering*. Vol. 44. Lecture Notes in Computational Science and Engineering. Springer Berlin Heidelberg, 2005, pp. 181–193.

[LM72] J.-L. Lions and E. Magenes. *Non-homogeneous Boundary Value Problems and Applications. Vol. I.* Die Grundlehren der mathematischen Wissenschaften, Band 181. Springer Berlin Heidelberg, 1972.

[LPS18] G. Li, D. Peterseim, and M. Schedensack. "Error analysis of a variational multiscale stabilization for convection-dominated diffusion equations in two dimensions". In: *IMA J. Numer. Anal.* 38.3 (2018), pp. 1229–1253.

[LT20] J. Liesen and P. Tichý. "The field of values bound on ideal GMRES". In: *arXiv preprint 1211.5969* (2020).

[Mai20] R. Maier. "Computational multiscale methods in unstructured heterogeneous media". PhD thesis. University of Augsburg, 2020.

[Mai21] R. Maier. "A high-order approach to elliptic multiscale problems with general unstructured coefficients". In: *SIAM J. Numer. Anal.* 59.2 (2021), pp. 1067–1089.

[Mål05] A. Målqvist. "Adaptive variational multiscale methods". PhD thesis. Chalmers University of Technology, 2005.

[Mål11] A. Målqvist. "Multiscale methods for elliptic problems". In: *Multiscale Model. Simul.* 9.3 (2011), pp. 1064–1086.

[MAS23] C. Ma, C. Alber, and R. Scheichl. "Wavenumber explicit convergence of a multiscale generalized finite element method for heterogeneous Helmholtz problems". In: *SIAM J. Numer. Anal.* 61.3 (2023), pp. 1546–1584.

[MB96] J. M. Melenk and I. Babuška. "The partition of unity finite element method: basic theory and applications". In: *Comput. Methods Appl. Mech. Engrg.* 139.1-4 (1996), pp. 289–314.

[Mel02] J. M. Melenk. *hp-Finite Element Methods for Singular Perturbations*. Springer Berlin Heidelberg, 2002.

[Mel95] J. M. Melenk. "On generalized finite element methods". PhD thesis. University of Maryland, College Park, 1995.

[Moi11] A. Moiola. "Trefftz-discontinuous Galerkin methods for time-harmonic wave problems". PhD thesis. ETH Zurich, 2011.

[MP14] A. Målqvist and D. Peterseim. "Localization of elliptic multiscale problems". In: *Math. Comp.* 83.290 (2014), pp. 2583–2603.

[MP20] A. Målqvist and D. Peterseim. *Numerical Homogenization by Localized Orthogonal Decomposition*. SIAM, Philadelphia, PA, 2020.

[MPS13] J. M. Melenk, A. Parsania, and S. Sauter. "General DG-methods for highly indefinite Helmholtz problems". In: *J. Sci. Comput.* 57.3 (2013), pp. 536–581.

[MR02] Y. Maday and E. M. Rønquist. "A reduced-basis element method". In: *J. Sci. Comput.* 17.1/4 (2002), pp. 447–459.

[MS02] A.-M. Matache and C. Schwab. "Two-scale FEM for homogenization problems". In: *ESAIM: Math. Model. Numer. Anal.* 36.4 (2002), pp. 537–572.

[MS10] J. M. Melenk and S. Sauter. "Convergence analysis for finite element discretizations of the Helmholtz equation with Dirichlet-to-Neumann boundary conditions". In: *Math. Comp.* 79.272 (2010), pp. 1871–1914.

[MS11] J. M. Melenk and S. Sauter. "Wavenumber explicit convergence analysis for Galerkin discretizations of the Helmholtz equation". In: *SIAM J. Numer. Anal.* 49.3 (2011), pp. 1210–1243.

[MS22] C. Ma and R. Scheichl. "Error estimates for discrete generalized FEMs with locally optimal spectral approximations". In: *Math. Comp.* 91 (2022), pp. 2539–2569.

[MSD22] C. Ma, R. Scheichl, and T. Dodwell. "Novel design and analysis of generalized finite element methods based on locally optimal spectral approximations". In: *SIAM J. Numer. Anal.* 60.1 (2022), pp. 244–273.

[MT78] F. Murat and L. Tartar. "H-convergence". In: *Séminaire d'Analyse Fonctionnelle et Numérique de l'Université d'Alger* (1978).

[Ngu89] G. Nguetseng. "A general convergence result for a functional related to the theory of homogenization". In: *SIAM J. Math. Anal.* 20.3 (1989), pp. 608–623.

[Ohl05] M. Ohlberger. "A posteriori error estimates for the heterogeneous multiscale finite element method for elliptic homogenization problems". In: *Multiscale Model. Simul.* 4.1 (2005), pp. 88–114.

[OR16] M. Ohlberger and S. Rave. "Reduced basis methods: success, limitations and future challenges". In: *Proceedings of Algoritmy*. 2016, pp. 1–12.

[OS15] M. Ohlberger and F. Schindler. "Error control for the localized reduced basis multiscale method with adaptive online enrichment". In: *SIAM J. Sci. Comput.* 37.6 (2015), A2865–A2895.

[OS19] H. Owhadi and C. Scovel. *Operator-Adapted Wavelets, Fast Solvers, and Numerical Homogenization*. Vol. 35. Cambridge Monographs on Applied and Computational Mathematics. Cambridge University Press, 2019.

[Osw93] P. Oswald. "On a BPX-preconditioner for P1 elements". In: *Computing* 51.2 (1993), pp. 125–133.

[Owh15] H. Owhadi. "Bayesian numerical homogenization". In: *Multiscale Model. Simul.* 13.3 (2015), pp. 812–828.

[Owh17] H. Owhadi. "Multigrid with rough coefficients and multiresolution operator decomposition from hierarchical information games". In: *SIAM Rev.* 59.1 (2017), pp. 99–149.

[OZ11] H. Owhadi and L. Zhang. "Localized bases for finite-dimensional homogenization approximations with nonseparated scales and high contrast". In: *Multiscale Model. Simul.* 9.4 (2011), pp. 1373–1398.

[OZB14] H. Owhadi, L. Zhang, and L. Berlyand. "Polyharmonic homogenization, rough polyharmonic splines and sparse super-localization". In: *ESAIM: Math. Model. Numer. Anal.* 48.2 (2014), pp. 517–552.

[PE03] A. Pokrovsky and A. Efros. "Diffraction theory and focusing of light by a slab of left-handed material". In: *Modern Phys. Lett. B* 338.1 (2003), pp. 333–337.

[Pen00] J. B. Pendry. "Negative refraction makes a perfect lens". In: *Phys. Rev. Lett.* 85 (18 2000), pp. 3966–3969.

[Pet16] D. Peterseim. "Variational multiscale stabilization and the exponential decay of fine-scale correctors". In: *Building bridges: Connections and Challenges in Modern Approaches to Numerical Partial Differential Equations*. Vol. 114. Lecture Notes in Computational Science and Engineering. Springer, 2016, pp. 341–367.

[Pet17] D. Peterseim. "Eliminating the pollution effect in Helmholtz problems by local subscale correction". In: *Math. Comp.* 86.305 (2017), pp. 1005–1036.

[Pin85] A. Pinkus. *n-widths in Approximation Theory*. Vol. 7. Results in Mathematics and Related Areas. Springer Berlin Heidelberg, 1985.

[PS12] D. Peterseim and S. Sauter. "Finite elements for elliptic problems with highly varying, nonperiodic diffusion matrix". In: *Multiscale Model. Simul.* 10.3 (2012), pp. 665–695.

[PSS06] J. B. Pendry, D. Schurig, and D. R. Smith. "Controlling electromagnetic fields". In: *Science* 312.5781 (2006), pp. 1780–1782.

[PST15] I. Polterovich, D. Sher, and J. Toth. "Nodal length of Steklov eigenfunctions on real-analytic Riemannian surfaces". In: *J. für die Reine und Angew. Math.* 2019 (2015).

[PT95] L. Piegl and W. Tiller. *The NURBS Book*. Springer Berlin Heidelberg, 1995.

[PV20] D. Peterseim and B. Verfürth. "Computational high frequency scattering from high-contrast heterogeneous media". In: *Math. Comp.* 89.326 (2020), pp. 2649–2674.

[PW60] L. E. Payne and H. F. Weinberger. "An optimal Poincaré inequality for convex domains". In: *Arch. Rational Mech. Anal.* 5 (1960), 286–292 (1960).

[QMN15] A. Quarteroni, A. Manzoni, and F. Negri. *Reduced Basis Methods for Partial Differential Equations: An Introduction*. Vol. 92. Springer, 2015.

[Rou13] T. Roubíček. *Nonlinear Partial Differential Equations with Applications*. Second. Vol. 153. International Series of Numerical Mathematics. Springer Basel, 2013.

[Saa03] Y. Saad. *Iterative Methods for Sparse Linear Systems*. Second. Other Titles in Applied Mathematics. SIAM, Philadelphia, PA, 2003.

[Spa68] S. Spagnolo. "Sulla convergenza di soluzioni di equazioni paraboliche ed ellittiche". In: *Ann. Sc. Norm. Super. Pisa Cl. Sci.* 22.4 (1968), pp. 571–597.

[SS22] J. Schleuß and K. Smetana. "Optimal local approximation spaces for parabolic problems". In: *Multiscale Model. Simul.* 20.1 (2022), pp. 551–582.

[ST18] S. Sauter and C. Torres. "Stability estimate for the Helmholtz equation with rapidly jumping coefficients". In: *Z. Angew. Math. Phys. 69, 139 (2018)* (2018).

[Szy06] D. B. Szyld. "The many proofs of an identity on the norm of oblique projections". In: *Numer. Algorithms* 42.3 (2006), pp. 309–323.

[Tar09] L. Tartar. *The General Theory of Homogenization*. Vol. 7. Lecture Notes of the Unione Matematica Italiana. Springer Berlin; UMI Bologna, 2009.

[Wey17] M. Weymuth. "Adaptive local (AL) basis for elliptic problems with L^∞-coefficients". In: *arXiv preprint 1703.06325* (2017).